FLEXURAL AND SHEAR RESPONSE OF PRECAST PRESTRESSED CONCRETE HOLLOWCORE SLABS UNDER FIRE CONDITIONS

By

Anuj Man Shakya

A DISSERTATION

Submitted to
Michigan State University
in partial fulfillment of the requirements
for the degree of

Civil Engineering - Doctor of Philosophy

2016

ABSTRACT

FLEXURAL AND SHEAR RESPONSE OF PRECAST PRESTRESSED CONCRETE HOLLOWCORE SLABS UNDER FIRE CONDITIONS

By

Anuj Man Shakya

Prestressed concrete (PC) hollowcore slabs are increasingly used in building applications due to numerous advantages they offer over traditional forms of slab construction. Structural fire safety is one of the primary considerations in building design and hence, building codes specify fire resistance requirements for these hollowcore slabs. PC hollowcore slabs, under fire conditions, are susceptible to failure through shear failure modes, in addition to flexural failure mode, due to presence of hollow cores. Moreover, these slabs are not provided with any additional shear reinforcement due to unique fabrication process aimed at achieving cost-effective construction. However, there is limited data and understanding in literature on the mechanism of shear failure in PC hollowcore slabs under realistic loading and fire conditions. To overcome some of these knowledge gaps, a comprehensive study was undertaken to develop an understanding on the fire performance of PC hollowcore slabs under fire conditions.

A three dimensional finite element based numerical model was developed for tracing performance of prestressed concrete hollowcore slabs under fire conditions. The model developed in ANSYS software, accounts for temperature induced degradation of properties of concrete and prestressing strands, cracking in concrete, material and geometrical nonlinearities, realistic fire, loading, and restraint conditions, as well as different failure limit states. For validating the numerical model, fire resistance tests were carried out on six PC hollowcore slabs under standard and realistic fire scenarios. The test variables included type of aggregate in concrete, load level, fire exposure and restraint conditions at the supports, and data generated

from fire tests showed that these parameters have significant influence on the fire performance of PC hollowcore slabs. Data obtained from these fire tests, as well as that reported in literature, were utilized to validate the above numerical model by comparing cross-sectional temperatures, mid-span deflection, axial restraint force, concrete cracking patterns and failure times.

The validated model was applied to carry out parametric studies to quantify the effect of various factors on the fire response of PC hollowcore slabs. Data from parametric studies show that slab depth, load level, loading pattern, axial restraint, level of prestressing and fire severity have significant influence on the fire response of PC hollowcore slabs. Results obtained from numerical study indicate that failure in hollowcore slabs under fire conditions can occur through shear limit state prior to reaching flexural limit state under loads inducing high shear force.

Results generated from the experimental and parametric studies are utilized to develop a rational design approach for evaluating fire resistance of PC hollowcore slabs. The proposed approach comprises of evaluating cross-sectional temperatures in the critical sections of the slab, and then determining moment and shear capacities at any given duration of the fire exposure by utilizing an approach similar to that at room temperature but incorporated with temperature dependent strength properties of concrete and prestressing steel. For predicting sectional temperatures in fire exposed hollowcore slabs, a simplified approach is developed by utilizing data obtained from parametric studies. Fire resistance of a PC hollowcore slab is determined as the time when external bending moment or shear force exceeds moment or shear capacity at the critical sections. The validity of the proposed approach is established by comparing resulting fire resistance predictions with those obtained from detailed finite element analysis and fire tests. This approach can be utilized for estimation of fire resistance of PC hollowcore slabs, and thus suited for incorporation in design codes and standards.

This dissertation is dedicated my beloved wife, Anila Rajbi	to my parents, Bhupendra handari. Without their sup been able to accomplish t	port and encouragem	apurna Tuladhar, and nent I would not have

ACKNOWLEDGMENTS

I would like to express my deep gratitude to my advisor, Prof. Venkatesh Kodur for his continued support and guidance during the course of my studies. I am very grateful for his motivation and perseverance, and for providing an opportunity for a valuable learning experience.

I would also like to thank Prof. Parviz Soroushian, Prof. Neeraj Buch and Prof. Thomas J. Pence for joining my Ph.D. committee, and for their valuable advice throughout my education at Michigan State University.

This research was partially supported by Precast/Prestressed Concrete Institute through Daniel P. Jenny Research Fellowship, and I would like to thank them for their resources. I am also grateful to Kerkstra Precast Inc. for fabricating and transporting the test slabs.

I would like to thank my friends Amir Arablouei, Ankit Agrawal, Mohannad Naser, Esam Aziz, Baolin Yu, Pratik Bhatt, Roya Solhmirzaei, Saleh Mohammad Alogla, Nikhil Raut, Wasim Khaliq and Purushutham Pakala for their support, particularly in the experimental part of this study.

I would also like to express my appreciation to Mr. Siavosh Ravanbakhsh for his support and help during the experimental program in this research. Additionally, I would like to extend my thanks to Laura Taylor, Margaret Conner and Laura Post for all the administrative assistance they provided.

TABLE OF CONTENTS

LIST	OF TABLES	ix
LIST	OF FIGURES	xi
CHA	APTER 1	1
1 In	troduction	1
1.1	General	1
1.2	Behavior of PC hollowcore slabs under fire conditions	3
1.3	Approaches for evaluating fire performance	5
1.4	Research objectives	6
1.5	Scope	
	APTER 2	
2 St	ate-of-the-Art Review	11
2.1	General	
2.2	Experimental studies	12
2.3	Numerical studies	18
2.4	Codal provisions	
2.5	Material properties at elevated temperatures	
2.	5.1 Concrete properties	25
	2.5.1.1 Thermal properties	25
	2.5.1.2 Mechanical properties	26
	2.5.1.3 Deformation properties	27
2.	5.2 Prestressing steel properties	28
	2.5.2.1 Thermal properties	28
	2.5.2.2 Mechanical properties	29
	2.5.2.3 Deformation properties	30
2.6	Knowledge gaps	67
CHA	APTER 3	69
3 Fi	re resistance experiments	
3.1	General	
3.2	Fabrication of test specimens	70
3.3	Instrumentation	72
3.4	Test equipment	73
3.5	Test conditions and procedure	73
3.6	Results and discussion	75
3.	6.1 Thermal response	75
3.	6.2 Structural response	77
3.	6.3 Crack propagation and spalling pattern	81
3.	6.4 Failure mode and fire resistance	84
3.7	Summary	101

CH	APTER 4		102
4 N	Iaterial proj	perty tests	102
4.1	Genera	1	102
4.2	Respon	se of prestressing strand under elevated temperatures	103
4.3	Experir	mental program	106
4.	3.1 Test	specimens	106
4.	3.2 Test	equipment	107
4.	3.3 Test	procedure	108
4.4	Results	and discussion	109
4.	4.1 Stres	ss-strain response	110
4.	4.2 Yield	d strength and ultimate strength	111
4.	4.3 Yield	d strain and failure strain	113
4.	4.4 Elast	tic modulus	114
4.	4.5 Failu	re patterns	115
4.	4.6 High	temperature property relations	116
4.	4.7 Relat	tion for stress-strain response	116
4.	4.8 Relat	tion for mechanical properties	118
4.5		implications	
4.6	Summa	nry	130
CH	APTER 5		131
5 N	umerical m	nodel and validation	131
5.1	Genera	1	131
5.2	Numeri	ical procedure	132
5.	2.1 Evalu	uating flexural and shear capacity	133
5.	2.2 Flexi	ural capacity based on simplified approach	134
5.	2.3 Shea	r capacity based on simplified approach	135
5.3		ization details	
5.4	Materia	al properties	140
5.5	Loading	g and boundary conditions	142
5.6	Failure	criteria	142
5.7	Mesh se	ensitivity study	143
5.8	Model	validation	144
5.	8.1 Slab	characteristics	145
5.	8.2 Anal	ysis details	145
5.	8.3 Resu	lts and discussion	146
	5.8.3.1	Thermal response	146
	5.8.3.2	Structural response	147
		Cracking pattern and failure modes	
		Fire resistance	
5.9		nry	
CH	APTER 6		164
		tudies	
6.1		1	
		influencing fire response	

6.3 I	Parametric studies	166
6.3.1	General	166
6.3.2	Range of parameters	166
6.3.3	Analysis details	168
6.3.4	Response parameters	169
6.4 I	Results of parametric studies	170
6.4.1	Effect of slab depth	170
6.4.2	Effect of load intensity	172
6.4.3	Effect of loading scenarios.	
6.4.4	Effect of axial restraint	
6.4.5	Effect of level of prestressing	176
6.4.6	Effect of fire severity	177
6.5	Summary	194
CHAPT	ER 7	195
	nal design methodology	
	General	
	Rational design approach	
	Simplified approach for predicting temperatures in PC hollowcore slabs	
7.3.1	General procedures	
7.3.2	Nonlinear regression analysis	198
7.3.3	Regression analysis results	
7.3.4	Verification of temperature equation	
7.4 I	Evaluating flexural and shear capacity under fire conditions	
7.4.1	General procedures	
7.4.2	Flexural and shear capacity at ambient conditions	204
7.4.3	Flexural and shear capacity under fire conditions	207
7.4.4	Case study	211
7.4.5	Validation of flexural and shear capacity equations	212
7.5 I	Limitations of proposed approach	213
7.6	Summary	228
CHAPT	ER 8	229
8 Concl	usions and recommendations	229
	General	
	Key findings	
	Recommendations for future research	
	Research impact	
APPENI	DIX	236
REFERE	ENCES	252

LIST OF TABLES

Table 2.1. Experimental studies on fire resistance of prestressed concrete hollowcore slabs 31
Table 2.2. Numerical/Analytical studies on fire resistance of prestressed concrete hollowcore slabs
Table 2.3. Provisions in building standards of various countries
Table 2.4. Prediction of fire resistance values for a typical hollowcore slab using different codes53
Table 2.5. Relationships for high temperature thermal properties of concrete (Eurocode 2) 54
Table 2.6. Constitutive relationship for high temperature properties of concrete (Eurocode 2) 55
Table 2.7. Values for the main parameters of the stress-strain relationships of NSC and HSC at elevated temperatures (Eurocode 2)
Table 2.8. High temperature thermal properties of prestressing steel (Eurocode 3)
Table 2.9. Constitutive relationships for high temperature properties of prestressing steel (Eurocode 2)
Table 2.10. Values for the main parameters of the stress-strain relationships of prestressing steel at elevated temperatures (Eurocode 2)
Table 2.11. Constitutive relationships for high temperature properties of prestressing steel (Eurocode 2)
Table 3.1. Geometric and material characteristics of tested slabs
Table 3.2. Batch proportions in concrete mixes
Table 3.3. Summary of test parameters and results
Table 4.1. Chemical compositions of prestressing strand and reinforcing bar
Table 4.2. Measured yield and ultimate strength and strain of prestressing strand (without and with preload) and reinforcing bars
Table 4.3. High temperature mechanical property relations for prestressing strand

Table 5.1. Comparison of mesh sizes and analysis results	152
Table 5.2. Summary of test parameters and results	152
Table 5.3. Comparison of measured and predicted fire resistance in tested slabs	152
Table 6.1. Comparison of predicted fire resistance in hollowcore slabs	179
Table 7.1. Summary of slab details and test parameters	215
Table 7.2. Comparison of temperature in prestressing strand at 1, 2 and 3 hour of fire	-
Table 7.3. Values for the main parameters of the stress-strain relationships of NSC are elevated temperatures (Eurocode 2)	
Table 7.4. Values for the main parameters of the stress-strain relationships of prestressi elevated temperatures (Eurocode 2)	_
Table 7.5. Comparison of predicted and test fire resistance	217

LIST OF FIGURES

Figure 1.1. Comparison of cross-sectional profiles of typical fire-exposed solid and prestressed concrete hollowcore slabs
Figure 1.2. Comparison of cross-sectional temperatures in a solid and equivalent hollowcore slab exposed to fire
Figure 2.1. Crack patterns in hollowcore slabs under fire conditions (Fellinger 2005) 60
Figure 2.2. Cross-sectional configuration of tested hollowcore slab (Breccolotti et al. 2006) 60
Figure 2.3. Variation of thermal conductivity of concrete with temperature based on Eurocode 2
Figure 2.4. Variation of specific heat of concrete with temperature based on Eurocode 2 61
Figure 2.5. Variation of density of concrete with temperature based on Eurocode 2
Figure 2.6. Variation of compressive strength and elastic modulus of concrete with temperature based on Eurocode 2
Figure 2.7. Stress-strain relationship of concrete in compression at various temperature based on Eurocode 2
Figure 2.8. Variation of thermal strain of concrete with temperature based on Eurocode 2 63
Figure 2.9. Stress-strain relationship of concrete in tension at various temperature based on Eurocode 2
Figure 2.10. Variation of thermal conductivity of steel with temperature based on Eurocode 3 . 64
Figure 2.11. Variation of specific heat of steel with temperature based on Eurocode 3
Figure 2.12. Variation of yield strength and elastic modulus of prestressing steel with temperature based on Eurocode 2
Figure 2.13. Stress-strain relationship of prestressing steel at various temperatures based on Eurocode 2
Figure 2.14. Variation of thermal strain of prestressing steel with temperature based on Eurocode 2

Figure 3.1. Location of thermocouples and strain gauges in PC hollowcore slab
Figure 3.2. Fabrication and curing of prestressed concrete hollowcore slabs
Figure 3.3. Test setup for undertaking fire resistance tests on PC hollowcore slabs
Figure 3.4. Four point loading scheme on hollowcore slab for fire tests
Figure 3.5. Time-temperature curves, simulated during fire tests
Figure 3.6. Variation of strand temperature with fire exposure time in tested slabs
Figure 3.7. Variation of mid-depth temperature with fire exposure time in tested slabs
Figure 3.8. Variation of quarter depth temperature with fire exposure time in tested slabs 92
Figure 3.9. Variation of unexposed surface temperature with fire exposure time in tested slabs 92
Figure 3.10. Variation of core bottom temperature with fire exposure time in tested slabs 93
Figure 3.11. Variation of core top temperature with fire exposure time in tested slabs
Figure 3.12. Variation of mid-span deflection in test hollowcore slabs with fire exposure time in tested slabs
Figure 3.13. Variation of axial restraint forces in Slab 5 with fire exposure time
Figure 3.14. Variation of strains in PC hollowcore slabs with fire exposure time in tested slabs 95
Figure 3.15. Cracking patterns in PC hollowcore slabs under fire exposure
Figure 3.16. Crack progression in tested slabs under combined loading and fire exposure 97
Figure 3.17. Extent of spalling in PC hollowcore slabs under fire exposure
Figure 4.1. Typical stress-strain response of prestressing strand and reinforcing at room temperature
Figure 4.2. Typical specimen anchorage system for tensile strength tests at elevated temperatures
Figure 4.3. Test setup for tensile strength tests on prestressing strand and reinforcing bar a elevated temperatures
Figure 4.4. Stress-strain response of prestressing strand at various temperatures

Figure 4.5. Stress-strain response of prestressing strand with 50% initial stress at various temperatures
Figure 4.6. Stress-strain response of reinforcing bar at various temperatures
Figure 4.7. Comparison of normalized yield stress of prestressing strand and reinforcing bar . 125
Figure 4.8. Comparison of normalized ultimate stress of prestressing strand and reinforcing bar
Figure 4.9. Comparison of normalized yield strain in prestressing strand and reinforcing bar 126
Figure 4.10. Comparison of normalized failure strain in prestressing strand and reinforcing bar
Figure 4.11. Comparison of normalized elastic modulus of prestressing strand and reinforcing bar
Figure 4.12. Failure patterns in of prestressing strand and reinforcing bars at various temperatures
Figure 4.13. Comparison of measured high temperature stress-strain curves of prestressing strands with predicted stress-strain curves (quadri-linear model)
Figure 4.14. Comparison of measured high temperature stress-strain curves of prestressing strands with stress-strain curves calculated based on Eurocode 2
Figure 5.1. Flowchart illustrating steps associated with fire resistance analysis of a hollowcore slab
Figure 5.2. Layout of a typical PC hollowcore slab and its discretization for finite element analysis
Figure 5.3. Comparison of mesh sizes used for mesh sensitivity study
Figure 5.4. Comparison of sectional temperatures with different mesh sizes
Figure 5.5. Comparison of mid-span deflections with different mesh sizes
Figure 5.6. Layout of PC hollowcore slab tested in the laboratory
Figure 5.7. Time-temperature curves, simulated during fire tests
Figure 5.8. Comparison of measured and predicted sectional temperatures for tested Slab 4 158
Figure 5.9. Comparison of measured and predicted sectional temperatures for tested Slab 5 159

Figure 5.10. Comparison of measured and predicted sectional temperatures for tested Slab G6
Figure 5.11. Comparison of measured and predicted mid-span deflections for test Slab 3, Slab 4 and Slab 5
Figure 5.12. Comparison of measured and predicted axial restraint force for test Slab 5 160
Figure 5.13. Comparison of predicted and observed failure modes in tested hollowcore slab under fire condition
Figure 5.14. Comparison of variations of moment capacity with fire exposure time for Slabs 3 to 6
Figure 5.15. Comparison of variations of shear capacity with fire exposure time for Slabs 3, 4 and 6
Figure 6.1. Flowchart showing steps associated with fire resistance analysis of hollowcore slabs
Figure 6.2. Cross-sectional configurations of various standard PC hollowcore slabs
Figure 6.3. PC hollowcore slab subjected various loading scenarios
Figure 6.4. Various fire scenarios encountered in buildings and parking structures
Figure 6.5. Variation of cross-sectional temperature in various hollowcore slabs under fire 183
Figure 6.6. Effect of slab depth on mid-span deflection, moment and shear capacity of hollowcore slabs exposed to fire
Figure 6.7. Effect of slab depth on crack pattern in hollowcore slabs under fire condition at failure
Figure 6.8. Effect of load level on mid-span deflection, moment and shear capacity in hollowcore slabs exposed to fire
Figure 6.9. Effect of loading scenario on mid-span deflection, moment and shear capacity in hollowcore slabs exposed to fire
Figure 6.10. Effect of loading scenarios on crack pattern in hollowcore slabs exposed to fire . 188
Figure 6.11. Effect of axial restraint on mid-span deflection, moment and shear capacity in hollowcore slabs exposed to fire

Figure 6.12. Effect of axial restraint on crack pattern in hollowcore slabs exposed to fire 190
Figure 6.13. Effect of level of prestressing on mid-span deflection, moment and shear capacity in hollowcore slabs exposed to fire
Figure 6.14. Effect of level of prestressing on crack pattern in hollowcore slabs exposed to fire
Figure 6.15. Effect of fire severity on sectional temperatures in hollowcore slabs
Figure 6.16. Effect of fire severity on mid-span deflection, moment and shear capacity in hollowcore slabs
Figure 7.1. Flowchart illustrating rational design approach for evaluating fire resistance of PC hollowcore slabs
Figure 7.2. Comparison of predicted temperature using proposed equations with temperatures obtained using finite element analysis for various depth hollowcore slabs
Figure 7.3. Time-temperature curves, simulated during fire tests
Figure 7.4. Comparison of predicted temperature in Slab 6 with that obtained from test conducted by Shakya and Kodur
Figure 7.5. Comparison of predicted temperature in Slab 4 with that obtained from test conducted by Shakya and Kodur
Figure 7.6. Comparison of predicted temperature in Slab G6 with that obtained from test conducted by Jansze et al
Figure 7.7. Comparison of predicted temperature in hollowcore slab with that obtained from test conducted by Breccolotti et al
Figure 7.8. Comparison of moment and shear capacity degradation using proposed equations and FEA in tested Slab 6
Figure 7.9. Comparison of moment and shear capacity degradation using proposed equations and FEA in tested Slab 4
Figure 7.10. Comparison of moment and shear capacity degradation using proposed equations and FEA in tested Slab G6
Figure 7.11. Comparison of moment and shear capacity degradation using proposed equations and FEA in tested Slab B
Figure A.1. Cross section, elevation and internal force diagram of PC hollowcore slab 251

CHAPTER 1

1 INTRODUCTION

1.1 General

Concrete is widely used as primary material in construction industry due to flexibility in application, locally available ingredients, superior properties and fire resistance. However, concrete is inherently weak in tension and this results in some limitations to its effective use without any reinforcement. One of the most effective methods of overcoming this drawback is through prestressing of concrete members. Prestressing of concrete members can be done either, by placing the concrete mix over pre-tensioned low relaxation steel strands and releasing after concrete attains required strength, or by post-tensioning of unbonded tendons placed inside structural members. The prestressing force in strands or tendons is transferred to the concrete as compressive stresses, which negate some of the tensile stresses developed in the member during service life of a structure. The improvement in tensile properties, through prestressing, can be utilized to achieve higher capacity, design longer span beams and slabs, smaller sectional sizes, and lighter structural members without cracking in the member during service life. In addition, use of prestressing technology also facilitates design of innovative and complex structural configurations.

One such innovative structural member, attainable through prestressing, is prestressed concrete (PC) hollowcore slabs, which are increasingly finding applications in buildings due to numerous advantages they offer over other forms of construction such as cost-effectiveness, architectural aesthetics, speedy construction, space utilization and low maintenance costs. On top of these benefits, these slabs exhibit significantly higher strength to weight ratio, as compared to solid slab of equivalent thickness.

Fire safety is one of the primary considerations in buildings and parking structures and thus, building codes specify certain fire resistance requirements for these hollowcore slabs to ensure the safety of occupants and fire fighters, control spread of fire, and minimize property damage during a fire incident. In an event of fire in a building, hollowcore slabs are required to ensure the containment of flame and smoke within the compartment, while sustaining service loads for fire exposure duration. In buildings fire safety is typically achieved through the provision of active and passive fire protection systems. Active fire protection systems, which include heat and smoke detectors, fire alarms, and sprinklers, get automatically triggered in a fire incident. Passive fire protection systems represent inherent fire resistance property of a structural member. The fire resistance of a structural member is defined as the duration during which the member exhibits passive fire protection, and is the earliest time to reach the end point criteria that is evaluated based on insulation, integrity and stability failure requirements (ASTM 2011). Structural members in building are typically required to have 0.5, 1, 1.5, 2, 3, 4 hours of fire resistance rating.

Currently, fire resistance ratings of a concrete slab is determined based on prescriptive approaches, wherein fire resistance is evaluated based on the depth of slab (or equivalent depth in the case of hollowcore slab) and the thickness of concrete cover to reinforcement. These prescriptive rules, derived based on data from standard fire tests, do not account for realistic failure limit states and critical influencing parameters, and thus, often do not yield realistic fire resistance. A rational approach that accounts for critical failure limit states and various factors affecting fire performance of PC hollowcore slabs can yield realistic fire resistance (Kodur and Dwaikat 2007).

1.2 Behavior of PC hollowcore slabs under fire conditions

The behavior of a PC hollowcore slab under fire conditions can be significantly different from that of a traditional solid slab, and this mainly arises due to the voids (cores) present in a hollowcore slab (see Figure 1.1). In a solid slab, temperature transmission from fire exposed surface to unexposed surface is mainly governed by conduction, whereas in a hollowcore slab, temperature transmission occurs via conduction in the solid concrete portion, and through convection and radiation in hollow cores. This can produce significant variations in progression of cross sectional temperatures in these slabs. A comparison of temperature progressions in a solid and an equivalent hollowcore exposed to fire is illustrated in Figure 1.2. It can be seen from this figure that the hollowcore slab experiences quicker transmission of heat to the unexposed side of the slab, as compared to a solid slab of equivalent depth.

Besides temperature transmission, structural behavior of hollowcore slabs can also be significantly different than that of solid slab, especially shear response. Hollowcore slabs possess lower shear capacity at room temperature, as compared to traditional solid slabs, due presence of core voids and lower cross-sectional concrete area. Moreover, these hollowcore slabs typically are not provided with any shear reinforcement due to unique fabrication process aimed at achieving cost-effective construction. Thus, unlike solid slabs in which failure is predominantly governed by flexural capacity, hollowcore slabs are susceptible to failure through shear limit state at ambient conditions (Rahman et al. 2012). Under fire conditions, the susceptibility of hollowcore slabs to shear failure is even higher as degradation of material properties occurs due to elevated cross-sectional temperature.

Under fire conditions, both concrete and prestressing strands experience temperature induced strength and modulus degradation, leading to degradation in moment and shear capacity with fire

exposure time. When the moment or shear capacity drops below the applied bending moment or shear force, failure of the slab occurs. In prescriptive based approaches, the moment capacity at which failure occurs is often linked to a critical temperature in prestressing strands, taken as 427°C. This critical temperature is the temperature at which the prestressing strand loses 50% of its ultimate strength (Hou et al. 2014). Evaluation of fire resistance of hollowcore slab by only gauging strand temperature might not yield realistic fire resistance, as failure in hollowcore slabs can also occur through other failure modes such as flexural cracking, shear cracking and spalling (Abrams 1976; Acker 2003; Aguado et al. 2012; Andersen and Lauridsen 1999; Bailey and Lennon 2008; Borgogno 1997; Breccolotti et al. 2006; Fellinger et al. 2005; Jensen 2005; Lennon 2003; Schepper and Anderson 2000; Zheng et al. 2010). Of these failure modes, shear cracking is the most critical failure modes in hollowcore slabs under fire condition, as it can occur abruptly without warning. Most of the previous fire resistance studies on PC hollowcore slabs considered only flexural response, without much consideration to failure under shear, in evaluating failure (Abrams 1976; Acker 2003; Aguado et al. 2012; Andersen and Lauridsen 1999; Bailey and Lennon 2008; Borgogno 1997; Breccolotti et al. 2006; Chang et al. 2008; Dotreppe and Franssen 2004; Fellinger et al. 2005; Jensen 2005; Lennon 2003; Min et al. 2010; Schepper and Anderson 2000; Zheng et al. 2010). Further, critical failure modes and their mechanisms in PC hollowcore slabs are not fully understood and have not been properly quantified under fire conditions. Thus, a significant knowledge gap exists in regards to failure modes and failure mechanisms of PC hollowcore slabs under fire conditions.

Besides shear failure, fire-induced spalling is another possible failure mode in hollowcore slabs exposed to fire, as reported by some researchers (Andersen and Lauridsen 1999; Breccolotti et al. 2006; Jensen 2005; Lennon 2003; Schepper and Anderson 2000). Spalling is rare but can occur

in hollowcore slabs as these slabs are currently fabricated with high strength concrete (HSC), with compressive strength greater than 70 MPa. Previous studies have shown that HSC is typically more susceptible to fire-induced spalling than normal strength concrete (NSC) due to lower percentage of interstitial voids (Kodur 2000; Kodur and McGrath 2001). Moreover, unlike solid slabs, hollowcore slabs are not provided with transverse reinforcement, and thus, fire-induced spalling in hollowcore slabs can cause rapid loss in strength due to direct exposure of strands to fire, leading to sudden failure. However, additional surface area in the core voids usually reduces the chances of spalling by facilitating release of temperature-induced pore pressure.

1.3 Approaches for evaluating fire performance

The prevalent method of evaluating fire resistance of hollowcore slabs is through prescriptive methods as specified in ACI 216.1 (ACI 216.1-14 2014), PCI (PCI 2011) and Eurocode 2 (Eurocode 2 2004a). These prescriptive methods are derived based on data from standard fire tests and prescribe tabulated fire resistance ratings linked to concrete cover thickness and effective slab depth of hollowcore slabs. These prescriptive methods do not account for actual design variables and realistic failure modes, and thus might not yield realistic fire resistance of PC hollowcore slabs.

Some codes such as PCI (PCI 2010) and Eurocode 2 (Eurocode 2 2004a) provide rational design approaches for evaluating fire resistance of concrete structures. These rational approaches are typically based on sectional analysis and utilize temperature induced strength reduction factors to evaluate reduction in capacity at the critical section of the structural member at a given fire exposure time. When the reduced sectional capacity drops below applied loading effect

(moment) during a fire event, failure is said to occur. Such a design approach for evaluating fire resistance of PC hollowcore slabs is not well established, especially based on shear limit state (Jansze et al. 2012; Min et al. 2012).

To overcome these limitations in current design approaches, a rational approach for evaluating fire resistance of PC hollowcore slabs can be developed through a performance-based fire design methodology. Undertaking performance-based fire design methodology requires a number of steps namely, assessing multiple fire scenarios, evaluating sectional temperatures, determining structural response, and then applying realistic failure criteria for evaluating fire resistance (Kodur and Dwaikat 2007). For implementing performance based methodology, a validated numerical model is required to perform thermo-structural analysis at various steps. Results from thermal and structural analysis can be utilized to evaluate failure at each time step, based on different failure criteria specified in standards such as ASTM-E119 (ASTM 2011), BS476 (BS 476–20 1987) or ISO834 (International Standard (E) 1999). Time to reach the (time) step at which failure occurs is taken as the fire resistance of the PC hollowcore slab. Through these steps, realistic fire performance of PC hollowcore slabs can be evaluated.

1.4 Research objectives

Observations from numerous fire tests on PC hollowcore slabs indicate that hollowcore slabs are susceptible to various failure modes, such as flexure and shear under fire conditions (Abrams 1976; Acker 2003; Aguado et al. 2012; Andersen and Lauridsen 1999; Bailey and Lennon 2008; Borgogno 1997; Breccolotti et al. 2006; Fellinger et al. 2005; Jensen 2005; Lennon 2003; Schepper and Anderson 2000; Zheng et al. 2010). The nature of failure mode in these slabs is governed by parameters like slab depth, load level, loading pattern, support restraint, level of

prestressing and fire scenarios. However, current fire design methodologies do not account for realistic failure modes and critical parameters. Thus, current design methods might not yield realistic fire resistance of PC hollowcore slabs.

To address some of these drawbacks, a fire design methodology based on rational approach needs to be developed. Thus, following objectives are proposed as part of this research.

- Undertake a detailed state-of-the-art review on the fire performance of PC hollowcore slabs and identify knowledge gaps relating to response of hollowcore slabs under fire conditions.
- Conduct full scale fire resistance tests on PC hollowcore slabs exposed to standard and design fire scenarios under different load levels, support conditions and with different concrete types.
- Develop finite element based numerical model to trace the response of PC hollowcore slabs under fire conditions. This model should account for geometric and material nonlinearities, temperature dependent thermal and mechanical properties of concrete, reinforcing steel and prestressing steel and all possible failure modes.
- Conduct high temperature tensile strength tests for evaluating stress-strain response for seven
 wire low relaxation prestressing strands, and incorporate the temperature dependent stressstrain relation in the numerical model.
- Validate the numerical model utilizing the data generated from fire resistance tests by comparing response predictions obtained from the model with data obtained from fire resistance experiments.
- Apply numerical model to undertake parametric studies, to quantify the influence of various critical parameters influencing the behavior and failure modes of PC hollowcore slabs under fire conditions.

 Develop rational methodology for fire design of PC hollowcore slabs based on the information generated from fire tests and numerical studies.

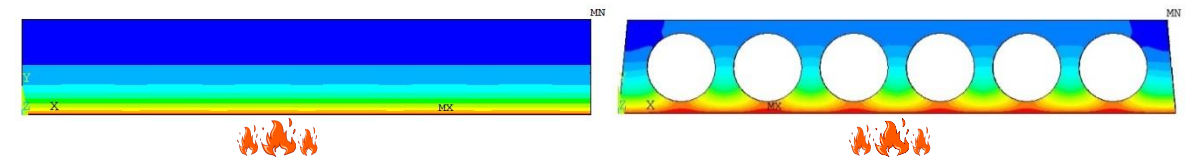


Figure 1.1. Comparison of cross-sectional profiles of typical fire-exposed solid and prestressed concrete hollowcore slabs

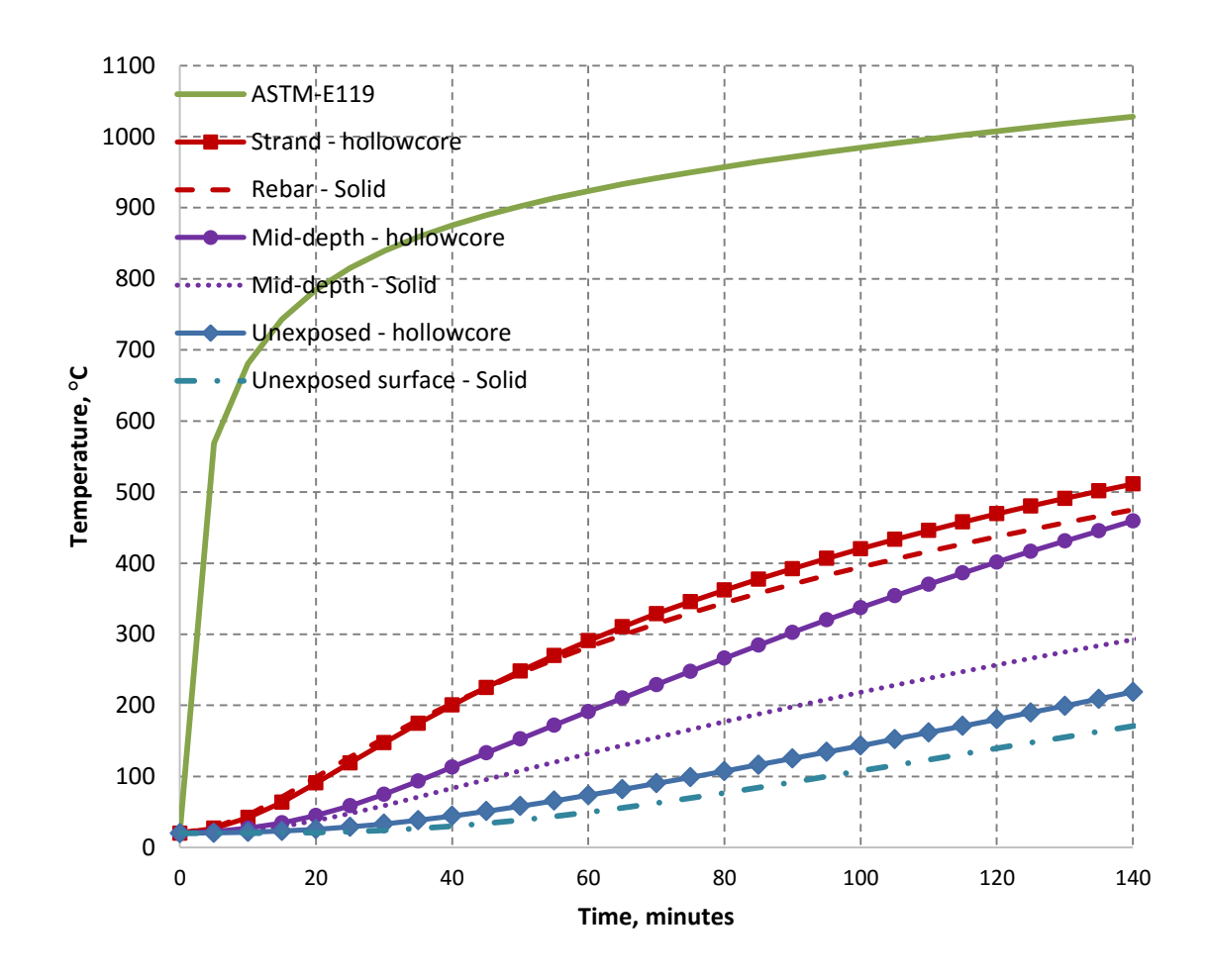


Figure 1.2. Comparison of cross-sectional temperatures in a solid and equivalent hollowcore slab exposed to fire

1.5 Scope

The research, undertaken to address the above objectives, is presented in eight chapters. Chapter 1 provides a general background to response of PC hollowcore slabs under fire conditions and layouts the objectives of the study. Chapter 2 summarizes a state-of-the-art review on the behavior of PC hollowcore slabs exposed to fire. The review includes summary of reported experimental and analytical studies, as well as presents fire design provisions for PC hollowcore slabs in current codes of practice. This chapter also reviews high temperature material property models for concrete and prestressing steel needed for modeling fire response of PC hollowcore slabs.

Chapter 3 presents fire resistance experiments on six PC hollowcore slabs under different aggregate types, fire scenarios, loading and support conditions. Data from the fire tests is used to discuss comparative response of PC hollowcore slabs under these conditions. Chapter 4 describes high temperature tensile strength tests on prestressing strands and reinforcing steel bars, and presents stress-strain relations for prestressing steel and reinforcing steel bars. Chapter 5 details a three dimensional finite element based numerical model developed for evaluating fire response of PC hollowcore slab. The validation of the finite element model (thermal and structural) is also presented by comparing predictions from the model with the results from fire tests.

Chapter 6 presents results from a parametric study on the influence of critical parameters on fire response of PC hollowcore slabs. A detailed discussion on the trends along with the ranges of parameters governing the fire resistance of PC hollowcore slabs is described in Chapter 6. In Chapter 7, rational design guidelines for predicting the fire resistance of PC hollowcore slabs are developed and simplified expressions for predicting sectional temperatures in hollowcore slabs

are proposed. Results from the fire resistance tests conducted as a part of this research and that available in the literature are applied to verify the proposed rational approach for evaluating the fire resistance of PC hollowcore slabs. Finally, Chapter 8 summarizes the main findings arising from the current study and lays out recommendations for further research.

2 STATE-OF-THE-ART REVIEW

This chapter is mainly based on the following journal papers:

- Shakya AM, Kodur VKR. Behavior of prestressed concrete hollowcore slabs under standard and design fire exposure. 8th Int. Conf. Struct. Fire, vol. 1, Shanghai China: 2014, p. 199–208.
- Shakya AM, Kodur VKR. Performance of prestressed concrete hollowcore slabs under standard and design fire exposure. PCI Conv. Natl. Bridge Conf., National Harbor, MD: Prestressed Concrete Institute; 2014.

2.1 General

Prestressed concrete hollowcore slabs are typically used in building and parking structures, where fire is one of the critical design parameters. Due to the presence of core voids, the fire behavior of hollowcore slabs is very complex and significantly different from that of traditional solid slabs. Fire resistance of PC hollowcore slabs is influenced by a number of factors including slab depth, size of cores, load level, loading pattern, support restraint, level of prestressing and fire scenarios. However, many of these factors are not taken into consideration in design of PC hollowcore slabs under fire conditions. The current code provisions for evaluating fire resistance of PC hollowcore slabs is based on prescriptive methodology and assumes the slab to have failed when prestressing strand reaches a critical temperature. These provisions are derived based on the standard fire tests carried out on PC hollowcore slabs.

In the last four decades, there have been numerous studies, both experimental and analytical, to develop an understanding on the behavior of PC hollowcore slabs under fire conditions. This section provides a state-of-the-art review on experimental and numerical studies, including drawbacks, related to fire performance of PC hollowcore slabs. Also, a review of fire resistance provisions in various codes and standards is provided. Finally, a review of high temperature thermal and mechanical properties of concrete and prestressing strand required for numerical modeling of PC hollowcore slabs is also presented.

2.2 Experimental studies

The performance of PC hollowcore slabs under fire conditions is typically evaluated through fire resistance tests. Several experimental studies carried have been carried out to evaluate fire resistance of precast prestressed hollowcore slabs. Some of the notable experimental studies on hollowcore slab are reviewed in detail, the main findings are discussed, and limitations and drawbacks in these studies are highlighted. In addition, details of reported fire resistance tests are also presented in Table 2.1. For each study, the objectives, the test parameters, the test methods and major conclusions are summarized in this table.

Abrams (Abrams 1976) was one of the early researchers to conduct fire tests on PC hollowcore slabs under standard fire conditions. The objective was to evaluate effect of fire insulation on temperature rise in prestressing strands. Fire tests were carried out on two hollowcore slabs supplemented with 70 mm (2¾ in.) of fire insulation on unexposed side of the slab. In addition, another two slabs were tested without any fire insulation. No loading was applied on the slabs in the fire tests. In the tests, the strand temperatures were slightly lower in the insulated slab, as

compared to the un-insulated slabs. This study evaluated only sectional temperatures, and did not study structural performance of hollowcore slabs under fire exposure.

Borgogno (Borgogno 1997) conducted tests on 20 hollowcore slabs to study their behavior at ambient and fire conditions. All hollowcore slabs were 1.2 m wide but with varying lengths and thickness, as well as provided with varying end conditions. The fire test details are illustrated in Table 2.1. Flexure, anchorage, shear, compression and shear-tension failures were identified as possible failure modes for hollowcore slabs under fire conditions. Further, flexible support and transverse bending of hollowcore slabs decreased the shear capacity under fire conditions. The study concluded that support conditions have significant effect on fire performance of hollowcore slabs.

Andersen and Lauridsen (Andersen and Lauridsen 1999) carried out fire tests on three hollowcore slabs to study fire induced spalling in high strength concrete hollowcore slabs. These simply supported slabs were 1.2 m wide, 6 m long and of varying thicknesses (185 to 270 mm), and were subjected to ISO 834 fire. Failure in all slabs occurred through shear failure. Also, fire resistance was evaluated through numerical analysis and compared with that obtained from the tests. Comparison of measured and predicted fire resistances (Andersen and Lauridsen 1999), indicated that calculated fire resistances were generally higher than the actual fire resistances measured in fire tests. Further, in the numerical analysis, failure occurred through flexural limit state in these slabs, but in the fire tests these slabs failed through shear and anchorage failures. Schepper and Anderson (Schepper and Anderson 2000) performed standard fire tests on hollowcore slabs to evaluate fire resistance of typical deck structures. Reinforced concrete topping was provided on top, which made these slabs behave as a single deck. Hollowcore slabs underwent cracking, spalling and bond failure during fire exposure. Test observations showed

that hollowcore slabs failed through crushing of the bottom concrete at supports due to negative restraint moment at supports.

Acker (Acker 2003) conducted fire tests on 24 hollowcore slab units to study global structural behavior of a deck structure. In first and fourth test slabs were 3 m in length and 1.2 m in width arranged in 2 by 2 setup, and slabs in the other two tests (second and third test) were 3 m in length and 0.6 m in width, arranged in 2 by 4 setup. Further details on the test setup are also illustrated in Table 2.1. Cross-sectional configuration of hollowcore slabs were varied in all four tests, and details on the cross-section can be found elsewhere (Acker 2003). All test floors measured 6 m by 3 m in overall dimensions, but two out of four tests (first and third test) received a reinforced concrete topping. Seven of these slabs failed through flexural failure mode at load level greater than serviceability live load, whereas one slab with topping failed through shear failure mode.

Lennon (Lennon 2003) carried out full-scale fire tests on two hollowcore slabs at Cardington Test Facility, Building Research Establishment (UK) to evaluate fire induced spalling of concrete and premature shear failure at supports of slabs. The hollowcore slabs were subjected to 60 minutes of design fire specified as per Eurocode 1 (Eurocode 1 2008). No premature shear failure or spalling occurred during tests, and hollowcore slabs survived the design fire conditions. Further, the study also concluded that spalling does not occur if adequate curing time is allowed.

Fellinger (Fellinger et al. 2005) conducted fire tests on 25 hollowcore slab units under ISO 834 fire. 21 out of 25 tests were performed on double ribbed hollowcore units sawn out of a full hollowcore slabs to study failure mechanism in core webs. Several parameters like slab thicknesses, type of (slab) production processes and continuity were considered. In addition to

slab tests, 60 small scale material property (calibration) tests were also conducted for calibrating constitutive models. The slabs under fire conditions failed through shear, anchorage, and combined shear and anchorage failure modes, as shown in Figure 2.1. The study concluded that, temperature induced thermal expansion leads to structural damage like cracking and slip of prestressing strands, starting within first 15 minutes of standard fire exposure. Further, the type of aggregate influences fire response of hollowcore slabs, and the restraints at supports are beneficial for improving fire resistance, which can only be generated through rigidity of vertical structures, and not by adjacent hollowcore slabs.

Jensen (Jensen 2005) performed three tests to evaluate shear capacity of hollowcore slabs under fire conditions. Hollowcore slabs were 2.935 m in length, 1.196 m in width and 265 mm in depth, and subsequently loaded with 65%, 75% and 80% of ultimate shear capacity measured at ambient conditions. Slabs were exposed to 60 minutes of standard fire and subsequent cooling phase of 90 min. Slab subjected to 80% load failed in 45 minutes and those subjected to 65% and 75% load did not undergo complete collapse or spalling. This study concluded that load level has significant effect on fire resistance of hollowcore slabs.

Breccolotti et al. (Breccolotti et al. 2006) performed two full-scale tests on four light weight concrete hollowcore slabs under ISO 834 fire. All slabs were 4.3 m in length, 1.2 m in width and 200 mm in depth The slab configuration is illustrated in Figure 2.2. One slab in each test was loaded, to induce 60 percent of ambient temperature moment capacity, with four point loading scheme, whereas second slab was unloaded. Further details on the test slabs are illustrated in Table 2.1. The unloaded slabs were loaded after fire tests to evaluate residual strength after exposing to fire. The study concluded that adequate curing under low humidity conditions

significantly reduces the risk of spalling. On the other hand, if fire-induced spalling occurs, load bearing capacity gets significantly reduced.

Engstrom et al. (Engström et al. 2007) performed full-scale experiments on ten hollowcore slabs units under ambient conditions to study the effect of different parameters that influence the shear and torsional response of slabs. The varied parameters were: loading pattern and support conditions that introduce shear and torsional stresses in hollowcore slabs. The slabs were of 200 mm and 400 mm depths and subjected to various shear and torsional loading combinations. It was concluded the capacity of the slab is significantly affected by the support conditions. Slabs, with depth of 400 mm, experienced cracking in the cover concrete below the strands at the supports leading to anchorage failure. However, no such cracks occurred in 200 mm slabs.

Bailey and Lennon (Bailey and Lennon 2008) tested 15 hollowcore slabs in two full scale fire tests. These hollowcore flooring units were supported on protected steel members and subjected to standard ISO384 (International Standard (E) 1999) fire conditions. Each slab was 1.2 m in width and 200 mm in depth. Restraint conditions were varied in two fire tests. Test results showed that steel supports did not provide lateral restraints, and thus, did not enhance fire resistance. However, lateral compression crack strips were formed at the ends due to some degree of restraints to expansion. This improved flexural and shear capacity of the units.

Peltonen and Plum (Peltonen and Plum November) performed fire tests on 8 hollowcore slabs (2 slabs per test) supported on "Peikko Deltabeams"; a proprietary beam section developed by Peikko Group. Even though these tests were primarily focused on evaluating the performance of the "Deltabeams", test data provide valuable information in the behavior of hollowcore slabs under fire conditions. The support beams ("Peikko Deltabeams") were un-insulated in order to evaluate the ability of these Deltabeams to carry the slabs under fire conditions. The hollowcore

slabs measured 2350 mm in width and the overall test panel with Deltabeam measured a width of 3915 mm and the length varied between 7.2 m and 9.6 m between tests. The load was applied at a distance of 715 mm from the end of the hollowcore slabs which corresponds to a distance of 675 mm (2.5 times depth of slab) from the theoretical support on the bottom flange. The tests were carried out under varied fire duration, cooling phase duration and loading. Further, details on the fire test are illustrated in Table 2.1. Temperature profiles were measured at various depths of hollowcore slabs. Based on the results from the tests, it was concluded that the Deltabeam can support the load from the hollowcore slab through the compression of the slab to the inclined web of the Deltabeam but not through the support on the bottom flange of the Deltabeam. Zheng et al (Zheng et al. 2010) carried out fire tests on 15 PC simply supported solid slabs and 9 two-span un-bonded prestressed continuous solid slabs to study spalling phenomena in PC slabs. Even though, this tests were conducted on solid slabs these tests can provide some information in understanding spalling in PC slabs. Thicknesses for 15 PC simply supported slabs varied among 80, 90 and 95 mm. Width and length were 0.6 and 3.3 m, and fire exposed length was 3.05 m for these 15 slabs. Thicknesses for 9 PC unbounded continuous slabs varied between 70, 80 and 85 mm, and width and length were 0.6 and 5.3 m (two spans of 2.55 m each). Fire exposed length varied between 2.35 and 2.12 m for these 9 slabs. Further, details on the fire test are illustrated in Table 2.1. In the tests, spalling occurred in concrete in the temperature range of 200-500°C. It was concluded that the nominal tensile strength and compressive strength of concrete have significant influence on the extent of spalling in concrete, but effect of water content on spalling is minimal. Also, the extent of spalling is increased when compressive stress of concrete is higher or concrete's tensile stress is lower on the surfaces exposed to fire.

Aguado el al. (Aguado et al. 2012) tested four hollowcore slabs with varying reinforcement arrangements to study its effect on fire response of PC hollowcore slabs. All four slabs were of 5.7 m in length, 1.2 m in width and 250 mm in depth, and comprised of nine void cores. Steel wires of 5 mm diameter and prestressing strands of 9.5 mm (3/8 in.) diameter were used. The average axis distances (distance from exposure surface to the center of the strands; cover thickness), ranging from 30.1 to 46.7 mm were studied. Slabs were loaded with four-point loading scheme and subjected to ISO 834 (International Standard (E) 1999) standard fire. Further, details on the fire test are illustrated in Table 2.1. Four types of cracking were evaluated during flexural loading namely, thermal, flexural, splitting and longitudinal cracking. Further, slabs with lowest moisture content, lowest tensile strength and highest compressive strength of concrete exhibited highest fire resistance.

The above review clearly illustrates that there have been numerous fire resistance tests on PC hollowcore slabs. However, information in the literature is not very consistent and show conflicting patterns from one test to other. Many of these fire tests were conducted under standard conditions and thus, do not provide any information regarding fire response under design or realistic scenarios (realistic fire, loading and support). Thus, to overcome this drawback, a fire test program needs to carried-out to evaluate the response of PC hollowcore slabs also under design fire, loading and support conditions.

2.3 Numerical studies

Fire tests are expensive and time consuming and thus, it is not possible to undertake numerous fire tests to evaluate effects of various parameters on fire performance of hollowcore slabs. Hence, numerical simulations can serve as an effective alternative to fire tests. Moreover, with

numerical modeling, there are no limitations on the parameters that can be accounted for, in order to better understand the behavior of hollowcore slabs. There have been number of numerical studies on fire performance of PC hollowcore slabs and most of these studies utilized finite element based models. Some of the notable studies are presented here and critical details are summarized in Table 2.2.

Dotreppe and Franssen (Dotreppe and Franssen 2004) performed numerical simulations on precast hollowcore slabs using computer program SAFIR (Franssen et al. 2004). The effects of hollow core (cavities) on temperature distribution, progression of transverse cracking across cross section due to thermal stresses and influence of restraint on deflection and cracking were studied. Further, details on the numeral model are illustrated in Table 2.2. Results from the study showed that thermal stresses were higher during first 30 minutes of fire. Further, the restraints enhanced the fire resistance calculated based on bending and shear failure criteria. It was concluded that cavities in the slab has significant effects on the temperature distribution and subsequent fire resistance.

Fellinger (Fellinger et al. 2005) performed numerical study of hollowcore slabs using DIANA finite element package (DIANA 2000). The model was validated and calibrated respectively based on, previously discussed, fire tests and material property tests (Fellinger et al. 2005). Finite element model was constructed to incorporate splitting cracking, verticals cracking and slip development in order to simulate realistic behavior of hollowcore slabs, under fire conditions. Further, details on the numeral model are illustrated in Table 2.2. The numerical study concluded that fire resistance is mainly affected by restraint to thermal expansion of the slab by lateral members.

Breccolotti et al. (Breccolotti et al. 2006) performed numerical analysis of tested light weight concrete prestressed hollowcore slabs using finite element code FIRES T3 (Iding et al. 1977). Load bearing capacity, based on bending failure criterion, was evaluated through thermostructural analysis. Further, details on the numerical study are illustrated in Table 2.2. However, spalling and shear failures were not incorporated in the model.

Engstrom et al. (Engström et al. 2007) developed three dimensional finite element numerical models of the hollowcore slabs using finite element package DIANA 8.1 and validated based on the previous experiments conducted on hollowcore slabs (Engström et al. 2007). Further, details on the numerical study are illustrated in Table 2.2. The model was successful in predicting the overall behavior, failure modes and maximum capacity that was in good agreement with the experimental results. The effects of parameters that influence the shear and torsion response of the hollowcore slabs were studied utilizing the model. However, this model is only applicable for ambient conditions and not for fire conditions.

Chang et al. (Chang et al. 2008) proposed a simple method for modeling the structural behavior of hollowcore concrete floor slabs under fire conditions. Grillage system was incorporated in finite element model, using beam elements, to capture thermal expansion in both directions, as illustrated in Table 2.2. Topping concrete layer was modeled using shell elements. The model was validated against test data on hollowcore slabs, and it was concluded that fire performance of hollowcore slab is significantly influenced by different arrangements of axial and rotational restraints at supports.

Min et al. (Min et al. 2010) developed a numerical model for evaluating fire resistance of PC hollowcore floors using multi-spring elements. Further, details on the numerical model are illustrated in Table 2.2. This model accounted for effects of starter (connector) rebars between

reinforcement toping slab and supporting beams. It was concluded that increasing number of starter bars enhances tensile capacity at supports, and hence increases fire resistance of hollowcore slabs.

The above review illustrates that limited numerical studies were conducted to evaluate fire performance of PC hollowcore slabs. These studies had several limitations and drawbacks, as these studies do not account for critical factors affecting response of hollowcore slabs under fire conditions namely fire scenario, loading patterns, restraint conditions, aggregate type and different failure modes. Thus, to overcome these drawbacks, there is a need of a robust computer model that can take in account critical parameters and realistic failure modes in hollowcore slabs under fire conditions.

2.4 Codal provisions

The specifications for fire resistance ratings of hollowcore slabs are provided in building codes and national standards. Most of these provisions are prescriptive in nature, which are derived based on results of standard fire tests. These tabulated fire resistance values are mostly dependent on concrete cover thickness to strand (reinforcement) and minimum dimensions (depth) of the slab. Current code provisions are discussed below and also summarized in Table 2.3. Further, to illustrate the variation in various code provisions, fire resistance of a typical hollowcore slab calculated based on various code provisions is compared in Table 2.4.

In the United States, concrete structures are to be designed in accordance with the American Concrete Institute (ACI 318) code (ACI 318 2011) and prestressed concrete structures are to be designed in accordance with the Precast and Prestressed Concrete Institute Handbook (PCI 2010) (PCI 2010). PCI Handbook (PCI 2010) gives the fire resistance ratings for prestressed concrete

floor or roof slabs in a tabular form based on the concrete cover thickness to reinforcement. In addition, PCI fire design manual (PCI 2011) lays out a rational design methodology for evaluating the fire resistance of PC slabs based on strength degradation of strand with temperature.

While ACI 318 (ACI 318 2011) does not contain any fire provisions, it refers to ACI 216.1 (ACI 216.1-14 2014) standard which gives prescriptive based tables for fire resistance ratings of concrete and masonry structures based on ASTM E119 (ASTM 2011) standard fire tests. ACI 216.1 (ACI 216.1-14 2014) specifies minimum sectional dimensions (slab thickness) and cover thickness (concrete cover over strands) for achieving a required fire resistance rating in slabs. For hollowcore slabs, effective slab thickness is obtained by dividing the net cross-sectional area by its width. Further, the fire ratings in both PCI publication (PCI 2010) and ACI 216.1 (ACI 216.1-14 2014) are given for different end conditions and aggregate types in concrete. ACI 216.1 (ACI 216.1-14 2014) provisions for determining fire resistance of PC slabs are similar to the provisions in PCI Design Handbook (PCI 2010) and International Building Code (IBC 2006) (ICC 2012).

Eurocode 2 (Eurocode 2 2004a) provides three approaches of determining fire resistance of PC slabs. These approaches are based on complexity, namely tabular (tables) approach, simplified approach and advanced methods. The tabular method, referred to as prescriptive approach, is the simplest and most direct method for evaluating fire resistance ratings. The table provides fire resistance based on the minimum thickness of the slab (excluding the floor finishes), axis distance of the reinforcement (equivalent to concrete cover thickness), and different configurations of slabs (simply-supported, continuous, flat and ribbed) (Eurocode 2 2004a).

The simplified approach, in Eurocode 2 (Eurocode 2 2004a) is based on cross-sectional analysis. Fire resistance is evaluated through sectional analysis by accounting for temperature induced strength reduction factors to evaluate the flexural capacity of slab at any given fire exposure time. The time when the flexural capacity drops below the applied bending moment, failure in the slabs is assumed, and this time is the fire resistance. Further, equations for calculating shear and anchorage capacity of hollowcore slabs under fire conditions are provided in Eurocode 2-Annex G (Jansze et al. 2012). This method is applicable where the slab is subjected to uniform fire exposure temperature and loading. The third approach for evaluating fire resistance in through advanced calculation method, wherein thermal and structural response of concrete structures (hollowcore slabs) is evaluated by applying heat transfer and structural mechanics principles. This method requires validation of numerical calculations with test data. Even though this method might lead to accurate estimation of fire resistance, there is lack of numerical models for evaluating fire response of prestressed concrete structures.

Other design codes such as Australian Code AS 3600 (AS 3600 2001), New Zealand Concrete Standard NZS 3101 (AS/NZS 2002) and Canadian National Building Code (NRC/CNRC 2010) provide tables for fire resistance ratings similar to PCI (PCI 2010) and ACI 216.1 (ACI 216.1-14 2014) provisions.

An overview of current design guidelines in codes and standards indicate that the prescriptive based methods are the most prevalent method for evaluating fire resistance of PC hollowcore slab, wherein these methods are mainly dependent on the critical strand temperature concrete. Fire resistance ratings are tabulated as a function of concrete cover thickness to the strands and slab thickness. The prescriptive approaches are developed solely based on critical temperature in strand as the limiting failure criteria, without any consideration for other critical failure modes

namely, flexural cracking, shear cracking and anchorage failure (Abrams 1976; Acker 2003; Aguado et al. 2012; Andersen and Lauridsen 1999; Bailey and Lennon 2008; Borgogno 1997; Breccolotti et al. 2006; Fellinger et al. 2005; Jensen 2005; Lennon 2003; Schepper and Anderson 2000; Zheng et al. 2010). Thus, these methods might not yield accurate fire resistance for hollowcore slabs, as illustrated in Table 2.4. For a 200 mm hollowcore slab, a fire resistance of 90 minutes is evaluated based on prescriptive approach, while such a slab exhibited more than 120 minutes of fire resistance during fire resistance tests (Shakya and Kodur 2015). Thus, to overcome this drawback, a rational fire design methodology which accounts for critical failure modes needs to be developed for evaluating realistic fire resistance of hollowcore slabs.

2.5 Material properties at elevated temperatures

The fire response of prestressed concrete hollowcore slabs is governed by thermal, mechanical and deformation properties of constituent materials, namely concrete and prestressing steel. The thermal properties determine heat transfer to the slab, mechanical properties determine the extent of strength loss and stiffness degradation, and deformation properties control deflection and deformation of the slab under fire conditions. All these properties vary as a function of temperature and are usually defined in codes and standards such as Eurocode 2 (Eurocode 2 2004a), Eurocode 3 (Eurocode 3 2005) and ASCE (ASCE 1992).

Thermal properties of concrete and prestressing steel include thermal conductivity, specific heat and density, mechanical properties include strength and modulus of elasticity, and deformation properties include mechanical and thermal strains of the constituent materials. All of the above material properties need to be properly accounted for in accurately tracing the fire response of

PC hollowcore slabs. This section provides a review on high temperature properties of concrete and prestressing steel.

2.5.1 Concrete properties

Until recently, PC hollowcore slabs were fabricated utilizing normal strength concrete (NSC) with concrete strengths ranging from 40-50 MPa. However, currently hollowcore slabs are fabricated with high strength concrete (HSC) with concrete strength greater than 70 MPa. Utilizing high strength concrete for fabricating PC hollowcore slabs usually prevents bond and anchorage failures under fire conditions (Shakya and Kodur 2015). There are relatively fewer material property models available for high strength concrete, as compared to normal strength concrete (NSC). These material property models are derived based on the data from material property tests and usually specified in codes. The most widely used constitutive models are specified in codes namely, the Eurocode 2 (Eurocode 2 2004a) and ASCE manual of practice (ASCE 1992). The thermal, mechanical and deformation property models specified in the ASCE model is valid for NSC only, while Eurocode model is valid for both NSC and HSC. Thus, material properties for high strength concrete as specified in Eurocode 2 (Eurocode 2 2004a) are discussed here. The constitutive model for high temperature material properties for concrete as specified in Eurocode 2 (Eurocode 2 (Eurocode 2 2004a) are also illustrated in Table 2.5 to Table 2.7.

2.5.1.1 Thermal properties

Properties of concrete that influence thermal behavior of PC hollowcore slabs include thermal conductivity, specific and density. The thermal conductivity, specific heat and density are expressed as a function of temperature for concrete in Eurocode 2 (Eurocode 2 2004a), are plotted in Figure 2.3, Figure 2.4 and Figure 2.5 respectively. It can be seen from Figure 2.3, Figure 2.4 and Figure 2.5 that temperature has significant effect on the thermal properties of

concrete. Eurocode model defines lower and upper bounds for thermal conductivity of concrete, wherein upper bound is applicable for siliceous aggregate concrete and lower bound is applicable for carbonate aggregate concrete. On the other hand, Eurocode constitutive model ignores significant changes in specific heat that occurs in carbonate aggregate concrete in the temperature range of 600-800°C and has the same heat capacity models for both siliceous and carbonate aggregate concrete. Lastly, density is defined to decrease in a linear fashion with temperature, as shown in Figure 2.5.

2.5.1.2 Mechanical properties

The most widely used constitutive model for concrete is specified in Eurocode 2 (Eurocode 2 2004a). These relations give the rate of degradation of concrete as a function of temperature only, without any consideration to variations in other significant parameters such as rate of loading, heating, material composition. Figure 2.6 shows variation of compressive strength and elastic modulus of concrete with temperature for HSC according to the models in Eurocode 2. It is evident both compressive strength and elastic modulus decrease with increase in temperature, wherein compressive strength of HSC degrades faster than elastic modulus. The strength property of HSC is also defined as stress-strain relationship at various temperatures, as shown in Figure 2.7. Previous studies have shown that the model proposed in Eurocode 2 (Eurocode 2 2004a) for Class 3 of HSC gives conservative values for concrete compressive strength reduction with temperature. However, Class 1 HSC is discussed in this chapter, which is slightly less conservative than Class 2 and Class 3 HSC, as concrete used for fabricating PC hollowcore slabs is represented by Class 1 HSC.

In addition, plastic behavior of concrete also needs to be defined and is represented using Willam and Warnke's constitutive model (Willam and Warnke 1975), which is capable of defining

concrete behavior in both tension and compression. The compressive plastic behavior is defined as isotropic multi-linear stress-strain curve varying with temperature while, tensile behavior is defined through damage parameters. For numerical analysis, the damage in concrete is defined in terms of crack opening and crack closing parameters. These parameters are defined through crack opening and closing shear transfer coefficients, (\beta t and \beta c respectively) and are taken to be 0.2 and 0.7 respectively (Willam and Warnke 1975). Shear transfer coefficients are taken to be zero when there is a total loss of shear transfer (representing a smooth crack) and 1.0 when there is full transfer of shear (representing a rough crack). In addition, concrete tensile strength is taken as $0.62\sqrt{f'_c}$ (f'_c in MPa), where f'_c is the compressive strength of concrete (ACI 318 2011; PCI 2010). Once concrete reaches its tensile rupture stress, a tensile stiffness multiplier of 0.6 is used to simulate a cracked (tension) condition with a sudden drop of the tensile stress to 60% of the initial rupture stress. Then, the drop is followed by a linearly descending response to zero stress at a strain value of six times the rupture strain (ANSYS 2014). The degradation of tensile strength of concrete with temperature is evaluated as specified in Eurocode 2 (Eurocode 2 2004a). The stress-strain relationship of concrete in tension at various temperatures is illustrated in Figure 2.9.

2.5.1.3 Deformation properties

Deformation property concrete is defined by thermal strain under fire conditions. The variation of thermal strain of concrete with temperature is plotted in Figure 2.8. Eurocode 2 provides two different models of thermal strain for carbonate and siliceous aggregate concrete, wherein siliceous aggregate concrete has higher rate of increase in thermal strain as can be seen in Figure 2.8.

2.5.2 Prestressing steel properties

There is limited information on high temperature properties of prestressing steel. For numerical analysis, properties for prestressing strands are typically utilized from Eurocode 3 (Eurocode 3 2005 p. 3) and Eurocode 2 (Eurocode 2 2004a). Thus, material properties of prestressing steel (thermal properties, mechanical properties, and deformation properties) that influence the fire response of prestressed structures are reviewed in this section. The constitutive model for high temperature material properties for concrete as specified in Eurocode 3 (Eurocode 3 2005 p. 3) and Eurocode 2 (Eurocode 2 2004a) are also illustrated in Table 2.8 to Table 2.11.

2.5.2.1 Thermal properties

Prestressing strand has very little influence in the progression of cross-sectional temperatures in hollowcore slabs, as prestressing steel is embedded in concrete and is of very small area as compared to concrete. Moreover, heat is distributed through prestressing strands quite rapidly, as the thermal conductivity of steel is significantly higher than that in concrete. Thus, typically in numerical analysis, steel reinforcement is generally assumed to be a perfect conductor, which implies that temperature is uniform within the steel area. The thermal properties that affect temperature in prestressing steel include thermal conductivity and specific heat. The thermal properties of steel depend on the composition of steel. However, as temperature rises, the thermal properties of steel become more dependent on temperature and are influenced less by steel composition (Williams B. K. 2004). Thus, thermal properties for steel is typically adopted from Eurocode 3 (Eurocode 3 2005) for numerical analysis, as thermal properties of steel are not specifically provided for prestressing steel in Eurocode 2 (Eurocode 2 2004a) or Eurocode 3 (Eurocode 3 2005).

It can be seen in Figure 2.10 that thermal conductivity of steel decreases with temperature in an almost linear fashion. On the contrary, specific heat of steel varies considerably between 700°C and 800°C, as can be seen in Figure 2.11. In general, the specific heat of steel increases with an increase in temperature with a large spike occurring around 750°C. The spike in the specific heat at around 750°C is due to the phase change that occurs in steel. As also reported previously, there are minor variations in the models specified in design codes and standards for high-temperature thermal properties of steel.

2.5.2.2 Mechanical properties

The mechanical properties of prestressing strands that govern fire behavior of PC hollowcore slabs include strength properties. Most of the previous tests on prestressing strand steel were conducted on individual wire specimens (Gales et al. 2012; Gálvez et al. 2011; Zheng et al. 2007) and thus, data obtained from these tests might not represent the response of the overall strand comprising of wire bundle, as typically used in practice. Thus, mechanical properties as specified in Eurocode 2 (Eurocode 2 2004a) are reviewed in this section. Figure 2.12 illustrates the variation of yield strength and elastic modulus of low relaxation (LR) prestressing strands (cold-worked (cw), Class B) with temperature, as specified in Eurocode 2 (Eurocode 2 2004a). Cold-worked Class B low relaxation strands represents the prestressing strands utilized for fabricating PC hollowcore slabs. It is evident from Figure 2.12 that both yield strength and elastic modulus decrease with increase in temperature, wherein elastic modulus of prestressing steel degrades faster than yield strength. The strength property of prestressing steel is also defined as stress-strain relationship at various temperatures, as shown in Figure 2.13.

The temperature dependent stress-strain relationship for prestressing steel in Eurocode 2 idealizes the mechanical behavior of prestressing strand into a tri-linear form, by truncating the

response at a stress level, typically taken as the yield stress (Eurocode 2 2004a) and ignoring any strain hardening phase. In addition, Eurocode 2 also assumes continuous increase in ductility with temperature, as reflected by progressing rupture strain in 20 to 1200°C temperature range, in prestressing strand. These idealized response trends might not be realistic, as indicated in some of the recent high temperature tensile tests on prestressing bars (Hou et al. 2014) and prestressing wires (Zheng et al. 2007). Data from these studies have clearly shown that high strength prestressing steel exhibits a distinct strain hardening phase beyond yield, and significant reduction in rupture strain in 200 to 500°C temperature range due to "blue brittleness" effect (Hou et al. 2014; Zheng et al. 2007). To overcome some of the drawback in Eurocode 2 model, mechanical tensile tests needs to be conducted to fully characterize the behavior of prestressing strands under elevated temperatures. However, the Eurocode 2 constitutive model for prestressing strands results in conservative response, and thus utilized for numerical analysis.

2.5.2.3 Deformation properties

Deformation property namely, thermal strain of prestressing steel has significant influence on the fire response of PC hollowcore slabs. Thus, temperature-induced thermal strain for steel as specified in Eurocode 3 (Eurocode 3 2005) is typically utilized for numerical analysis and is also plotted in Figure 2.14. The thermal strain of steel increase in a linear fashion with temperature increase. However, in the temperature range of 700°C-850°C, the Eurocode model accounts for the phase change that occurs in steel in this temperature range by assuming a constant thermal strain from 750°C to 850°C, followed by an increasing thermal strain up to 1000°C.

Table 2.1. Experimental studies on fire resistance of prestressed concrete hollowcore slabs

Study/Investigation	Study Objectives / Detail	Features and Methodology	Observations / Conclusions	Strengths/Draw backs
Abrams M. S. (1976)	The study presents the results of the 2 standard fire tests carried on 4 PC hollowcore slabs. Objective: • To evaluate the effects of roofing insulation on the temperature of the prestressing strand.	 All the slabs were 40 in. long, 24 in. wide and 8 in. thick. One slab in each test had 3/8 in. strands and other had ½ in. strands. Both types of slabs had 1½ in. clear cover over the strands. Only one test had 2¾ in. thick roof insulation on the side away from the fire. Two slabs were placed adjacently and subjected to ASTM E-119 fire. All slabs were simply supported. 	 The slab with insulation registered slightly lower strand temperature than the one without insulation, thus achieving somewhat higher fire resistance. Fire resistance of the slab was evaluated based on the critical strand temperature of 426 °C. Slabs without insulation achieved fire resistance of about 95 min. for both strand diameters and two slabs with insulation achieved 100 min. fire resistance. 	 This test provides a good understandin g of the temperature increase in prestressing strands in hollowcore slabs. Drawbacks This test is only based on standard fire and does not study realistic fire. The slabs were unloaded, which does not reflect realistic application scenarios.

Table 2.1. (cont'd)

Borgogno W. (1997)	The study studies the	• All hollowcore slabs were 1.2	Possible failure modes were	• This study
Doigugilo W. (1997)	results of the 20 fire			
	tests conducted on PC	m wide but with varying	observed to be bending,	provides
		lengths and thickness.	anchorage, shear	ample
	hollowcore slabs.	• 7 tests conducted at ETH	compression, and shear	amount of
		involved following slabs, one	tension failures.	tests data for
	Objective:	with 16 cm thickness and 8 cm	• The structural behaviour of	variety of
	• To identify the	concrete cover and six with 20	the hollowcore elements	cases.
	possible failure	cm thickness with no concrete	was significantly influenced	Drawbacks
	modes and develop	cover. The supports were	by the conditions at the	 These tests
	structural model of	flexible for 5 tests and rigid	supports. In particular, a	do not
	the hollowcore	for 2 tests with unrestrained	flexible support on a beam	account for
	slabs.	end condition for all tests.	and the transverse bending	design or
		• 8 tests conducted at CTICM	of the hollowcore slab	realistic fire
		involved following slabs, all	decreased the shear	scenarios.
		with 16 cm thickness, 4	resistance significantly.	• Many
		without concrete cover and	• The least fire resistance was	important
		other 4 with 5 cm concrete	observed in one of the tests	parameters
		cover. Supports were flexible	reported by Richter (1987)	like concrete
		for 3 tests and rigid for other 5	which achieved only 32	strength and
		tests. The end condition was	min. and failed by brittle	aggregate
		unrestrained in most of the	web failure.	type were not
		cases expect for 2 cases.	Maximum fire resistance	considered in
		-	was observed in two of the	the study.
		• 3 tests reported by Richter		me study.
		(1987/2) involved slabs with	tests performed in ETH,	
		14 cm thickness and no	which achieved more than	
		concrete cover. Support	122 min. for slab with	
		conditions were all rigid and	flexible support and	
		unrestrained.	unrestrained end condition.	
		• 2 tests conducted at Sevilla as		
		reported by Rui-Wamba		
		(1994) involved slabs with 14		

Table 2.1. (cont'd)

Andersen N. E. and Lauridsen D. H.	The study presents the results of three fire	cm thickness with 6 cm concrete cover. The support condition were both rigid but end condition was toggled between restrained and unrestrained. • All hollowcore units were of	The critical failure mode was observed to be shear	• This study
(1999)	testits of three fire tests on hollow core slabs and compares the results to the fire resistance calculations performed by four participants. Objective: To study spalling of high strength concrete To identify potential failure modes.	6m length and 1.2 m width but with different thicknesses, 185mm (SP 18), 220mm (SP 22) and 270mm (SP 27). Each tests consisted of two identical slabs and comprised no topping concrete • The slabs were subjected to ISO834 fire • All slabs were simply supported	failure. Bond failure between the strand and the concrete was observed after around 10 min. of fire. Slabs SP 18 and SP 22 exhibited very similar shear failure with 45 degrees rupture line approximately 1m from the support and shear failure for slab SP 27 occurred at the supports due to snapping off of supporting concrete. Significant discrepancy is seen between the test and calculations in prediction of fire resistance and failure modes. Spalling was not observed in any of the tests.	provides good information on the performance of high strength concrete under fire and studies its spalling phenomena. Drawbacks • The huge discrepancy between tests and the calculated results are not studied.

Table 2.1. (cont'd)

Schepper L. and Anderson N. E. (2000)	The study presents the results of fire tests on the hollowcore slab elements in a deck structure. • To determine the fire resistance of deck structures in the strong rooms • To determine the failure modes.	 The decks consisted of PC hollowcore slabs 220 mm thick with an 80 mm cast-in-place reinforced concrete topping and partly filled hollowcores with shear reinforcement. The deck was subjected to ISO 834 fire. 	 The failure mode was observed to be compression failure on the bottom of the hollowcore slab due to the negative end restraint moment at the support. The hollowcore slab elements with cast-in-place reinforced concrete topping failed around 23 minutes of fire with the maximum 	• This study provides information about behavior of hollowcore slab units when used as a single deck structure.
Acker A.V. (2003)	The study presents results of four fire tests conducted on hollowcore slabs arranged 2 by 2 in first and fourth tests and 2 by 4 in second and third test set up. Objective: • To study the global structural behavior of the hollowcore units in a decking structure. • To evaluate the magnitude and location of thermal stresses caused by the different fire	 All four comprised of two floor spans of 3 m supported on three beams. The cross sectional properties of hollowcore slabs varied in all four tests. All the slabs in first and fourth tests were 3 m in length and 1.2 m in width arranged 2 by 2 in test setup and all the slabs in second and third tests were 3 m in length and 0.6 m in width arranged 2 by 4 in the test setup. The units were connected to the perimeter and mid support beam through 12 mm diameter bars. Two of the setup received insitu reinforced concrete 	 deflection of 250 mm. The tests results showed that the critical failure mode was bending as it was observed in 7 out of 8 cases at load level exceeding serviceability load limit with an average load factor of 2.72. The eighth case showed shear failure. The study concluded that the fire resistance of the concrete structures can be governed by indirect stresses developed in the units due thermal expansion restricted by the edge structures rather than the degradation of material strength at elevated 	• This study provides valuable information in understandin g the global structural behavior of hollowcore slabs under fire conditions.

Table 2.1. (cont'd)

	exposure times. • To examine the influence of parameters like restraint to thermal expansion, the cable effect of the deflection, and the size of the cross section on the fire response.	topping. • The arrangement was subjected to 2 hours of ISO 834 fire.	temperature. It also states that shear can be significantly transferred to the prestressing strands through the longitudinal joints.	
Lennon T. (2003)	The study presents the results of two full scale fire tests on hollow core slabs. Objectives: To study the spalling phenomena of the hollow core slabs and premature shear failure at the supports.	 The test set ups were identical except for the structural concrete topping. One set up had slab joints filled and was provided with 50 mm of concrete topping with reinforcement mesh. Other set up had reinforcing bars placed in the joints at the support on top of filling the joints. The hollowcore slab setup was subjected to 60 min of design fire designed as per Eurocode (EC1-1991). 	 No significant spalling was observed even at temperatures in excess of 1200 °C and very rapid heating. Thus, concluded that spalling does not occur when sufficient curing time is allowed. No premature shear failure was observed. 	• This study provides good test data from full scale testing which can be utilized for understandin g spalling and shear failure of hollow core slabs.
Fellinger J. H. H. (2005)	The study presents the results of 25 fire tests performed on the hollowcore slabs after conducting a thorough	• 21 out of 25 tests were performed on the double ribbed hollowcore units sawn out of the full hollowcore slabs.	• Failure modes were observed to be shear, anchorage and combined shear and anchorage failures.	• The study provides crucial information on the failure

Table 2.1. (cont'd)

• To study the failure mechanism in the All tests were done under ISO splitting crack. and aggregate aggregate					
		study also presents 60 new small scale calibration tests for calibrating constitutive models. • To identify failure modes of hollowcore slabs under fire conditions. • To study the failure mechanism in the web of the hollow cores. To observe the expected cracking along the web and measure the slip between the strands and the concrete. • To study the effects of various parameters like slab thickness, production process and support condition on the fire resistance of the hollowcore	studied. Four types of slab thicknesses (200, 260, 265 and 400mm), two types of production processes (extrusion and slip form) and three types of end conditions (simple support, restraint in spanning direction and reinforced end beam) were studied. All tests were done under ISO	developed over the entire length of the specimen. One of the slabs (VX265) exhibited horizontal crack through the smallest section of the web throughout the entire slab length. Two slabs (HVP260 and K400) developed horizontal cracks along the strand as splitting crack. Aggregate type is an important parameter that affects the fire resistance of hollowcore slab. The restraints can only be generated through the rigidity of vertical structures rather than	and failure modes of hollowcore slabs under fire. • Drawbacks: Some of the vital parameters like concrete and aggregate type, spalling is not taken

Table 2.1. (cont'd)

Jensen J. P. (2005)	The study provides the structural performance of hollowcore slabs with varying loading level. • To identify the effect of loading level on the fire resistance of the slab.	 The hollowcore slab comprised of one whole and two halves units with 2935 mm length and 265 mm thickness. Each element consists of 8 normal ribs and two longitudinal joints with side ribs. The tests were done under 60 min. of standard fire with 90 min. of subsequent cooling. 	 No spalling or breaking occurred in slabs with 65% and 75% loading based on shear capacity exposed to 60 min. of fire and 90 min. of cooling. On the other hand the slab with 80% loading with respect to ultimate shear capacity, failed after 45 min. due to breaking. The test results concluded that the load level has significant effect on the fire resistance. 	 This tests provides useful data on the structural performance of the slab under fire in terms of mid span vertical deflection. Drawbacks Various important parameters with respect to fire response are not accounted for.
Breccolotti M. et al. (2006)	The study presents the results of two full-	• All the slabs were 4.3 m in length, 1.2 m in width and 0.2	• In the first tests, the loaded slab underwent brittle	• This study provides
(2000)	scale tests on total of	m deep and made from C48/58	collapse in shear after 76	valuable
	four high performance	N/mm ² concrete with 1.9	min. of the fire exposure. At	information
	light weight concrete	KN/m ³ unit weight. Each slab	40 th min. vertical pass-	regarding
	(HPLWC) hollowcore	comprised seven 3/8 in.	through holes formed due to	temperature
	slabs.	prestressing strands.	local spalling were closed	distribution
	• To assess the load	Additional shear	using insulating material to	and structural
	bearing capacity of	reinforcements were placed at	continue the test until	performance
	hollowcore slabs	both the ends of the slabs.	failure.	under fire in

Table 2.1. (cont'd)

under fire conditions along with the charcteristics of the thermal field and residual strength after the fire exposure.	 One slab in each test was loaded whereas other one was unloaded to evaluate the residual strength after exposing to fire. Four point loading scheme was used. Vertical load used was of magnitude that caused 60% of the service bending moment in the mid span. Test was conducted under ISO 834 fire. Thermal boundary conditions varied between tests. In the first test the holes were left open whereas in the second test the holes were plugged using mineral wool to prevent air circulation. After the first test, the slabs for the second test were stored near the furnace area under extreme dry conditions. 	 In the second test no cover spalling or brittle failure occurred. The failure time was 90 min. and was close to the theoretical value. Moisture content of concrete affects the spalling. No effect of insulating material used to plug the holes at the end on the slab temperature. It was concluded that the horizontal cores exhibit low exchange of heat between slab and atmosphere due to convection. The unloaded slabs in both the tests showed same residual mechanical strength. The duration of the heat had insignificant effect on the residual strength. Both unloaded slabs during heating showed around 50% strength reduction after cooling when compared to the theoretical value. 	hollowcore slabs. The information can be utilized for developing and validating numerical model of fire tests on hollowcore slabs. Drawbacks The spalling phenomena is not studied in details, as from the experiment it is apparent that it has significant effect on the load bearing capacity. Only one concrete type is studied

Table 2.1. (cont'd)

Broo H. et al. (2007)	The study presents the	• Two typical thickness of	• The cracks in the cover	• This study
D100 11. Ct al. (2007)	results of the	hollowcore slabs were used	concrete below the strands	provides
	experiments	one with 200 mm and other		valuable data
	1 *		at the supports were	
	performed on seven	with 400 mm thickness. Total	observed in the 400 mm	on
	hollowcore slabs	of four 200 mm and five 400	slabs leading to anchorage	understandin
	under ambient	mm slabs were tested with	failure. However, no such	g of shear
	conditions.	various loading patterns	cracks were seen in 200 mm	and torsional
	• To study the effects	causing various shear and	slabs.	performance
	of parameters like	torsion combinations. 200 mm	• In 200 mm slabs the cracks	of
	loading patterns	slabs had seven and 400 mm	were observed in the webs	hollowcore
	and support	lab had eleven12.5 mm dia.	in the form of shear tension	slab
	conditions that	strands.	cracks which progressed	Drawbacks:
	influence the shear	• The slabs were 7 m in length	from outer to inner webs.	• This study is
	and torsional	and 1.2 m in width for all	Longitudinal cracks were	only based
	response of the	cases.	also observed in case of	on ambient
	slab.	• The support conditions were	mortar supports.	condition and
		varied between bearing strip of	• All 400 mm slabs showed	is valid at
		neoprene and mortar bearing	longitudinal cracks above	elevated
		with grout ends. Only one	one of the outer most void.	temperatures.
		mortar bearing case was tested	The shear cracks followed	• The higher
		=		_
		for each type of slab.	that same pattern as the 200	strength
			mm slabs.	achieved
			• In both the slabs, the end	with mortar
			condition with mortar bed	supports is
			and grouted ends achieved	not explained
			higher capacities.	in the case of
			Study concluded that the	200 mm
			capacity of the slab is	slabs.
			significantly affected by the	
			support conditions.	

Table 2.1. (cont'd)

Bailey C. G. and Lennon T. (2008)	The study presents the results of two full scale fire tests on hollowcore floor system supported on protected steel work. • To identify the effectiveness and significance of lateral structural and thermal on the fire response of hollowcore slab.	 The tests setup was housed on a fire compartment of 7.02m x 17.76m, with an internal floor to soffit height of 3.6m. Total of 15 hollowcore slabs were tested. Each slab was 1200 mm in width and 200 mm in thickness. Joints between the units were infilled with grout. Two tests were identical except for the different restraint conditions. The second test consisted T12-U bars at each unit end cores, 19 mm shear stud was fixed to the steel beam and gaps were ingrouted. 	 The tests results showed that the steel supports did not provide lateral restraint thus did not help in increasing fire resistance. Lateral compression strips were formed at the end due to some sort of restraints to expansion. The study concluded that the formation of lateral strip can enhance fire resistance by improving flexural and shear capacity of units. The study also identifies that the small-scale standard fire tests can be very unrealistic to predict fire resistance time as it ignores 	 This study identifies the effectiveness of lateral supports and its significance in enhancing fire resistance. Drawbacks This study does not take in account various parameter affecting the fire resistance of
Peltonen S. and	The study presents the	The hollowcore slabs	the whole building behavior. • None of the specimen failed	• The study
Plum C. M. (2009)	results of four fire tests on hollowcore slabs supported on Peikko Deltabeams without insulation. • To evaluate the ability of these Deltabeams to support the	measured 2350 mm in width and the overall test panel with Deltabeam measured a width of 3915 mm. The length varied between 7.2 m and 9.6 m between tests. • The load was applied at a distance of 715 mm from the end of the hollowcore slabs.	during the entire tests. The maximum fire induced deflection for 60 min. test was 82 mm for the slab and 75 mm for the Deltabeam and for 120 min. test were 145 mm and 110 mm respectively.	provides good tests results of behavior of hollowcore slabs under fire when combined with other

Table 2.1. (cont'd)

	hollowcore slabs under fire conditions.	Four tests varied in fire duration, cooling phase duration and the loading. (I) 60 min. with 120 min. cooling with 48 KN/m load (II) 60 min. with 120 min. cooling with 57.6 KN/m load (III) 120 min. with 247 min. cooling with 48 KN/m load and (IV) 180 min. with no. cooling phase with 30 KN/m load	The study concluded that the Deltabeam was able to carry the load from the hollowcore slab through the compression of the slab to the inclined web of the Deltabeam but not through the support on the bottom flange of the Deltabeam. Temperature profiles were generated at various depths of hollowcore slabs.	structures, Deltabeam in this case. Drawbacks: The study in focused on the proprietary Deltabeams and doesnot provide detailed performance of the hollowcore slabs.
Zheng W. Z. et al. (2010)	The study presents the fire tests results on 15 PC simply supported slabs and 9 two-span unbonded prestressed continuous slabs. • To study the spalling phenomena on prestressed concrete. • To propose expressions for top envelope curve and surface of concrete	 The thickness for 15 PC simply supported slabs varied between 80, 90 and 95 mm and the width and length were 600 and 3300 mm for all 15 slabs. Fire exposed length was 3050 mm. The thickness for 9 PC unbounded continuous slabs varied between 70, 80 and 85 mm and the width and length were 600 and 2550X2 mm for all 9 slabs. Fire exposed length varied between 2350 and 2120 mm. 	 The spalling was observed in the concrete temperature range of 200-500 °C The study concludes that the nominal tensile stress of concrete and concrete strength have significant influence on the extent of spalling in concrete but effect of water content on the spalling is minimal. Also the spalling occurs more easily when the compressive stress in higher or the tensile stress is lower 	 The experimental study provides a good understandin g of spalling behavior of prestressed concrete in prestressed slabs. Drawbacks: Only one type of

Table 2.1. (cont'd)

	spalling.	The fire curve was given by ISO834 fire.	on the surface exposed to fire and the concrete strength and water content are higher at ambient condition. • Expressions are proposed for the top envelope curve and surface of concrete spalling.	aggregate (Calcareous) is considered. • The specimens are relatively small and might not represent the spalling behavior in a full scale slab.
Aguado J. V. el al. (2012)	The study presents the results of four full scale fire tests on PC hollowcore slabs under flexure. • To study the influence of the reinforcement arrangement and strands axis distance in the fire resistance of hollowcore slabs.	 All four slabs were of 5.7 m long, 1.2 m wide and 250 mm thick and comprised of nine hollowcores. Four different reinforcement arrangements/patterns and average axis distance ranging from 30.1 to 46.7 mm were studied. 5 mm steel wires and 3/8" diameter prestressing strands were used. The slabs were loaded with four point loading scheme. The slabs were subjected to ISO 834 standard fire. 	 The fire resistance of the hollowcore slabs ranged from 84 to 105 min. Four types of cracking were observed during the bending test namely thermal, flexural, splitting and longitudinal cracking. The structural response of hollowcore slab is divided into three stages Initial deflection driven by thermal cracking and final driven by loss of strength of steel. Highest fire resistance was observed at lowest moisture content, lowest tensile strength and highest 	 This study provides valuable information on variations in fire response with different reinforcemen t patterns. Drawbacks: The experiment is limited to only one type of concrete and aggregate

Table 2.1. (cont'd)

	compressive strength of concrete among the four hollowcore slabs. • Non-prestressed wires showed optimal performance without failure. • The third stage of the deflection of hollowcore slab under fire is significantly governed by the reinforcement arrangement.	type only. • Spalling is not discussed. • The effect of strand axis distance is not conclusive.
--	---	---

Table 2.2. Numerical/Analytical studies on fire resistance of prestressed concrete hollowcore slabs

Study	Objective / Study Details	Analysis/Model Features	Observations / Conclusions	Strengths/Drawbacks
Dotreppe J. and Franssen J. (2004)	The study analyses the results of the numerical analysis performed on the PC hollowcore slabs. • To develop a numerical model based on the test results.	Analysis Technique: Finite Element Method using FE code SAFIR. • 2D- thermal analysis was performed on the cross section assuming uniform distribution along longitudinal direction. The subdivision of cross- sections in mesh was used and heat transmission by conduction in concrete and radiation in the cores was considered. Features: • Standard fire was given by ISO 834 fire Constitutive model: • Adopted from Eurocode. Validation against: • The numerical simulation was used to prepare the experimental fire tests which also validated the numerical model itself.	 The study concluded that cavities in the slab affect the temperature distribution. The fire resistance measured based on bending increases with restraint level. Thermal stresses are higher during first 30 min of fire. Longitudinal restraints are favorable to the fire. 	 This study studies important parameter affecting the fire response of hollowcore slabs. Drawbacks: Spalling was not considered. Some other important parameters like concrete strength, aggregate type are not studied.

Table 2.2. (cont'd)

Fellinger J. H. H. (2004)	 To develop finite element model for shear and anchorage behavior of hollowcore slabs exposed to fire. To validate and calibrate the numerical model based on the fire tests performed by Fellinger J. H. H. (2004). 	 Analysis Technique: Finite Element Method using FE package DIANA. Features: Standard fire was given by ISO 834 fire. Splitting cracks, verticals cracks and slip development were included in the FE model. Constitutive model: Adopted from Eurocode Validation against: Fire tests performed by Fellinger J. H. H. (2004). Calibration against: 60 new small tests performed by Fellinger J. H. H. (2004) up to 600°C. 	 The results from the numerical analysis showed that the fire resistance of the slab is mainly affected by thermal expansion, restrained against thermal expansion and ductility of concrete in tension. This study identifies the shortcoming of Eurocode 2 in incorporating shear and anchorage failure. The fire resistance of the slab is significantly influenced by the aggregate type which governs the fracture energy and thermal expansion of the concrete. 	 This study is successful in identifying the critical failure mechanisms and modes in the hollowcore slabs. Various new parameters are taken into account. Drawbacks The model is only limited to standard fire.
Breccolotti et al. (2006)	To develop a numerical model to predict the temperature field in the cross section of the hollowcore	Analysis Technique: Finite Element Method using FE code FIRES T3. • 2D- thermal analysis was performed on the cross section assuming uniform distribution along longitudinal direction.	• The numerical model is proposed to be reliable when realistic thermal and mechanical properties are incorporated and spalling of the concrete is ignored.	 This model can be reliably used to predict the load bearing capacity of the hollowcore slab exposed to fire conditions as it is well validated against the test data. Drawbacks. This model is incapable of

Table 2.2. (cont'd)

	slabs and evaluate the load bearing capacity of the slabs under fire conditions. To validate the numerical model against fire test.	 Temperature inside the cores assumed to be constant. Parametric analysis was performed for different constant core temperatures (100, 200, 300, 400°C). Features: Standard fire was given by ISO 834 fire Thermal Properties: Adopted from experiments performed by Felicetti and Gambarova (2002, 2003). Constitutive model: Adopted from Eurocode and experiments. Validation against: Fire tests performed by Breccolotti et al. (2006). 		handling spalling.
Engstrom et al. (2007)	• To establish a three dimensional finite element numerical models of the hollowcore to analyze the	Analysis Technique: Finite Element Method using FE package DIANA 8.1. Features: • Analysis was done for ambient conditions. • The interation between	 Good agreement was observed between the test results and numerical model for various combinations of shear and torsion. All of the analysis showed same failure modes of shear tension failure. 	 The numerical model proposed can be very viable in terms of simplicity and time required to do the analysis. Detailed fracture criteria for concrete and yield criteria for steel are considered which makes the model able to

Table 2.2. (cont'd)

effects of	strands and concrete was	• Combination of coarse solid	capture the realistic
parameters that influence the	done by a bond-slip relation.	element for critical parts and	response. Drawbacks:
		beam element for the rest	
shear and	Relatively coarse mesh	showed quite reasonable	• This model is only good for
torsion	was used.	reliability.	ambient condition and
response of the			might not be applicable for
hollowcore slabs.	bearing strips were		elevated temperatures.
	modeled using eight node		• Even though the mesh is
• To validate the			verified, the accuracy of
model with the			model could be increased
experiments.	Constitutive model:		by further refining the
	Concrete		mesh.
	• Adopted from linear		
	fracture mechanics for		
	concrete. A rotating crack		
	model based on total		
	strain was used for		
	concrete. The harding		
	was defined by		
	Thorenfeldt exopression		
	in compression and		
	Horjdijk, TNO in tension.		
	Material data for concrete		
	was based on		
	experiments conducted at		
	VTT. Steel		
	• Von-Mises yield criteria		
	was used for steel with an		
	associative flow law and		
	isotropic hardening.		

Table 2.2. (cont'd)

		 Material data was used from the experiments carried at VTT. Neoprene 10 mm thick neoprene was used. The stiffness was calculated from experiments at VTT. Poissons ratio was assumed to be 0.49 and young's modulus as 15 MPa. Validation against: Fire tests performed by Broo H. et al. (2007 Mesh: Mesh verification was done. 		
Chang J. et al. (2008)	 To propose a simple method for modeling structural behavior of hollowcore concrete floor slabs under fire conditions. To validate model against 	Analysis Technique: Finite Element Method using FE code SAFIR. • Grillage system was incorporated in the finite element model using beam elements. • The topping concrete layer was modeled using shell elements. Features:	• The study concludes that the fire performance of the slab is significantly influenced by different arrangements of axial and rotational restraints at supports.	 The study provides a simple finite element method using beam and shell elements. Drawbacks: Shear, anchorage and bond failures cannot be predicted by the proposed model. The model considers no spalling occurs.

Table 2.2. (cont'd)

	experimental data and do a parametric study with different arrangements of axial and rotational restraints at supports.	 Standard fire was given by ISO 834 fire Constitutive model: Adopted from Eurocode. Validation against: Fire tests performed by Acker A.V. (2003) Jensen J. P. (2005). 		
et al. (2010)	 To developed a numerical model for evaluating the fire resistance of PC hollowcore floors using multi-spring elements. To validate against test data. 	 Analysis Technique: Finite Element Method using FE code SAFIR. Multi-springs elements were used to account for the effects of starter bars between the reinforcement toping slab and the supporting beams. Perfect bond between concrete and steel was assumed Spalling was ignored. The model was based on Bernoulli hypothesis and cannot detect shear failure. Features: Standard fire was given by ISO 834 fire 	• It was concluded that that increasing the number of starter bars enhances the tensile capacity at the support and hence increases the fire resistance of the hollowcore slabs.	 The proposed model replaces the previous model with beam element and shell elements proposed by Chang J. et al. (2008) which assumes the tendons are anchored to the supporting beams in the prestressed flooring system where steel tendons terminate at the ends. Drawbacks: Shear and bond failures cannot be predicted by the proposed model. The model considers no spalling occurs.

Table 2.2. (cont'd)

Constitutive model: • Adopted from Eurocode. Validation against:	
• Fire tests performed by Acker A.V. (2003) and Dotreppe J. and Franssen J. (2004) conducted at University of Liege, Belgium.	

Table 2.3. Provisions in building standards of various countries

Standard	Provisions	Strengths/Drawbacks
PCI 2010, USA	 The fire resistance provisions have been given based on the concrete cover thickness for prestressed concrete floor or roof slabs (PCI 2010 Table 10.8.2). The provision also distinguishes between restrained and unrestrained end condition and among different aggregate type namely siliceous, carbonate and sandlightweight or lightweight aggregate. The fire resistance provisions have also been specified based on the slab thickness faced with 5/8 in. of Type-X gypsum wallboard for two cases of air space (with no air space and with 6 in. air space) and three types of aggregates (PCI 2010 Table 10.5.1). For a hollowcore slab, this thickness may be obtained by dividing the net cross-sectional area by its width. PCI 2010 provides a rational design method for prestressed beam but not for prestressed slabs. 	 The provisions are strictly prescriptive in nature. The fire resistance ratings are based on the concrete cover of the PC slabs and does not account for the factor affecting the fire resistance. Assumes concrete density, moisture condition, air content, and maximum aggregate size as less important factors that influence heat transmission.
ACI 216, USA	 The fire resistance provisions have been given based on the equivalent slab thickness for plain and reinforced including PC bearing or non-bearing walls and floor and roof slabs (ACI 216 Table 2.1). The equivalent thickness of the precast hollowcore slabs is evaluated by dividing the net cross sectional are by the width of the slab. For hollowcore slab filled with grout or loose insulating materials the effective thickness is taken to be same as the slab thickness. The fire resistance has also been specified based on the concrete cover thickness over the reinforcement (ACI 216 Table 2.3). The table provides different fire resistance ratings for both non-prestressed and 	 The provisions are strictly prescriptive in nature. The fire resistance ratings are based on the concrete cover and the slab thickness and does not account for the factor affecting the fire resistance.

Table 2.3. (cont'd)

	 prestressed floor and roof slabs. It also differentiated bet two end conditions (restrained and unrestrained). Both fire provisions in both the table provide different values for different concrete type namely siliceous, carbonate, semi-lightweight and lightweight. 	
Eurocode 2, Europe	 Part 1–2: Structural fire design, provides three ways of determining fire resistance of PC slabs as tables, simplified or advanced methods for determining fire resistance of slabs The table provides the fire resistance based on the minimum thickness of the slab excluding the floor finishes and axis distance of the reinforcement. Total of four types of slabs are identified simply supported solid slabs (EC2-1 Table 5.8), continuous solid slabs (EC2-1 Table 5.8), flat slabs (EC2-1 Table 5.9) and ribbed slabs (EC2-1 Table 5.10 and 5.11). The simplified method specified by Eurocode (EC2-1 section 4) uses strength reduction factors and applies where the loading is predominantly uniformly distributed and ambient condition design has been based on linear analysis or linear analysis with limited redistribution. New equations for calculating the shear and anchorage capacity of hollowcore slabs under fire were introduced in Eurocode 2-Annex G. 	 The tabular methods prescriptive. The advanced method provisions can be used in performance-based design.

Table 2.3. (cont'd)

AS 3600, Australia	 The fire ratings are provided in tabular form based on the effective thickness of the slab. For simple prestressed slabs, the provisions have also been provided to determine fire resistance based on concrete cover to the bottom tendons and end supports as simply supported and continuous slab. For ribbed slabs, the provisions are based on end conditions (simply supported and continuous), minimum width of the rib and cover thickness. 	 The method is prescriptive. No spalling is considered in the calculations. Aggregate types are not considered in the equation.
NZS 3101, New Zealand	 The fire ratings are provided in tabular form based on the effective thickness of the slab. The fire ratings are based on the minimum concrete cover. 	The method is strictly prescriptive.Various important parameters are not considered.
National Building code, Canada	 Simple empirical formulas are provided to compute the minimum slab thickness based on the required fire resistance rating in hours. Similarly the minimum cover thickness required for given fire resistance rating is also provided. 	 The provisions are prescriptive in nature. The fire resistance is only based on concrete cover thickness, aggregate type and the dimension of the slab and ignores a number of other factors influencing fire resistance.

Table 2.4. Prediction of fire resistance values for a typical hollowcore slab using different codes

Slab depth –	Measured	PCI,	ACI216.1,	Eurocode 2,	AS 3600,	NZS 3101,	NBC,
200 mm	in tests	United States	United States	Europe	Australia	New Zealand	Canada
Fire resistance, minutes	>120	90	90	90	90	90	90

Table 2.5. Relationships for high temperature thermal properties of concrete (Eurocode 2)

		Normal strength and high strength concrete
Thermal Conductivity (W/m K)	All types	$Upper\ limit: \\ k_c = 2 - 0.2451\ (T/100) + 0.0107\ (T/100)2 \\ for\ 20^{\circ}C \leq T \leq 1200^{\circ}C \\ Lower\ limit: \\ k_c = 1.36 - 0.136\ (T/100) + 0.0057\ (T/100)2 \\ for\ 20^{\circ}C \leq T \leq 1200^{\circ}C$

	Specific heat (J/kg°C)							
Specific heat (J/kg°C)	$c = 900,$ for $20^{\circ}C \le T \le 100^{\circ}C$							
	$c = 900 + (T - 100),$ for $100^{\circ}C < T \le 200^{\circ}C$							
	$c = 1000 + (T - 200)/2$, for $200^{\circ}C < T \le 400^{\circ}C$							
	$c = 1100,$ for $400^{\circ}C \le T \le 1200^{\circ}C$							
	Density change (kg/m ³)							
	$\rho = \rho(20^{\circ}C) = Reference\ density$							
ıea	for $20^{\circ}C \le T \le 115^{\circ}C$							
ic I	$\rho = \rho(20^{\circ}C) (1 - 0.02(T - 115)/85)$							
cif	for $115^{\circ}C < T \le 200^{\circ}C$							
Spe	$\rho = \rho(20^{\circ}C) (0.98 - 0.03(T - 200)/200)$							
3 1	for $200^{\circ}C < T \le 400^{\circ}C$							
	$\rho = \rho(20^{\circ}C) (0.95 - 0.07(T - 400)/800)$							
	$for 400$ ° $C < T \le 1200$ ° C							
	Thermal Capacity = $\rho \times c$							

Strain	Siliceous aggregate	$ \varepsilon_{th} = -1.8 \times 10^{-4} + 9 \times 10^{-6} T + 2.3 \times 10^{-11} T^{3} $ $ for 20^{\circ}C \leq T \leq 700^{\circ}C $ $ \varepsilon_{th} = 14 \times 10^{-3} $ $ for 700^{\circ}C < T \leq 1200^{\circ}C $
Thermal Strain	Carbonate aggregate	$ \varepsilon_{th} = -1.2 \times 10^{-4} + 6 \times 10^{-6} T + 1.4 \times 10^{-11} T^{3} $ $ for 20^{\circ}C \leq T \leq 805^{\circ}C $ $ \varepsilon_{th} = 12 \times 10^{-3} $ $ for 805^{\circ}C < T \leq 1200^{\circ}C $

Table 2.6. Constitutive relationship for high temperature properties of concrete (Eurocode 2)

	Normal strength and high strength concrete
Stress-strain relationships	$\sigma_c = \frac{3\varepsilon \ f_{c,T}^{'}}{\varepsilon_{c1,T} \left(2 + \left(\frac{\varepsilon}{\varepsilon_{c1,T}}\right)^3\right)} \ , \varepsilon \leq \varepsilon_{cu1,T}$ For $\varepsilon_{c1(T)} < \varepsilon \leq \varepsilon_{cu1(T)}$, the Eurocode permits the use of linear as well as nonlinear
ress	descending branch in the numerical analysis.
Sti	For the parameters in this equation refer to Table 2.7

Table 2.7. Values for the main parameters of the stress-strain relationships of NSC and HSC at elevated temperatures (Eurocode 2)

Toma	Temp.	NSC						HSC		
Temp.		Siliceous Agg.			Calcareous Agg.			$f_{c,T}^{'}/f_{c}^{'}(20^{\circ}C)$		
		$\frac{f_{c,T}^{'}}{f_c^{'}(20^{\circ}C)}$	$arepsilon_{cl,T}$	$\mathcal{E}_{cu1,T}$	$\frac{f_{c,T}^{'}}{f_c^{'}(20^{\circ}C)}$	$\mathcal{E}_{cl,T}$	$\varepsilon_{cu1,T}$	Class1	Class2	Class3
68	20	1	0.0025	0.02	1	0.0025	0.02	1	1	1
212	100	1	0.004	0.0225	1	0.004	0.023	0.9	0.75	0.75
392	200	0.95	0.0055	0.025	0.97	0.0055	0.025	0.9	0.75	0.70
572	300	0.85	0.007	0.0275	0.91	0.007	0.028	0.85	0.75	0.65
752	400	0.75	0.01	0.03	0.85	0.01	0.03	0.75	0.75	0.45
932	500	0.6	0.015	0.0325	0.74	0.015	0.033	0.60	0.60	0.30
1112	600	0.45	0.025	0.035	0.6	0.025	0.035	0.45	0.45	0.25
1292	700	0.3	0.025	0.0375	0.43	0.025	0.038	0.30	0.30	0.20
1472	800	0.15	0.025	0.04	0.27	0.025	0.04	0.15	0.15	0.15
1652	900	0.08	0.025	0.0425	0.15	0.025	0.043	0.08	0.113	0.08
1832	1000	0.04	0.025	0.045	0.06	0.025	0.045	0.04	0.075	0.04
2012	1100	0.01	0.025	0.0475	0.02	0.025	0.048	0.01	0.038	0.01
2192	1200	0	-	_	0	-	-	0	0	0

Table 2.8. High temperature thermal properties of prestressing steel (Eurocode 3)

Thermal conductivity (W/m K)	$k_{s} = \begin{cases} 54 - 3.33 \times 10^{-2} T & 20^{\circ} C \le T < 800^{\circ} C \\ 27.3 & 800^{\circ} C \le T \le 1200^{\circ} C \end{cases}$
Specific heat (J/kg K)	$c_{s} = \begin{cases} 425 + 7.73 \times 10^{-1} T - 1.69 \times 10^{-3} T^{2} + 2.22 \times 10^{-6} T^{3} & 20^{\circ} C \leq T < 600^{\circ} C \\ 666 + \frac{13002}{738 - T} & 600^{\circ} C \leq T < 735^{\circ} C \\ 545 + \frac{17820}{T - 731} & 735^{\circ} C \leq T < 900^{\circ} C \\ 650 & 900^{\circ} C \leq T \leq 1200^{\circ} C \end{cases}$
Thermal strain (valid for structural steel only)	$\varepsilon_{ths} = \begin{cases} 1.2 \times 10^{-5} T + 0.4 \times 10^{-8} T^2 - 2.416 \times 10^{-4} & 20^{o} C \le T \le 750^{o} C \\ 1.1 \times 10^{-2} & 750^{o} C < T \le 860^{o} C \\ 2 \times 10^{-5} T - 6.2 \times 10^{-3} & 860^{o} C < T \le 1200^{o} C \end{cases}$

Table 2.9. Constitutive relationships for high temperature properties of prestressing steel (Eurocode 2)
$$\sigma_s = \begin{cases} \varepsilon_p E_{p,T} & \varepsilon_p \leq \varepsilon_{pp,T} \\ f_{pp,T} - c + (b/a) \left(a^2 - \left(\varepsilon_{py,T} - \varepsilon_p \right)^2 \right)^{0.5} & \varepsilon_{pp,T} < \varepsilon_p \leq \varepsilon_{py,T} \\ f_{py,T} & \varepsilon_{py,T} < \varepsilon_p \leq \varepsilon_{py,T} \\ f_{py,T} & \varepsilon_{px,T} < \varepsilon_p \leq \varepsilon_{px,T} \\ f_{py,T} & \varepsilon_{px,T} - \varepsilon_{px,T} \\ 0.0 & \varepsilon_p > \varepsilon_{px,T} \end{cases}$$
Parameters
$$\varepsilon_{pp,T} = \frac{f_{pp,T}}{E_{p,T}} \quad \varepsilon_{py,T} = 0.02 \quad \varepsilon_{px,T} = 0.15 \quad \varepsilon_{px,T} = 0.2$$
Functions
$$a^2 = \left(\varepsilon_{py,T} - \varepsilon_{pp,T} \right) \left(\varepsilon_{py,T} - \varepsilon_{pp,T} + \frac{c}{E_{p,T}} \right)$$

$$b^2 = c \left(\varepsilon_{py,T} - \varepsilon_{pp,T} \right) E_{p,T} + c^2$$

$$c = \frac{\left(f_{py,T} - f_{pp,T} \right)^2}{\left(\varepsilon_{py,T} - \varepsilon_{pp,T} \right) E_{p,T} - \left(f_{py,T} - f_{pp,T} \right)}$$
Values of $f_{pp,T}$, $f_{py,T}$, $f_{py,T}$, $f_{p,T}$, $f_{p,T}$, and $f_{px,T}$ can be obtained from Table 2.10

Table 2.10. Values for the main parameters of the stress-strain relationships of prestressing steel at elevated temperatures (Eurocode 2)

Steel temp.	teel temp. $\frac{F_{py,T}}{\beta f_{yp}}$			$\frac{F_{pp,T}}{\beta f_{yp}}$		$\frac{E_{p,T}}{E_p}$		$arepsilon_{pt,T}[-]$	$arepsilon_{pu,T}[-]$
T°C	Class A	w Class B	q and t	cw	q and t	cw	q and t	cw,	cw,
1	2a	2b	3	4	5	6	7	8	9
20	1	1	1	1	1	1	1	0.05	0.1
100	1	0.99	0.98	0.68	0.77	0.98	0.76	0.05	0.1
200	0.87	0.87	0.92	0.51	0.62	0.95	0.61	0.05	0.1
300	0.7	0.72	0.86	0.32	0.58	0.88	0.52	0.055	0.105
400	0.5	0.46	0.69	0.13	0.52	0.81	0.41	0.06	0.11
500	0.3	0.22	0.26	0.07	0.14	0.54	0.2	0.065	0.115
600	0.14	0.1	0.21	0.05	0.11	0.41	0.15	0.07	0.12
700	0.06	0.08	0.15	0.03	0.09	0.1	0.1	0.075	0.125
800	0.04	0.05	0.09	0.02	0.06	0.07	0.06	0.08	0.13
900	0.02	0.03	0.04	0.01	0.03	0.03	0.03	0.085	0.135
1000	0	0	0	0	0	0	0	0.09	0.14
1100	0	0	0	0	0	0	0	0.095	0.145
1200	0	0	0	0	0	0	0	0.1	0.15

Note: For intermediate values of temperature, linear interpolation may be used.

Where,

cw = cold worked, q and t = quenched and tempered

$$\beta = \begin{cases} \left(\frac{\varepsilon_{ud} - f_{po,1T} / E_{p}}{\varepsilon_{uT} - \varepsilon_{po,1T} / E_{p}}\right) \times \left(\frac{f_{pT} - f_{po,1T}}{f_{pT}}\right) + \frac{f_{po,1T}}{f_{pT}} & ClassA \\ 0.9 & ClassB \end{cases}$$

 \mathcal{E}_{ud} , \mathcal{E}_{uT} , $f_{po,1T}$, f_{pT} and E_p are material properties at room temperature as per EN1992-1-1

Table 2.11. Constitutive relationships for high temperature properties of prestressing steel (Eurocode 2)

(Edifocode 2)							
Thermal Strain	$\varepsilon_{ths} = \left\{ 1.0 \times 10^{-5} T + 0.4 \times 10^{-8} T^2 - 2.016 \times 10^{-4} 20^{\circ} C \le T < 1200^{\circ} C \right\}$						

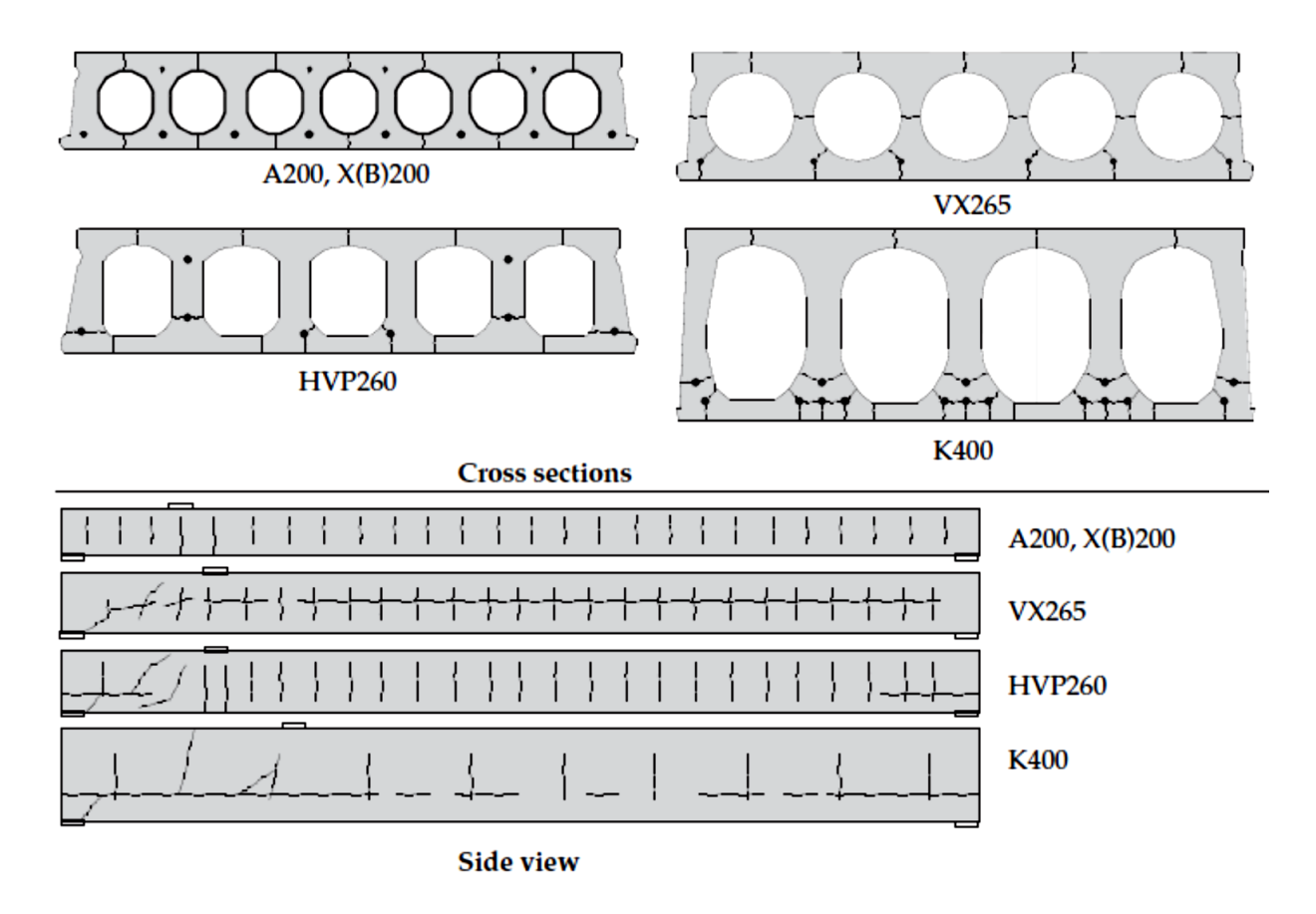


Figure 2.1. Crack patterns in hollowcore slabs under fire conditions (Fellinger 2005)

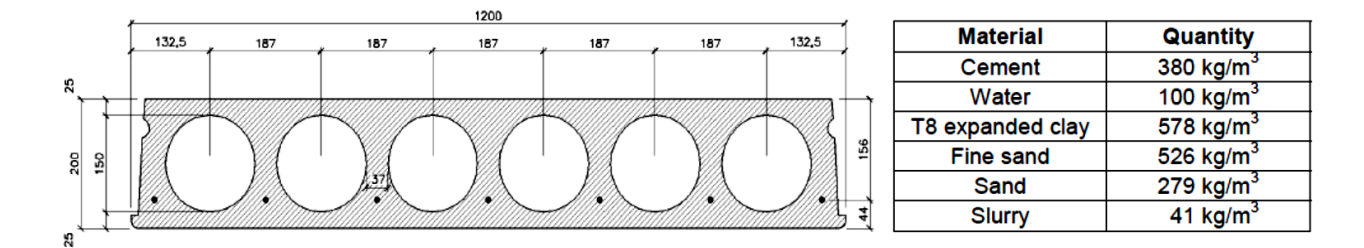


Figure 2.2. Cross-sectional configuration of tested hollowcore slab (Breccolotti et al. 2006)

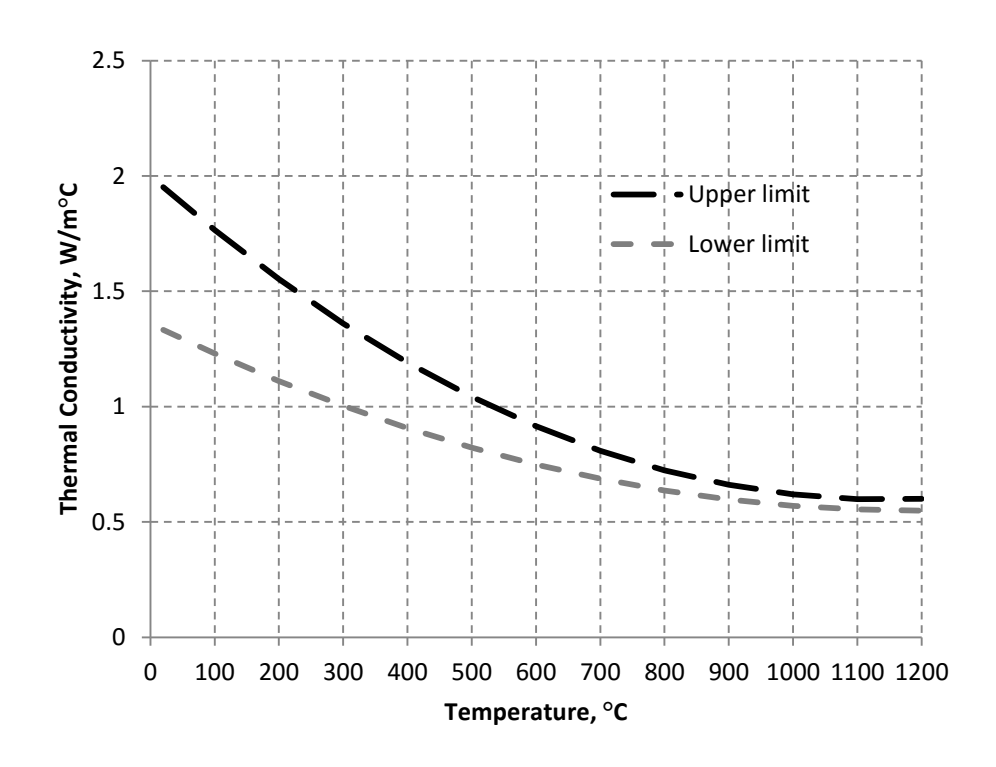


Figure 2.3. Variation of thermal conductivity of concrete with temperature based on Eurocode 2

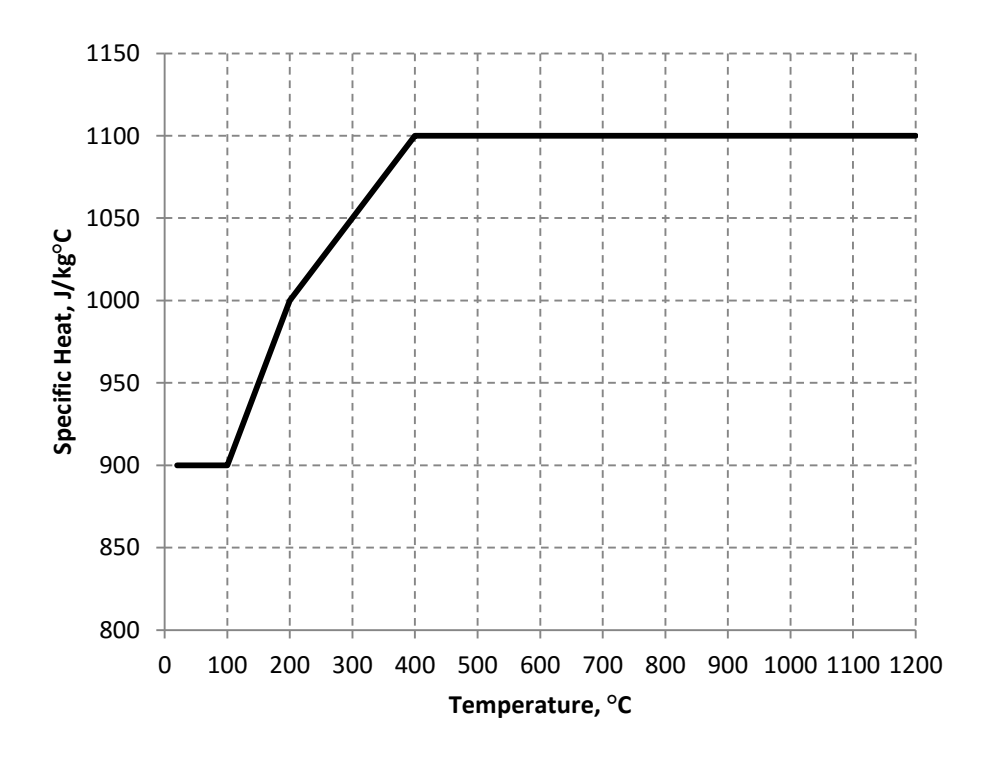


Figure 2.4. Variation of specific heat of concrete with temperature based on Eurocode 2

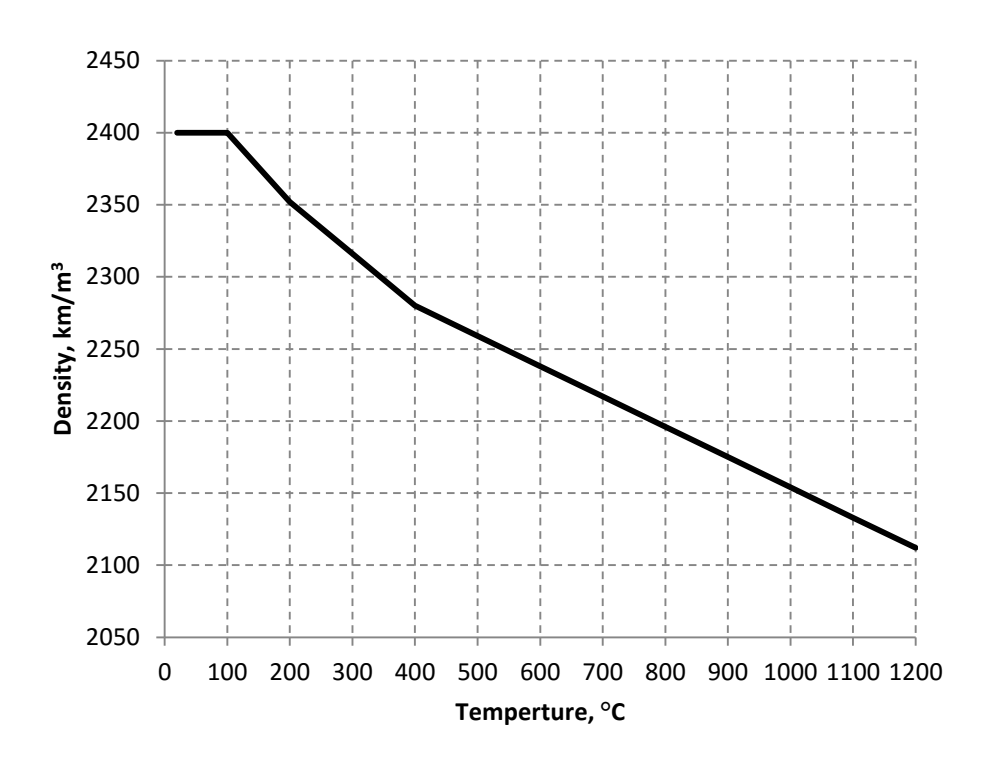


Figure 2.5. Variation of density of concrete with temperature based on Eurocode 2

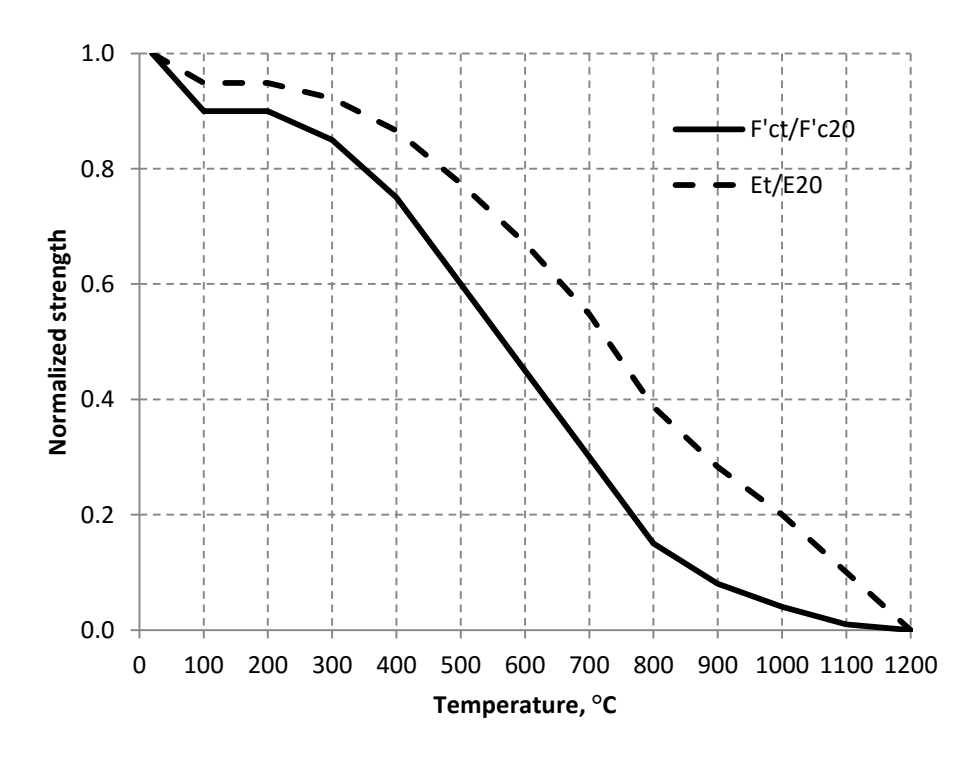


Figure 2.6. Variation of compressive strength and elastic modulus of concrete with temperature based on Eurocode 2

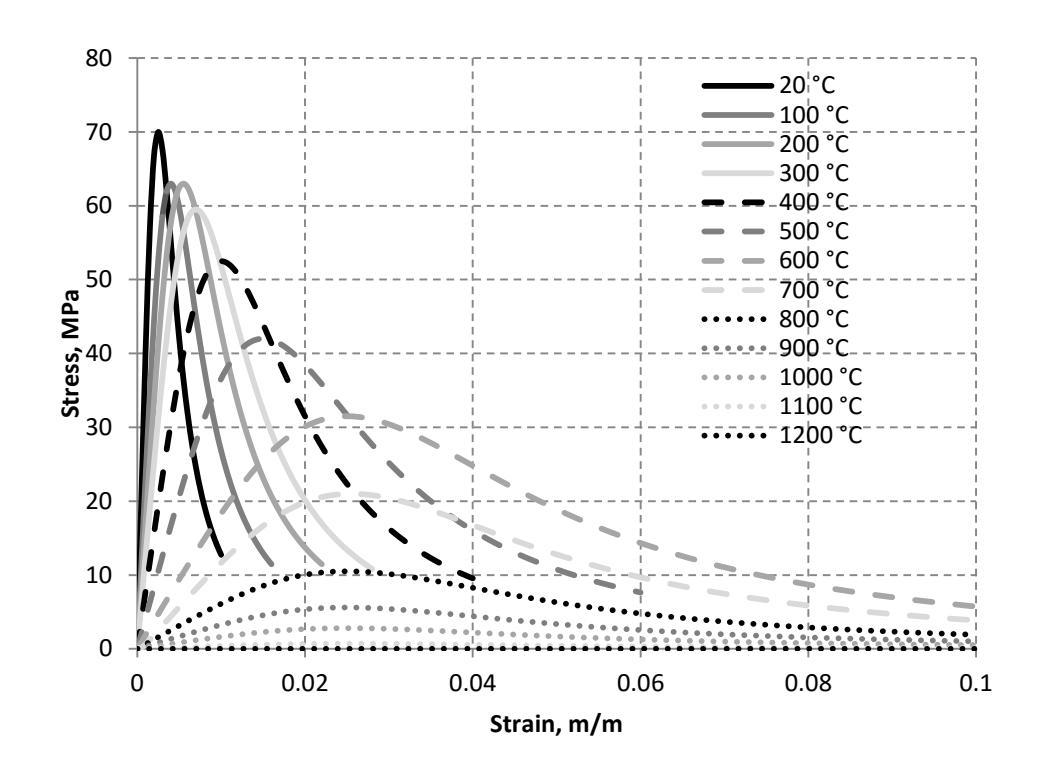


Figure 2.7. Stress-strain relationship of concrete in compression at various temperature based on Eurocode 2

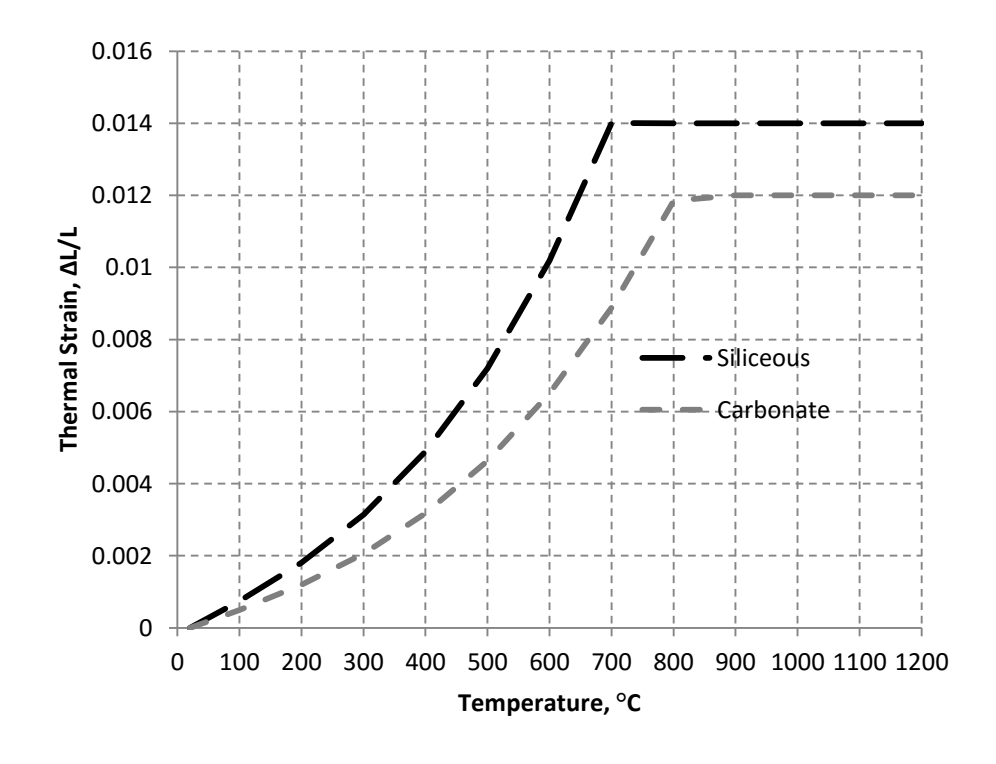


Figure 2.8. Variation of thermal strain of concrete with temperature based on Eurocode 2

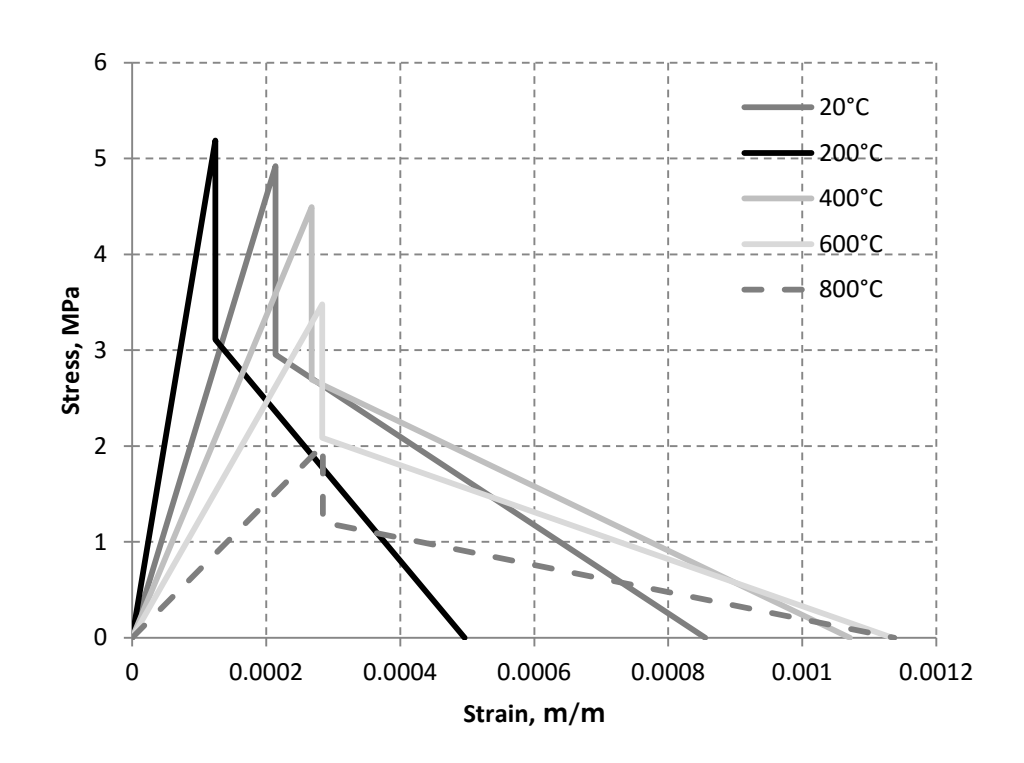


Figure 2.9. Stress-strain relationship of concrete in tension at various temperature based on Eurocode 2

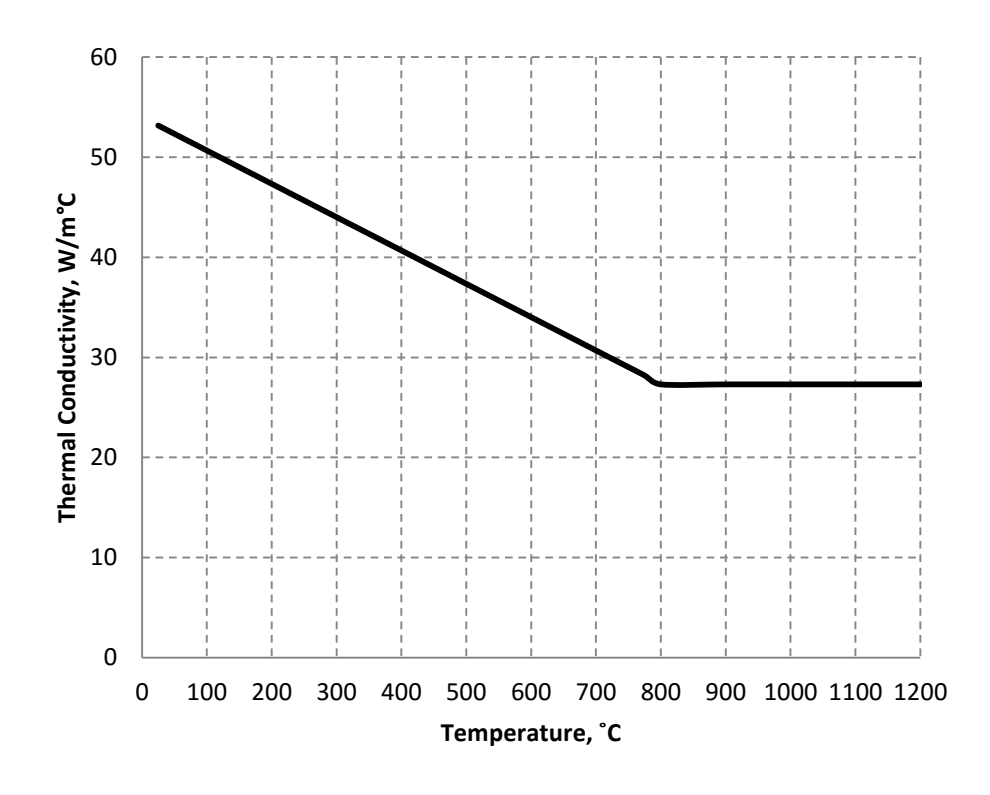


Figure 2.10. Variation of thermal conductivity of steel with temperature based on Eurocode 3

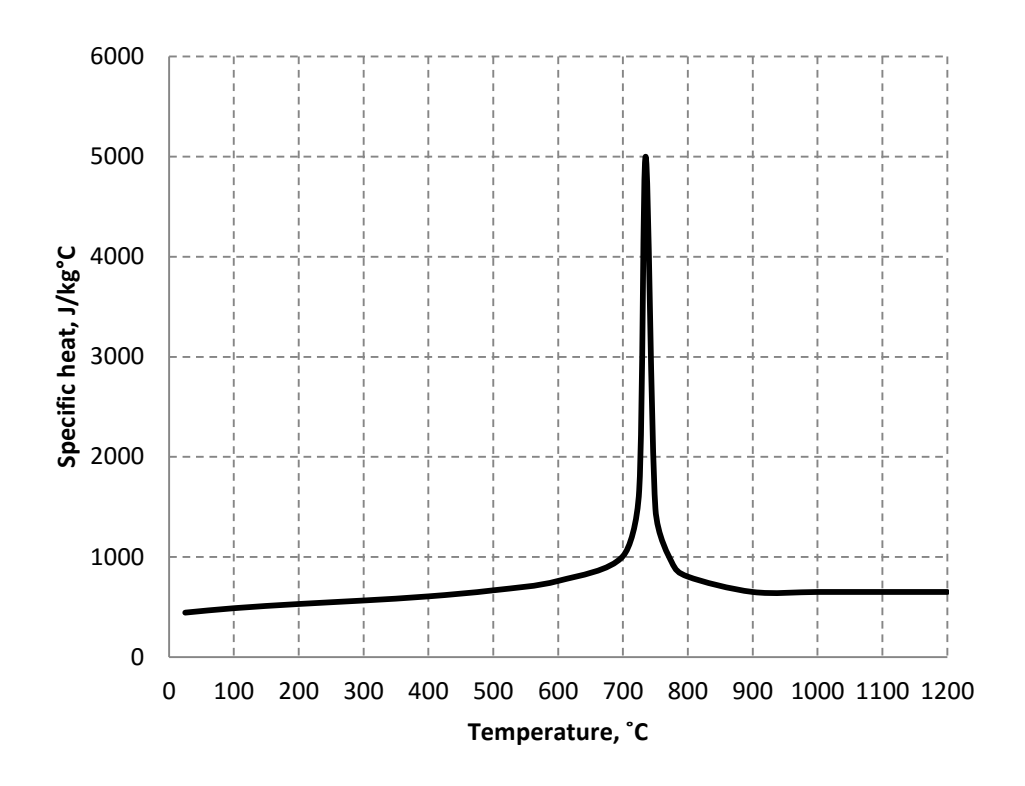


Figure 2.11. Variation of specific heat of steel with temperature based on Eurocode 3

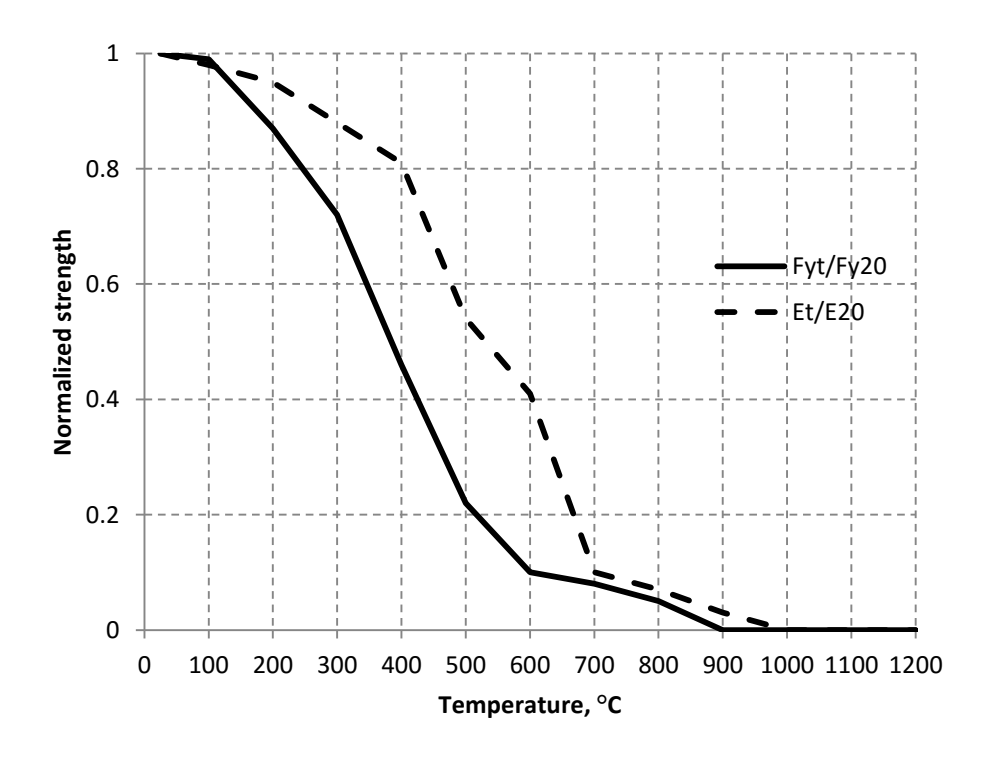


Figure 2.12. Variation of yield strength and elastic modulus of prestressing steel with temperature based on Eurocode 2

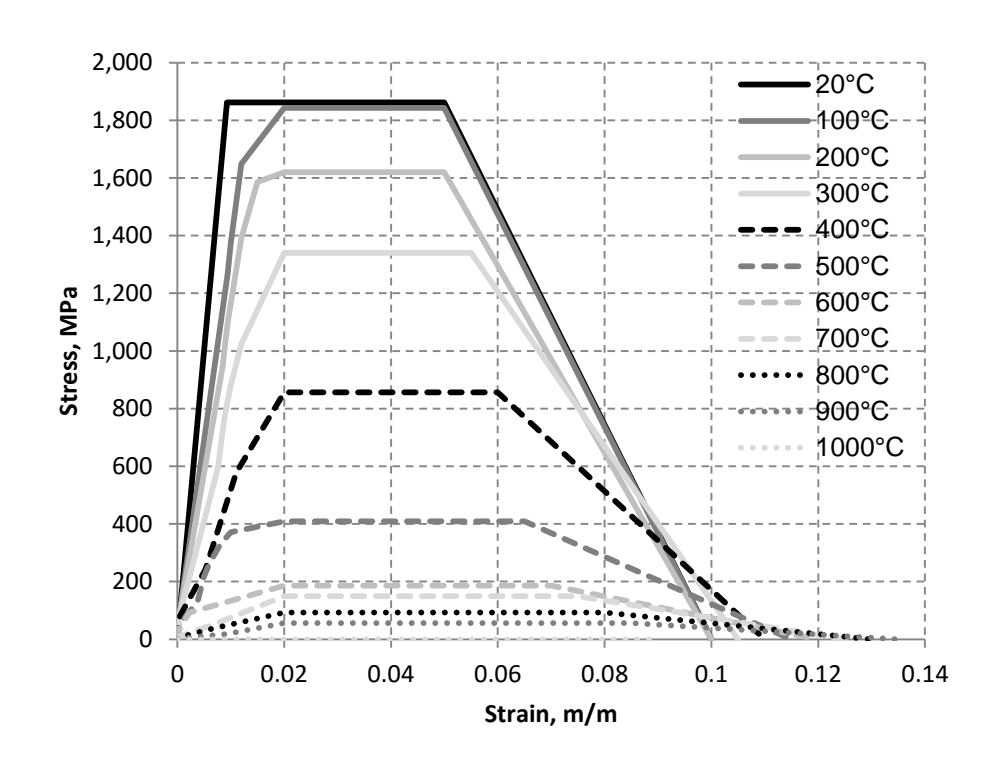


Figure 2.13. Stress-strain relationship of prestressing steel at various temperatures based on Eurocode 2

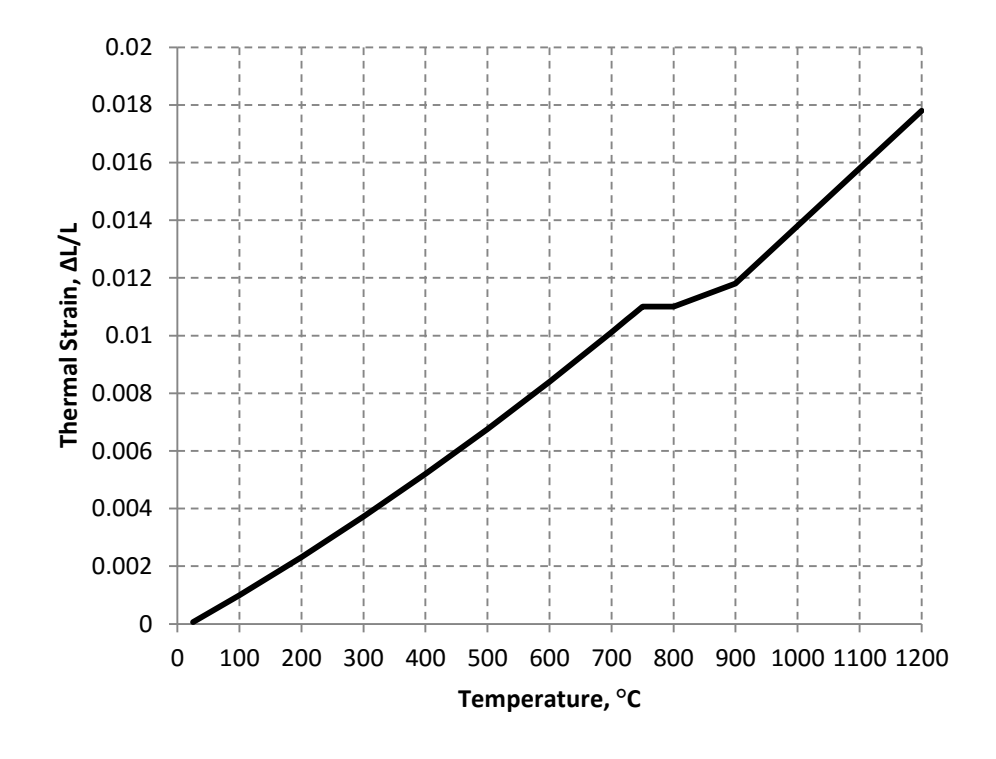


Figure 2.14. Variation of thermal strain of prestressing steel with temperature based on Eurocode 2

2.6 Knowledge gaps

Based on the state-of-the-art review, several drawbacks have been identified in previously conducted studies. Most of the fire tests and numerical studies were conducted under standard fire scenarios and did not address critical issues encountered in building fires such as realistic fire scenario, load level, support restraint and aggregate type. Thus, performance of these slabs under design fire conditions is still largely unknown. Moreover, failure modes and mechanisms in hollowcore slabs under fire conditions have not been well understood or established. In addition, current codal provisions for fire design of hollowcore slabs are derived from standard fire tests and mostly prescriptive in nature. These methods are limited in design parameters and thus, might not yield realistic fire resistance of hollowcore slabs. Few rational design methods are available, but are also limited in design parameters and do not account for realistic failure modes.

The major knowledge gaps relating to fire performance of PC hollowcore slabs are:

- There is no test data on the behavior of hollowcore slabs under realistic (design) fire, loading scenarios.
- The effect of restraint support conditions on fire performance of hollowcore slabs is not well established.
- Few numerical models are available, but are limited to only specific type of hollowcore configurations. Further, these models do not account for realistic fire scenario, load level, restraint condition and critical failure modes.
- Factors that influence failure modes in PC hollowcore slabs under fire conditions are not well
 established.

- There is lack of data on the mechanical property of prestressing strands. Available
 mechanical property relations of prestressing strands are not properly defined under fire
 conditions.
- Prevalent fire design methodologies of PC hollowcore slabs are prescriptive in nature, and are limited in design parameters. Thus, these methods might not yield realistic fire resistance of hollowcore slabs.

CHAPTER 3

3 FIRE RESISTANCE EXPERIMENTS

This chapter is mainly based on the following journal papers:

- Shakya, A. M., and Kodur, V. K. R. (2015). "Response of precast prestressed concrete hollowcore slabs under fire conditions." Engineering Structures, 87, 126–138
- Shakya A. M., Kodur V. K. R. (2014). Behavior of prestressed concrete hollowcore slabs under standard and design fire exposure. 8th Int. Conf. Struct. Fire, vol. 1, Shanghai China: p. 199–208.
- Shakya A. M., Kodur V. K. R. (2014) Performance of prestressed concrete hollowcore slabs under standard and design fire exposure. PCI Conv. Natl. Bridge Conf., National Harbor, MD: Prestressed Concrete Institute; 2014.

3.1 General

The state-of-the-art literature review presented in Chapter 2 clearly indicates that there have been number of fire tests on prestressed concrete hollowcore slabs. However, most of these fire tests were carried out under standard fire conditions without full considerations to field conditions, including design fire scenarios, loading and axial restraints (Abrams 1976; Acker 2003; Aguado et al. 2012; Andersen and Lauridsen 1999; Bailey and Lennon 2008; Borgogno 1997; Breccolotti et al. 2006; Fellinger et al. 2005; Jensen 2005; Lennon 2003; Schepper and Anderson 2000; Zheng et al. 2010). Thus, there is lack of reliable fire test data on hollowcore slabs including, detailed sectional temperature profile, progression of strain distribution and fire induced axial restraint forces. Moreover, failure modes have been presented qualitatively without much

consideration to mechanism of these failure modes and factors affecting such failure modes. To overcome some of these drawbacks, an experimental study was undertaken to develop better understanding of the behavior of hollowcore slabs and to study critical factors affecting these failure modes under fire conditions. As a part of this experimental study, fire resistance tests were performed on six PC hollowcore slabs to evaluate the fire behavior of PC hollowcore slabs under different fire scenarios, load levels and restraint conditions. Full details on fabrication, instrumentation, test procedures together with measured response parameters are presented in this chapter (Shakya and Kodur 2015).

3.2 Fabrication of test specimens

The fire resistance tests were conducted on six PC hollowcore slabs designated as Slab 1 to Slab 6. All tested PC hollowcore slab units were of 4 m in length, 1.2 m in width and 200 mm in depth, and had six cores and seven prestressing strands as reinforcement. The cores in the slabs were of 150 mm diameter, with 25 mm concrete thickness at the bottom of the core. The prestressing strands were of 12.7 mm diameter and low relaxation strand type, with yield stress of 1860 MPa. Effective concrete cover thickness over the strands, measured from the center of the strands, was 44 mm. Geometric and material characteristics of these slabs are presented in Table 3.1 and a detailed cross sectional configuration of a typical tested PC hollowcore slab is shown in Figure 3.1.

All six slabs were cast at a local fabrication plant (Kerkstra Precast Inc. in Michigan) through concrete extrusion process. This extrusion process involved specialized extrusion die of predetermined hollowcore configuration (die with 200 mm depth and six 150 mm diameter cores was used for these slabs), which run over a 150 m long bed. The prestressing strands were laid

on the bed, based on design strand configuration, and anchored using steel chucks at ends. Prestressing was done by stretching the strands, using hydraulic jacks to predetermined prestressing force (70% of yield strength of strand). The bed surface was lubricated for easy stripping of slabs from casting bed. The concrete hopper continuously fed concrete mix to the extrusion equipment, wherein slab was extruded by forcing the concrete mix through the vibrating die. The vibration of die ensured production of continuous and well compacted slab. Slabs of required span length were cut using wet sawing process before stripping from casting bed.

The hollowcore slabs were designed as per PCI design manual provisions (PCI 2011) and met specifications of commercially produced slabs in USA. Two batch mixes of concrete were used to fabricate the slabs, namely carbonate aggregate batch mix for four slabs (Slab 1, Slab 3, Slab 5 and Slab 6) and siliceous aggregate batch mix for the remaining two slabs (Slab 2 and Slab 4). The mix proportions used in two batch mixes of concrete are tabulated in Table 3.2. Concrete used for fabrication of these slabs was designed to achieve minimum required transfer compressive strength of 21 MPa, within 10 hours of concrete pouring, for facilitating speedy casting and stripping process. The measured compressive strengths of two batches of concrete, at the time of transfer and stripping, were in the range of 35 to 37 MPa (5 to 5.4 Ksi.). All six slabs were stored for 2 months in the plant yard and then shipped to MSU Civil Infrastructural Laboratory, where they were stored for 7 to 8 months at 25°C and 40% relative humidity till fire tests were undertaken. Figure 3.2 shows fabrication of hollowcore slabs through extrusion process and storage of these slabs for curing, prior to fire tests.

The compressive strength of concrete and relative humidity of slabs were measured periodically during curing stage. The average compressive strength of concrete measured at 28 and 90 day are

tabulated in Table 3.2 and that measured on test day along with the relative humidity of test slabs measured on test day are tabulated in Table 3.3. As can be seen from tabulated values, the compressive strength of siliceous aggregate concrete is slightly higher than that of carbonate aggregate concrete. This can be attributed to the fact that the concrete with siliceous aggregate exhibits better bonding and interlocking between cement paste and aggregate, due to angular shape, compared to carbonate aggregate which is typically characterized as rounded (Kodur and Harmathy 2012).

3.3 Instrumentation

The instrumentation in PC hollowcore slabs consisted of thermocouples, strain gauges, LVDTs (linear variable displacement transducer) and load cells. Thermocouples were placed at various locations within the slab namely, strand, mid depth, quarter depth, core bottom, core top and on unexposed (top) surface to monitor temperature progression throughout fire exposure duration. Strain gauges (operational up to 300°C) were also installed to measure progression of thermal and mechanical strains in strand and top surface of slab and load cells were installed to measure fire induced axial restraint force. In addition, LVDTs were installed on slabs to record progression of mid-span deflection during fire tests. Location of thermocouples, strain gauges and deflection gauges on the slab is illustrated in Figure 3.1. Due to the nature of fabrication process, instrumentation had to be installed in the slabs after the extrusion process, wherein thermocouples were placed by drilling holes at specific locations, and strain gauges were attached on the concrete surface. Special care was taken in placing the instrumentation at exact depths and locations of the slabs. Thermocouples were placed right after casting, but just before hardening of concrete, while strain gauges, LVDTs and load cells were placed prior to fire tests.

3.4 Test equipment

Fire resistance tests on PC hollowcore slabs were conducted in a structural fire test furnace at MSU Civil Infrastructure Laboratory. The test furnace is designed to simulate simultaneous application of thermal and structural loading, as well as, restraint conditions to which a structural member might be subjected to, in a fire event. Details of the furnace, together with test set-up, are illustrated in Figure 3.3.

The fire furnace at MSU consists of a steel framework supported by four steel columns and a fire chamber of 3.05 m in length, 2.44 m in width and 1.78 m in height. The furnace is equipped with six gas burners, which are capable of producing maximum heat power of 2.5 MW. These six burners are strategically placed, on four walls of the furnace, for uniform progression of heat energy within the furnace chamber. Six type-K Chromel-Alumel thermocouples, as per ASTM E119 specifications (ASTM 2011), are also placed on four walls of the furnace to monitor furnace temperature during fire tests. The input gas and ventilation are controlled manually to maintain the average furnace temperature consistent with a specified fire curve (standard or design fire scenario). All thermocouple, strain gauge and LVDT channels are connected to a data acquisition system, which display and record temperatures, strains and displacements respectively in real time during a fire resistance test. There are two view ports on two opposite walls of the furnace for taking visual observations during a fire test.

3.5 Test conditions and procedure

Two PC hollowcore slabs were tested in each fire test by subjecting them to predetermined fire, loading and boundary conditions. The slabs were stored for 7 to 8 months at 25°C and 40% relative humidity before fire tests were undertaken. Middle portion of each slab, 2.44 m (8 ft.) of

clear span of 3.65 m (12 ft.), was exposed to fire. Five out of six slabs were tested under simply-supported conditions, in which a slab was supported on steel sections (W14×96). Semicircle rods were welded to steel sections to allow free rotation of slab at the ends. The sixth slab (Slab 5) was restrained for longitudinal/axial expansion. Superimposed loading was applied using hydraulic actuators through extension columns, and were distributed along the slab width, using hollow steel sections (HSS $8\times8\times\frac{1}{2}$). Four point loading scheme was adopted to apply loading on the slabs. Figure 3.4 illustrates loading setup on a PC hollowcore slab during a fire test.

In the case of slab with restrained boundary conditions (Slab 5), two hollow steel sections (HSS $8\times8\times\frac{1}{2}$) were used to provide axial restraint to the slab. Two post tensioning rods, of 25.4 mm diameter and with ultimate capacity of 534 kN, were run through the cores of the slabs to bind the steel hollow sections to slab ends, as can be seen in Figure 3.3 (g). Load cells were attached to the ends of these post-tensioning rods to monitor the extent of temperature induced axial force that develop during fire exposure.

To study the behavior of PC hollowcore slabs under different fire scenarios, the slabs were tested under three different fire scenarios, as shown in Figure 3.5. In Test 1, Slab 1 and Slab 2 were tested under design fire exposure (DF1) to simulate a typical office/library fire without a decay phase. In Test 2, Slab 3 and Slab 4 were tested under design fire (DF2) exposure simulating similar office/library fire, comprising of 120 minutes of growth phase followed by a decay phase with a cooling rate of 10°C/minute. These fire scenarios represent typical ventilation controlled conditions encountered in buildings. In Test 3, Slab 5 and 6 were tested under standard ASTM E119 fire (ASTM 2011).

The load level on tested slabs was varied in fire tests. Slabs 1 and 2 were tested under 50% load level (57.8 kN, representing 50% of the flexural capacity of the slab at room temperature) and

Slabs 3 to 6 were tested under 60% load level (69.4 kN, representing 60% of the flexural capacity of the slab at room temperature). During fire tests, care was taken to maintain a uniform load level on slabs throughout the fire exposure duration. The loading on slabs was chosen to simulate typical service load levels on hollowcore slabs. In addition, end support conditions were also varied. Slabs 1, 2, 3, 4 and 6 were tested with simply supported end conditions while Slab 5 was tested under axially restrained end conditions.

3.6 Results and discussion

Results obtained from fire tests on six PC hollowcore slabs are utilized to evaluate thermal response, structural response, cracking and spalling progression, as well as failure times.

3.6.1 Thermal response

The thermal responses of tested hollowcore slabs are illustrated in Figure 3.6 to Figure 3.11, by plotting temperature progression as a function of fire exposure time. The progression of temperatures in strand, mid depth, quarter depth, unexposed surface, core bottom and core top of the slabs are compared, for six tested slabs, in Figure 3.6, Figure 3.7, Figure 3.8, Figure 3.9, Figure 3.10 and Figure 3.11 respectively. Slabs 1 and 2 were exposed to fire scenario DF1, Slab 3 and 4 were exposed to design fire DF2, and Slab 5 and 6 were exposed to ASTM E119 fire [15] (See Figure 3.5). In all tested slabs, cross-sectional temperatures plateau at about 100°C, generally within 20-40 minutes of fire exposure. This plateau can be attributed to utilization of heat for evaporation of free moisture present in concrete which occurs around 100°C. However, at strand and core bottom locations, close to the fire exposed surface of the slab, the plateau around 100°C is not observed. This is attributed to migration of moisture from these concrete layers to inner layers induced by increased pore pressure due to high thermal gradients generated

along the depth of slab, at early stage of fire exposure (Ichikawa and England 2004). After attaining this phase, the temperatures in prestressing strands and concrete increase with fire exposure time. It can also be seen from Figure 3.6 through Figure 3.11 that, the temperatures in concrete layers farther from the fire exposure surface is lower than those layers closer to the exposure surface. This can be attributed to lower thermal conductivity and higher specific heat of concrete, which delays temperature transmission through the slab. This delay also produces higher thermal gradient along the slab depth, in the early stages of fire exposure.

Unlike in solid concrete slabs, temperature progression in hollowcore slabs exposed to fire is significantly affected by presence of void cores. The effect of cores on temperature transmission through the slab is reflected in measured temperature in the cores, particularly at the bottom surface of cores. A comparison of Figure 3.6 and Figure 3.10 reveal that, the temperature in prestressing strands is typically higher than the temperatures at the bottom surface of the core, even though the core bottom surfaces are closer to fire exposure surface than the strands. This is mainly due to dissipation of heat through the core. As air exhibits higher specific heat than concrete, the presence of voids leads to faster dissipation of heat from the surfaces closer to the voids.

The effect of aggregate type in concrete on temperature progression in slabs can be gauged from Figure 3.6 through Figure 3.11. It can be seen that the rate of temperature rise is relatively higher in slabs (Slab 2 and Slab 4) made of siliceous aggregate than slabs (Slab 1 and Slab 3) made of carbonate aggregate. This can be directly attributed to the fact that siliceous aggregate concrete possesses higher thermal conductivity than carbonate aggregate concrete (Kodur and Harmathy 2012), and thus leads to faster heat transmission through the slab.

3.6.2 Structural response

The structural response of PC hollowcore slabs under different fire exposure conditions is illustrated through progressions of mid span deflection, restraint force and strain level in Figure 3.12, Figure 3.13 and Figure 3.14 respectively. The mid-span deflection in all slabs progress with fire exposure time and follow similar trend. The deflections in all six slabs plotted in Figure 3.12 can be grouped into three stages. In Stage 1, in first 20 minutes of fire exposure, the deflections increase at a slow pace in all slabs. This trend mainly arises from thermal strains generated due to high thermal gradients, generated along the slab depth, occurring in early stage of fire exposure. However, concrete and strands undergo very little strength degradation in this stage due to low temperatures in strands (below 150°C) and inner layers of concrete (below 100°C). In Stage 2, after 20 minutes into fire exposure and up to 75 minutes, deflections in all slabs increase at a slightly slower pace. This increase in deflection is due degradation of strength and modulus in concrete and strand, as temperatures increase in inner layers of concrete reducing thermal gradients.

Finally, in Stage 3 (beyond 75 minutes), deflections in all slabs increase at a rapid pace, and this is mainly attributed to high mechanical and creep strains resulting from very high temperatures in concrete and strands, which reach above 500°C. Difference in the level of deflection in different slabs is pronounced in this stage. Slabs 1 and 2 show lower deflections than Slab 3 and 4, and this is due to the lower load levels in Slabs 1 and 2, as compared to Slab 3 and 4. Slabs 5 and 6 show much higher deflections as compared to Slabs 3 and 4, and this is due to the fact that ASTM-E119 fire scenario produce slightly higher fire intensity than DF2 fire scenario (see Figure 3.5). Slab 5 shows lower deflections than Slab 6, and this is can be attributed to the presence of restraint supports which enhances the stiffness of the slab.

Deflections in Slab 1 and Slab 2, plotted in Figure 3.12, show some abrupt variations. This can be attributed to slight problems encountered in maintaining exact level of loading during fire test (Test 1), wherein actuators with a capacity of 2720 kN were used for loading the two slabs. The hydraulic system connected to these actuators is capable of maintaining desired preset load by automatically adjusting required hydraulic pressure to match initially set pressure in the system. However, the accuracy in adjusting hydraulic pressure range goes down at very low levels of loading (below 5% of the actuator capacity), as compared to capacity of actuators. Since, the level of applied loading on Slab 1 and Slab 2 represented less than 1% of full capacity of these actuators, the required hydraulic pressure in these actuators was very low. Due to this low hydraulic pressure, maintaining required loading necessitated frequent manual readjustment of hydraulic pressure in the actuators throughout the first fire test. This resulted in slight fluctuation in applied loading (±10% of load level on slabs). This loading setup was later modified for Test 2 and Test 3, wherein actuators with smaller capacity (250 kN) were used for loading. Thus, in fire tests 2 and 3, 25% of actuator capacity was utilized and this led to proper load stabilization during test duration with no abrupt variation in deflection.

Deflection trends from fire tests, plotted in Figure 3.12, show that slabs made of siliceous aggregate concrete (Slab 2 and Slab 4) experienced higher deflections (up to 10 percent) than slabs made of carbonate aggregate concrete (Slab 1 and Slab 3). This is mainly due to the fact that siliceous aggregate concrete slabs experienced higher rate of temperature rise than carbonate aggregate concrete slabs (see Figure 3.6 to Figure 3.11). The higher cross-sectional temperatures in siliceous aggregate concrete slabs lead to faster strength and stiffness degradation in concrete and strands, which in turn resulted in higher deflections.

Temperature induced axial restraint force that gets developed in Slab 5 due to restriction on free expansion of the slab, and the variation of this axial force with fire exposure time is plotted Figure 3.13. Fire induced axial force (P_t) in the slab at any specific fire exposure time is directly proportional to strain level and modulus, and this relationship can be used to explain the trends in measured axial restraint force in Slab 5, given as:

$$P_{t} = \sum A \times E_{t} \times \varepsilon_{t} \tag{3.1}$$

where, A is the cross-sectional area, E_t is the modulus of concrete and strand, and ε_t is the total strain in the slab measured at the level of neutral axis. Similar to deflection progression, the progression of axial restraint force in Slab 5 can be grouped into three stages, as shown in Figure 3.13. In Stage 1, in the first 20 minutes of fire exposure, the restraint force rapidly increases with fire exposure time. This can be clearly attributed to higher thermal strain (ε_t in Equation 3.1) generated in concrete and prestressing strand due to high thermal gradients developing in the early stage of fire exposure. However, in this stage there is not much degradation of modulus in concrete and strand due to relatively lower temperatures in the strand and inner layers of concrete. After 20 minutes, in Stage 2, temperature increases in inner layers of concrete and this leads to degradation of modulus (E_t in Equation 3.1) of prestressing strand and concrete, which in turn leads to rapid decrease in axial restraint force up to about 75 minutes. The degradation of modulus in concrete and prestressing strand in Stage 2 occurs at a much higher pace than increase in thermal strains. In Stage 3 (beyond 75 minutes), axial restraint force could not be properly measured in the fire tests due to sensitivity of instrumentation at temperatures beyond 500°C.

The variation in strains, measured at strand level and at top layer of concrete in all six slabs is plotted in Figure 3.14. Strain data is only reliable up to 25 minutes into fire exposure at strands

and 60 minutes of fire exposure on unexposed (top) surface concrete. This is due to the fact that strain gauges got damaged or dysfunctional at temperatures above 250°C, and the strain data beyond this temperature is not reliable. The plotted strain data clearly show that prestressing strands are in tension and top surface concrete is in compression in all simply-supported slabs (Slabs 1 to 4 and Slab 6) in initial stage of fire exposure. In the restrained Slab 5, strands experience compression for a brief duration (10 minutes) in the initial stage of fire exposure before reverting to tension. This can be attributed to slight increase of camber in slab resulting from restriction to expansion facilitated by axial restraint effect at supports. However, the top layer of concrete, in Slab 5, is in compression for the entire duration of fire exposure. The strain in strands increases at a higher rate as compared to that in top surface of concrete in the first 20 minutes of fire exposure. This can be attributed to the much higher temperatures in the strands than top most layer of concrete, occurring due to development of high thermal gradient at the initial stages of fire exposure. After 20 minutes, the strain in concrete, on the top surface of all the slabs, increase gradually, and is attributed to degradation in strength and modulus in concrete and strand.

A closer review of strain data in different slabs reveal that aggregate type, load level, fire scenario and support condition have significant influence on the level of strains that develop in PC hollowcore slabs. Strains at strand and top layer of concrete in Slabs 2 and 4, fabricated with siliceous aggregate concrete, are higher, as compared to their carbonate aggregate counterparts (Slabs 1 and 3), and this mainly results from higher sectional temperature (see Figure 3.6 to Figure 3.11), which induces higher thermal expansion in Slabs 2 and 4. As discussed earlier, siliceous aggregate concrete possesses higher thermal conductivity and thus, produces higher sectional temperatures in Slabs 2 and 4 (Kodur and Harmathy 2012). On the other hand, strains

in Slabs 3 and 4 are higher, as compared to that in Slabs 1 and 2, and this is due to higher level of applied loading on Slabs 3 and 4, which induces higher mechanical strains. The higher strains in Slabs 5 and 6, as compared to that in Slabs 1 to 4, are due to higher intensity of ASTM-E119 (ASTM 2011) fire exposure in Slabs 5 and 6 leading to higher sectional temperatures which in turn produces higher thermal strains. A comparison of strain progression in Slab 5 and Slab 6 further indicates that restraint supports lower level of strains in hollowcore slabs, and this can be attributed to the restriction to free expansion due to axial restraints.

3.6.3 Crack propagation and spalling pattern

Visual observations made during and after fire tests is used to gauge the progression of cracking and spalling in hollowcore slabs. The visual observations during fire tests were made through two view ports on the fire furnace walls. Prestressing force in strands produced compressive stresses in bottom layers of concrete, and this generated a residual camber in all slabs. Prior to fire exposure, there were no visible cracks in any of the slabs under applied loading.

In early stage of fire exposure, concrete (directly exposed to fire) and strands undergo expansion at slightly different rates, due to high thermal gradients. Because of this, tensile stresses develop in the bottom concrete layers of the slab and this led to gradual development of longitudinal cracks in the weakest sections (cores) of the bottom surface of the slab. With increasing fire exposure time, these cracks grew in size and progressed from the support ends towards the midspan of the slabs. Longitudinal cracks also developed in the top sections of the cores within 60 minutes into fire exposure. This can be also be attributed to high thermal gradients, which leads to the development of thermal strains at different rates in the top and bottom layers of the slabs in transverse direction. Bottom concrete layers exhibited higher thermal strains than top concrete layers, leading to tension cracks in the weakest sections (cores) of the top surface of the slab.

Such longitudinal cracks have also been previously reported in literature in hollowcore slabs during fire tests (Fellinger et al. 2005). However, longitudinal cracks have insignificant effect on the structural response of the slab, as each separated segment (with a single web) of the hollowcore slab acts as an individual beam. This is also reflected by the deflection progression in hollowcores slabs, illustrated in Figure 3.12, which shows no abrupt increase in deflection during first 60 minutes of fire exposure.

Beyond 60 minutes into fire exposure, flexural cracks get widened with time. In the case of carbonate aggregate concrete slabs (Slabs 1, 3 and 6) shear cracks started to develop around 75 minutes, and this is mainly due to the fact that carbonate aggregate (due to rounded shape) exhibit weaker bond and interlocking between cement paste and aggregate surface than siliceous aggregate which is angular in shape (Kodur and Harmathy 2012). However, shear cracks were not observed in restrained Slab 5 and siliceous aggregate concrete Slabs 2 and 4. This infers that carbonate aggregate concrete slabs are more susceptible to shear cracking than siliceous aggregate concrete slabs. Typical crack progression patterns in hollowcore slabs are illustrated in Figure 3.15 and successive progression of these cracks initiating at various times to fire exposure is illustrated for all six slabs in Figure 3.16.

Slabs 1 to 4, subjected to design fire scenario, sustained load for the entire fire duration and did not experience failure for 120 minutes. Slab 6 failed through widening of flexural cracks at 140 minutes, and axially restrained slab (Slab 5) failed in 170 minutes through excessive cracking and crushing of concrete at the mid-span section. The typical failure modes observed in these slabs are illustrated in Figure 3.15. During fire tests, water seeping out of concrete and strand interface through both ends of slabs could be seen. After 20 minutes of heating, water vapor escaping through the unexposed surface and inner core surfaces was also observed.

A review of literature indicate that high strength concrete structural members are prone to spalling under fire exposure [20]. Since, the tested hollowcore slabs were fabricated with concrete of 70 MPa compressive strength, special attention was paid to monitor spalling during fire tests. No fire induced spalling occurred in carbonate aggregate concrete slabs (Slabs 1, 3 and 6). However, minor spalling in the form of pitting on the fire exposed bottom surface was observed in siliceous aggregate concrete slabs, Slab 2 and Slab 4, and this spalling occurred in early stages (in the first 20 minutes) of fire exposure. This minor spalling in siliceous aggregate concrete slabs can be attributed to higher compaction and lower pore volume facilitated through better interlocking and bond between cement paste and aggregate surface (Kodur and Harmathy 2012).

Observations from fire tests indicated there was no spalling in the initial stages of fire exposure in restrained Slab 5, but occurrence of severe spalling in later stages of fire exposure and this is illustrated in Figure 3.17(b). This spalling is due to high internal stresses generated from restrained supports in this slab indicating that restraint conditions has an influence on the extent of fire induced spalling. Unlike spalling in siliceous aggregate concrete slabs, the spalling in restrained carbonate aggregate concrete Slab 5 did not occur in the early stage of fire exposure, but occurred in later stages of fire exposure (100-120 minutes), when high levels of restraint force gets developed in the slab. Figure 3.17, shows the extent of spalling in PC hollowcore slabs under different conditions, after fire tests.

Fire induced spalling in concrete structures typically occur when temperature induced pore pressure within concrete exceeds the tensile strength of concrete (Kodur 2014; Kodur and Shakya 2014). The pore pressure generated in concrete gets released through the exterior surfaces of a structural member (Ichikawa and England 2004). In the case of hollowcore slabs,

unlike in other types of concrete structural members, pore pressure can get relieved not only through bottom surface of the slab but also through inner core surfaces, and this helps to mitigate pore pressure more effectively. Moreover, temperature induced micro cracks, which develop during fire exposure, also help to release pore pressure and mitigate any noticeable fire induced spalling of concrete.

3.6.4 Failure mode and fire resistance

Visual observations during and post fire tests is utilized to evaluate comparative failure modes in these slabs. Based on literature review, PC hollowcore slabs, under fire conditions, are susceptible to various failure modes such as, flexural, shear, spalling, bond and anchorage failure modes (Abrams 1976; Acker 2003; Aguado et al. 2012; Andersen and Lauridsen 1999; Bailey and Lennon 2008; Borgogno 1997; Breccolotti et al. 2006; Fellinger et al. 2005; Jensen 2005; Lennon 2003; Schepper and Anderson 2000; Zheng et al. 2010). All six test slabs showed some flexural cracks originating from the bottom fire exposed surface, but did not exhibit any bond or anchorage failure. Slab 1, Slab 3 and Slab 6 also showed some shear cracks. However, these shear cracks did not affect the load carrying capacity of the slabs, as can also be seen from deflection profiles in Figure 3.12, wherein no abrupt drop in deflection occurred. This can be attributed to the fact that the shear cracks were not fully propagated through the slab depth. Further, Slab 6, exposed to ASTM-E119 fire, failed through widening of flexural cracks, and axially restrained Slab 5 failed though severe flexural cracking at the mid-span section, as shown in Figure 3.15. In spite of being fabricated with high strength concrete (~70 MPa) no major spalling occurred in all six slabs.

The failure times of hollowcore slabs were evaluated based on different failure limit states specified in ASTM-E119 (ASTM 2011). Accordingly, failure of horizontal members (floors and

slabs) under fire exposure occurs through reaching integrity, insulation and stability limit states. Based on integrity criteria, failure occurs when flame breaches through unexposed side of the slab. Based on insulation criteria, failure of slab is said to occur when the average temperature measured at 9 points on the unexposed surface of the slab exceeds 139°C or temperature at any point exceeds 181°C above initial temperature. As per stability (strength) criteria, failure is said to occur when the slab cannot sustain the applied loading and such a condition is determined when the flexural or shear capacity of the slab drops below the applied bending moment or applied shear loading respectively. In prescriptive based approaches, stability failure in hollowcore slabs is assessed by relating degradation in capacity to the critical temperature in prestressing strand, taken as 427°C.

In addition to the above three limit states, British Standard (BS 476) (BS 476–20 1987) specifies deflection or deflection rate as a possible failure limit state for horizontal members (beams or slabs). Based on BS 476 (BS 476–20 1987) criteria, failure of concrete slabs, occur when the maximum deflection in the slab exceeds L/20 at any fire exposure time, or the rate of deflection exceeds the limit given by $L^2/9000d$ (mm/min) after attaining a maximum deflection of L/30, where, L = span length of the slab (mm), and d = effective depth of the slab (mm).

Based on thermal limiting criterion specified in ASTM E119 (ASTM 2011), all tested slabs attained minimum of 120 minutes of fire resistance. Based on structural criteria, Slabs 1 to 4, exposed to design fires, did not exceed deflection or strength limit state throughout the fire exposure duration. Further, Slabs 5 and 6 also did not exceed deflection limit state, but failed through strength limit state, at 170 and 140 minutes respectively, as illustrated in Figure 3.12. Slab 5, being axially restrained, exhibited significantly higher fire resistance, than Slab 6.

Table 3.1. Geometric and material characteristics of tested slabs

Parameter	Slab 1 to Slab 6			
Dimension (length×width×thickness)	$4\times1.2\times0.2~m^3$			
Cores	Six 150 mm Ø			
Concrete design compressive strength	75 MPa			
Prestressing strand	Seven wire – 12.7 mm 1860 MPa low relaxation			

Table 3.2. Batch proportions in concrete mixes

Tuote 5.2. Butter proportions in concrete mixes						
Description (per m ³)	Batch 1	Batch 2				
Slabs	Slab 1, Slab 3, Slab 5, Slab 6	Slab 2, Slab 4				
Cement (Type I), kg	315	315				
Fine aggregate (2NS), kg	911	950				
Course aggregate, kg	1002.64	943				
	(Carbonate - Natural Stone -	(Siliceous - #67 LS -				
	Rounded)	Angular)				
Fly ash, kg	56	56				
AE 260, kg	0.3	0.3				
Visco 4100, kg	1.001	1.001				
Sikatard 440, kg	0.26	0.0				
Water, litre	95	95				
Water cement ratio (W/C)	0.334	0.334				
Fine aggregate ratio	0.378	0.397				
Coarse aggregate ratio	0.416	0.395				
Fine aggregate moisture	~4%	~4%				
Coarse aggregate moisture	~1%	~1%				
Mixing time, sec	100	100				
Unit weight of concrete, kg/m ³	2410	2390				
Concrete strength $f_{\mathcal{C}}$ '(28 days), MPa	56	58				
Concrete strength f_C '(90 days), MPa	65	78				

Table 3.3. Summary of test parameters and results

Test slab	Aggregate type	Test day Compressive strength (f'c), MPa	Applied Loading (% of capacity)	Support	Test day RH %	Fire scenario	Failure modes	Spalling
Slab 1	Carbonate	74	50	SS	60	DF1	n.f.	None
Slab 2	Siliceous	87	50	SS	60	DF1	n.f.	Minor
Slab 3	Carbonate	75	60	SS	55	DF2	n.f.	None
Slab 4	Siliceous	91	60	SS	55	DF2	n.f.	Minor
Slab 5	Carbonate	75	60	AR	55	ASTM - E119	Flexural cracking	None
Slab 6	Carbonate	75	60	SS	55	ASTM - E119	Flexural crushing	None

Note: SS = simply supported, AR = axially restrained, RH = relative humidity, 'n.f.' = no failure

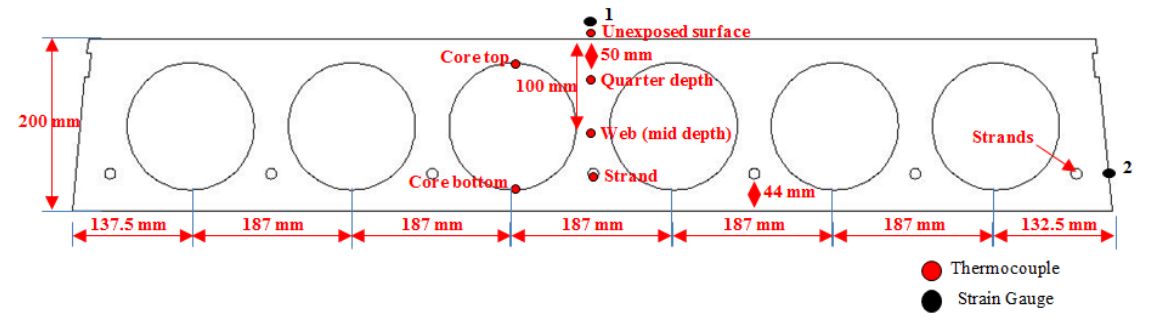


Figure 3.1. Location of thermocouples and strain gauges in PC hollowcore slab



Figure 3.2. Fabrication and curing of prestressed concrete hollowcore slabs

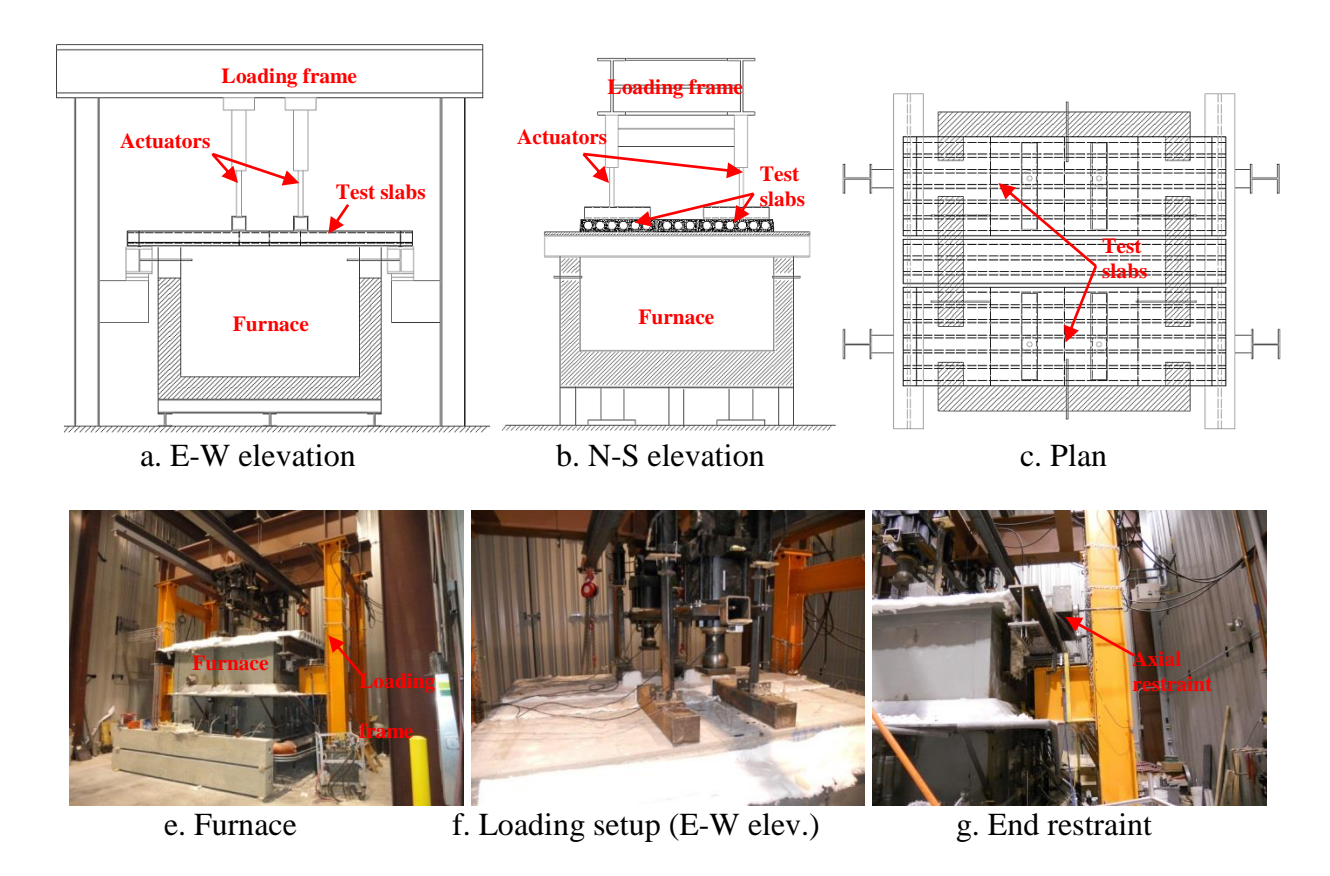


Figure 3.3. Test setup for undertaking fire resistance tests on PC hollowcore slabs

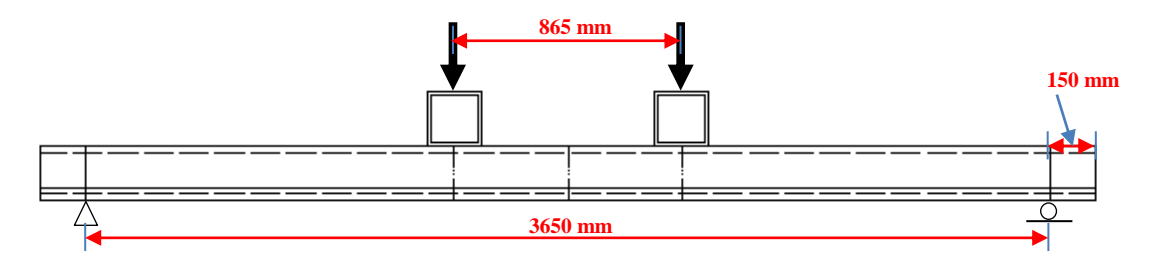


Figure 3.4. Four point loading scheme on hollowcore slab for fire tests

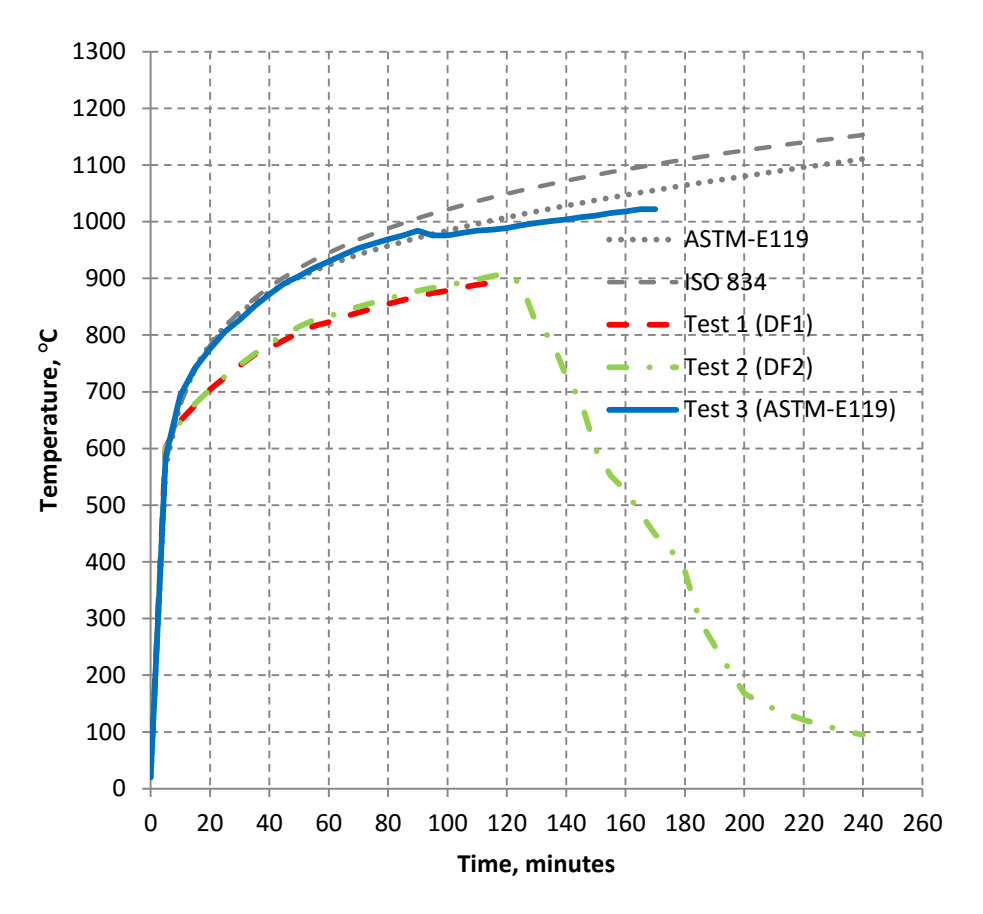


Figure 3.5. Time-temperature curves, simulated during fire tests

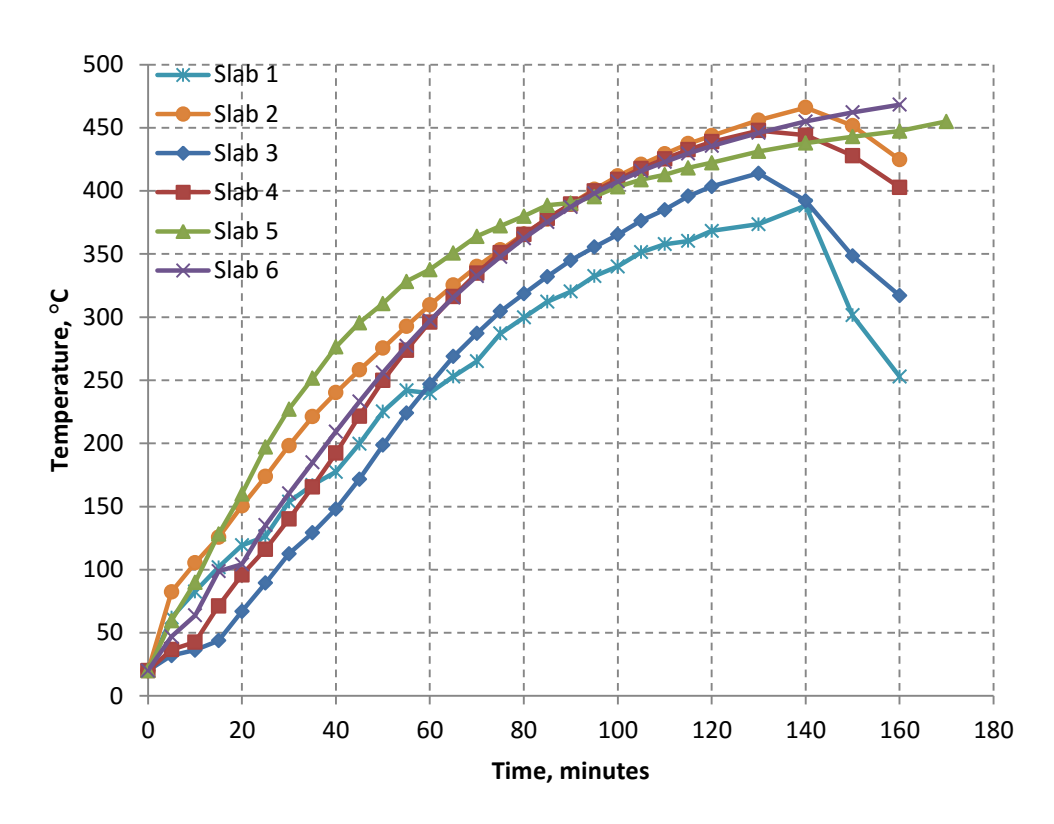


Figure 3.6. Variation of strand temperature with fire exposure time in tested slabs

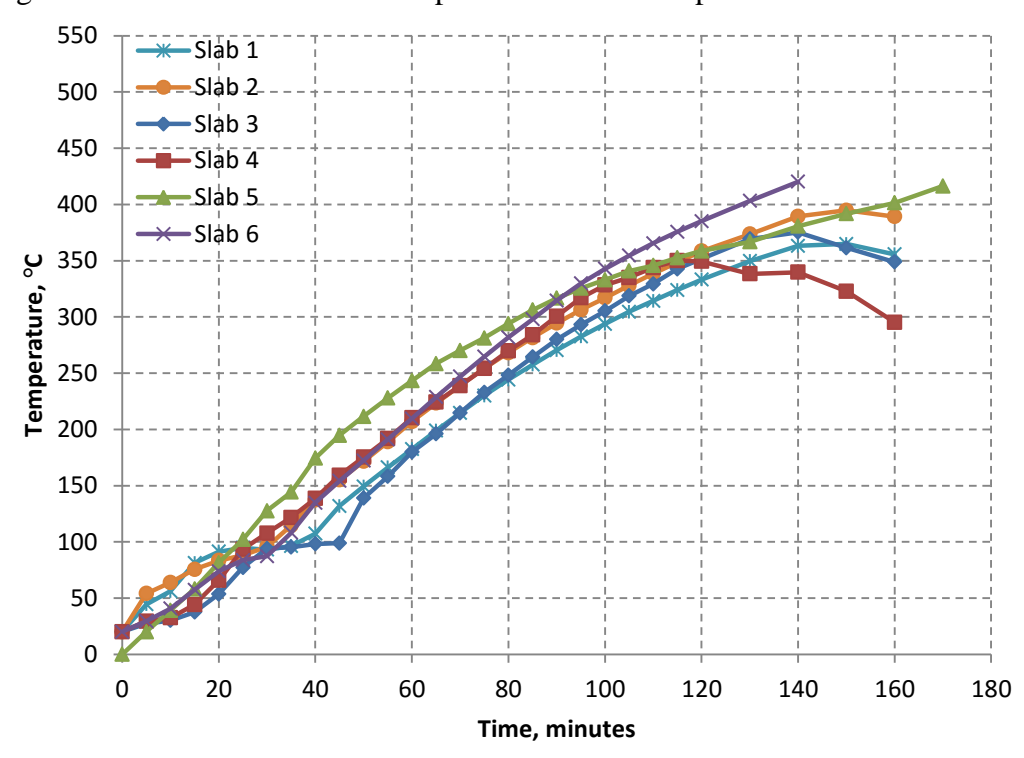


Figure 3.7. Variation of mid-depth temperature with fire exposure time in tested slabs

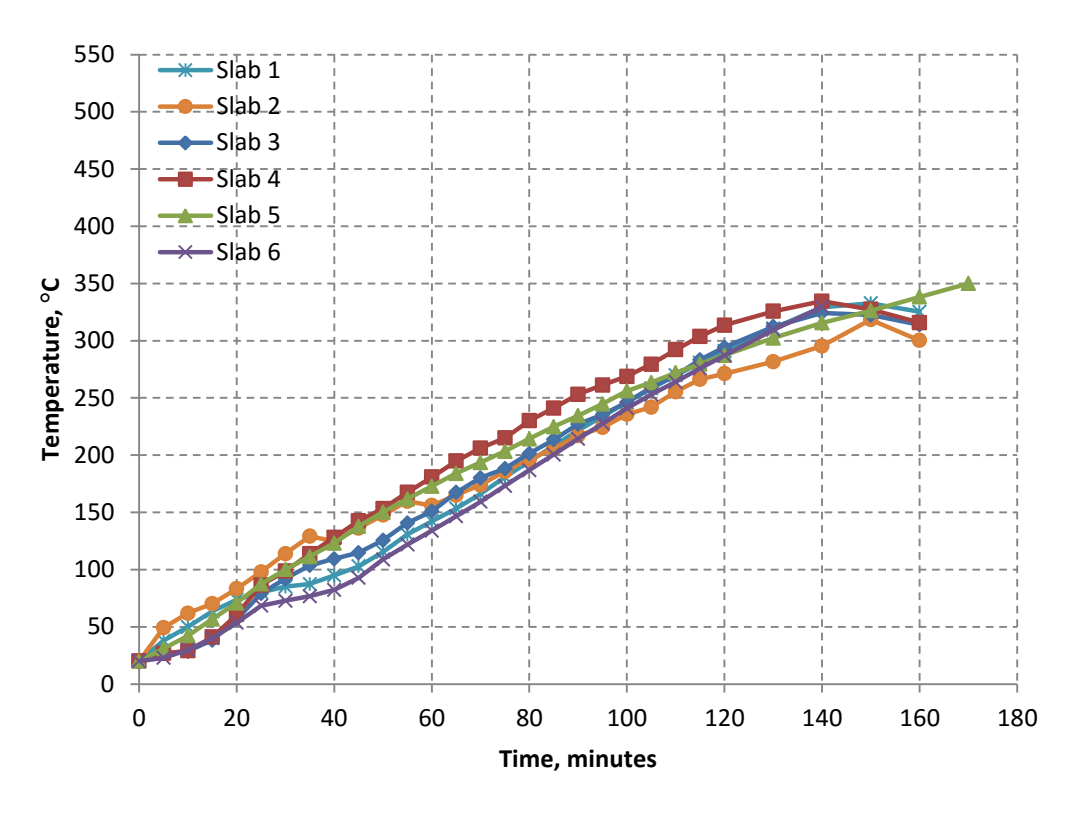


Figure 3.8. Variation of quarter depth temperature with fire exposure time in tested slabs

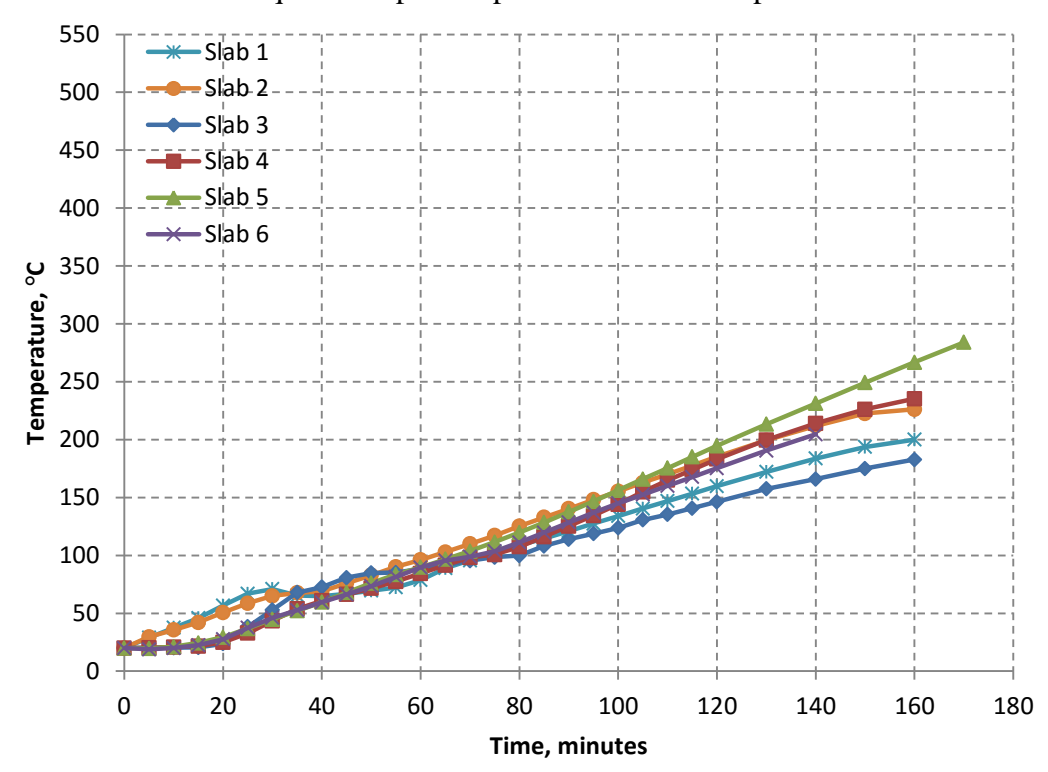


Figure 3.9. Variation of unexposed surface temperature with fire exposure time in tested slabs

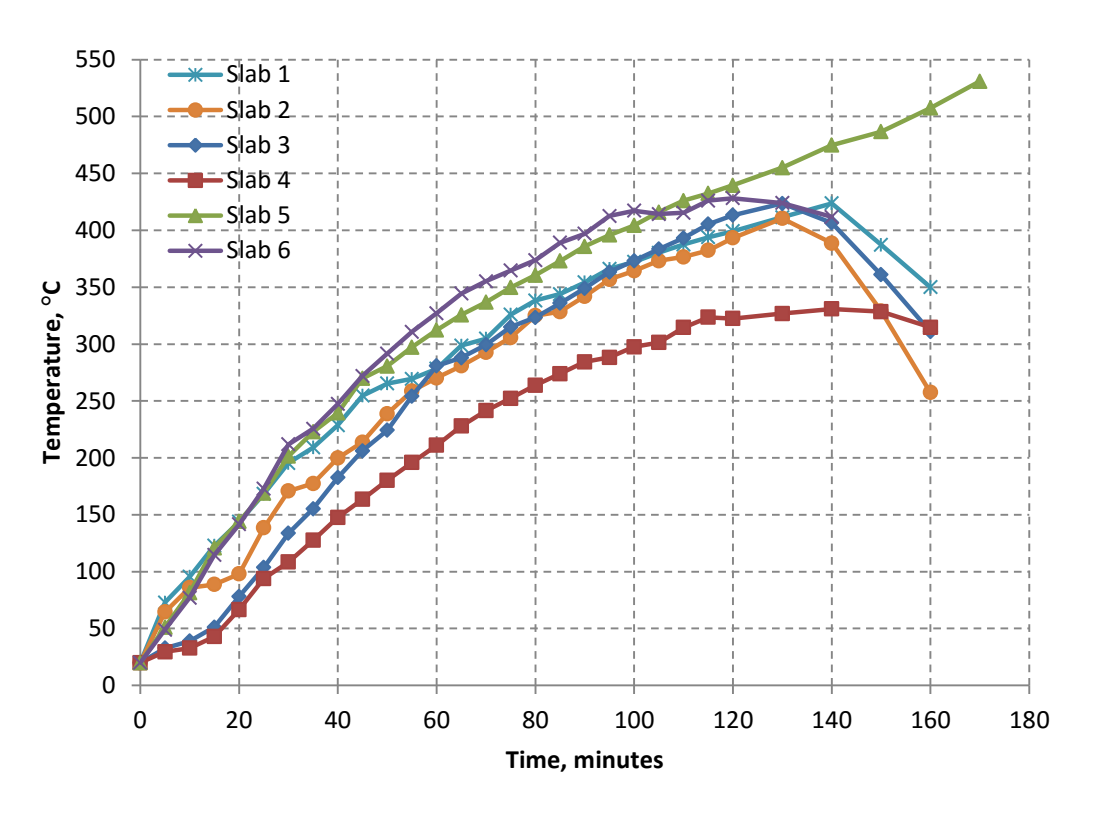


Figure 3.10. Variation of core bottom temperature with fire exposure time in tested slabs

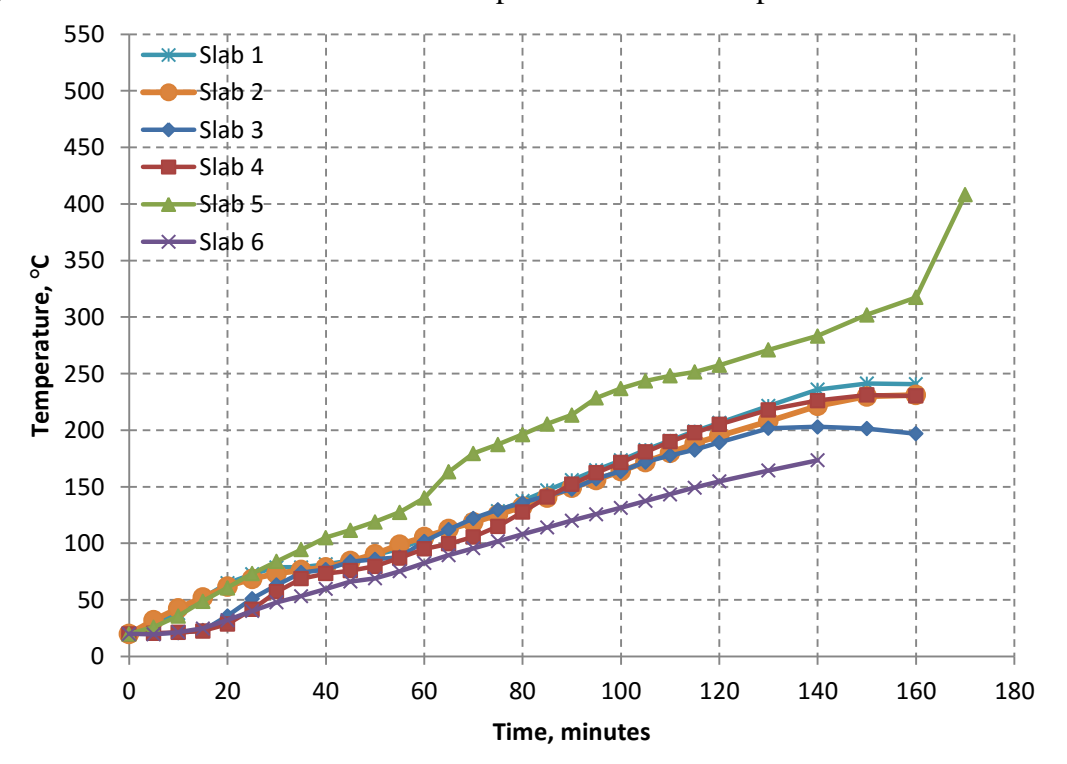


Figure 3.11. Variation of core top temperature with fire exposure time in tested slabs

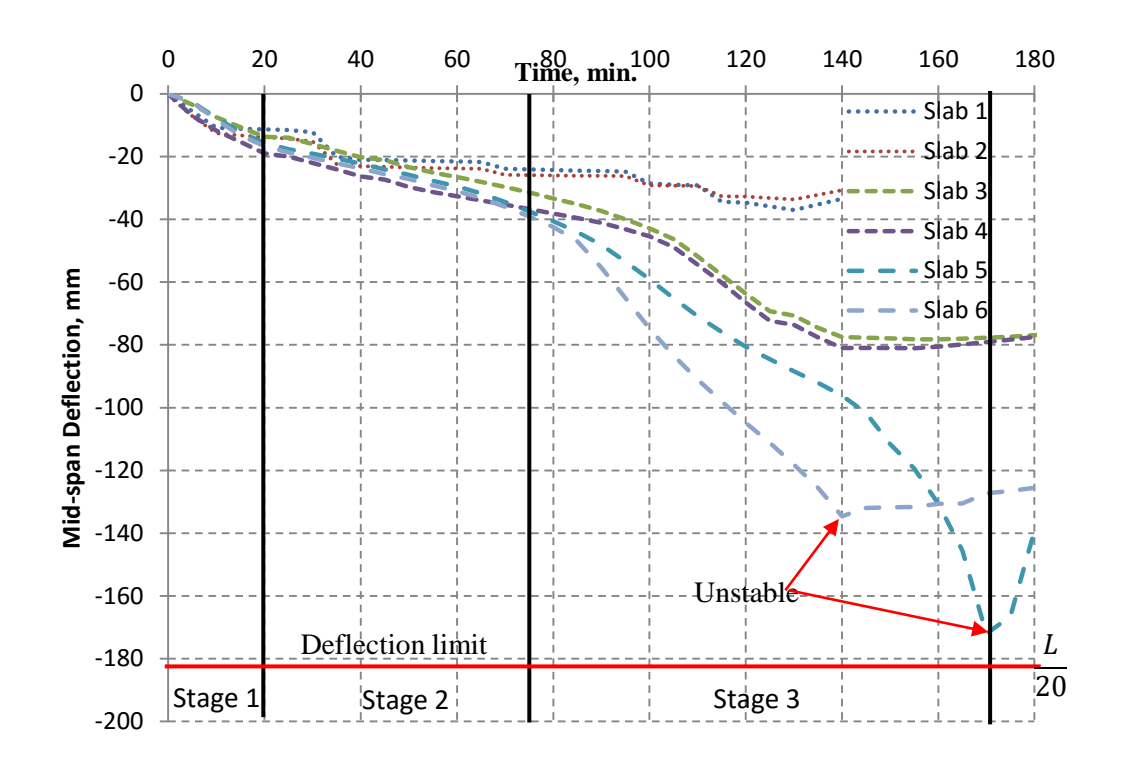


Figure 3.12. Variation of mid-span deflection in test hollowcore slabs with fire exposure time in tested slabs

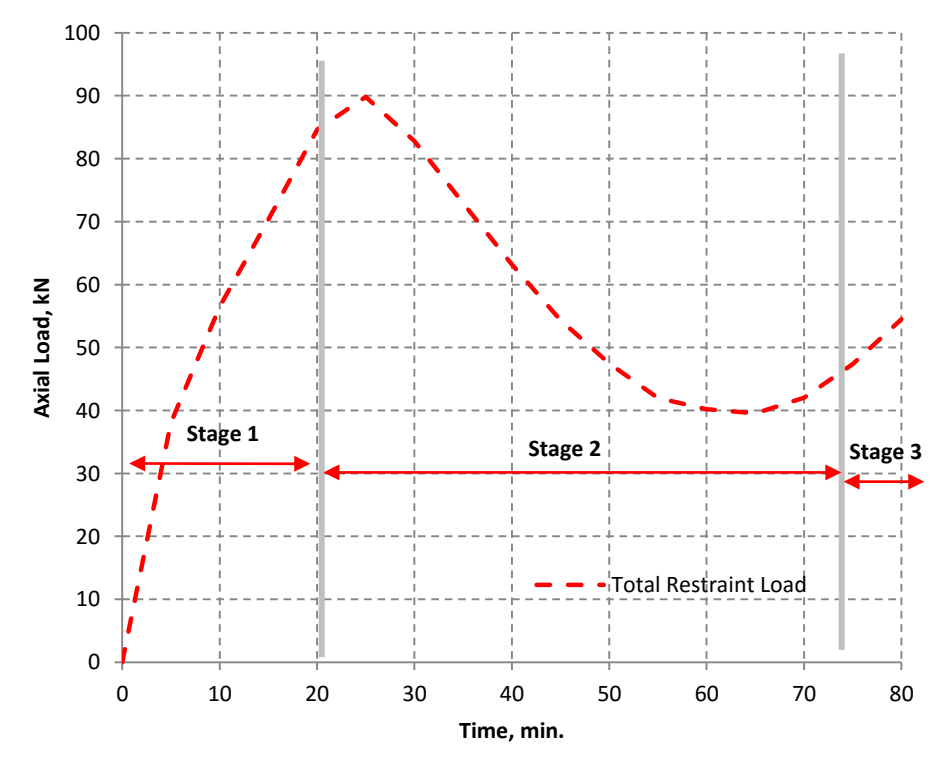


Figure 3.13. Variation of axial restraint forces in Slab 5 with fire exposure time

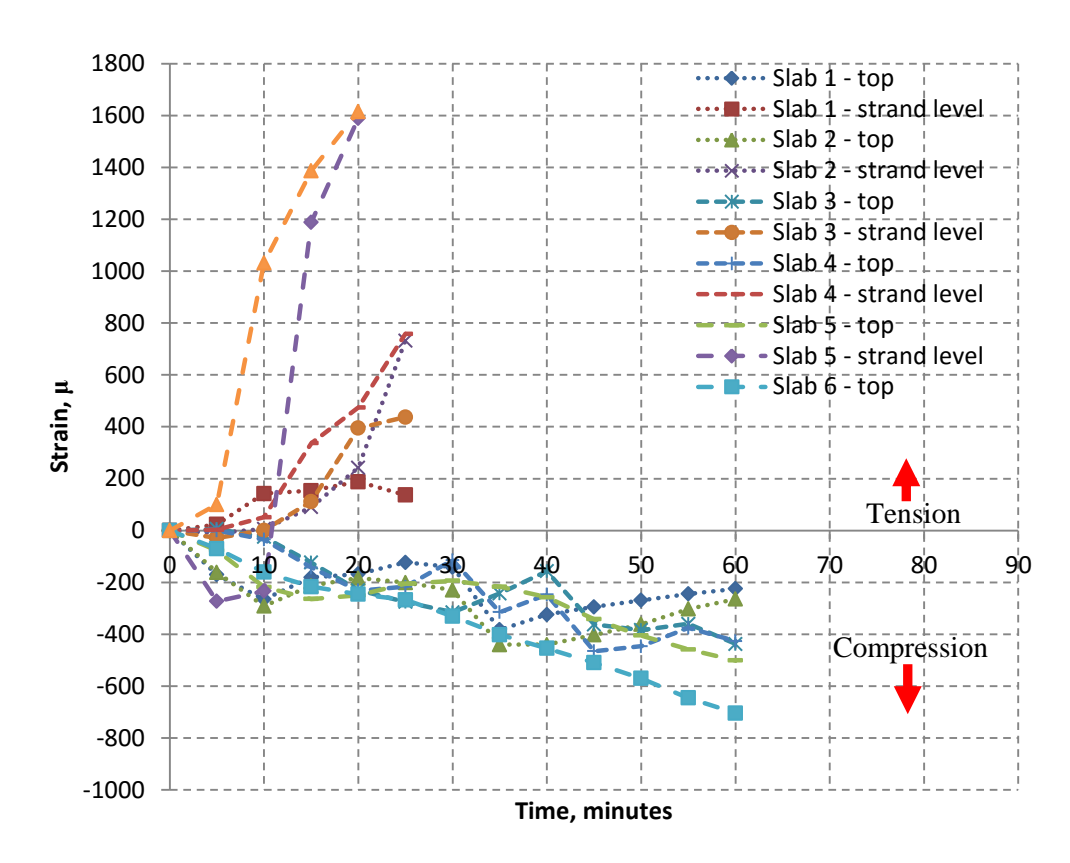
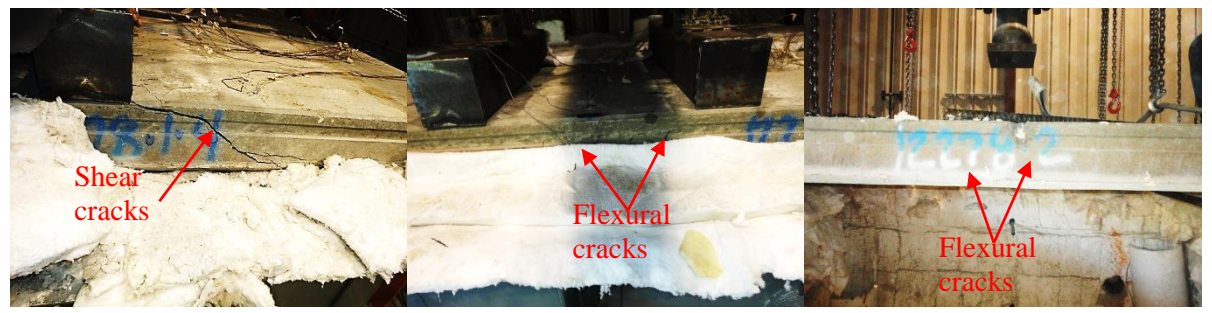


Figure 3.14. Variation of strains in PC hollowcore slabs with fire exposure time in tested slabs



a. Slab 2, longitudinal cracks b. Slab 5, longitudinal cracks c. Slab 6, longitudinal cracks



d. Slab 1, shear cracks

e. Slab 3, flexural cracks

f. Slab 4, flexural cracks



g. Slab 5, flexural cracks

h. Slab 5, mid-span crushing

i. Slab 6, shear cracks

Figure 3.15. Cracking patterns in PC hollowcore slabs under fire exposure

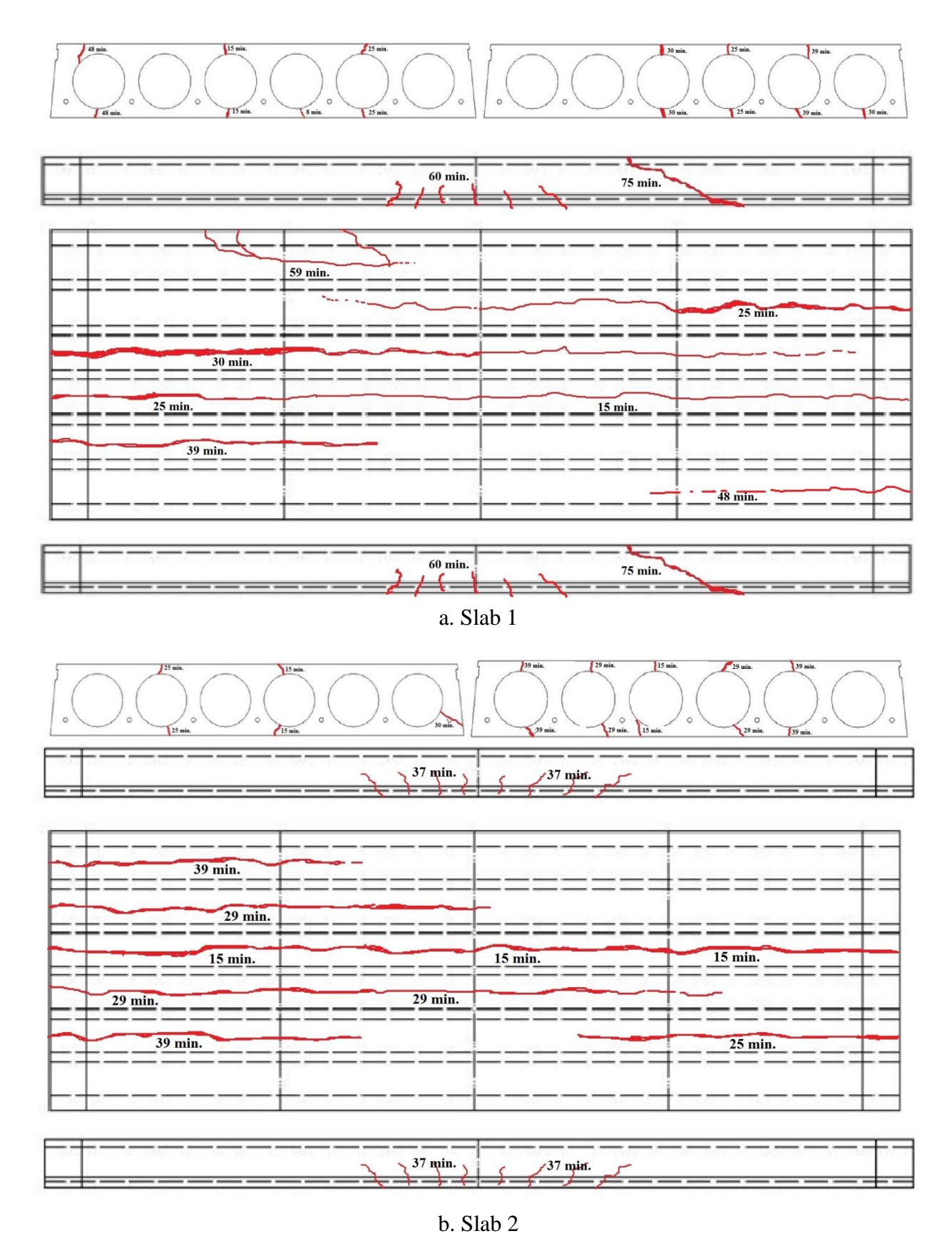
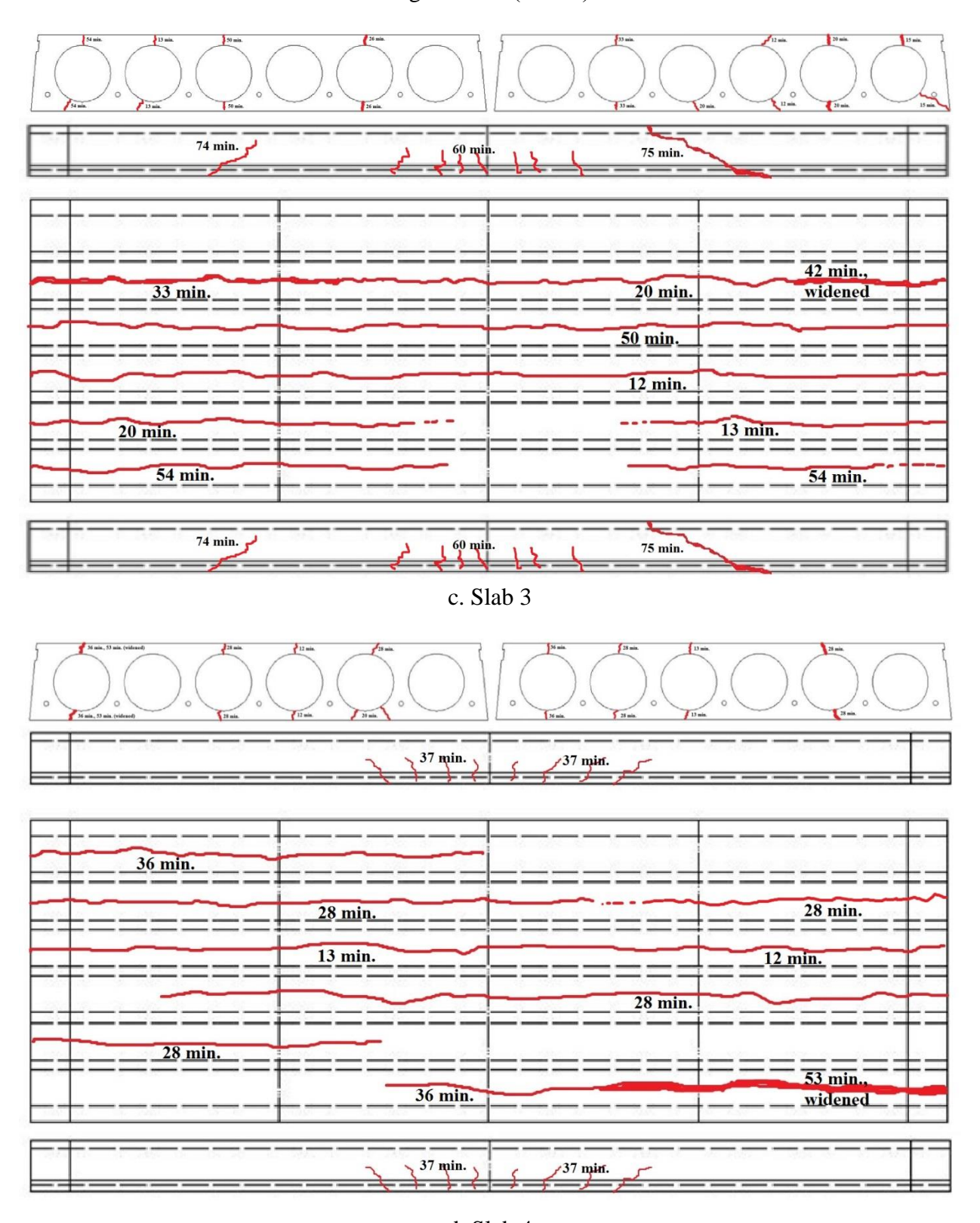


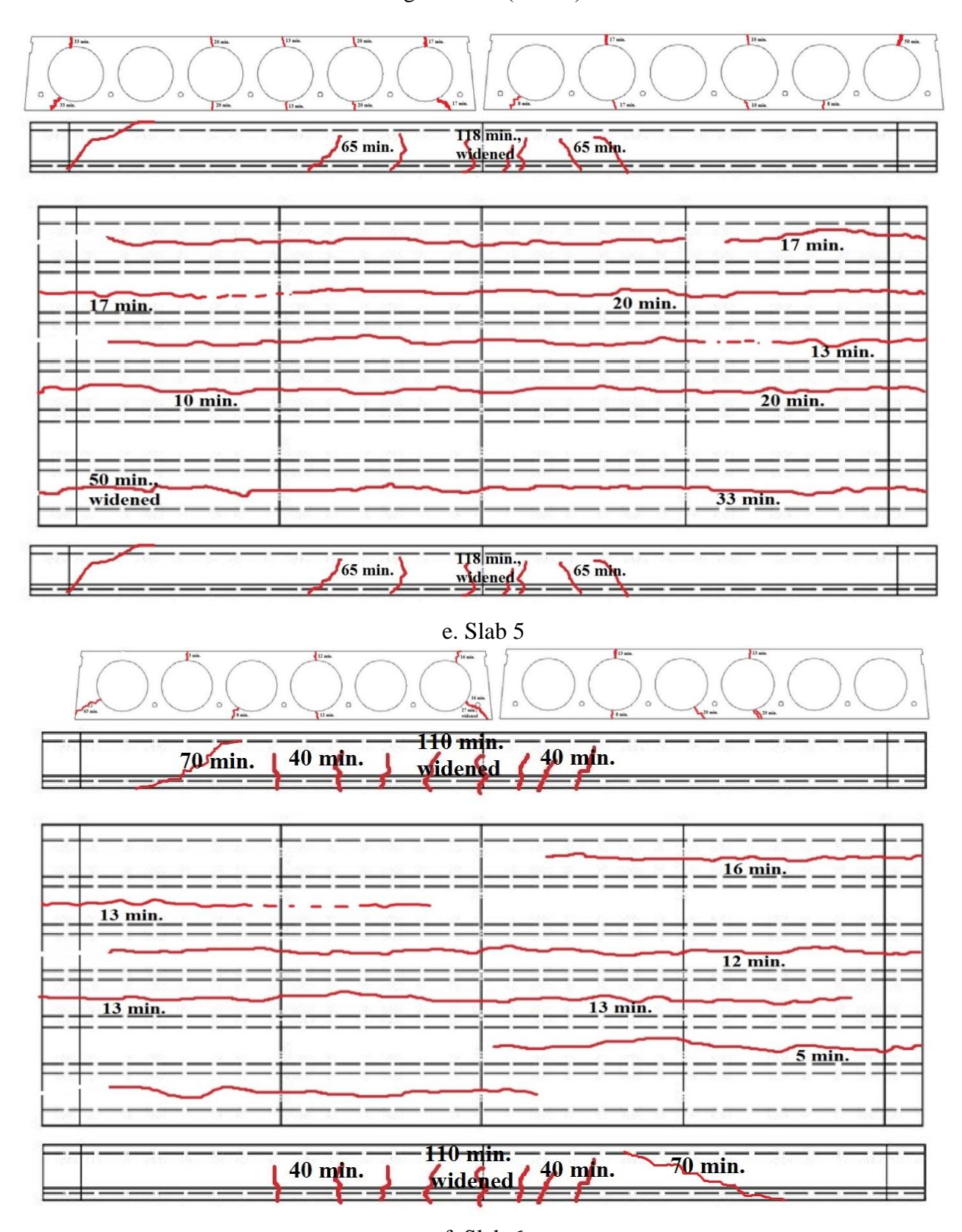
Figure 3.16. Crack progression in tested slabs under combined loading and fire exposure

Figure 3.16. (cont'd)



d. Slab 4

Figure 3.16. (cont'd)



f. Slab 6



Figure 3.17. Extent of spalling in PC hollowcore slabs under fire exposure

3.7 Summary

Fire resistance tests were conducted to study the behavior of PC hollowcore slabs under standard and design fire scenarios, different loading levels, axial restraints and different aggregate types in concrete. Based on these fire tests, the following observations can be drawn on the behavior of PC hollowcore slabs under fire scenarios:

- Hollowcore slabs, similar to the ones discussed in this chapter, can sustain fire exposure for two hours, under service level loading (60% of flexural capacity).
- Fire scenario and load level have significant influence on the fire performance of prestressed hollowcore slabs. Hollowcore slabs exhibit better performance under design fire scenarios than under standard fire scenarios.
- Presence of axial restraint conditions at supports has significant influence on the fire response of hollowcore slabs, and can enhance fire resistance of typical hollowcore slabs by at least 30 minutes.
- Hollowcore slabs fabricated with carbonate aggregate exhibit higher fire resistance than those with siliceous aggregate by up to 10 percent. Siliceous aggregate concrete slabs are more susceptible to fire induced spalling than carbonate aggregate concrete slabs. Also, carbonate aggregate concrete slabs are more prone to shear cracking than siliceous aggregate concrete slabs.

4 MATERIAL PROPERTY TESTS

This chapter is mainly based on the following journal papers:

 Shakya A. M., Kodur V. K. R. Effect of temperature on the mechanical properties of low relaxation seven wire prestressing strand. Journal of Construction and Building Materials, January 2015. (under review)

4.1 General

High-temperature properties of prestressing strand are crucial for evaluating response of PC hollowcore slabs under fire conditions. However, there is very few data on the mechanical properties of prestressing strands under elevated conditions, as previous tests on prestressing strand steel were conducted on individual wire specimens (Gales et al. 2012; Gálvez et al. 2011; Zheng et al. 2007). Data generated for prestressing wires might not represent the response of the prestressing strand comprising of seven wires, as typically used in practice.

Currently, the variation of strength and modulus properties of low relaxation prestressing strand with temperature is specified in various codes namely, ACI 216.1 (ACI 216.1-14 2014), PCI (PCI 2011) and Eurocode 2 (Eurocode 2 2004a). The mechanical properties of prestressing strand are typically specified in terms of strength and modulus degradation in ACI 216.1 and PCI, and in terms of stress-strain relation in Eurocode 2. Thus, mechanical property relations specified in Eurocode 2 are typically utilized for numerical analysis. However, temperature dependent stress-strain relations in Eurocode 2 idealizes the response of prestressing strand into a tri-linear form, by truncating the response at a stress level (typically taken as the yield stress) and

ignoring any strain hardening phase. In addition, Eurocode 2 also assumes continuous increase in ductility in prestressing strand with temperature, as reflected by progressing rupture strain in 20 to 1200°C temperature range. These idealized trends might not represent actual response, as also indicated by some of the recent studies on prestressing bars (Hou et al. 2014) and prestressing wires (Zheng et al. 2007). Data from these studies have clearly shown that high strength prestressing steel exhibits a distinct strain hardening phase beyond yield, and significant reduction in rupture strain in 200 to 500°C temperature range due to "blue brittleness" effect (Hou et al. 2014; Zheng et al. 2007).

To overcome some of the above drawbacks, a series of steady state tensile strength tests were conducted on low relaxation seven-wire prestressing strands, conforming to ASTM-A416 (ASTM 2012a), in the temperature range of 20 to 800°C. To compare the response of prestressing strand with conventional reinforcing bar, series of similar tests were also conducted on Grade 60 rebars with characteristic yield strength of 420 MPa, conforming to ASTM-A615 (ASTM 2012b). Also, additional tests were conducted on prestressing strands under 50 percent stress to evaluate the effect of initial stress on the overall mechanical response of prestressing strand. Data from these tensile tests are utilized to evaluate and propose empirical relations for expressing stress-strain response, variation of elastic modulus, yield point, ultimate point and rupture point as a function of temperature.

4.2 Response of prestressing strand under elevated temperatures

Prestressing strand wires are typically produced by cold-drawing AISI/SAE (American Iron and Steel Institute/ Society of Automotive Engineers) 1080 carbon steel hot-rolled wire rod, of 1185 MPa tensile strength, through a series of 8 or 9 carbide dies to achieve desired mechanical

strength. In this process the cross-sectional area of the rod gets decreased by 85% and thus, the tensile strength gets increased by up to 50% to 1860 MPa, due to "work hardening". Also, these processes introduce low relaxation properties in the prestressing wires which ensure long lasting prestressing force in prestressed concrete members. As required by ASTM-A416 (ASTM 2012a), prestressing strands are fabricated as bundle of seven wires with a larger diameter center wire and other six surrounding wires.

Prestressing strand experiences degradation of mechanical properties at elevated temperatures. For evaluating fire resistance of PC structures the variation of properties of prestressing strand, together with concrete, is required. A review of literature in Chapter 2, show that, there have been number of investigations to study the behavior of prestressing wires and reinforcing bars at elevated temperature (Gales et al. 2011, 2012; Gálvez et al. 2011; Tao et al. 2013; Wang et al. 2013, 2007; Zheng et al. 2007), however there is very limited information on the behavior of low relaxation seven-wire prestressing strand at elevated temperature. Further, there is lack of data on the effect of preload on the degradation of properties of prestressing strands at elevated temperatures.

Stress-strain response of prestressing strand differs significantly from that of reinforcing bar, wherein the prestressing strand exhibits brittle response and lacks a clear demarcation of yield plateau even at room temperature. A typical stress-strain response of prestressing strand at room temperature is compared with that of reinforcing bar in Figure 4.1. Main characteristic points along the stress-strain curve namely, proportional limit, yield point, ultimate strength, plastic deformation, necking and rupture point that bear significant importance for structural design are indicated in Figure 4.1. The proportional limit, in Figure 4.1, represents linear portion of stress-strain curve, wherein the slope is the elastic modulus (E). The yield point is taken as the

intersection of the stress-strain curve and 0.2% strain offset line of the proportional line as recommended in Eurocode 2 (Eurocode 2 2004b) and Eurocode 3 (Eurocode 3 2005). On the other hand, ultimate strength is maximum value of stress in the stress-strain curve, and the rupture point is the point where the strands rupture or break. Deformation up to yield point is typically taken as elastic deformation and any deformation beyond elastic limit is expressed as plastic deformation.

The higher yield strength and ultimate strength in prestressing strand, as compared to that of reinforcing bar, is due to differences in chemical composition and mechanical treatment during manufacturing process. The chemical composition of prestressing strand and steel reinforcing bar are tabulated and compared in Table 4.1. Steel used in prestressing strands has much higher carbon content and also prestressing strand is manufactured through cold-drawing process which significantly increases its tensile strength and also makes it brittle (Hou et al. 2014). Reinforcing bar, on the other hand, has considerably lower carbon content and is typically hot-rolled, without any work hardening process, which results in higher ductility. In addition, steel used in reinforcing bars comprise of additional elements like copper, nickel, vanadium, aluminium and molybdenum, and these elements enhance properties of reinforcing bars such as higher elastic modulus and better retention of strength after exposure to high temperatures (Hou et al. 2014). Much of the currently available data on temperature induced property degradation is for prestressing wires and there is a lack of data on temperature induced property degradation in prestressing strands.

4.3 Experimental program

An experimental program was designed to evaluate mechanical properties of prestressing strand in the temperature range of 20 to 800°C. To study the effect of initial stress (preload) on the stress-strain response of prestressing strand, strand specimens were also tested under initial stress corresponding to 50 percent of room temperature tensile strength before exposing to elevated temperature. Further, to compare the high temperature mechanical response of strand with that of reinforcing bar, tensile tests were also conducted on reinforcing bars in 20 to 800°C temperature range.

4.3.1 Test specimens

For tensile strength tests, 26 prestressing strand specimens of 820 mm length and 12.7 mm diameter were cut from 7 wire prestressing strand spool, fabricated from low-relaxation steel with a characteristic tensile strength of 1860 MPa. Of these specimens, 18 prestressing strand specimens were used for tests without any initial stress and remaining 8 specimens were used for tests with initial stress. For tensile strength tests on reinforcing bars, 18 reinforcing bar specimens of 750 mm in length were cut from Grade 60 - #4 reinforcing bar having 12.7 mm diameter and characteristic tensile strength of 517 MPa. The chemical composition of steel used in prestressing strand and reinforcing bar are tabulated in Table 4.1.

For anchoring prestressing strand specimens to the tensile strength test equipment, steel grips, usually termed as chucks, of 220 kN capacity were used. In the case of reinforcing bar, anchor bolts were welded at reinforcing bar ends for anchoring the reinforcing bars. These two types of anchoring mechanisms for prestressing strand and reinforcing bar are illustrated in Figure 4.2. No slippage of the chuck or the welded anchor bolts after execution of tensile tests at ambient

conditions can be seen in Figure 4.2. This infers that these systems can be reliably used for tensile strength tests at elevated temperature.

4.3.2 Test equipment

For undertaking high temperature tensile strength tests, a specialized test set-up, as shown in Figure 4.3, was designed and fabricated. The test equipment comprises of tensile strength testing machine, an electric furnace, and a data acquisition system. In the tensile strength testing machine, two ends of specimens are anchored at the top and bottom beams through two pairs of clamping brackets. Steel chucks are used in the case of strand, and welded bolt ends are used in the case of reinforcing bar to anchor the specimens, as discussed earlier. The distance between the top and the bottom beams can be adjusted to set to a specific gauge length (approximately 600 mm, as per ASTM-A416 (ASTM 2012a)). Two hydraulic jacks, located at the bottom steel beam, can directly apply specified load to the top beam through high strength extension rods. When hydraulic jacks apply an increasing load, the top beam moves upward and thus, tensile force is applied on the specimen. The load applied to the specimen is measured by a pair of load cells attached to extension rods and the axial deformation of the specimen is measured through an externally placed linear variable displacement transducer (LVDT), with a range of ±38 mm and with an accuracy of 0.0254 mm. The LVDT is attached to the top loading frame through a rigid steel bracket assembly. During the test, the top beam is always maintained in a perfectly horizontal position to minimize eccentric loading during the test.

A small scale electric furnace, fixed in between upper and lower ends of beams, can heat the test specimen to a desired target temperature. The electric furnace comprises of cylindrical chamber with an inner diameter of 203 mm and an inner height of 254 mm. The temperature in the furnace can reach up to 1000°C, and target temperature, heating rate and stabilization duration

can be programmed into the furnace through a control module. Three internal thermocouples mounted on the interior walls of furnace monitor the furnace temperature at upper, middle and lower zones. The average reading of these three thermocouples is taken as the furnace temperature. In addition, two thermocouples were directly attached to the specimen to monitor the actual specimen temperature during high temperature tests. The load cells, LVDT, and specimen thermocouples are connected to a data acquisition system, wherein applied load, displacement and furnace and specimen temperatures on the specimen can be recorded every 0.01 second. Through this setup, tensile strength test can be conducted by heating prestressing strand or reinforcing bar specimens to a desired temperature and then subjecting it to tensile loading.

4.3.3 Test procedure

After anchoring the test prestressing strand or reinforcing bar specimen between the top and the bottom clamping brackets, two thermocouples were attached to the specimen, one at the midlength and other at a depth of 250 mm above the mid length, to monitor temperatures in the specimen. The furnace door was then closed and heating was turned-on so as to attain a target temperature. The heating rate in the furnace was set to 10°C per minute as specified by Twilt (1988) (Twilt 1988). This rate of heating has also been adopted in previous tensile tests on prestressing and reinforcing bars (Hou et al. 2014; Zheng et al. 2007), and ensures reaching the target temperature without much effect of temperature induced creep in the specimens. All tests were conducted under steady state condition wherein, once the target temperature was reached it was maintained at that temperature for about 30 minutes so as to ensure uniform temperature (± 5°C) along the length of the specimen. After temperature along the specimen stabilized, hydraulic pumps, attached to loading jacks, were turned-on and loading was applied on the

specimen at strain rate of 0.005±0.002 per minute (ASTM 2003), until failure occurred in the specimen. The applied loading and displacement, along with the temperature on the specimen, were recorded through a data acquisition system.

In the case of prestressing strand with initial stress, the strand specimens were loaded to 50 percent of the room temperature tensile strength, and then exposed to a predetermined target temperature. After temperature was stabilized, additional loading was applied in increments until failure occurred in the strand.

Tensile strength tests on prestressing strand were carried out at nine temperature points, namely 20, 100, 200, 300, 450, 500, 600, 700 and 800°C. Tests on strand with 50 percent initial stress were carried out at four temperature points of 100, 200, 300 and 450°C. Tests with initial stress were limited to temperature 450°C or below, as a test at 500°C with 50 percent initial stress resulted in sudden failure of the strand indicating that high temperature creep effects dominate at temperatures beyond critical temperature of strand (~450°C). Thus, no results are presented for temperatures beyond 450°C for specimens with initial stress.

Similarly, tests on reinforcing bar were carried out at nine target temperatures of 20, 100, 200, 300, 400, 500, 600, 700 and 800°C. In each of these tests, two specimens were tested at each temperature and the average of the two readings is taken to evaluate the response parameters.

4.4 Results and discussion

Data generated from tension tests is utilized to plot temperature-dependent stress-strain curves for prestressing strand and reinforcing bar. These stress-strain curves were further utilized to derive yield strength, ultimate tensile strength, elastic modulus, and failure characteristics of prestressing strand and reinforcing bar at various temperatures.

4.4.1 Stress-strain response

The stress-strain response at various temperatures for prestressing strands is plotted in Figure 4.4, whereas that for prestressing strands with 50 percent initial stress and reinforcing bars are plotted in Figure 4.5 and Figure 4.6 respectively. Prestressing strand exhibits only a slight loss of strength up to 200°C and thus, the stress-strain response at 100°C and 200°C follow a trend similar to that at room temperature (20°C). Beyond 200°C, prestressing strand starts to lose its strength at a rapid pace with increase in temperature. Also a significant reduction in failure strain occurs in 200 to 500°C temperature range. This reduction in failure strain in 200-500°C can be attributed to blue brittleness effect (Hou et al. 2014; Zheng et al. 2007), which decreases the ductility of prestressing steel. At 600°C, prestressing strand undergoes large deformations due to softening of steel, with yielding occurring at lower stress levels which leads to reduction in the slope of the linear-elastic section of the stress-strain curve. At 700°C and 800°C, there is no clear demarcation in the initial linear-elastic portion of the stress-strain curve due to further softening of steel. Beyond 500°C, strain at which failure occurs rapidly increases showing significant increase in ductility.

Prestressing strand with 50 percent initial stress exhibits similar stress-strain response as that of prestressing strand without any initial stress. However, there is slight decrease in ultimate strength in strands with initial stress. Also, as can be seen in Figure 4.5, there is reduction of failure strain in 200 to 450°C temperature range, which is similar to the trend as that of strand without initial stress. In this temperature range, the presence of initial stress for a relatively short duration does not significantly affect the behavior of prestressing strand.

Reinforcing bar exhibits similar overall response, but do not undergo significant strength loss in 20 to 400°C range (see Figure 4.6). Reinforcing bar also exhibits a reduction in failure strains in 20 to 500°C temperature range due to blue brittleness effect, similar to that observed in

prestressing strand. Beyond 400°C, reinforcing bar undergoes significant reduction in strength, combined with large increase in failure strains beyond 500°C. These large deformations beyond 500°C in reinforcing bars are due to softening of steel from exposure to very high temperature. The distinct demarcation on linear-elastic portion of the curve disappears in 700 to 800°C temperature range, similar to that in prestressing strand.

4.4.2 Yield strength and ultimate strength

The mechanical behavior of steel is typically characterized based on its yield strength, ultimate strength and elastic modulus. From the generated stress-strain response, yield strength, ultimate strength, elastic modulus, yield strain and failure strain values were evaluated at various temperatures and these values are tabulated in Table 4.2. The normalized yield and ultimate strength with respect to room temperature yield and ultimate strength are plotted as a function of temperature in Figure 4.7 and Figure 4.8 respectively. The yield strength of prestressing strand and reinforcing bar correspond to the 0.2% offset strain, while ultimate strength corresponds to peak stress just prior to commencement of necking phase (see Figure 4.1).

Tests results show that both yield strength and ultimate strength degrade in both reinforcing bar and prestressing strand in 20 to 800°C temperature range. The rate of degradation of yield and ultimate strength is higher in prestressing strand, as compared to that of reinforcing bar, as can be seen in Figure 4.7 and Figure 4.8. Further, both yield and ultimate strength values are slightly lower in strand with 50 percent initial stress, but the rate of strength degradation is slightly higher. This can be attributed to the fact that under the combined action of initial stress and temperature, steel undergoes significant thermal creep due to movement and rearrangement of dislocations within the microstructure (Hou et al. 2014). However, the extent of creep deformations largely depends on the duration of exposure to high temperature. Since the

exposure duration in current tests is relatively short (30 minutes), the differences between the unloaded and loaded tension tests are within 5 percent and can be deemed somewhat to be insignificant in 20 to 450°C temperature range.

Close observations of Figure 4.7 and Figure 4.8 also show that strength retention in prestressing strand is generally lower than that in reinforcing bar over the temperature range of 20 to 800°C. Prestressing strand does not experience any loss of yield strength and only slight loss of ultimate strength in 20 to 200°C range, whereas reinforcing bar experience an insignificant loss of yield and ultimate strength in 20 to 400°C. Beyond 200°C, prestressing strand undergoes a faster reduction in yield and ultimate strength as compared to reinforcing bar wherein, rapid loss of strength in reinforcing bar occur only beyond 400°C. At 800°C, prestressing strand loses about 95% of ultimate strength, which is higher than that of reinforcing bar which loses about 80 percent ultimate strength at 800°C, as can be seen in Figure 4.8.

The differences in the rate of strength degradation in prestresssing strand and reinforcing bar can be attributed to differences in the chemical composition and heat treatment process during production of these steels (Chawla 2008). Prestressing strands are made from steel with much higher carbon content (0.83% by weight, that is more than double) as compared to the type of steel used in reinforcing bars (0.39% by weight) (see Table 4.1). Further, reinforcing bars are manufactured through hot-forging method, whereas prestressing steel strands are manufactured through cold-drawn process (inducing work hardening), to achieve higher strength at room temperature. Due to this cold-drawn process the microstructure of prestressing strand steel undergoes formation of martensite crystalline structures, which is metastable and temperature sensitive (Hou et al. 2014). When prestressing steel is exposed to elevated temperature, the microstructure changes from martensite to pearlite which is very ductile and soft with reduced

strength (Chawla 2008). On the other hand, the reinforcing steel possesses a more regular microstructure, referred to as ferrite-cementive, which has a smaller dislocation density and a lower strength than martensite (Hou et al. 2014). The strength degradation in steels at elevated temperatures is caused by recovery of these dislocations and recrystallization process. Thus, at high temperature, reinforcing steel exhibits limited recovery of dislocations and recrystallization (Felicetti et al. 2009) which leads to less severe strength degradation in reinforcing bar than in prestressing steel strand.

4.4.3 Yield strain and failure strain

To illustrate the variation of ductility with temperature rise, the ratio of yield strain (ε_y) and ultimate strain (ε_k) to corresponding room temperature strains are plotted as a function of temperature in Figure 4.9 and Figure 4.10. The measured yield and ultimate strain of prestressing strand and reinforcing bar corresponding to various temperatures are also tabulated in Table 4.2. The yield and failure strain corresponds to the strains at which yield and fracture of prestressing strand occur, as discussed in Section 4.2.

Data from tests show that yield strain (ε_y) decreases in both prestressing strand and reinforcing bar throughout 20 to 800°C temperature range. At 450°C, the yield strain of prestressing bar is about 70 percent of failure strain at room temperature. Similarly, results plotted in Figure 4.10 show that there is no significant change in failure strain (ε_k) up to 200°C and there is rapid decrease in the failure strain in 200 to 500°C temperature range in prestressing strand. However, in the case of reinforcing bar, failure strain decrease in 20 to 500°C range. This decrease in failure strain in both strand and reinforcing bar is due to aging of carbon and nitrogen interstitial atoms typically occurring below 500°C range, which is also referred to as blue brittleness effect (Dolzhenkov 1971). The temperature range at which this phenomenon occurs varies with the

chemical composition of steel (Wang et al. 2013). Beyond 450°C, the prestressing strand experiences significant increase in failure strain, reflecting higher ductility, and at 800°C failure strain increases 1.8 times of its original strain at room temperature, which is significantly higher than that observed in reinforcing bar. This is due to the fact that the ductility of prestressing strand at elevated temperatures is significantly improved through purification by removal of interstitial impurities (Abiko 1995). Reinforcing steel exhibits similar increase in failure strain and ductility at temperatures above 500°C.

Both prestressing strand and reinforcing bar possess highest ductility at 800°C. At 800°C, test specimens continued to stretch without experiencing rupture and the tests had to be terminated due to reaching maximum extension (limiting) lengths in the loading jacks. Thus, failure strains for specimens at 800°C were calculated indirectly by readjusting the extension length of loading jacks and continuing the tests until failure occurred in the specimens.

4.4.4 Elastic modulus

The elastic modulus of the prestressing strand and reinforcing bar are deduced at various temperatures from plotted stress-strain curves, as the secant modulus of the initial elastic portion of corresponding curves. The elastic modulus ratio, defined as the ratio of the elastic modulus at a given temperature to that at ambient temperature, are compared in Figure 4.11 for prestressing strand and reinforcing bar. The elastic modulus of prestressing strand is slightly lower than that of reinforcing bar, as can be seen in Figure 4.4 and Figure 4.6 and this is due to differences in chemical compositions in steels (see Table 4.1). Unlike reinforcing bar, prestressing strand does not have additional elements such as copper, nickel, vanadium, aluminium and molybdenum (see Table 4.1) resulting in the lower elastic modulus (Hou et al. 2014).

A close observation of trends in Figure 4.11 indicate that the elastic modulus decrease with increase in temperature and show a similar degradation trend in both prestressing strand and reinforcing bar. However, the rate of degradation of elastic modulus in prestressing strand is slightly higher than that in reinforcing bar, especially beyond 500°C. On the other hand, presence of preload is observed to have minimal effect on the degradation rate of elastic modulus of prestressing strand and this can be attributed to relatively shorter exposure (temperature) duration.

4.4.5 Failure patterns

The failure patterns in prestressing strand and reinforcing bar at various temperatures are shown in Figure 4.12. It can be seen from this figure that the necking length decrease in both strand and reinforcing bar in 20 to 500°C temperature range. This decrease in necking length indicates reduction in ductility which leads to lower failure strains as discussed in Section 4.4.3. On the other hand, necking length continuously increase beyond 500°C in prestressing strand and reinforcing bar due to interstitial purification process (Hou et al. 2014). In Figure 4.12, this is also reflected by higher degree of tapering of critical section in 500 to 800°C temperature range. In the case of prestressing strand with 50 percent initial stress, a distinct fraying failure pattern is noticed in 20 to 300°C range and this is attributed to the fact that the failure in these strands occur by breakage of individual wires in succession, as can be seen in Figure 4.12(c). Presence of initial stress introduces stress concentrations at critical locations (points) in these strands leading to failure of strand by breakage of each individual wire at different times in succession. A similar failure pattern is observed in strands without initial stress at 20 and 100°C (see Figure 4.12(a)) due to higher stress level at low temperatures. This fraying failure pattern does not occur

when the ductility of the strand increases at high temperature, wherein failure rather occurs by necking and tapering of the critical section (see Figure 4.12 (a) and (c)).

4.4.6 High temperature property relations

Data generated from the above property tests are utilized to generate high temperature stress-strain relationships for prestressing strand. Relations for yield strength, tensile strength, failure strain and elastic modulus are expressed as a function of temperature in 20 to 800°C range.

4.4.7 Relation for stress-strain response

Based on data generated from high temperature tensile tests, a stress-strain response relation is derived. This relation, similar to that for stress-strain relation at room temperature (see Figure 4.1), captures different salient features as observed in stress-strain tests at elevated temperatures. The proposed relations for representing temperature dependent mechanical behavior of seven-wire prestressing strand is similar to the one proposed by Hou et al. (Hou et al. 2014) for prestressing strand and by Tao et al. (Tao et al. 2013) for reinforcing bars. The proposed relations for stress-strain response given in Equation 1 is a quadri-linear stress-strain curve to represent four important stages of the behavior namely, proportional limit, yield point, ultimate point, and rupture point. This relation is applicable over 20 to 800°C temperature range.

$$\sigma = E_{T} \times \varepsilon \qquad 0 \leq \varepsilon \leq \frac{\sigma_{pT}}{E_{T}} \qquad (4.1)$$

$$\sigma = \frac{\sigma_{yT} - \sigma_{pT}}{\varepsilon_{yT} - \frac{\sigma_{pT}}{E_{T}}} \times \left(\varepsilon - \frac{\sigma_{pT}}{E_{T}}\right) \qquad \frac{\sigma_{pT}}{E_{T}} < \varepsilon < \varepsilon_{yT}$$

$$\sigma = \frac{\sigma_{uT} - \sigma_{yT}}{\varepsilon_{uT} - \varepsilon_{yT}} \times \left(\varepsilon - \varepsilon_{yT}\right) + \sigma_{0.2T} \qquad \varepsilon_{0.2T} < \varepsilon < \varepsilon_{uT}$$

$$\sigma = \frac{\sigma_{kT} - \sigma_{uT}}{\varepsilon_{kT} - \varepsilon_{uT}} \times \left(\varepsilon - \varepsilon_{uT}\right) + \sigma_{uT} \qquad \varepsilon_{uT} < \varepsilon < \varepsilon_{kT}$$

$$20^{\circ}\text{C} \leq \text{T} \leq 800^{\circ}\text{C}$$

where,

 σ_p = stress values in proportional limit

 ε_p = strain values in proportional limit

 σ_v = yield stress

 $\varepsilon_{\rm v}$ = yield strain

 σ_u = ultimate stress

 $\epsilon_u = ultimate \ strain$

 σ_k = failure or rupture stress

 ε_k = failure or rupture strain

E = Elastic modulus

Subscripts:

_p = prestressing strands

_{pl} = prestressing strands with preload

 $_{rs}$ = reinforcing bars

 $_{\rm b}$ = prestressing bars

 $_{T}$ = temperature

To illustrate the applicability of proposed quadri-linear stress-strain model, stress-strain response predicted from proposed equation is compared with the measured stress-strain curve for various temperatures, as shown in Figure 4.13. A good correlation between these two sets of curves indicates that the proposed quadri-linear stress-strain expression can be utilized to represent stress-strain relation for low relaxation seven-wire prestressing strand.

The stress-strain response predictions from Equation 4.1 is also compared with that from Eurocode 2 (Eurocode 2 2004a) in Figure 4.14. Eurocode 2 expresses the stress-strain relation

for prestressing strand as a tri-linear model, unlike the proposed model which expresses the response as a quadri-linear model. From the figure it is evident that, the equation specified in Eurocode 2 ignores the strain hardening phase of the prestressing strand and gives a continuous increase in failure strains, even in 200 to 500°C, which is not representative of the trends observed in many previous studies (Hou et al. 2014; Zheng et al. 2007). Further, Eurocode 2 material property model yields slightly higher elastic modulus in 20 to 200°C temperature range as compared to the proposed model. The stress-strain relationship of prestressing strand proposed by Eurocode 2 is over conservative based on strength and under conservative based on failure or rupture strains and thus, might not be representative of the entire range of stress-strain behavior.

4.4.8 Relation for mechanical properties

In addition to stress-strain relations, empirical equations for variation of yield strength (σ_{yT}/σ_y) , ultimate strength (σ_{uT}/σ_u) , failure strain $(\epsilon_{kT}/\epsilon_k)$ and elastic modulus (E_T/E) , are proposed as a function of temperature, and are listed in Table 4.3. These relations are derived through a regression analysis or curve fitting of data generated from tensile strength tests. The accuracy of the regression analysis is represented by the coefficient of determination (R^2) , and is calculated to be the ratio of the sum of squares of deviations of the response values to their predictor. The value of R^2 has to lie between 0 and unity, with '1' showing a perfect fit to the curve (Kodur and Shakya 2013). These generated relations obtained through regression analysis show R^2 values ranging from 0.96 to 1, showing reasonably good fit. To illustrate the applicability of proposed relationships, predicted property response is compared with measured response for prestressing strand, as shown in Figure 4.7, Figure 4.8, Figure 4.10 and Figure 4.11. A good correlation shows that the proposed relation can be effectively utilized to represent the response under elevated temperature.

4.5 Design implications

Accurate definition of mechanical properties of prestressing strand is critical in evaluating realistic fire resistance of prestressed concrete members. Currently, high temperature mechanical response of prestressing steel are evaluated using individual wire specimens, which does not represent the true response of strand comprising of multiple wires. One of the direct implications of this discrepancy is in numerical simulations on fire response of prestressed concrete structures, wherein prestressing strand is modeled as a single steel wire which requires material property definition of the strand (wire bundle) rather than that of individual wire. On the other hand, material model for prestressing strand currently available in Eurocode 2, ignores some of the important features of the response, such as strain hardening phase and decrease in failure strain in 200 to 500°C temperature range. The stress-strain relation proposed in this study overcomes some of these drawbacks and presents a high temperature mechanical behavior of low relaxation seven-wire prestressing strand. The proposed high temperature mechanical property relations for prestressing strand can be utilized as input in the computer programs for evaluating the response of prestressed concrete structures exposed to fire.

Table 4.1. Chemical compositions of prestressing strand and reinforcing bar

Type of steel	Prestressing strand (Cold-drawn)	Reinforcing bar (Hot- rolled)
Composition	% by weight	% by weight
Carbon	0.810-0.840	0.390
Silicon	0.220-0.300	0.380
Manganese	0.660-0.720	0.76
Phosphor	0.012-0.015	0.022
Sulfur	0.011-0.014	0.030
Chromium	0.130-0.220	0.130
Copper	n.p.	0.110
Nitrogen	n.p.	0.02
Nickel	n.p.	0.070
Vanadium	n.p.	0.020
Aluminium	n.p.	0.005
Molybdenum	n.p.	0.020

Note: 'n.p.' = not present

Table 4.2. Measured yield and ultimate strength and strain of prestressing strand (without and with preload) and reinforcing bars

Temp (°C)	Yield strength (σ _v), MPa		Ultimate strength (σ _u), MPa		Yield strain (ε_{v}) , m/m		Failure strain (ε_k) , m/m					
	PS	PS – 50%	RS	PS	PS – 50%	RS	PS	PS – 50%	RS	PS	PS – 50%	RS
20	1690	1690	509	1893	1893	701	0.021	0.021	0.0100	0.064	0.064	0.130
100	1644	1628	527	1897	1811	702	0.020	0.019	0.0090	0.068	0.068	0.097
200	1482	1416	495	1712	1629	678	0.018	0.017	0.0080	0.060	0.055	0.075
300	1170	1162	500	1441	1366	670	0.015	0.013	0.0085	0.040	0.039	0.068
400	-	-	490	-	-	599	-	-	0.0079	_	-	0.052
450	962	836	-	971	843	-	0.016	0.014	-	0.031	0.030	-
500	604	-	399	606	-	403	0.013	-	0.0070	0.033	-	0.020
600	291	-	270	324	-	281	0.007	-	0.0055	0.083	-	0.027
700	158	-	188	175	-	200	0.007	-	0.0045	0.104	-	0.070
800	65	-	120	98	-	158	0.004	-	0.0038	0.120	-	0.120

Note: 'PS' = prestressing strand, 'PS – 50%' = PS with preload, 'RS' = reinforcing bar, '-' = not available

Table 4.3. High temperature mechanical property relations for prestressing strand

Property	Relationship	R^2	Equation
Floperty	Relationship	Value	no.
Yield strength (σ _y), MPa	$\sigma_{yT}/\sigma_{y} = 6^{-12} \times T^{4} - 6^{-09} \times T^{3} - 9^{-08} \times T^{2} - 0.0006 \times T + 1.0196$	0.989	(4.2)
Ultimate strength (σ_u), MPa	$\sigma_{uT}/\sigma_{u} = 1^{12} \times T^{4} + 3^{09} \times T^{3} - 6^{06} \times T^{2} + 0.0006 \times T + 0.9895$	0.996	(4.3)
Failure strain (ε_k), m/m	$\epsilon_{kT}\!/\epsilon_k = -7^{-11}\times T^4 + 1^{-07}\!\times\! T^3 - 6^{-05}\!\times\! T^2 + 0.0082\!\times\! T + 0.8276$	0.967	(4.4)
Elastic modulus (E), MPa	$E_{T}\!/E = 7^{-12}\!\times\! T^4 - 9^{-09}\!\times\! T^3 + 2^{-06}\!\times\! T^2 - 0.0002\!\times\! T + 1.0099$	0.968	(4.5)

Note: 'T' = temperature

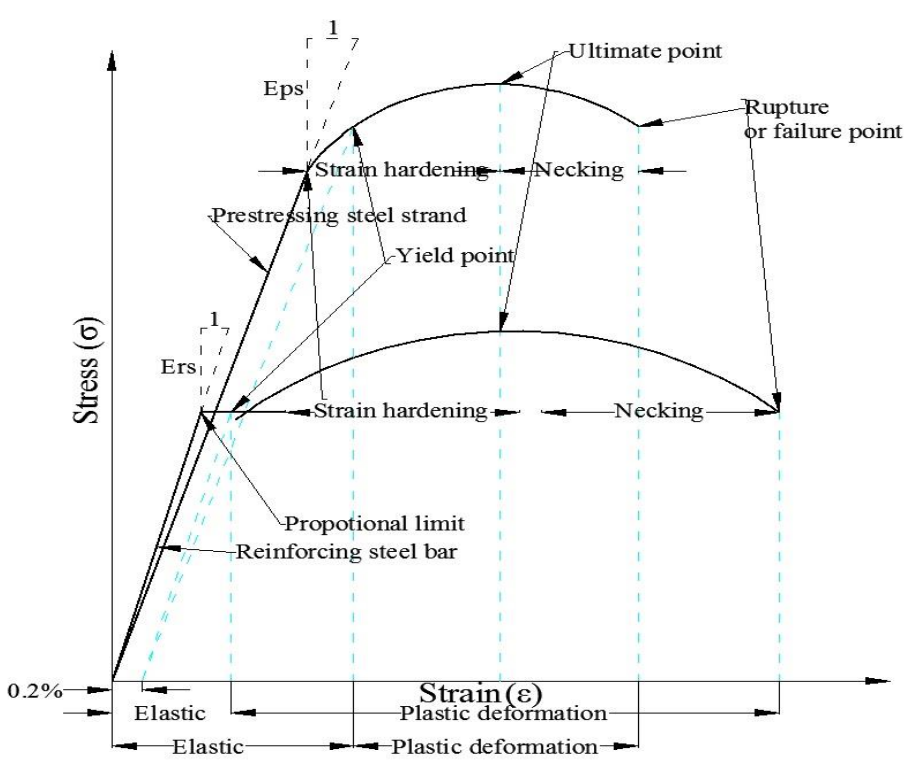
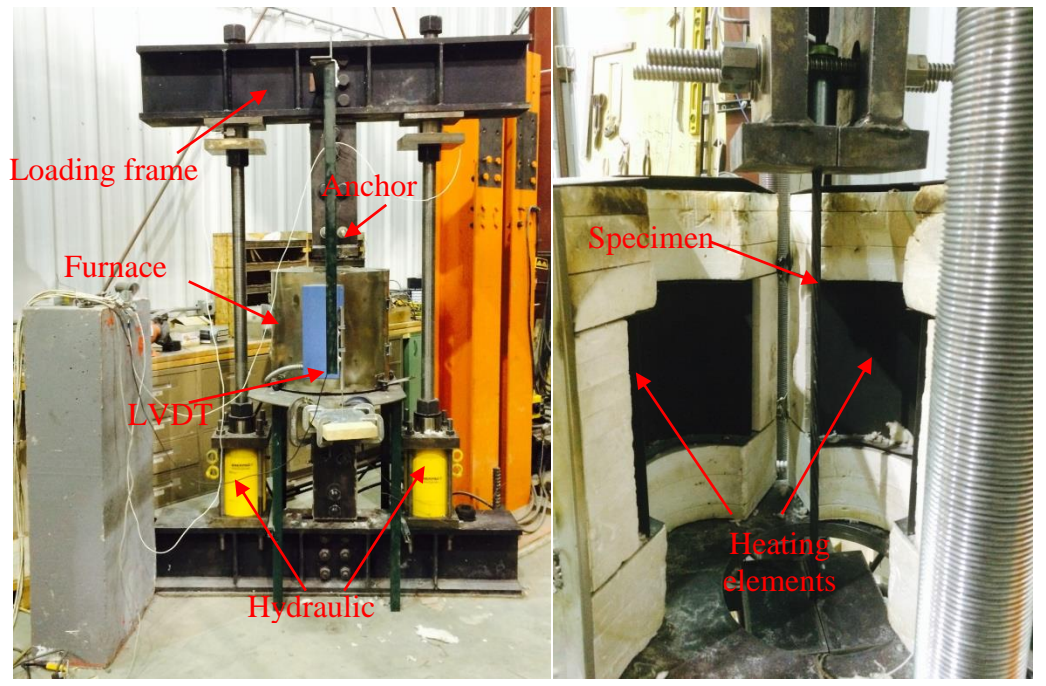


Figure 4.1. Typical stress-strain response of prestressing strand and reinforcing at room temperature

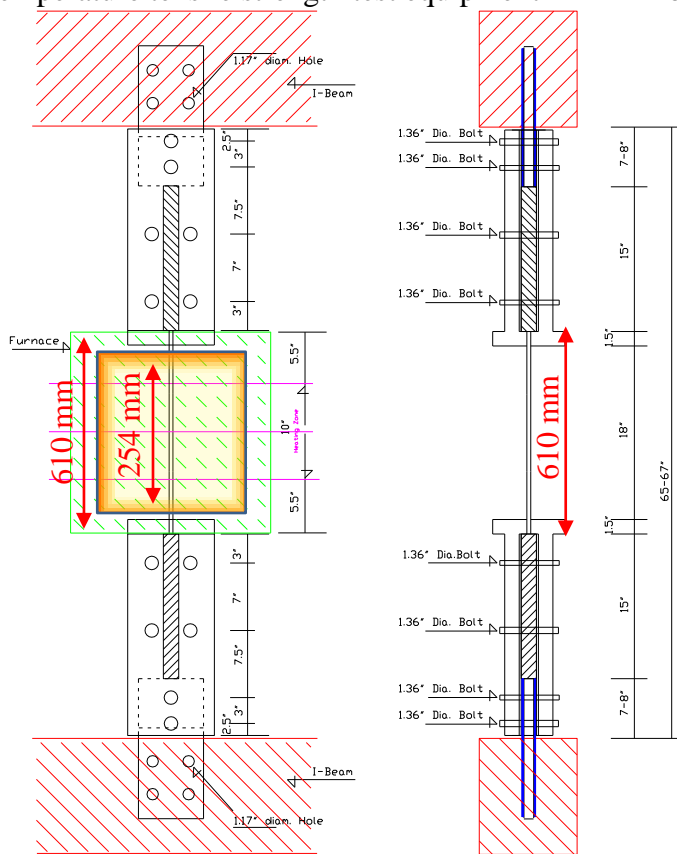


a. Chucks for prestressing strand b. Welded anchor bolts for reinforcing bar Figure 4.2. Typical specimen anchorage system for tensile strength tests at elevated temperatures



a. High temperature tensile strength test equipment

b. Furnace



c. East-West elevation d. North-South elevation

Figure 4.3. Test setup for tensile strength tests on prestressing strand and reinforcing bar at elevated temperatures

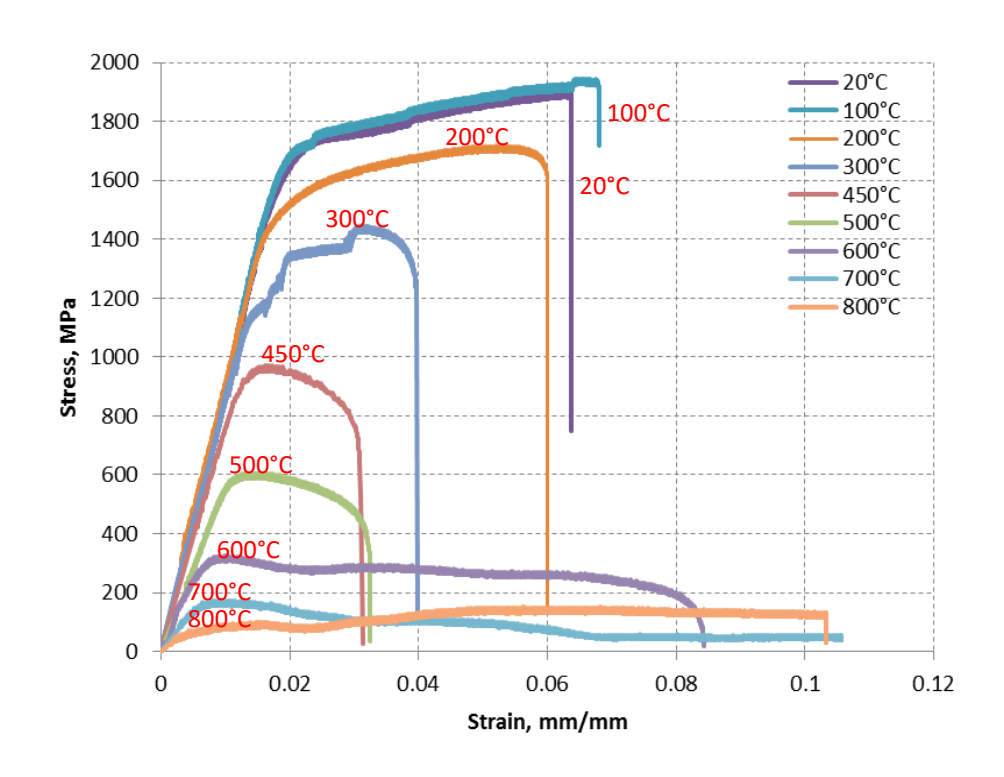


Figure 4.4. Stress-strain response of prestressing strand at various temperatures

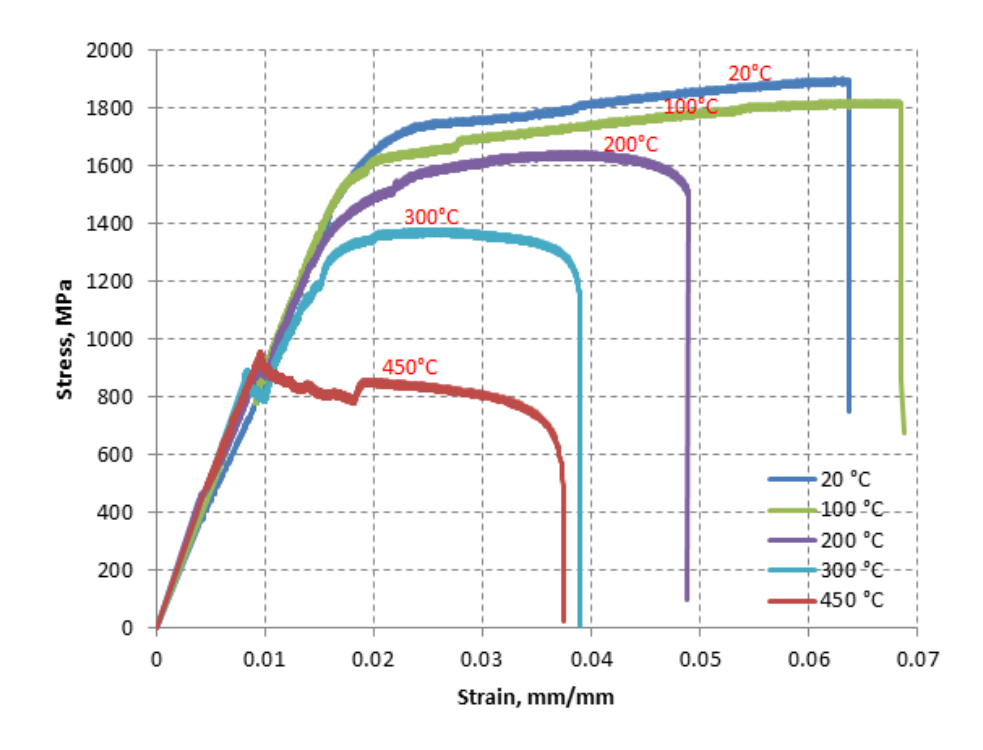


Figure 4.5. Stress-strain response of prestressing strand with 50% initial stress at various temperatures

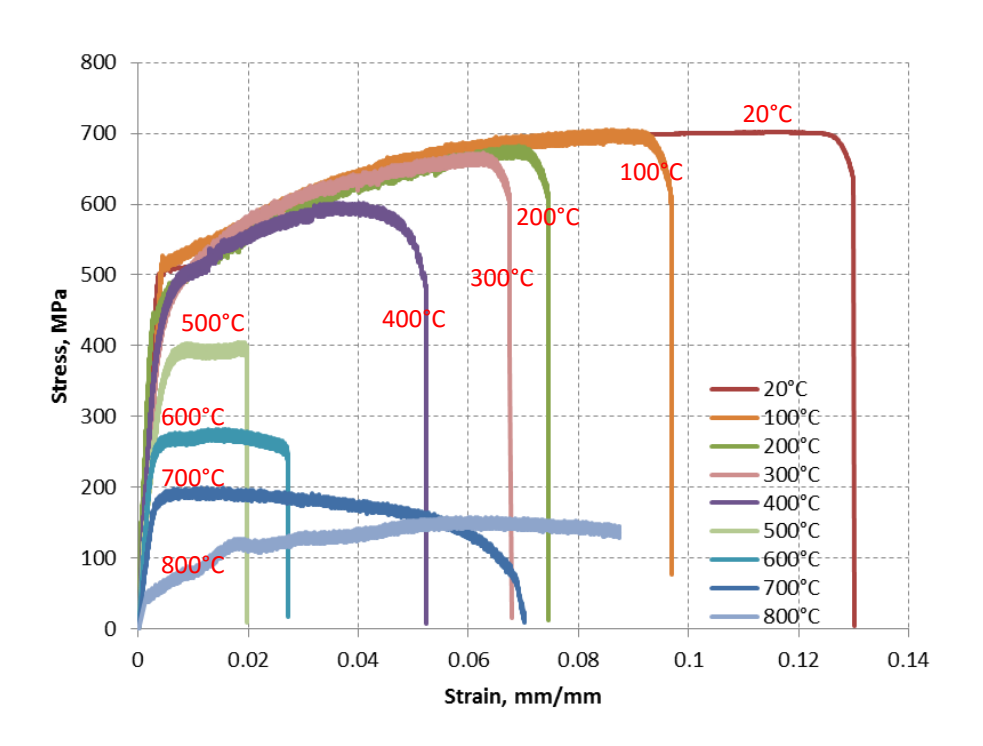


Figure 4.6. Stress-strain response of reinforcing bar at various temperatures

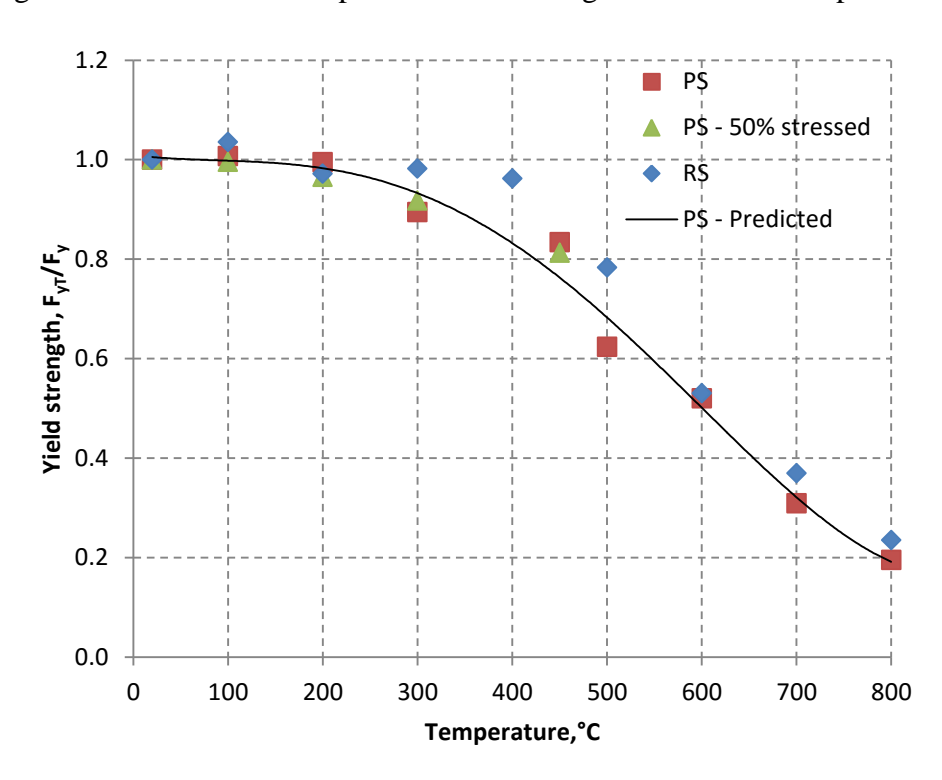


Figure 4.7. Comparison of normalized yield stress of prestressing strand and reinforcing bar

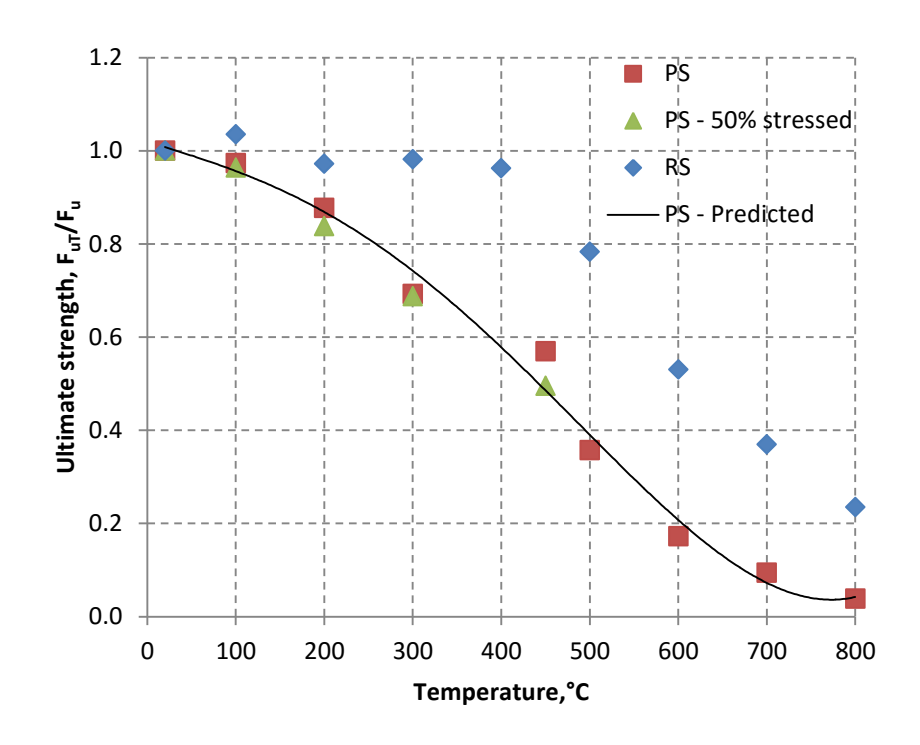


Figure 4.8. Comparison of normalized ultimate stress of prestressing strand and reinforcing bar

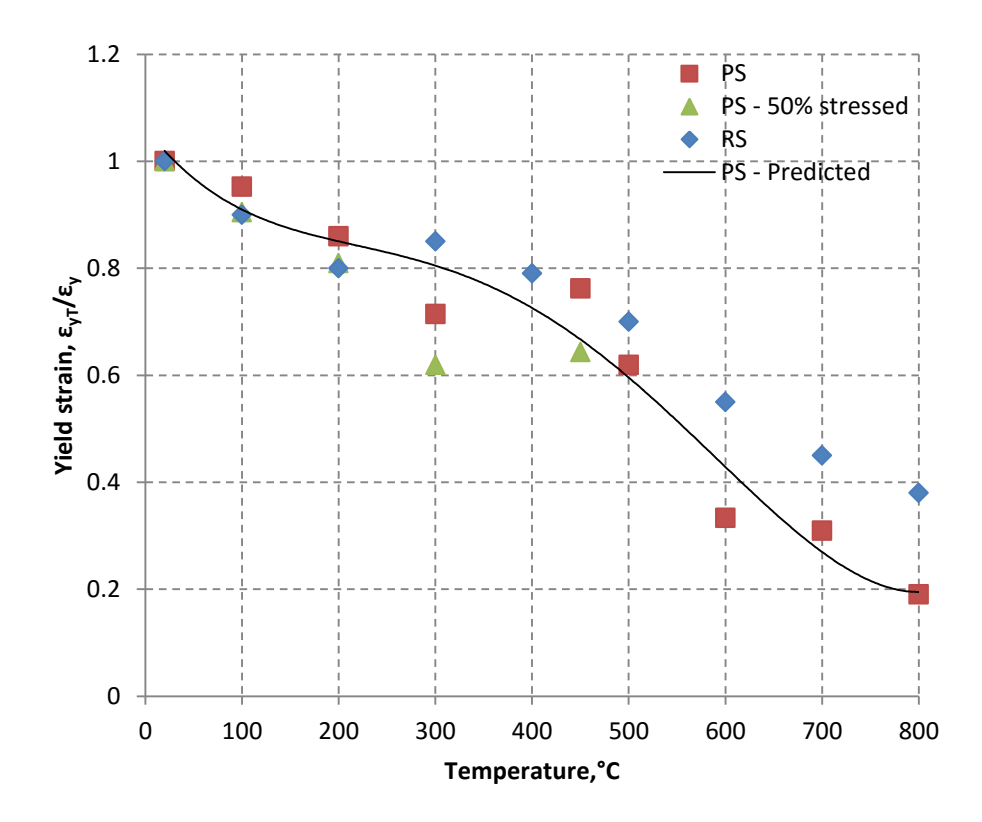


Figure 4.9. Comparison of normalized yield strain in prestressing strand and reinforcing bar

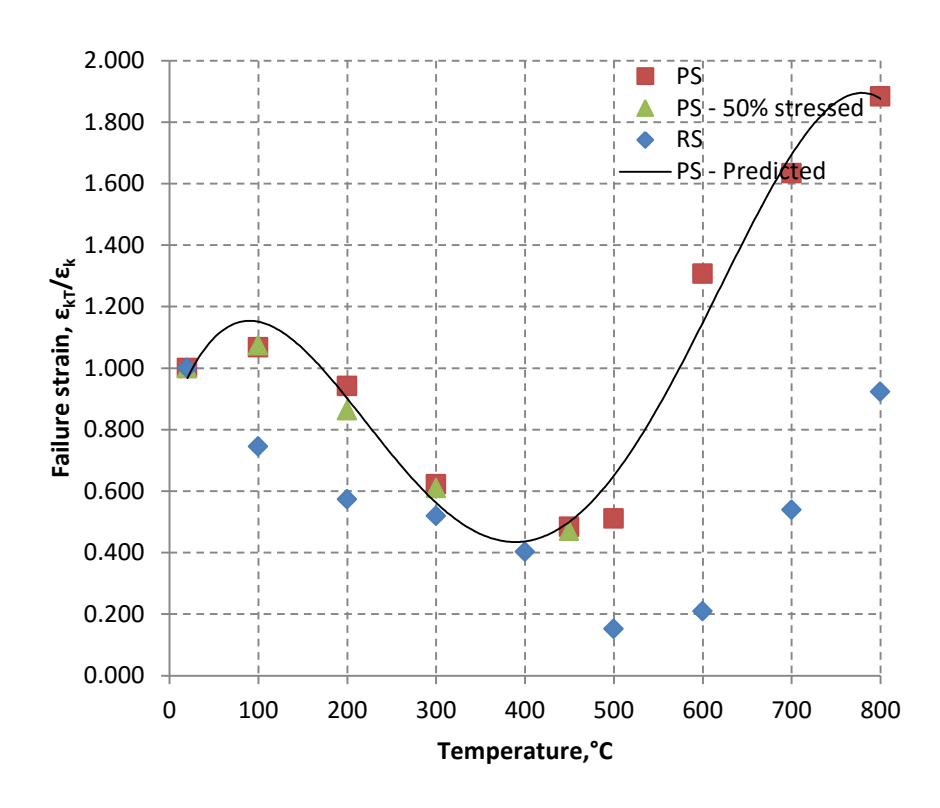


Figure 4.10. Comparison of normalized failure strain in prestressing strand and reinforcing bar

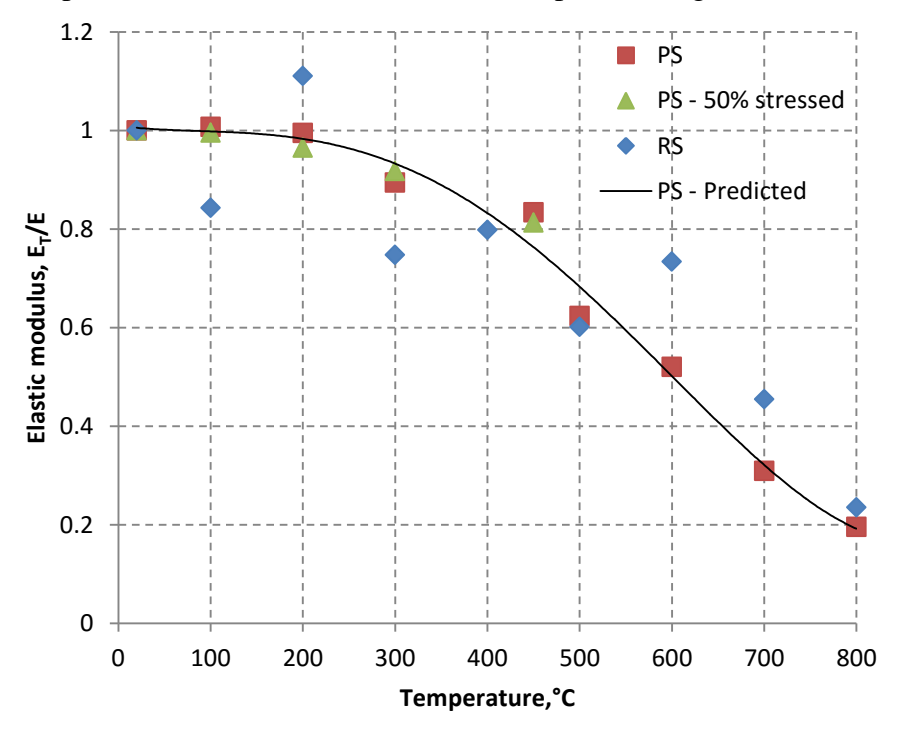
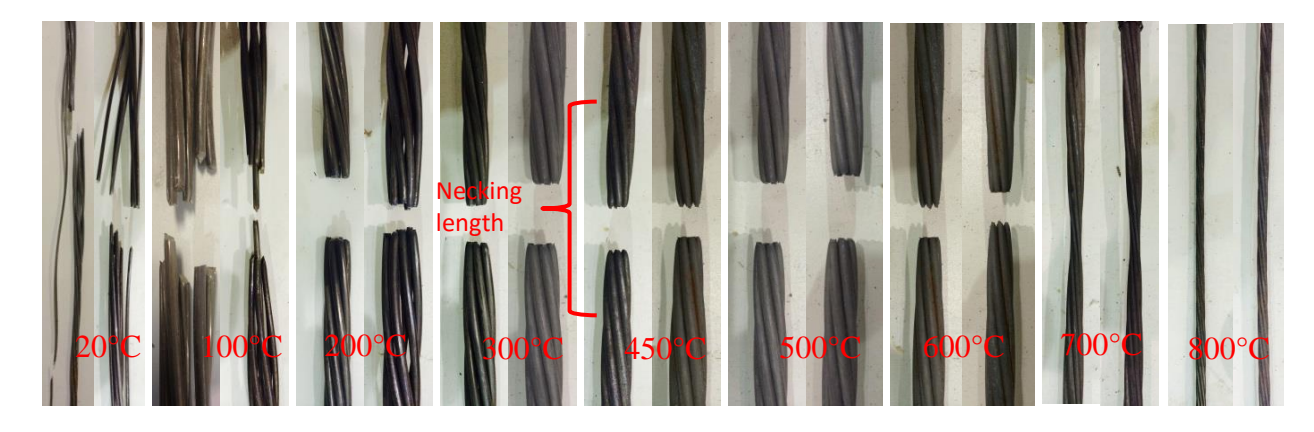


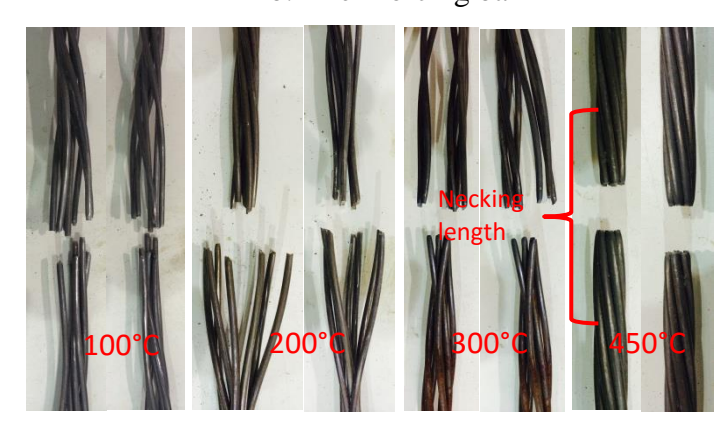
Figure 4.11. Comparison of normalized elastic modulus of prestressing strand and reinforcing bar



a. Prestressing strand



b. Reinforcing bar



c. Prestressing strand under 50% initial loading (stress)

Figure 4.12. Failure patterns in of prestressing strand and reinforcing bars at various temperatures

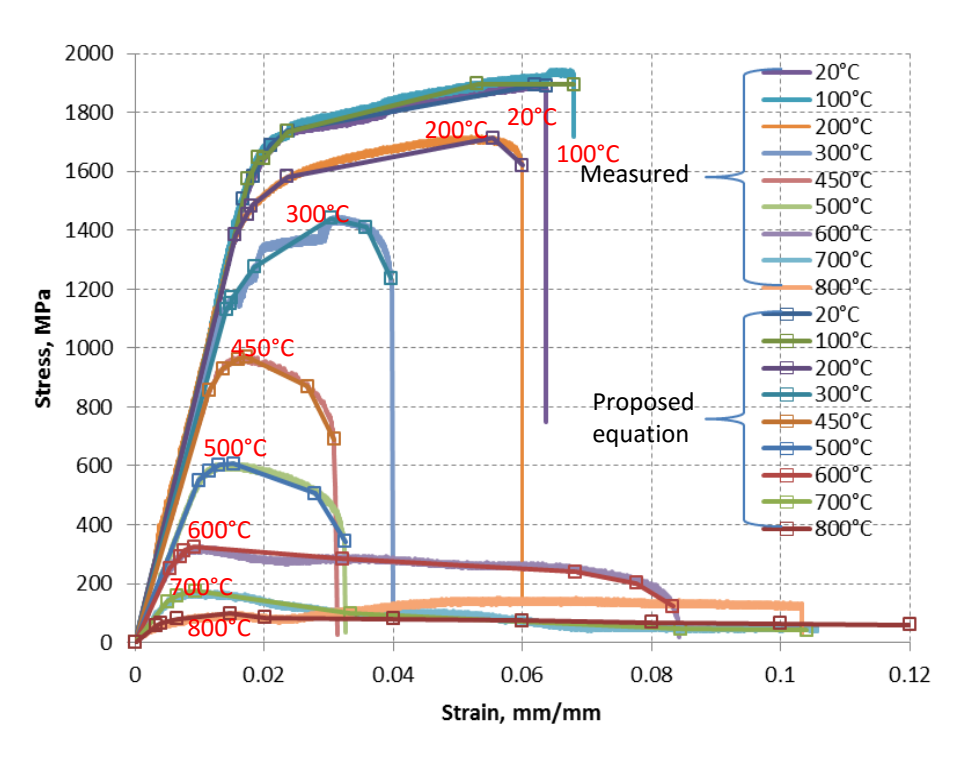


Figure 4.13. Comparison of measured high temperature stress-strain curves of prestressing strands with predicted stress-strain curves (quadri-linear model)

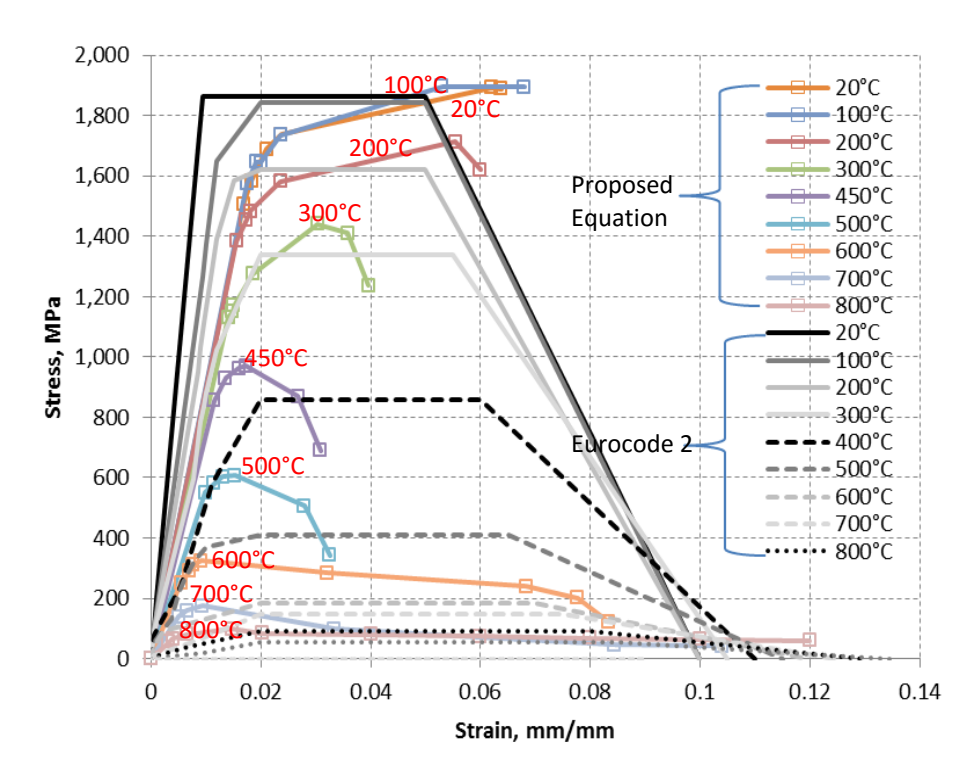


Figure 4.14. Comparison of measured high temperature stress-strain curves of prestressing strands with stress-strain curves calculated based on Eurocode 2

4.6 Summary

A set of steady-state tensile strength tests were carried out on prestressing strands and reinforcing bars at various temperatures. Based on these material level tests, the following observations can be drawn on the behavior of low relaxation seven-wire prestressing strand.

- Prestressing strand exhibits higher strength degradation, as compared to that of reinforcing bar, throughout 20 to 800°C temperature range. The rate of degradation is slightly higher under the presence of 50 percent initial stress on prestressing strand in 20 to 450°C temperature range.
- The failure (rupture) strain in prestressing strand does not change in 20 to 200°C temperature range. However, rupture strain decreases in 200 to 500°C range due to blue brittleness effect. Beyond 500°C, rupture strain significantly increases due to increased ductility resulting from interstitial purification process.
- The effect of initial stress on yield and ultimate strength of prestressing strand is somewhat insignificant in 100 to 450°C range, when the duration of high temperature exposure is relatively short. But, presence of initial stress can have significant influence beyond 450°C due to domination of thermal creep effects.
- The proposed stress-strain response for prestressing strand, evaluated based on test data, is slightly different than that of Eurocode 2 model. This is because Eurocode 2 model ignores strain hardening, specifies continuous increase in failure strain even in 200 to 500°C range, and yields slightly higher elastic modulus till 200°C.
- The proposed high temperature mechanical property relations for prestressing strand can be
 utilized as input in the computer programs for evaluating the response of prestressed
 concrete structures exposed to fire.

5 NUMERICAL MODEL AND VALIDATION

This chapter is mainly based on the following journal papers:

- Kodur V K. R., Shakya A. M., Modeling the response of precast prestressed concrete hollowcore slabs exposed to fire. PCI Journal, 59-3, May-July 2014.
- Shakya AM, Kodur VKR. Behavior of prestressed concrete hollowcore slabs under standard and design fire exposure. 8th Int. Conf. Struct. Fire, vol. 1, Shanghai China: 2014, p. 199–208.
- Shakya AM, Kodur VKR. Performance of prestressed concrete hollowcore slabs under standard and design fire exposure. PCI Conv. Natl. Bridge Conf., National Harbor, MD: Prestressed Concrete Institute; 2014.

5.1 General

Fire tests are expensive, time consuming and require sophisticated test facilities and thus, it is not always feasible to undertake fire tests to evaluate fire performance of structural members. Moreover, in fire tests, only limited number of parameters can be studied and interdependency of parameters cannot be established. The alternative to overcome many of the limitations in fire tests is to apply numerical modeling approach for evaluating fire response of structures.

The detailed literature review presented in Chapter 2 indicated that limited numerical studies have been undertaken to evaluate fire performance of hollowcore slabs (Breccolotti et al. 2006; Chang et al. 2008; Dotreppe and Franssen 2004; Fellinger et al. 2005; Min et al. 2010). However, most of these studies did not account for various failure modes in these slabs under fire conditions. These numerical models typically evaluate sectional temperatures through two

dimensional finite element analyses, and utilize simplified methods to predict flexural response of hollowcore slabs at various fire exposure times without any consideration to other critical failure limit states, especially shear. Thus, these numerical models might not yield the realistic response of hollowcore slabs under fire conditions.

To overcome some of these limitations, development of a three dimensional finite element based numerical model for tracing performance of PC hollowcore slabs under fire conditions, utilizing ANSYS APDL (ANSYS 2014), is presented in this chapter. The validity of the finite element model is established by comparing predictions from the analysis with results from fire tests undertaken as part of this research and also tests undertaken by other researchers.

5.2 Numerical procedure

A sequentially un-coupled thermal and structural analysis is applied for tracing response of PC hollowcore slabs exposed to fire conditions. The analysis is carried out in various time steps by incrementing time from the start of fire exposure (ignition) till failure of the slab, under fire conditions. The analysis procedure as illustrated through a flowchart in Figure 5.1, comprise of following main steps at each step.

- Establishing fire temperature resulting from fire exposure.
- Applying heat transfer principles namely, radiation, convection and conduction to obtain
 cross-sectional temperature profiles at various time steps. Radiation and convection heat
 transfer principles are used for transfer of heat from fire source to the exposed surface of the
 structure (slab) and from bottom surfaces of the cores to the top core surfaces, and
 conduction is used for transfer of heat through the solid concrete layers.

- Applying nodal temperatures results obtained from thermal analysis to the structural model.
 In ANSYS, element switching allows for nodal compatibility between thermal and structural analysis modes.
- Calculating deflection, flexural and shear capacity of hollowcore slab at various time steps into fire exposure.
- Applying failures limit states to determine fire resistance of PC hollowcore slabs based on various failure modes.
- If the failure occurs, analysis is stopped. Fire resistance is the duration to the last time step. If failure does not occur, the above steps are repeated in the subsequent time step.

5.2.1 Evaluating flexural and shear capacity

The main outputs from ANSYS are nodal sectional temperatures, deflection and stresses at each time step. The stresses, generated at individual elements, are integrated across the depth of the section in a separate spreadsheet calculations to evaluate flexural and shear capacity at critical sections of the slab. The sectional flexural and shear capacity of the slab can be evaluated at any given time steps into fire exposure, using Equations 5.1 and 5.2.

$$M_{nT} = \sum \sigma_{zT} A_{e} d_{naT}$$
 (5.1)

$$V_{nT} = \sum \tau_{vzT} A_e \tag{5.2}$$

where,

 M_{nT} = flexural capacity of slab under fire conditions

 V_{nT} = shear capacity of slab under fire conditions

 $A_e =$ cross-sectional area of the element

 σ_{zT} = normal stress along longitudinal direction of member under fire conditions

 au_{yzT} = shear stress along transverse direction of member at shear critical section at elevated temperature

 d_{naT} = distance of centroid of element to neutral axis of the slab under fire conditions. Neutral axis represents the point along the depth of the slab, where change of direction in normal stress is detected.

5.2.2 Flexural capacity based on simplified approach

Flexural capacity of hollowcore slabs at elevated temperature can also be derived based on relations specified in Eurocode 2 (Eurocode 2 2004a), PCI (PCI 2011) and ACI318 (ACI 318 2011), by accounting for material degradation and axial restraint force. This approach has also been utilized in previous studies (Abrams 1976; Acker 2003; Aguado et al. 2012; Andersen and Lauridsen 1999; Bailey and Lennon 2008; Borgogno 1997; Breccolotti et al. 2006; Chang et al. 2008; Dotreppe and Franssen 2004; Fellinger et al. 2005; Jensen 2005; Lennon 2003; Min et al. 2010; Schepper and Anderson 2000; Zheng et al. 2010). The modified equation for flexural capacity under fire conditions is given as;

$$M_{nT} = A_{ps} f_{psT} \left(d_p - \frac{a_T}{2} \right)$$

$$f_{psT} = f_{puT} \left[1 - \frac{\gamma_p}{\beta_1} \left(\frac{\rho_p f_{puT}}{f'_{cT}} \right) \right]$$

$$\beta_1 = 0.85 - \left(\frac{f'_{cT} (in psi) - 4000}{1000} \right) \times 0.05$$

$$\rho_p = \frac{A_{ps}}{bd_p}$$

where,

 M_{nT} = flexural capacity under fire condition, kN-m

 A_{ps} = area of prestressed reinforcement, m²

 f_{psT} = stress in prestressed reinforcement at elevated temperature, Pa (or N/m²)

 f_{puT} = tensile strength of prestressing steel at elevated temperature, Pa (or N/m²)

 f'_{cT} = compressive strength of concrete at elevated temperature, Pa (or N/m²), utilize average sectional temperature to evaluate f'_{cT}

 γ_p = factor for type of prestressing strand (0.28 for low relaxation strand)

 β_1 = factor relating depth of equivalent rectangular compressive stress block to neutral axis depth

 ρ_p = ratio of area of prestressed reinforcement to concrete area

 d_p = distance from extreme compression fiber of concrete section to centroid of prestressed reinforcement

 a_T = depth of equivalent compression stress block under fire conditions = $\frac{A_{ps}f_{psT}}{0.85f_{cT}'}b$

5.2.3 Shear capacity based on simplified approach

PC hollowcore slabs have inherently reduced shear capacity due to significant reduction in cross-sectional concrete due to presence of core voids. Moreover, these slabs are not provided with any additional shear reinforcements due to unique fabrication process adopted to achieve cost-effective construction. Thus, hollowcore slabs can experience abrupt shear failure in ambient as well as during fire conditions. However, there is limited information on the shear behavior of hollowcore slabs under fire condition, as most of the previous studies (Abrams 1976; Acker 2003; Aguado et al. 2012; Andersen and Lauridsen 1999; Bailey and Lennon 2008; Borgogno 1997; Breccolotti et al. 2006; Chang et al. 2008; Dotreppe and Franssen 2004; Fellinger et al. 2005; Jensen 2005; Lennon 2003; Min et al. 2010; Schepper and Anderson 2000; Zheng et al. 2010) conducted on PC hollowcore slabs were focused on tracing flexural behavior under fire conditions without much consideration to failure in shear.

Unlike solid slabs in which design (failure) is typically governed by flexural capacity, PC hollowcore slabs need to be checked for shear capacity in both ambient and elevated temperatures (Rahman et al. 2012). Design equations for evaluating shear capacity of these slabs have been well established for ambient conditions as specified in several codes namely Eurocode (Eurocode 2 2004a), FIP (FIP 1999), ACI (ACI 318 2011) and PCI (PCI 2010). These equations specified for estimating shear capacity at ambient temperature can be utilized to evaluate shear capacity at elevated temperature by accounting for temperature-induced material degradation in concrete and prestressing strand.

One such equation for shear capacity was proposed by Borgogno (Borgogno 1997) by modifying the ambient design equation specified in the FIP (FIP 1999). The FIP equation gives shear capacity of hollowcore slabs, in the regions that have undergone flexural cracking and does not take into account any shear reinforcement. The modified equation for shear capacity under fire conditions is given as,

$$V_{uk} = 0.068 b_w d\xi \left[1 + \frac{50 A_p f_{pyT}}{b_w df_{py}} \right] \sqrt{f'_{cT}}$$
 (5.4)

where,

 V_{uk} = shear capacity in regions undergone flexural cracking under fire conditions

 $b_w = \text{total web width}$

d = effective depth

 $\xi = 1.6 - d \ge 1$ (scale factor), where d is measured in m

 A_p = total cross sectional area of prestressing strands at the bottom face of the section

 \vec{f}_{cT} = compressive strength of concrete under fire conditions

 f_{py} = yield strength of prestressing strands at ambient temperature

 f_{pyT} = yield strength of prestressing strands under fire conditions

Similar approach was followed by Acker (Acker 2003) for evaluating shear capacity of hollowcore slabs under fire conditions by modifying ambient shear equation specified in Eurocode 2 (Eurocode 2 2004a). The modified equation accounts for temperature-induced property degradation in concrete and prestressing strand and is given as,

$$V_{Rd,c,fi} = \left[C_{Rd,c} k \left(100 \rho_{l,fi} f_{c,fi,m} \right)^{\frac{1}{3}} + k_1 \sigma_{cp,fi} \right] b_w d$$
 (5.5)

where,

 $V_{\rm Rd,c,fi}=$ shear capacity in regions un-cracked in flexure under fire conditions in N $C_{\rm Rd,c}=0.18/\gamma c$ (γc is partial safety factor for concrete)

$$k = 1 + \sqrt{(200/d)} \le 2.0$$

where,

d = effective depth at ambient temperature measured in mm

 $\rho_{l,fi}$ = force-equivalent ratio of longitudinal reinforcement = $\frac{A_{sl}}{b_w d} \le 0.02$

where,

 A_{sl} = area of the tensile reinforcement (prestressing strands)

 b_w = smallest width of the cross-section in the tensile area measured in mm $f_{\rm c,fi,m}$ = average compressive strength of concrete under fire conditions in MPa ($f_{\rm c,fi,m}$ can be taken equal to the strength of concrete for the temperature at mid height of the web)

$$k_1 = 0.15$$

$$\sigma_{cp,fi} = N_{Ed}/A_c$$

where,

 N_{Ed} = axial force in the cross-section due to loading or prestressing in N A_c = area of concrete cross-sectional measured in mm²

Similar procedure can also be applied to evaluate fire-induced shear capacity degradation based on room temperature shear equation specified in ACI 318 (ACI 318 2011) or PCI (PCI 2010) manual. Min at el. (Min et al. 2012) compared shear capacity evaluated from modified Eurocode (Eurocode 2 2004a) and FIP (FIP 1999) equations and showed that the modified Eurocode 2 (Eurocode 2 2004a) equation typically yields better estimate of degrading shear capacity of hollowcore slabs under fire conditions. Thus, Eurocode 2 equations are utilized in this study. The above simplified equations provide a convenient means of evaluating flexural and shear capacity under fire conditions. However, the accuracy of this approach has not been properly established. To overcome this drawback, in the current study fire resistance evaluated based on above discussed flexural and shear capacity equations is compared with that obtained from series of numerical studies carried on PC hollowcore slabs under fire conditions.

5.3 Discretization details

For fire resistance analysis, the given PC hollowcore slab is discretized into various elements. Two sets of elements are needed for undertaking thermal and structural analysis in ANSYS. For thermal analysis, SOLID70, LINK33 and SURF152 can be used, and for structural analysis SOLID65, LINK180 and COMBIN40 can be utilized.

SURF152 is a surface effect element and capable of simulating heat transfer to structural members through radiation and convection. This element was overlaid onto fire exposed surface of slab to simulate radiation and convection of heat from fire source onto the bottom surface of the slab. Similarly, SURF152 element was also overlaid onto open surfaces of the hollow cores, to simulate radiation and convection of heat from lower surface of cores to upper surfaces. The boundary conditions are different for the heat transmission from fire source to the bottom surface

and within the cores. To take this in to account, different reference time-temperature curves needed for SURF152 elements, are utilized for bottom and core surfaces for evaluating temperatures transmitted through radiation and convection. A defined fire time-temperature curve is utilized as the reference temperature for the heat transmission from fire source to the bottom surface of the slab, whereas average nodal temperature at the bottom half surface of the cores is utilized as the reference temperature for heat transmission within the cores. As heat due to convection is transmitted through upward movement of hot particles and heat transmission due to radiation occurs by outward emission of energy from surfaces at higher energy level (core bottom surface), SURF152 elements are overlaid on the top half surface of the cores only. SOLID70 element, which is capable of simulating 3-D thermal conduction, is used to simulate transmission of heat into the concrete slab from the surface of slab. This element has eight nodes with a single degree of freedom namely, temperature, at each node and is applicable to a threedimensional, steady-state or transient thermal analysis. LINK33 is a uniaxial element with a capability to conduct heat between nodes. Like SOLID70, LINK33 element has a single degree of freedom, temperature, at each nodal point. This conducting line element is capable of simulating steady-state or transient thermal analysis. The thermal elements are transformed (switched) into structural elements after completion of thermal analysis. The conversion is performed as follows.

- SOLID70 3-D solid elements were converted to SOLID65 3-D concrete solid elements.
- LINK33 thermal line elements were converted to LINK180 prestressing strands line elements.

In structural analysis, SOLID65 3-D element is utilized to model concrete behavior. This SOLID65 element is capable of simulating cracking in tension (in three orthogonal directions),

crushing in compression, plastic deformations and creep by utilizing concrete damage plasticity model proposed by Willam and Warnke (Willam and Warnke 1975). This element is defined by eight nodes having three degrees of freedom at each node: translation in nodal x, y, and z directions.

LINK180 3-D spar element is used to model prestressing strands. This element can capture uniaxial tension or compression and has three degrees of freedom at each node: translation in the nodal x, y, and z directions. Plasticity, creep, rotation, and large strain deformations in prestressing steel can also be simulated using this element. Surface effect elements (SURF152) do not have any role (contribution) in structural analysis and thus are deleted from structural model. A typical PC hollowcore slab, discretized into various elements, is shown in Figure 5.2. Further, for simulating axially restrained supports, COMBIN40 element is used. COMBIN40 element is a combination of a spring-slider and a damper, and is defined by two nodes with one degree of freedom at each node, two spring constants, a damping coefficient and a limiting sliding force. Compressive behavior of the COMBIN40 element is defined as a linear load-deformation curve with a limiting sliding force (corresponding to the resistance force against axial expansion provided by the supports), whereas tensile behavior is ignored to allow free contraction of the member.

5.4 Material properties

When a hollowcore slab is subjected to fire, the properties of concrete and prestressing steel degrade with increasing temperature. For evaluating realistic fire response, the variation of properties with temperature is to be taken into account. Thus, for finite element analysis, temperature dependent thermal and mechanical properties are to be provided as input data. The

thermal properties include thermal conductivity, specific heat and emissivity factors, while mechanical properties include density, elastic modulus, poison's ratio, stress-strain relations and thermal expansion. All these properties for concrete, reinforcing steel and prestressing steel are defined as varying with temperature using the relations specified in Eurocode 2 (Eurocode 2 2004a).

In ANSYS, plastic behavior of concrete is represented using Willam and Warnke's constitutive model (Willam and Warnke 1975), which is capable of defining concrete behavior in both tension and compression. Under gravity loading, top fibers of the slab are subjected to compression, while bottom fibers are subject to tension. Hence, it is necessary to define concrete behavior in both compression and tension regimes. The compressive plastic behavior is defined as isotropic multi-linear stress-strain curve varying with temperature, while tensile behavior is defined through tensile constitutive relations and damage parameters. Concrete tensile strength is taken as $0.62\sqrt{f'_c}$ (f'_c in MPa), where f'_c is the compressive strength of concrete (ACI 318 2011; PCI 2010). Once concrete reaches its tensile rupture stress, a tensile stiffness multiplier of 0.6 is used to simulate a cracked (tension) condition with a sudden drop of the tensile stress to 60% of the initial rupture stress. Then, the drop is followed by a linearly descending response to zero stress at a strain value of six times the rupture strain (ANSYS 2014). The degradation of tensile strength of concrete with temperature is evaluated as specified in Eurocode 2 (Eurocode 2 2004a). In additional, the damage in concrete is defined in terms of crack opening and crack closing parameters. These parameters are defined through crack opening and closing shear transfer coefficients, (\beta t and \beta c respectively) and are taken to be 0.2 and 0.7 respectively (Willam and Warnke 1975). Shear transfer coefficients are taken to be zero when there is a total loss of shear transfer (representing a smooth crack) and 1.0 when there is full transfer of shear

(representing a rough crack). Utilizing Willam and Warnke's constitutive model (Willam and Warnke 1975) in ANSYS, discrete concrete cracking in hollowcore slabs can be identified. Based on cracking patterns, the nature of failure (failure mode) in these slabs under fire conditions can be evaluated.

5.5 Loading and boundary conditions

A PC hollowcore slab, under fire conditions, is subjected to both thermal and mechanical loading. To simulate realistic scenario, analysis starts with the application of applied loading on slab, which is generally a percentage of flexural capacity of the slab. After initial deflection, due to loading stabilize, the slab is exposed to fire (thermal loading). Both mechanical and thermal loading are continued until failure occurs in the slab. The slab can be subjected to any specified fire exposure conditions, which is to be input as time-temperature curve (points). This can be a standard fire (ASTM E119, ISO834) or a typical design fire comprising of heating and cooling phase. Support condition is defined by fixing nodal degrees of freedom at the support nodes. A simple support is allowed to deform in longitudinal direction and rotate freely, whereas in the case of restraint supports, additional spring elements are introduced to restrict longitudinal deformations in outward direction. However, the slab ends are allowed to rotate freely in restraint condition. Figure 5.2 shows a layout of a typical hollowcore slab with applied loading and boundary conditions.

5.6 Failure criteria

The failure times of hollowcore slabs are evaluated based on different failure limit states specified in ASTM-E119 (ASTM 2011). Accordingly, failure of horizontal members (floors and

slabs) under fire exposure occurs through reaching integrity, insulation and stability limit states. Based on integrity criteria, failure occurs when flame breaches through unexposed side of the slab. Based on insulation criteria, failure of slab is said to occur when the average temperature measured at 9 points on the unexposed surface of the slab exceeds 139°C or temperature at any point exceeds 181°C above initial temperature. As per stability (strength) criteria, failure is said to occur when the slab cannot sustain the applied loading. Such a condition occurs when the flexural or shear capacity of the slab drops below the applied bending moment or applied shear loading respectively. In prescriptive based approaches, stability failure in hollowcore slabs is assessed by relating degradation in capacity to the critical temperature in prestressing strand, taken as 427°C.

In addition to the above three limit states, British Standard (BS 476) (BS 476–20 1987) specifies deflection or deflection rate as a possible failure limit state for horizontal members (beams or slabs). Based on BS 476 (BS 476–20 1987) criteria, failure of concrete slabs, occur when the maximum deflection in the slab exceeds L/20 at any fire exposure time, or the rate of deflection exceeds the limit given by $L^2/9000d$ (mm/min) after attaining a maximum deflection of L/30, where, L = span length of the slab (mm), and d = effective depth of the slab (mm).

5.7 Mesh sensitivity study

In finite element analysis mesh size adopted in discretizing the member (slab) can have significant influence on the response parameters. Effect of mesh size on the results from numerical model was evaluated through a mesh sensitivity analysis. For this purpose, the slab was analyzed by discretizing with three different mesh sizes namely, coarse, medium and fine. The mesh sizes in longitudinal and transverse directions were selected to be 100 mm and 25 mm

for coarse mesh, 50 mm and 20 mm for medium mesh, and 40 mm and 10 mm for fine mesh. The slabs were analyzed by exposing to ASTM-E119 fire, as shown in Figure 5.3.

The comparison of sectional temperatures and deflections from these three analysis cases are plotted in Figure 5.4 and Figure 5.5 respectively. From these figures it can be evaluated that results obtained using medium mesh is seven times more accurate than that compared to that obtained using coarse mesh, as shown in Table 5.1. In addition, analysis duration was approximately 3 hours, 10 hours and 24 hours for coarse, medium and fine mesh sizes respectively, which show that finer mesh takes significantly longer than medium or coarse mesh. Thus, based on the trade-off between level of accuracy and analysis duration, medium size is the optimum mesh size for numerical studies.

5.8 Model validation

The above developed numerical model is validated by comparing response predictions from the analysis with data measured in fire tests. For this validation, fire resistance tests on PC hollowcore slabs carried out as a part of this research (Shakya and Kodur 2015) and those reported in chapter are selected. Four tested slabs (at Michigan State University), designated as Slabs 3 to 6, are analyzed using the numerical model. In addition, one of the hollowcore slabs tested by Jansze et. al (Jansze et al. 2012, 2014), designated as Slab G6, are also analyzed. Characteristics of these tested slabs are tabulated in Table 5.2. Identical test conditions including aggregate type, fire scenario, load level and support condition are simulated in the analysis. The fire behavior of these slabs is evaluated and presented in terms of temperature progression, mid span deflection, axial restraint force, failure mode and fire resistance. The fire resistance is evaluated by applying failure criteria discussed in Section 5.6.

5.8.1 Slab characteristics

All four slabs (Slabs 3 to 6), tested at Michigan State University (Shakya and Kodur 2015), are of 4 m in length, 1.2 m in width and 200 mm in depth, and has six cores and seven prestressing strands as reinforcement. The cores in the slabs are of 150 mm diameter, with 25 mm concrete thickness at the bottom of the core. The prestressing strands are of 12.7 mm diameter and are of low relaxation strand type with tensile strength of 1860 MPa. Concrete cover thickness over the strands is 44 mm.

Similarly, Slab G6 is of 3.9 m in length, 1.2 m in width and 265 mm in depth, and has five cores and six prestressing strands as reinforcement. The cores in the slabs are of 200 mm height and 167 mm width, with 30 mm concrete thickness at the bottom of the core. The prestressing strands in Slab G6 are of 12.7 mm diameter and similar to those in Slabs 3 to 6. Concrete cover thickness over the strands is 50 mm. Detailed configurations of these hollowcore slabs tested in the laboratory are shown in Figure 5.6.

Slab 3, Slab 5, Slab 6 and Slab G6 were fabricated with carbonate aggregate concrete and Slab 4 with siliceous aggregate concrete. Compressive strengths of concrete on test day was 75 MPa in Slabs 3, 5 and 6, 91 MPa in Slab 4, and 56 MPa in Slab G6, as also listed in Table 5.2 . Full details of fire resistance tests on PC hollowcore slabs is given in Chapter 4 and in literature (Jansze et al. 2014; Shakya and Kodur 2015).

5.8.2 Analysis details

The above selected PC hollowcore slabs are analyzed by discretizing the slab in to various elements as discussed in Section 5.3. The thermo-mechanical analysis is carried out at 5 minute time intervals till failure of the slab. The slab is subjected to simultaneous fire and structural loading, as in the tests. Fire exposure is continued until failure in Slabs 3 to 6, but in the case of

Slab G6, fire exposure is stopped at 120 minutes and load is increased until failure occurred in the slab, similar to that in the fire resistance tests.

The analysis starts by subjecting the slab to static loads. Transient thermal load corresponding to design fire (DF) or ASTM-E119 (ASTM 2011) (which is equivalent to ISO 834 (International Standard (E) 1999) standard fire curve), as shown in Figure 3.5, is applied after steady state has been achieved from static mechanical loading. The slab is assumed to have failed when capacity (moment or shear capacity), or deflection or rate of deflection exceeds the permissible limits. Moment and shear capacity at any time step can be evaluated by utilizing internal bending and shear stresses generated from ANSYS analysis, after the slab is loaded to maximum capacity. These internal moment and shear capacity can also be evaluated by utilizing equations provided in Eurocode (Eurocode 2 2004a), ACI (ACI 318 2011) or PCI (PCI 2010) modified to account for temperature dependent material degradation.

Results generated from the analysis, namely cross sectional temperatures, deflections, axial restraint force, failure modes and failure times are utilized for validation. Arbitrary failure, based on temperature on unexposed surface exceeding critical temperatures, is also evaluated.

5.8.3 Results and discussion

The validation of above numerical model is established by comparing thermal response, structural response, failure modes and fire resistance of tests PC hollowcore slabs obtained from fire tests and numerical analysis.

5.8.3.1 Thermal response

Validation of thermal response is established by comparing measured and predicted temperatures at various cross-sectional locations in Slabs 4, 5 and G6, and these are plotted in Figure 5.8, Figure 5.9 and Figure 5.10 respectively.

In the initial stages of fire exposure, in the first 20 minutes, temperatures at the level of prestressing strand, mid-depth, quarter depth and unexposed surface increase gradually with time. As expected, temperatures in concrete layers farther from the fire exposure surface are lower than those layers closer to the exposure surface. This temperature progression trend is also predicted by the numerical model, as can be seen in Figure 5.8, Figure 5.9 and Figure 5.10. Beyond 20 minutes of fire exposure, temperatures at all locations increase at a gradual pace with time. Overall, temperature progression trends in these three slabs are similar and there is a good agreement between the measured and the predicted temperatures. The temperatures on the unexposed surface of Slabs 4 and 5 reach the limiting temperature of 181°C at 120 minutes into fire exposure as seen in both test and model predictions, and this marks the failure point in these slabs according to insulation criteria as specified in ASTM-E119 (ASTM 2011). The unexposed surface temperature data could not be compared for Slab G6, since this test data is not reported by authors (Jansze et al. 2014). However based on data obtained from the numerical model, the unexposed temperature did not exceed at 120 minutes into fire exposure in Slab G6.

5.8.3.2 Structural response

The validity of the model for structural response is established by comparing predicted and measured mid-span deflections for Slabs 3 to 6 and Slab G6, and axial restraint force in restrained Slab 5. The deflections are compared in Figure 5.11 and the axial restraint force is compared in Figure 5.12.

The deflection response in Figure 5.11 can be grouped into three stages. In Stage 1, in first 20 minutes of fire exposure, the deflections in all slabs increase at a rapid pace. These result mainly from thermal strains generated due to high thermal gradients, generated along the slab depth, occurring in early stage of fire exposure. However, concrete and strands undergo very little

capacity degradation in this stage due to low temperatures in strands and inner layers of concrete. In Stage 2, after 20 minutes into fire exposure, deflections in all slabs increase at a slightly slower pace decrease rapidly up to 75 minutes into fire exposure. This increase in deflection is due to degradation of capacity and modulus in concrete and strand, as temperatures increase in inner layers of concrete reducing thermal gradients

Finally, in Stage 3 beyond 75 minutes, deflections increase at a rapid pace and are mainly due to creep effects, which get pronounced at very high temperatures in concrete and prestressing strand. Overall, there is a good agreement in predicted and measured deflections in Stage 1 and Stage 2. However, in Stage 3, the model predicts slightly lower deflections in these slabs, and this can be mainly attributed to the fact that the temperature dependent stress-strain curves for concrete and steel are adopted from Eurocode 2 (Eurocode 2 2004a), which does not fully account for high temperature creep strains.

Similar to deflection, axial restraint force in Slab 5 plotted can also be grouped into three stages, as shown in Figure 5.12. In Stage 1, in the first 20 minutes of fire exposure, the restraint force rapidly increases with fire exposure time. This can be clearly attributed to higher thermal strain generated in concrete and prestressing strand due to high thermal gradients developing in the early stage of fire exposure. However, in this stage there is not much degradation of modulus in concrete and strand due to low temperatures in strand and inner layers of concrete. After 20 minutes, in Stage 2, temperature increases in inner layers of concrete, and this leads to degradation of modulus of prestressing strand and concrete which in turn leads to rapid decrease in axial restraint force up to about 75 minutes. The degradation of modulus in concrete and prestressing strand in Stage 2 occurs at a much higher pace than increase in thermal strains, which leads to decrease in axial restraint force. Finally, in Stage 3 (beyond 75 minutes), based on

the results from numerical model, the axial restraint force continues to decrease due to further degradation in strength and modulus properties in concrete and prestressing strand due to reaching very high temperatures. However, in the fire tests, axial restraint force could not be properly measured in Stage 3, beyond 500°C, due to sensitivity of instrumentation. Overall, there is reasonable agreement between predicted and measured axial restraint force.

In the case of Slab G6, fire exposure is stopped at 120 minutes and load is increased until failure, as per fire test conducted by Janzse et al. (Jansze et al. 2014). Thus, for Slab G6, only maximum deflections at failure can be compared after 120 minutes. This deflection is around 60 to 65 mm from both test and model.

5.8.3.3 Cracking pattern and failure modes

The crack pattern and failure modes obtained from finite element analysis are compared with that obtained from fire resistance tests in Figure 5.13. In the fire resistance tests, Slab 5 and 6, subjected to ASTM-E119 fire, underwent abrupt failure due to flexural crushing and cracking respectively at 170 and 140 minutes in the test. The crack patterns at failure predicted by numerical model show similar patterns wherein, crack patterns in Slab 6 show discrete vertical cracking along mid-span of the slab (see Figure 5.13(c)), indicating flexural cracks, and crack patterns in Slab 5 show higher density of cracks at mid span (see Figure 5.13(a)), indicating higher level of cracking of concrete. The difference in the failure pattern in these two slabs is mainly due to presence of support restraints in Slab 5. The presence of axial restraints leads to higher accumulation of internal stresses in concrete, in turn resulting in higher degree of concrete damage.

In addition to flexural cracks, shear cracks observed in Slab 6, shown in Figure 5.13(f), during fire resistance test is also captured by the model. In Figure 5.13(e), Shear cracking is indicated

by inclined cracks at the locations of application of loads. However, failure in these slabs is not governed by shear failure mode as the shear cracks do not extend into the entire depth of Slab 6. In the case of Slab G6, the slab survived 120 minutes of ISO 834 fire (International Standard (E) 1999), but failed in shear when loading is increased after fire exposure is stopped. The inclined cracks along the depth of the slab originating from the point of application of load indicate occurrence of failure through shear failure mode, as also illustrated in Figure 5.13(g).

5.8.3.4 Fire resistance

The failure times of all five slabs are evaluated based on model predicted response parameters is compared with those obtained from fire tests for five slabs in Table 5.3. Accordingly, none of the slabs failed under integrity criteria, as no holes were formed in any of the slabs in the fire resistance tests and thus, no flame breached through the unexposed side of the slab. However, current numerical model is not capable of directly predicting formation of pass-through holes, as the model cannot model concrete spalling. However, temperatures in the unexposed surface obtained from the model are well below the fire temperature in the entire range of fire exposure, which indirectly indicates no breach of flame through the unexposed surface. Based on insulation a criterion, limiting unexposed surface temperatures of 181°C is reached at 120 minutes into fire exposure in Slabs 4, 5 and 6. These failure times from model based on insulation criterion compare well with those evaluated in fire tests. Lower fire resistance of Slab 4, as compared to Slab 3, can be attributed to higher thermal conductivity and lower specific heat of siliceous aggregate concrete (Kodur and Harmathy 2012), which leads to faster transmission of temperatures into Slab 4. It should be noted that fire resistance based on insulation criterion in Slab 5 and Slab 6 (exposed to ASTM-E119 fire) is same as Slab 4 (exposed to design fire DF), as ASTM-E119 is of slightly higher intensity than DF. In the case of Slab G6, critical unexposed

surface temperature obtained from model was not exceeded at 120 minutes into ISO 834 fire, when the fire exposure is stopped.

Slabs 3 to 6 sustained load beyond 120 minutes, which infer that reaching unexposed surface limiting temperature does not represent strength failure in these slabs. Application of flexural capacity criterion results in failure times of 165, 140, 160 and 130 minutes in Slab 3, Slab 4, Slab 5 and Slab 6 respectively, as illustrated in Figure 5.14. Similarly, application of shear capacity degradation criterion results in failure times of 180, 150 and 145 minutes in Slab 3, Slab 4 and Slab 6 respectively, while no shear failure occurs in Slab 5, as illustrated in Figure 5.15. Higher fire resistance in Slab 5, as compared to Slab 6, is due to the presence of axial restraints which enhances the stiffness of the slabs. These failure times, based on strength limit state, compare well with that observed in fire tests, wherein the failure times were measured to be 170 and 140 minutes in Slab 5 and Slab 6 corresponding to flexural failure mode. However, in the tests, no strength failure was seen in Slabs 3 and 4, since decay phase was initiated in Slabs 3 and 4 at 120 minutes. In the case of Slab G6, fire exposure was stopped at 120 minutes in the test and thus, fire resistance based on strength criteria is not evaluated. However, maximum load sustained by the slab obtained from the model, before failure after fire exposure is stopped, compared well with the test value.

Overall there is a good agreement between the model prediction and the test data, indicating that the proposed model is capable of predicting fire behavior of PC hollowcore slabs, including failure under shear limit state.

Table 5.1. Comparison of mesh sizes and analysis results

Mesh description	Coarse	Medium (Adopted)	Fine
Max. longitudinal mesh size (mm)	100	50	40
Max. lateral mesh size (mm)	25	20	10
Max. error in thermal results, relative to results with fine mesh (%)	22	3	0
Max. error in structural results, relative to results with fine mesh (%)	7	1	0
Approx. run duration (hours)	3	10	24

Table 5.2. Summary of test parameters and results

Test slab	Aggregate type	Test day compressive strength (f'c), MPa	Applied loading (% of capacity)	Support condition	Test day moisture content	Fire scenario
Slab 3	Carbonate	75	60	SS	56% RH	DF
Slab 4	Siliceous	91	60	SS	55% RH	DF
Slab 5	Carbonate	75	60	AR	55% RH	ASTM-E119
Slab 6	Carbonate	75	60	SS	55% RH	ASTM-E119
Slab G6	Carbonate	56	70	SS	2.5-3.2% MC	ISO 834

Note: SS = simply supported, AR = axially restrained, RH = relative humidity, MC = moisture content

Table 5.3. Comparison of measured and predicted fire resistance in tested slabs

Test slab	Fire resistance (minutes)								
	Measured				Predicted				
	Insulation	Capa	Capacity Fai		Failure T. 1.	D.C.	Capacity		Failure
		Flexure	Shear	mode	Insulation	Deflection	Flexure	Shear	mode
Slab 3	145	n.f.	n.f.	n.f.	140	n.f	165	180	Flexure
Slab 4	120	n.f.	n.f.	n.f.	120	n.f	140	150	Flexure
Slab 5	120	170	n.f.	Flexure	120	160	160	n.f.	Flexure
Slab 6	120	140	n.f.	Flexure	120	130	→130	145	Flexure
Slab G6	n.a.	>120	>120	Shear	>120	n.a.	n.a.	n.a.	Shear

Note: 'n.f.' = no failure, 'n.a.' = not available

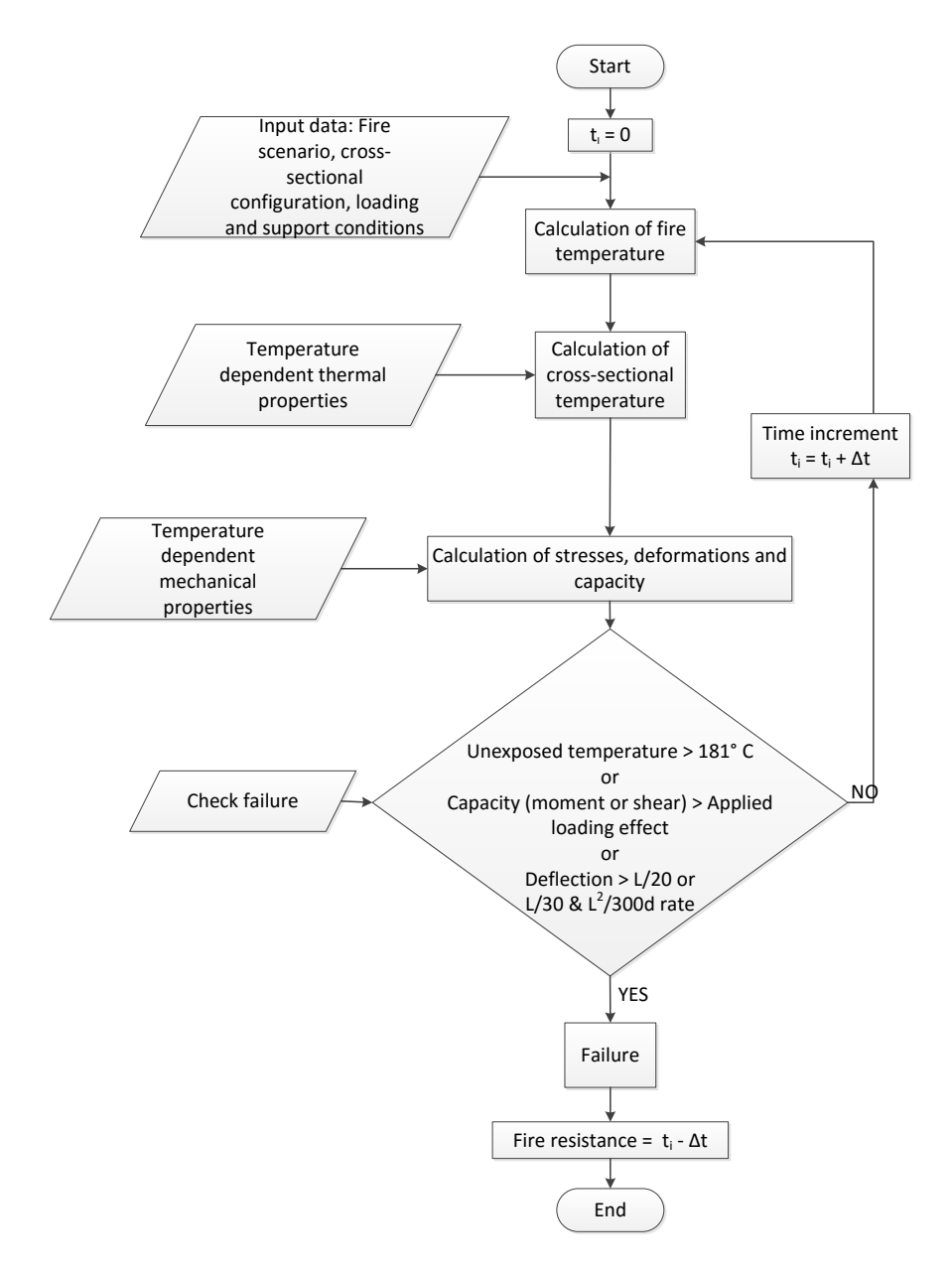
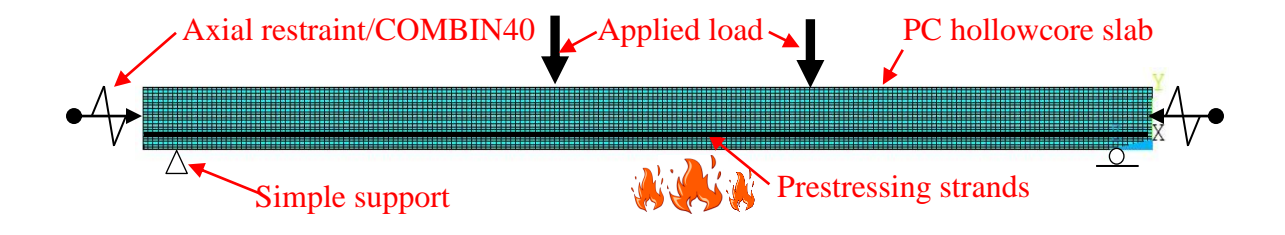
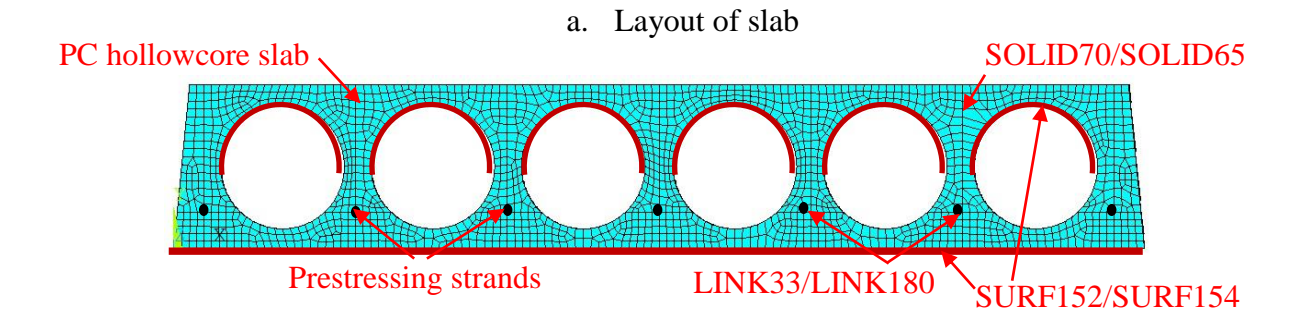
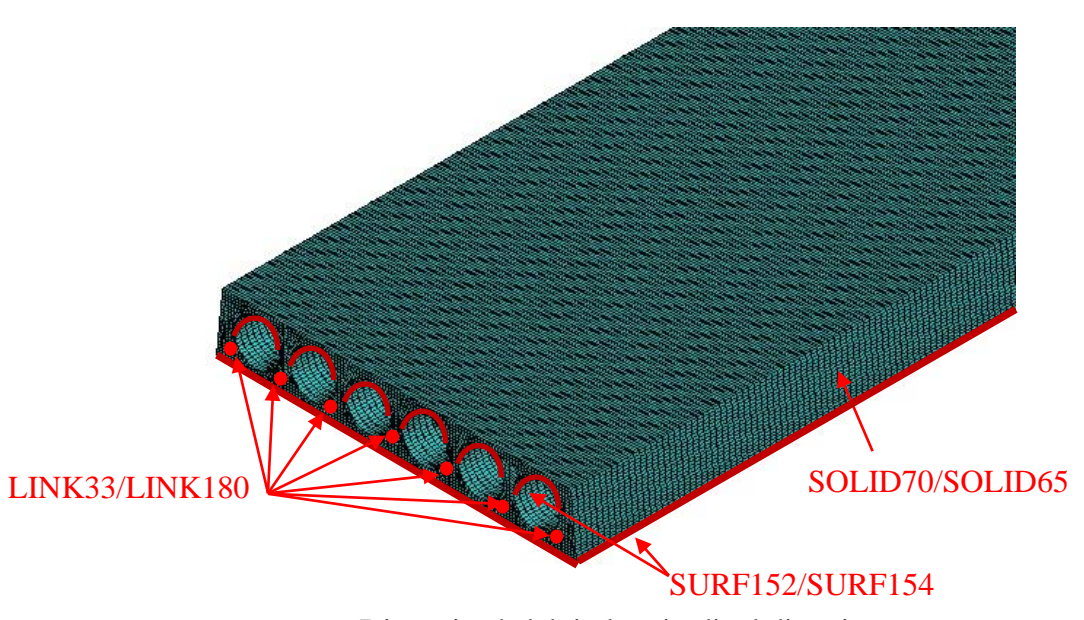


Figure 5.1. Flowchart illustrating steps associated with fire resistance analysis of a hollowcore slab





b. Discretization of cross-section



c. Discretized slab in longitudinal direction

Figure 5.2. Layout of a typical PC hollowcore slab and its discretization for finite element analysis

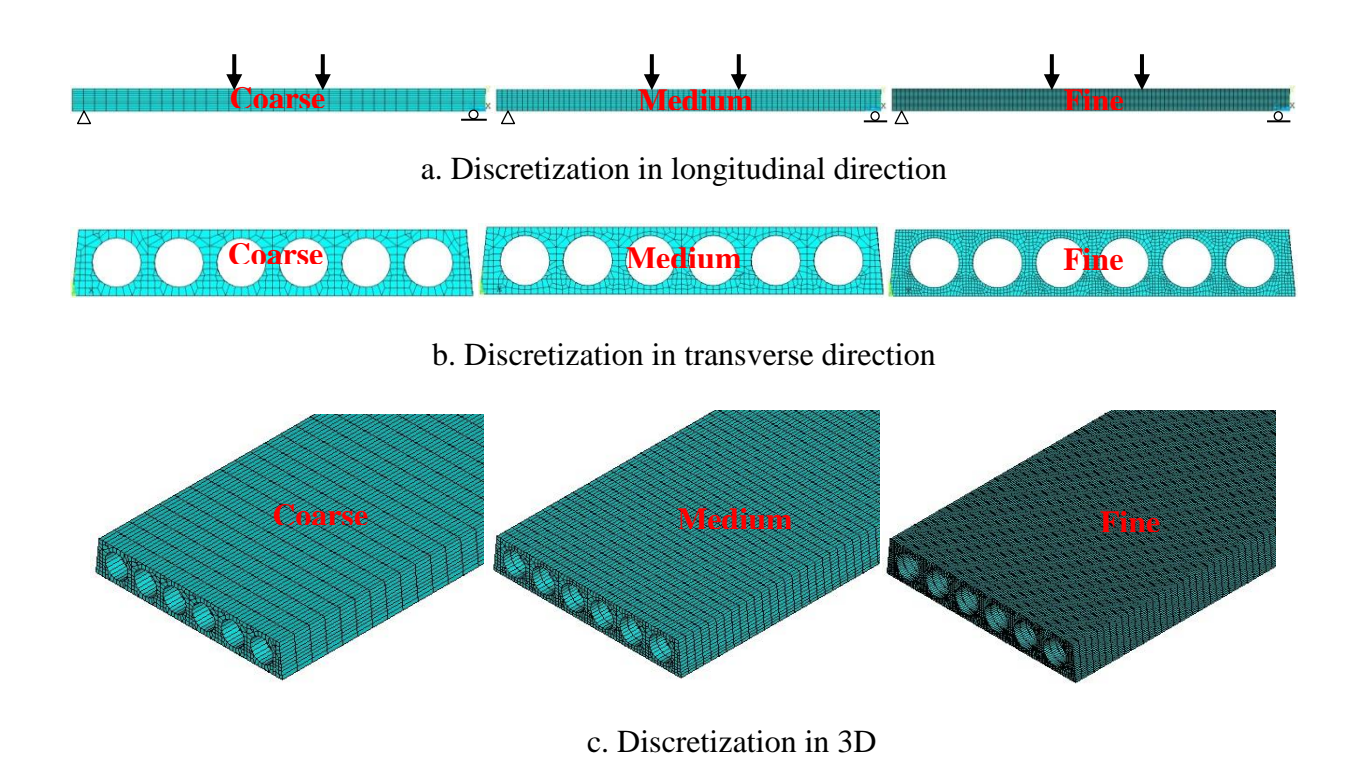


Figure 5.3. Comparison of mesh sizes used for mesh sensitivity study

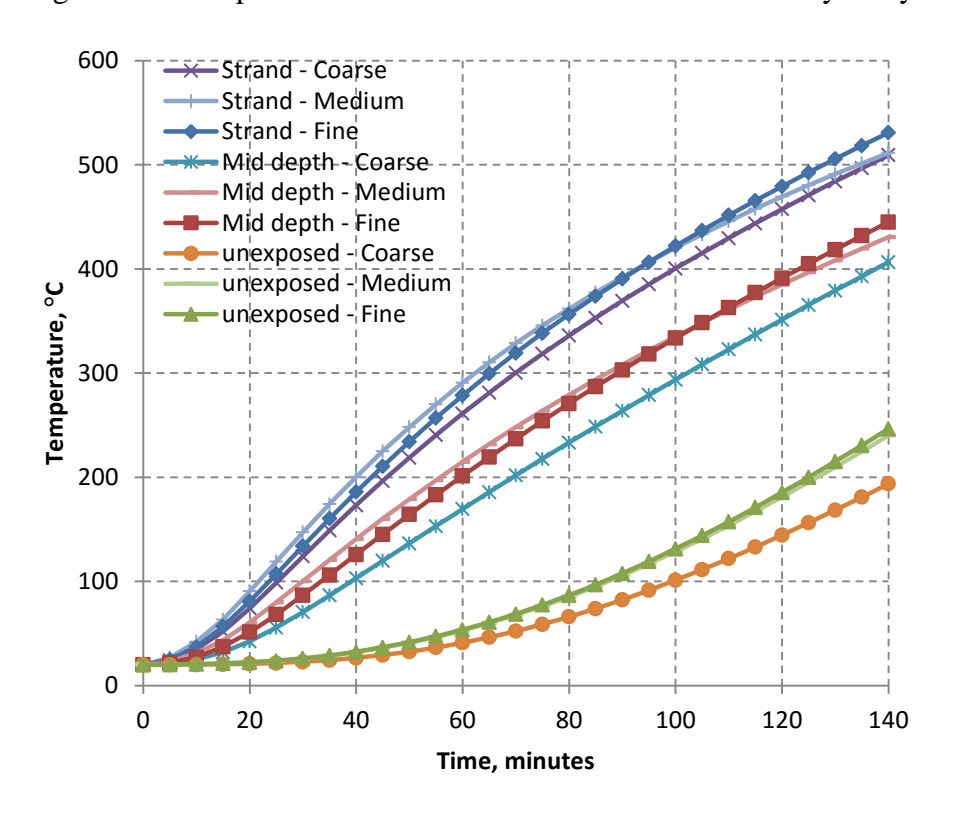


Figure 5.4. Comparison of sectional temperatures with different mesh sizes

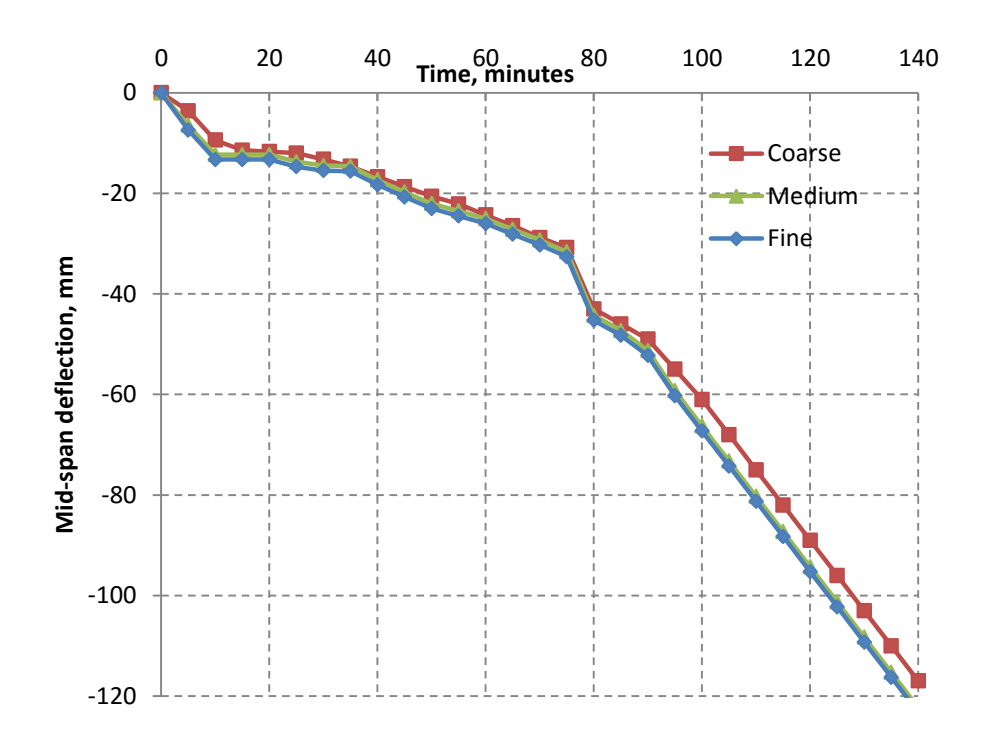
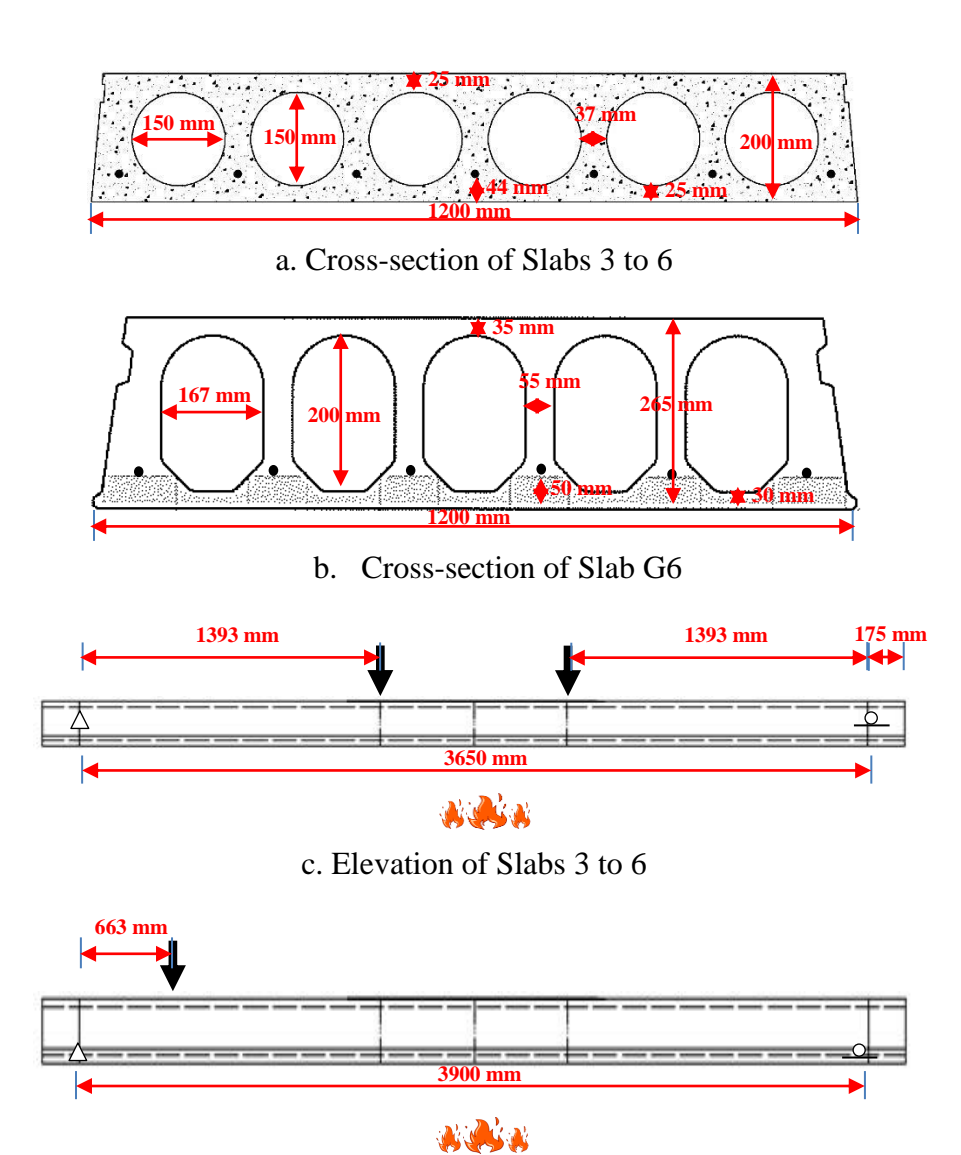


Figure 5.5. Comparison of mid-span deflections with different mesh sizes



d. Elevation of Slab G6

Figure 5.6. Layout of PC hollowcore slab tested in the laboratory

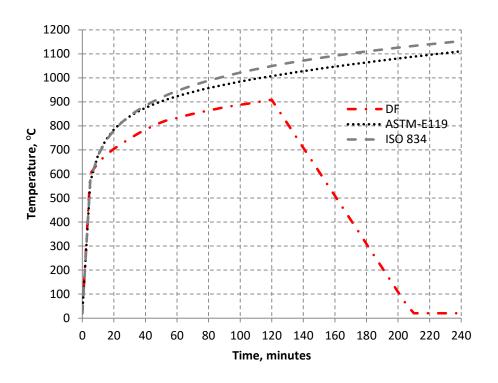


Figure 5.7. Time-temperature curves, simulated during fire tests

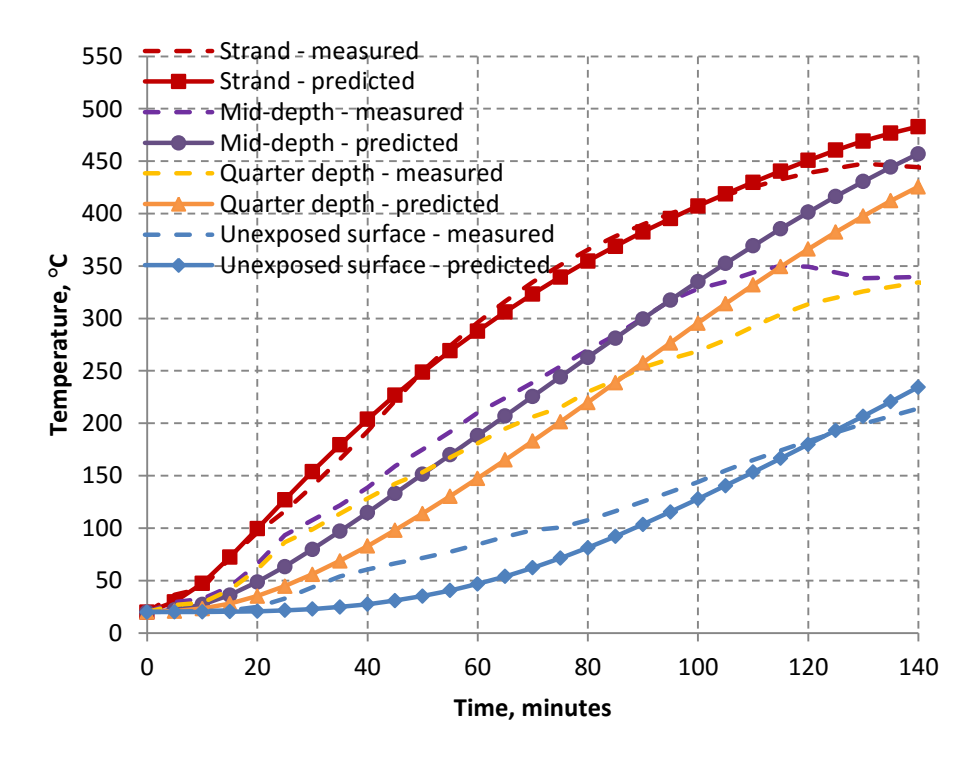


Figure 5.8. Comparison of measured and predicted sectional temperatures for tested Slab 4

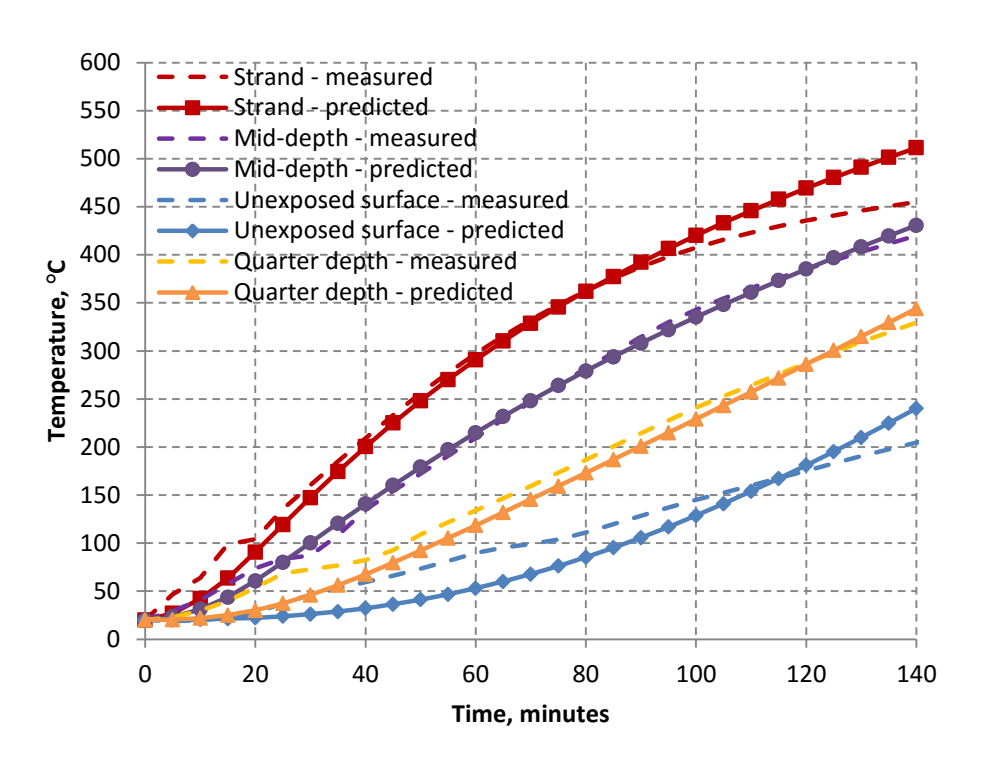


Figure 5.9. Comparison of measured and predicted sectional temperatures for tested Slab 5

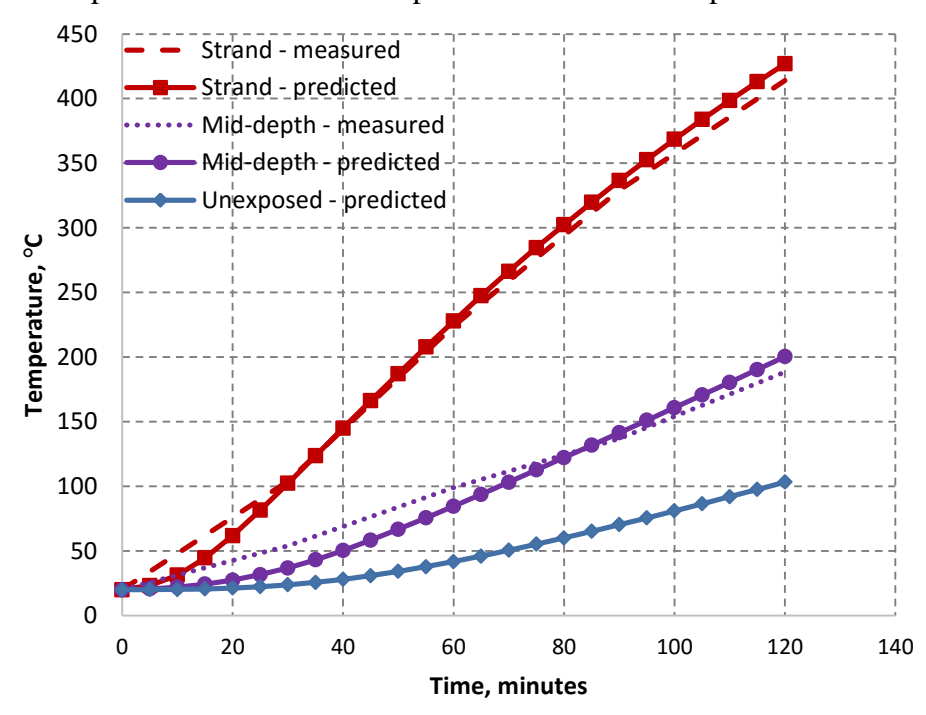


Figure 5.10. Comparison of measured and predicted sectional temperatures for tested Slab G6

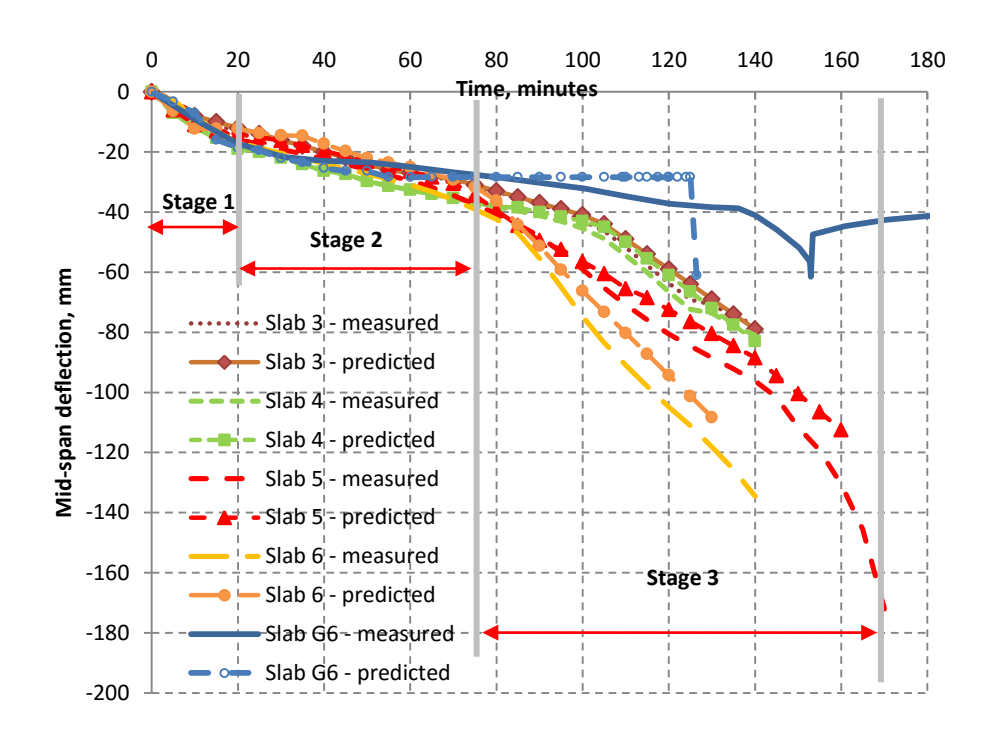


Figure 5.11. Comparison of measured and predicted mid-span deflections for test Slab 3, Slab 4 and Slab 5

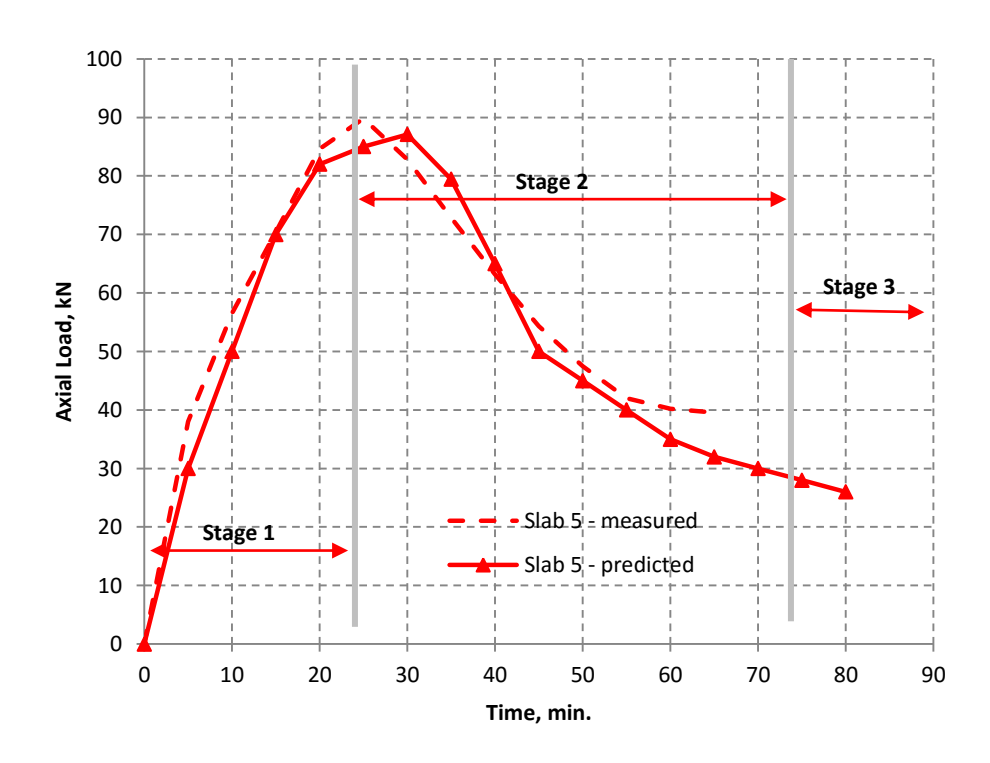


Figure 5.12. Comparison of measured and predicted axial restraint force for test Slab 5

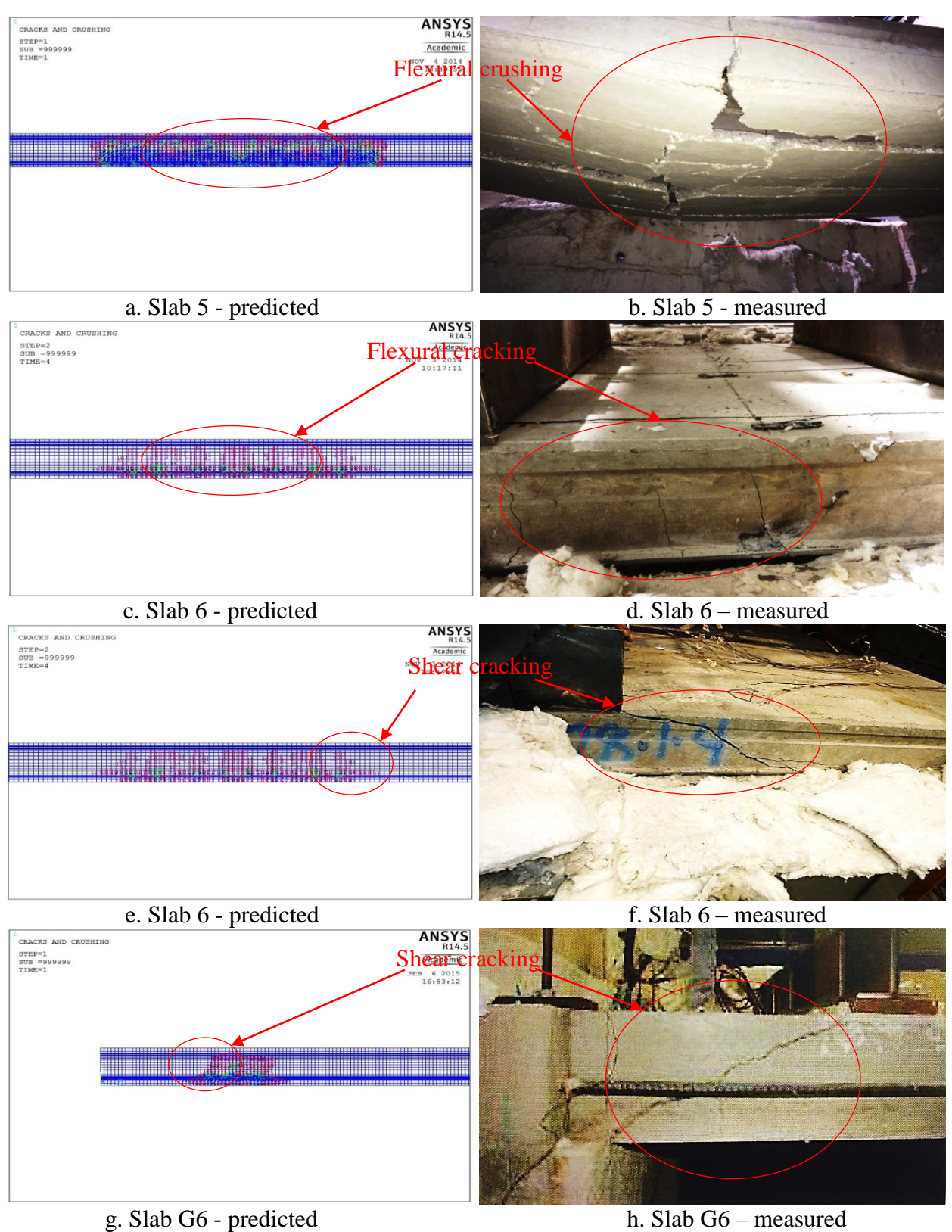


Figure 5.13. Comparison of predicted and observed failure modes in tested hollowcore slab under fire condition

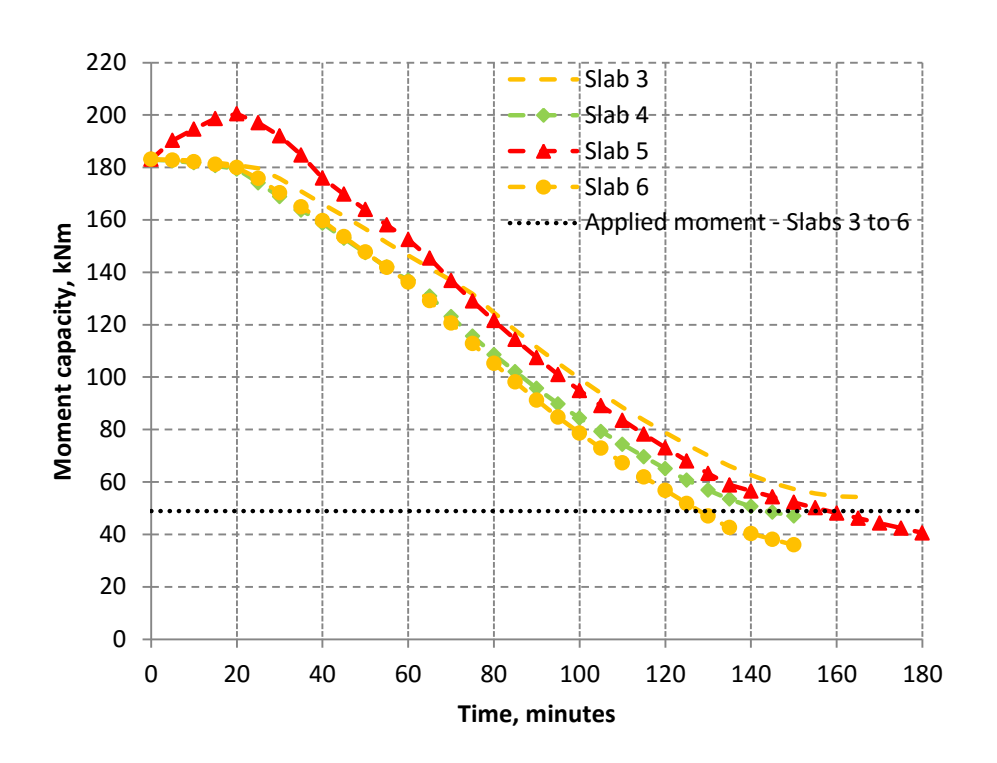


Figure 5.14. Comparison of variations of moment capacity with fire exposure time for Slabs 3 to 6

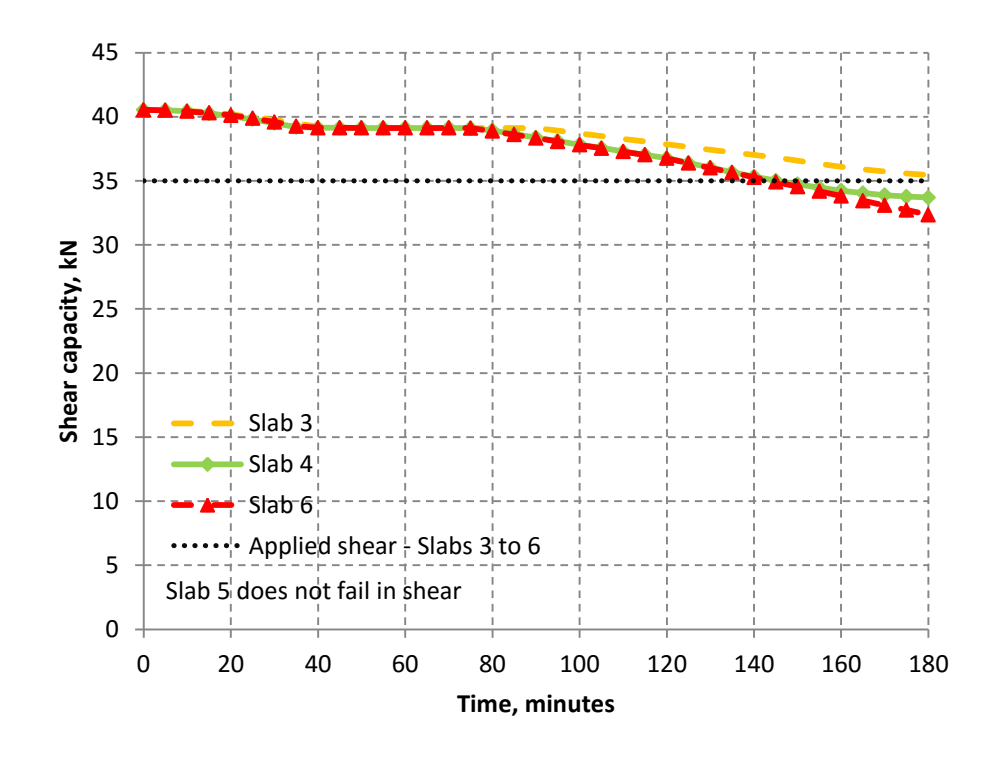


Figure 5.15. Comparison of variations of shear capacity with fire exposure time for Slabs 3, 4 and 6

5.9 Summary

A three-dimensional finite element based numerical model is developed to trace the realistic behavior of PC hollowcore slabs under fire conditions. Based on the results, the following observations can be made:

- The proposed numerical model is capable of tracing the response of PC hollowcore slabs under realistic fire, loading and support conditions.
- The proposed model is capable of predicting realistic failure modes in PC hollowcore slabs under fire conditions by predicting cracking patterns in concrete.
- The model developed in ANSYS software [6], accounts for temperature induced degradation of properties of concrete and prestressing strands, cracking in concrete, material and geometrical nonlinearities, realistic fire, load and restraint conditions, as well as different failure limit states.
- Output parameters from the numerical model include sectional temperature, mid-span deflection, axial restraint force, sectional stresses and cracking pattern. Sectional stresses can be utilized to evaluate flexural and shear capacity at any given time into fire exposure. Alternatively, Eurocode 2 equations can also be utilized to evaluate flexural and shear capacity of PC hollowcore slab at any given fire exposure time, by accounting for temperature induced strength degradation.

This chapter is mainly based on the following journal papers:

- Kodur VKR, Shakya AM. Factors governing the shear response of PC hollowcore slabs under fire conditions. Fire Safety Journal, 2015 (under review)
- Shakya AM, Kodur VKR. Behavior of prestressed concrete hollowcore slabs under standard and design fire exposure. 8th Int. Conf. Struct. Fire, vol. 1, Shanghai China: 2014, p. 199–208.
- Shakya AM, Kodur VKR. Performance of prestressed concrete hollowcore slabs under standard and design fire exposure. PCI Conv. Natl. Bridge Conf., National Harbor, MD: Prestressed Concrete Institute; 2014.

6.1 General

Fire performance of PC hollowcore slabs is influenced by number of factors. It is crucial to identify and quantify the effects of these factors to understand the behavior and failure modes of hollowcore slabs under fire conditions. Parametric studies can generate data that can be utilized to identify significant factors and also to quantify the effect of these factors on overall performance. The validated numerical, presented in Chapter 5, is applied to evaluate the effects of various factors influencing the response of PC hollowcore slabs under fire conditions. The results from parametric studies can be utilized to develop design guidelines on fire response of PC hollowcore slabs. Details on procedure and results of parametric studies are discussed in the

following sections, and the numerical approach is also illustrated through a flowchart, as shown in Figure 6.1.

6.2 Factors influencing fire response

A state-of-the-art review presented in Chapter 2 indicated that, the fire response and failure modes of PC hollowcore slabs are influenced by several factors. Also, hollowcore slabs are typically susceptible to flexure and shear failure modes under both ambient as well as fire conditions. Among other failure modes, shear failure is the critical failure mode in hollowcore slabs due to significant reduction in cross-sectional concrete, and is significantly dependent on various parameters (Abrams 1976; Acker 2003; Aguado et al. 2012; Andersen and Lauridsen 1999; Bailey and Lennon 2008; Borgogno 1997; Breccolotti et al. 2006; Fellinger et al. 2005; Jensen 2005; Lennon 2003; Schepper and Anderson 2000; Zheng et al. 2010). The main factors influencing the fire response and failure modes of PC hollowcore slabs are:

- Slab depth
- Load intensity
- Loading scenario
- Axial restraint
- Level of prestressing
- Fire severity

Previous studies have studied effects of some of these parameters on the fire response of hollowcore slabs, such as slab depth and load level. However, effects of these factors have not been fully studied over a wide range due to lack of a numerical model capable of predicting realistic failure modes in hollowcore slabs under fire conditions. Thus, a detailed parametric

study was undertaken using the developed numerical model to quantify the effect of slab depth, load level, loading scenario, axial restraint, level of prestressing and fire severity on the fire response and failure modes of PC hollowcore slabs.

6.3 Parametric studies

The results from parametric studies undertaken to quantify the effect of above parameters on the response and failure modes of hollowcore slabs under fire conditions is discussed in the following section.

6.3.1 General

Parametric study on PC hollowcore slabs under fire conditions is performed utilizing the three dimensional finite element based numerical model developed in Chapter 5. The model is validated against the data obtained from fire test discussed in Chapter 3 (Shakya and Kodur 2015) and in the literature (Jansze et al. 2012). The validated model accounts for temperature induced degradation of properties of concrete and prestressing strands, realistic fire, load and restraint conditions, as well as different failure limit states. Moreover, the developed model is capable of predicting cracking patterns in concrete under fire, and thus can be utilized to predict critical failure modes in these PC hollowcore slabs.

6.3.2 Range of parameters

To quantify the effect of critical parameters on fire resistance of slabs, a set of slabs were analyzed by varying above parameters over a wide range. In total, 38 PC hollowcore slabs were analyzed and the factors varied included slab depth, load level, loading scenario, axial restraint, level of prestressing and level of prestressing.

The depth of hollowcore slabs utilized in building applications range from 150 mm to 400 mm. Structural capacity and cross-sectional configurations for these slabs vary slightly from one country to another, however general use in United States is governed by PCI design handbook (PCI 2010). For this study, five different PC hollowcore slabs are selected from PCI design handbook (PCI 2010) with depths of 150, 200, 250, 300 and 400 mm. These slabs are made of concrete of 75 MPa compressive strength and prestressing strands of 12.7 mm (0.5 in.) diameter with a tensile strength of 1860 MPa. The detailed cross-sectional configurations of these slabs showing slab depth, core dimension, prestressing strand layout, and concrete cover to strand, are shown in Figure 6.2. These slabs are simultaneously subjected to a four point loading scheme with a load equivalent to 60 percent of room temperature moment capacity and exposed to ASTM-E119 standard fire (ASTM 2011), as shown in Figure 6.3(a) and Figure 6.4 respectively. Fire exposure is continued until failure occurs in this slab.

To study the effect of other critical parameters, two of the slabs selected above, with 200 mm and 400 mm depth, are analyzed under different levels of loading, loading scenarios, levels of axial restraint, levels of prestressing and various fire intensities. However, slabs subjected to three load levels are analyzed namely, 50, 60 and 85 percent, under the four point loading scheme shown in Figure 6.3(a). These loading cases are selected to cover a wide range of load intensities and are designated as L50, L60 and L85. Similarly, three cases of loading scenarios are analyzed; concentrated bending loading, designated as BL (see Figure 6.3(a)), uniformly distributed loading, designated as UDL (see Figure 6.3(b)), and shear loading, designated as SL (see Figure 6.3(c)). In the fourth set, two cases of axial restraint are considered, which include partially restraint case, with 50 percent axial restraint, and fully restraint case, with 100 percent

axial restraint, at supports. These cases are designated as AR50 and AR100 respectively. Results from axially restraint cases are compared with simply supported case, designated as SS.

Similarly, three cases of prestressing level is also studied, namely, 50, 70 and 85 percent of tensile strength of prestressing strands, designated as PS50, PS70 and PS85 respectively. Finally, effect of fire severity on performance of hollowcore slabs is studied by analyzing slabs under five different fire scenarios namely, ASTM-E119 standard fire (ASTM 2011), ASTM-E1529 (ASTM 2014) hydrocarbon fire, mild (intensity) design fire (DF1), medium (intensity) design fire (DF2) and severe (intensity) design fire (DF3), and these are illustrated in Figure 6.4. The design fires (DF1, DF2 and DF3) represent fire scenarios typically encountered in building and parking structures and are calculated based on Eurocode 1 compartment fire provisions (Eurocode 1 2008). All these parameters are also listed in Table 6.1.

6.3.3 Analysis details

For ANSYS analysis, hollowcore slab is discretized in to various elements as discussed in Chapter 5. The thermo-mechanical analysis is carried out at 5 minute time intervals, by subjecting the slab to simultaneous fire and structural loading, till failure occurs. The analysis starts by subjecting the slab to static loading. Transient thermal (fire) loading corresponding to specified fire scenario is applied after a steady state is reached under static mechanical loading. Sequential uncoupled thermo-mechanical analysis is carried out at incrementing time steps. At the end of each time step the failure of the slab is checked by applying different failure criteria, as discussed in Chapter 5. Accordingly, the slab is assumed to have failed when capacity (moment or shear capacity), or deflection exceeds the permissible limits. The fire resistance of analyzed slabs evaluated based on these failure criteria, as discussed in Chapter 5, is compared in Table 6.1.

6.3.4 Response parameters

The response parameters generated from ANSYS include sectional temperatures, mid-span deflections, axial restraint force in axially restrained slabs, elemental stresses, and cracking patterns.

The deflection computed at each time step, can be directly utilized to gauge the failure of the hollowcore slab. However, such strength failure at critical sections might occur through moment or shear limit state. To check this, flexural and shear capacity at any given time step can be evaluated using ANSYS generated sectional stresses, as discussed in Chapter 5. The elemental stresses, generated at individual elements, are integrated across the depth of the section in a separate spreadsheet calculation to evaluate internal flexural and shear capacity. These internal flexural and shear capacity calculated from spreadsheet are checked against bending moment and shear force due to applied loading to evaluate failure at critical sections. Alternatively, as discussed in Chapter 5, Eurocode (Eurocode 2 2004a) equations can also be used to evaluate the moment and shear capacity at critical section of a slab at any given time into the fire exposure duration (Acker 2003; Borgogno 1997).

The failure is assumed when the internal flexural capacity or shear capacity drops below bending moment or shear force due to applied loading. In ANSYS, based on cracking pattern in concrete, failure location in slabs can be gauged, wherein discrete vertical cracks originating from the midspan of the slab typically represent critical flexural cracking, and inclined cracks originating from location of high shear forces (loading points) typically represent shear cracking.

6.4 Results of parametric studies

Results from the parametric studies are presented in Table 6.1 and Figure 6.6 to Figure 6.16. The fire resistance, evaluated by applying different failure criteria, are compared in Table 6.1 for all analyzed slabs. While thermal response is presented, in terms of sectional temperatures, structural response is presented in terms of progression of deflection, degradation of moment and shear capacity. The effect of each of the above established parameters on the fire response of hollowcore slabs is discussed below.

6.4.1 Effect of slab depth

To study the effect of slab depth on the shear response of PC hollowcore slabs under fire exposure, results from analysis on five PC hollowcore slabs of five depths (150, 200, 250, 300 and 400 mm), is utilized (see Table 6.1). The cross-sectional temperatures, plotted in Figure 6.5, show that the progression of sectional temperature in all five slabs follow similar trend. However, sectional temperatures typically decrease with increase in slab depth, which can be attributed to higher thermal inertia of thicker slabs, as compared to thinner slabs. Lower sectional temperatures in thicker slabs in turn lead to higher fire resistance, as compared to that of thinner slabs.

The mid-span deflection is compared for all five slabs in Figure 6.6(a). The deflections in all five slabs increase with fire exposure time, but the level of deflection significantly varies from one slab to another. As expected, thinner slabs undergo higher deflections, as compared to thicker slabs, and this is mainly due to higher sectional temperatures (see Figure 6.5) and lower stiffness of thinner slabs than that in thicker slabs. Failure in these five slabs (of 150, 200, 250, 300 and 400 mm thickness) based on deflection limit state occurred at 90, 125, 145, 155 and 200 minutes respectively, when numerical analysis experienced non-convergence indicating imminent failure.

Comparison of these fire resistance values, based on deflection criteria, with that evaluated based on strength (moment and shear) failure criteria, as shown in Table 6.1 and Figure 6.6(b) and (c), infer that there is good correlation between the two.

Further, the failure modes in these slabs are illustrated in Figure 6.7, which show that failure is through flexural cracking in thinner slabs (150 and 200 mm), through flexure-shear cracking in medium depth slab (250 mm) and shear cracking in thicker slabs (300 and 400 mm). These results infer that thicker slabs are more susceptible to shear failure as compared to thinner slabs. Moment and shear capacity, evaluated as per Eurocode (Eurocode 2 2004a) equations, is utilized to plot moment and shear capacity degradation as a function of the fire exposure duration, and these responses are illustrated in Figure 6.6. The degradation in moment capacity in hollowcore slab mainly depends on the strand strength, as most of the flexural capacity of the slab is mostly governed by tensile strength of the prestressing strands. In all slabs moment capacity decreases with reduction in strand strength, which is a function of temperature in strand. There is no significant loss of moment capacity up to first 20 minutes of fire exposure and this is mainly due to low temperatures (below 125°C) in the strands. After this stage, moment capacity gradually decreases with increase in temperatures until failure occurs (see Figure 6.5). The failure based on flexural capacity occurs at 90, 130, 150, 165 and 220 minutes in 150, 200, 250, 300 and 400 mm slabs respectively (see Table 6.1). These fire resistance times evaluated based on Eurocode 2 (Eurocode 2 2004a) flexural capacity equation correspond well with that based on deflection failure limit state obtained through the numerical model (see Figure 6.6(a)) for 150 and 200 mm slabs, but not for 250, 300 and 400 mm thick slabs. This is mainly attributed to the fact that failure in thinner slabs (150 and 200 mm) is governed by flexural failure mode, whereas failure in thicker slabs (250, 300 and 400 mm) is governed by flexure-shear or shear failure mode.

Shear capacity, which mainly depends on concrete strength, decrease in a gradual pace in the first 40 minutes. This can be attributed to the fact that the temperatures increase in a gradual pace in inner concrete layers (see Figure 6.5). There is no significant degradation in shear capacity from 40 to 80 minutes into fire exposure and this is due to the fact that concrete experiences no significant degradation in compressive strength below 200°C temperature range (Eurocode 2 2004a). After about 75 to 80 minutes, shear capacity starts to degrade in linear fashion until failure occurs in these slabs, as concrete temperatures gradually increase (above 200°C) in the inner layers of the slab. Failure occurs when the shear capacity drops below the shear force due to applied external loading. Based on shear limit state, the fire resistance of slabs with 150, 200, 250, 300 and 400 mm depth is 235, 145, 145, 155 and 200 minutes respectively. The fire resistance evaluated based on shear limit state compare well with the fire resistance based on deflection criteria for thicker slabs namely 250, 300 and 400 mm slabs, which undergo failure through flexure-shear or shear failure mode. Thus, it is evident that shear limit states is to be considered in evaluating failure in thicker hollowcore slabs, especially when the thickness exceeds 250 mm.

6.4.2 Effect of load intensity

To study the effect of load level on shear response, 200 mm and 400 mm slabs are analyzed under three different levels of loading, 50% (L50), 60% (L60) and 85% (L85) of room temperature moment capacity, as discussed in Section 6.3.2.

Results from the analysis indicate that load level has no effect on thermal response of hollowcore slabs, but has significant influence on structural response. Both 200 mm and 400 mm slabs exhibit similar deflection trend under different load levels, as shown in Figure 6.8(a). As expected, higher load levels result in higher deflections and lower fire resistance, indicating that

load level has significant effect on the fire resistance of hollowcore slabs. Fire resistance based on deflection limit state for 200 mm – L50, 200 mm – L60, 200 mm – L85 slabs is 140, 125, 105 minutes, and for the case of 400 mm – L50, 400 mm – L60, 400 mm – L85 slabs is 230, 200, 180 minutes respectively (see Figure 6.8(a)). The fire resistance evaluated based on strength criteria (flexural or shear strength degradation), as illustrated in Figure 6.8(b) and (c), corresponds well with deflection based failure times, as also shown in Table 6.1. A review of cracking patterns from ANSYS analysis clearly show that 200 mm slabs fail through flexural failure mode, while 400 mm slabs fail through shear failure mode under all three cases of loading, similar to that shown in Section 6.4.1. These results further infer that in thicker slabs, failure occurs through shear limit state under fire conditions irrespective of the load level.

6.4.3 Effect of loading scenarios

To study the effect of loading pattern, 200 mm and 400 mm thick hollowcore slabs are analyzed under three different loading scenarios, concentrated bending loading (BL), distributed loading (UDL) and shear loading (SL), as discussed in Section 6.3.2. However, loading scenario causing high shear force (SL) is only applied on 200 mm slabs in order to evaluate if shear failure is possible even in thinner slabs under high level of shear loading.

Results from the analysis indicate that loading pattern has no effect on thermal response of hollowcore slabs, but has significant influence on structural response. The deflection progression in these slabs under loading cases of BL and UDL is similar, as plotted in Figure 6.9(a), and this is due to the fact that under both cases of loading, slabs are basically subjected to higher bending moments. On the other hand, slab 200 mm – SL shows similar deflection progression to that of slabs 200 mm – BL and 200 mm – UDL in Stages 1 and 2, but in Stage 3 (beyond 75 minutes), 200 mm – SL shows rapid increase in deflection with failure occurring around 90 minutes. This

can be attributed to the fact that, slab 200 mm - SL is subjected to higher shear forces, as compared to slabs 200 mm - BL and 200 mm - UDL and thus, shear failure occurs much earlier in slab 200 mm - SL.

The fire resistance of analyzed slabs is also evaluated based on flexural or shear strength criteria, as illustrated in Figure 6.9(b) and (c), and these values compare well with deflection-based failure times. The computed fire resistance is also compared in Table 6.1. Higher fire resistance in slab 400 mm – UDL (which is 220 minutes), as compared to slab 400 mm – BL (which is 200 minutes), can be attributed to the shift in failure mode from shear in 400 mm – BL slab to flexural in 400 mm – UDL slab, as shown in Figure 6.10(c) and (d). However, there is no noticeable difference in the failure mode and fire resistance between 200 mm – BL and 200 mm – UDL slabs. Further, the cracking pattern composed of inclined cracks at loading zones and absence of flexural cracking close to mid span also infer that the failure in slab 200 mm – SL is through shear, as illustrated in Figure 6.10(e).

These results infer that shear limit state can govern failure even in thinner hollowcore slabs when subjected to certain loading patterns under fire conditions.

6.4.4 Effect of axial restraint

To study the effect of axial restraint on the behavior of hollowcore slabs under fire conditions, 200 mm and 400 mm hollowcore slabs are analyzed under 50 percent and 100 percent (full) axial restraints, designated as AR50 and AR100, as discussed in Section 6.3.2.

Results from the analysis show that axial restraint has no effect on the temperature profile of hollowcore slabs but have significant effect on the structural response of these slabs under fire conditions. As discussed in Chapter 5, presence of axial restraint enhances fire resistance of hollowcore slabs through redistribution of stresses and in turn offsetting (delaying) the failure. In

addition, the extent of increase in fire resistance depends on the level of axial restraint, as also reflected in Figure 6.11(a), wherein slabs with 100 percent (full) axial restraints (AR100) undergo lower deflections and exhibit higher fire resistance, as compared to those with 50 percent axial restraint at supports. Similarly, slabs with 50 percent axial restraints (AR50) undergo lower deflections and exhibit higher fire resistance than those without any axial restraints (SS). As per deflection limit state, the fire resistance of slabs 200 mm – SS, 200 mm – AR50 and 200 mm – AR100 is 125, 140 and 160 minutes, while that of slabs 400 mm – SS, 400 mm – AR50 and 400 mm – AR100 is 200, 230 and 240 minutes respectively.

These fire resistance values correspond well with that evaluated based on strength criteria, as shown in Table 6.1 and Figure 6.11(b) and (c). The enhanced moment capacity due to second order moments induced by the presence of axial restraints results in higher fire resistance in these slabs. Thus, fire resistance based on strength limit state in slabs 200 mm – AR50 and 200 mm – AR100 is 140 and 160 minutes respectively, and in slabs 400 mm – AR50 and 400 mm – AR100 is 230 and 240 minutes respectively. These fire resistance times are greater than those in slabs without any axial restraint (SS), as also can be seen in Table 6.1.

The axial restraint also influences the resulting failure mode in hollowcore slabs under fire conditions. As illustrated in Figure 6.12, extent of flexural cracking increases with increase in the level of axial restraint in 200 mm slab, while the failure mode in 400 mm – SS slab shifts from shear to flexure-shear in slab 400 mm – AR50 and then to flexure in slab 400 mm – AR100. This is mainly due to the fact that fire-induced axial force, generated due to presence of axial restraint, enhances both moment capacity and shear capacity. However, the relative increase in shear capacity is much higher than that of moment capacity and thus, presence of axial restraint in hollowcore slabs helps in avoiding shear failure even in thicker hollowcore slabs under fire

conditions. These results infer that presence of high axial restraint at supports can enhance fire resistance and also prevent shear failures in thicker slabs.

6.4.5 Effect of level of prestressing

To study the effect of level of prestressing on fire resistance of slabs, 200 mm and 400 mm hollowcore slabs are analyzed under three different levels of prestressing, namely 50% (PS50), 70% (PS70) and 85% (PS85), as discussed in Section 6.3.2. Results from the analysis indicate that level of prestressing has no effect on the temperature profile of hollowcore slabs, but has significant effect on the structural response of these slabs. As per deflection limit state, fire resistance of 200 mm – PS50, 200 mm – PS70, 200 mm – PS85 slabs is 110, 125, 140 minutes and corresponding values in 400 mm – PS50, 400 mm – PS70, 400 mm – PS85 slabs is 195, 200, 200 minutes, as shown in Figure 6.13(a) and Table 6.1.

Even though deflection trends (see Figure 6.13(a)) in these slabs under fire exposure do not show significant variation under various levels of prestressing, the level of prestressing has significant effect on the degradation of moment and shear capacity in these slabs, as shown in Figure 6.13(b) and (c). Slabs with higher level of prestressing have higher flexural and shear capacity at ambient conditions. The higher capacity, resulting from higher prestressing, becomes less effective at higher temperatures, as prestressing strands start to lose their strength due to increase in temperature, which is evident in Figure 6.13. The fire resistance based on strength criteria (moment and shear capacity) compare well with the failure times evaluated based on deflection limit state, as also shown in Table 6.1.

Further, cracking patterns generated from ANSYS, as shown in Figure 6.14, also show that level of prestressing has significant effect on failure modes of hollowcore slabs exposed to fire. In 200 mm slab, intensity of flexural cracking increases with increase in level of prestressing, while

failure mode in 400 mm slab shifts from flexure-shear mode to shear mode when the level of prestressing is increased from 50 to 70 and then to 85 percent.

These results infer that, although an increase in level of prestressing can lead to improved structural (moment and shear) performance at ambient conditions, the effectiveness of prestressing gets diminished at elevated temperature, due to loss in strand strength leading to insignificant improvement in the overall fire resistance.

6.4.6 Effect of fire severity

To study the effect of fire severity, 200 mm and 400 mm hollowcore slabs are analyzed under five different fire scenarios (see Figure 6.4), as discussed in Section 6.3.2. Results from the analysis indicate that fire severity has significant effect on thermal as well as structural response of PC hollowcore slabs. As expected, higher intensity fire exposure leads to higher sectional temperatures in these slabs, as shown in Figure 6.15, and due to this, slabs undergo higher deflections under severe fires. As illustrated in Figure 6.16(a) and (b), mid-span deflections under ASTM-E1529 and DF3 are higher than that under ASTM-E119 and DF2, which are in turn higher than that under DF1. These deflection profiles show that 200 mm slab does not fail under DF1 fire, and 400 mm slab does not fail under both DF1 and DF2 fires. However, failure in 200 mm slab occurs at 60 minutes under both DF3 and ASTM-E1529 fires and at 125 and 150 minutes under ASTM-E119 and DF2 fire scenarios respectively. Similarly, failure in 400 mm slab occurs at 200, 120 and 110 minutes under ASTM-E119, ASTM-1529 and DF3 fires respectively. These results indicate that failure times are similar under ASTM-E1529 and DF3 and ASTM-E119 and DF2 fire scenarios which are of similar or of equivalent fire severity. These fire resistance values evaluated based on deflection criteria, correlate well with that based on strength criteria (moment and shear capacity), as shown in Table 6.1 and Figure 6.16(c) to (f).

A review of cracking patterns generated in ANSYS indicate that, there is no significant variation in failure modes in 200 mm slab under different fire scenarios, as failure in thinner slab (200 mm) occurs through flexure under all fire scenarios except under DF1, wherein failure did not occur due to low intensity of fire. However, slightly higher extent of concrete cracking is evaluated in 200 mm slab under higher intensity fires namely ASTM-E1529 and DF3, as compared to that under ASTM-E119 and DF2.

On the other hand, the failure mode in 400 mm slab shifted from shear failure mode to flexural failure mode when subjected to higher severity fires such as ASTM-E1529 and DF3. This can be attributed to the fact that the flexural capacity of hollowcore slab is mainly dependent on the strand temperature, and under higher fire intensity, temperature in strands increase at a much higher rate than inner concrete layers causing faster degradation in moment capacity than shear capacity. The failure modes under various fire severities are very similar to the ones presented in Section 6.4.1.

These results infer that fire intensity has significant influence on fire response and failure modes of PC hollowcore slabs, wherein higher intensity fire exposure can shift mode of failure in hollowcore slabs from shear to flexure.

Table 6.1. Comparison of predicted fire resistance in hollowcore slabs

		Fire resistance (minutes)					
Study parameter	Slab description	Insulation- model	Deflection- model	Flexure - based on EC2	Shear - based on EC2	Code EC2/ ACI216.1 /PCI	Failure mode
Slab depth	150 mm	90	90 🕌	▶90	235	60 (OC)	Flexure
	200 mm	120	125	130	145	90 (OC)	Flexure
	250 mm	130	145	150	145	120(OC)	Flexure- Shear
	300 mm	150	155	165	155	180 (UC)	Shear
	400 mm	180	200	220	200	240 (UC)	Shear
Load level	200 mm - L50	120	140	135	155	90 (OC)	Flexure
	$200\;mm-L60\;$	120	125	130	145	90 (OC)	Flexure
	200 mm – L85	120	105	105	105	90 (OC)	Flexure- Shear
	$400\;mm-L50\;$	180	230	230	220	240 (UC)	Shear
	$400\;mm-L60\;$	180	200	220	200	240 (UC)	Shear
	400 mm – L85	180	180	190	170	240 (UC)	Shear
Loading scenario	200 mm - BL	120	125	130	145	90 (OC)	Flexure
	200 mm - UDL	120	125	130	155	90 (OC)	Flexure
	200 mm - SL	120	90 🕶	130	90	90	Shear
	400 mm - BL	180	200	220	200	240 (UC)	Shear
	400 mm - UDL	180	220	220	230	240 (UC)	Flexure
Axial restraint	200 mm - SS	120	125	130	145	90 (OC)	Flexure
	200 mm - AR50	120	140	140	160	90 (OC)	Flexure
	200 mm – AR100	120	160	160	180	90 (OC)	Flexure
	400 mm – SS	180	200	220	200	240 (UC)	Shear
	400 mm – AR50	180	230	230	230	240 (UC)	Flexure- Shear
	400 mm – AR100	180	240	240	260	240	Flexure
Level of prestressing	200 mm – PS50	120	110	110	145	90 (OC)	Flexure
	200 mm – PS70	120	125	130	145	90 (OC)	Flexure
	200 mm – PS85	120	140	140	150	90 (OC)	Flexure
	400 mm – PS50	180	195	195	195	240 (UC)	Flexure- Shear
	$400\;mm-PS70$	180	200	220	200	240 (UC)	Shear
	400 mm – PS85	180	200	230	205	240 (UC)	Shear
Fire scenario	200 mm – E119	120	125	130	145	90 (OC)	Flexure
	200 mm - E1529	120	60◀──	60	75	90 (OC)	Flexure
	200 mm – DF1	120	n.f.	n.f.	n.f.	90	n.f.
	200 mm - DF2	120	150◀──	150	n.f.	90 (OC)	Flexure
	200 mm – DF3	120	60	65	80	90 (UC)	Flexure
	400 mm – E119	180	200	220	200	240 (UC)	Shear
	400 mm – E1529	120	120	→ 120	140	240 (UC)	Flexure
	400 mm – DF1	180	n.f.	n.f.	n.f.	240	n.f.
	400 mm - DF2	180	n.f.	n.f./240	n.f.	240 (UC)	n.f.
	400 mm - DF3	120	110	→ 115	125	240 (UC)	Flexure

Note: 'n.f.' = no failure, 'n.a.' = not available, 'OC' = over conservative, 'UC' = under conservative

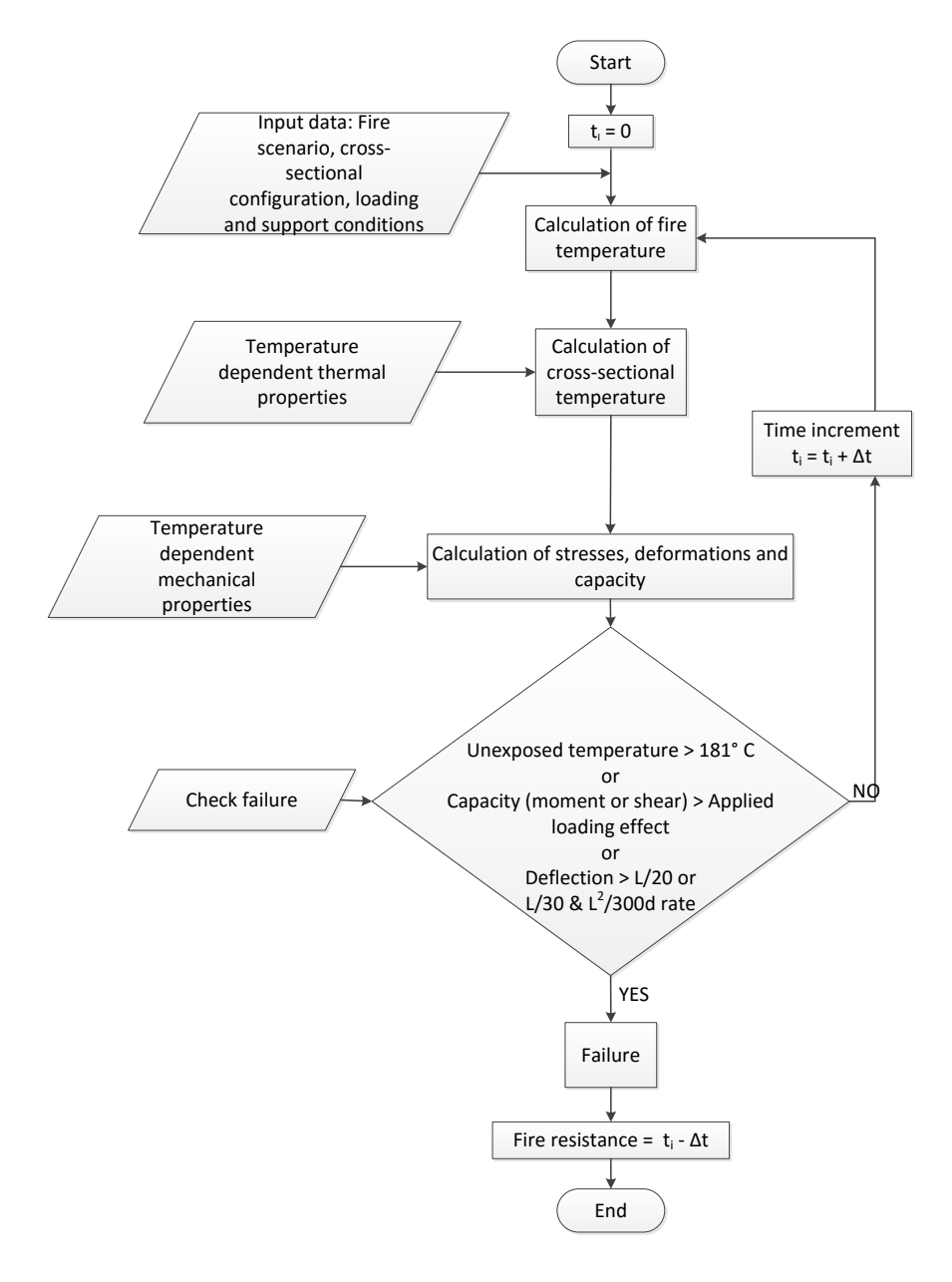


Figure 6.1. Flowchart showing steps associated with fire resistance analysis of hollowcore slabs

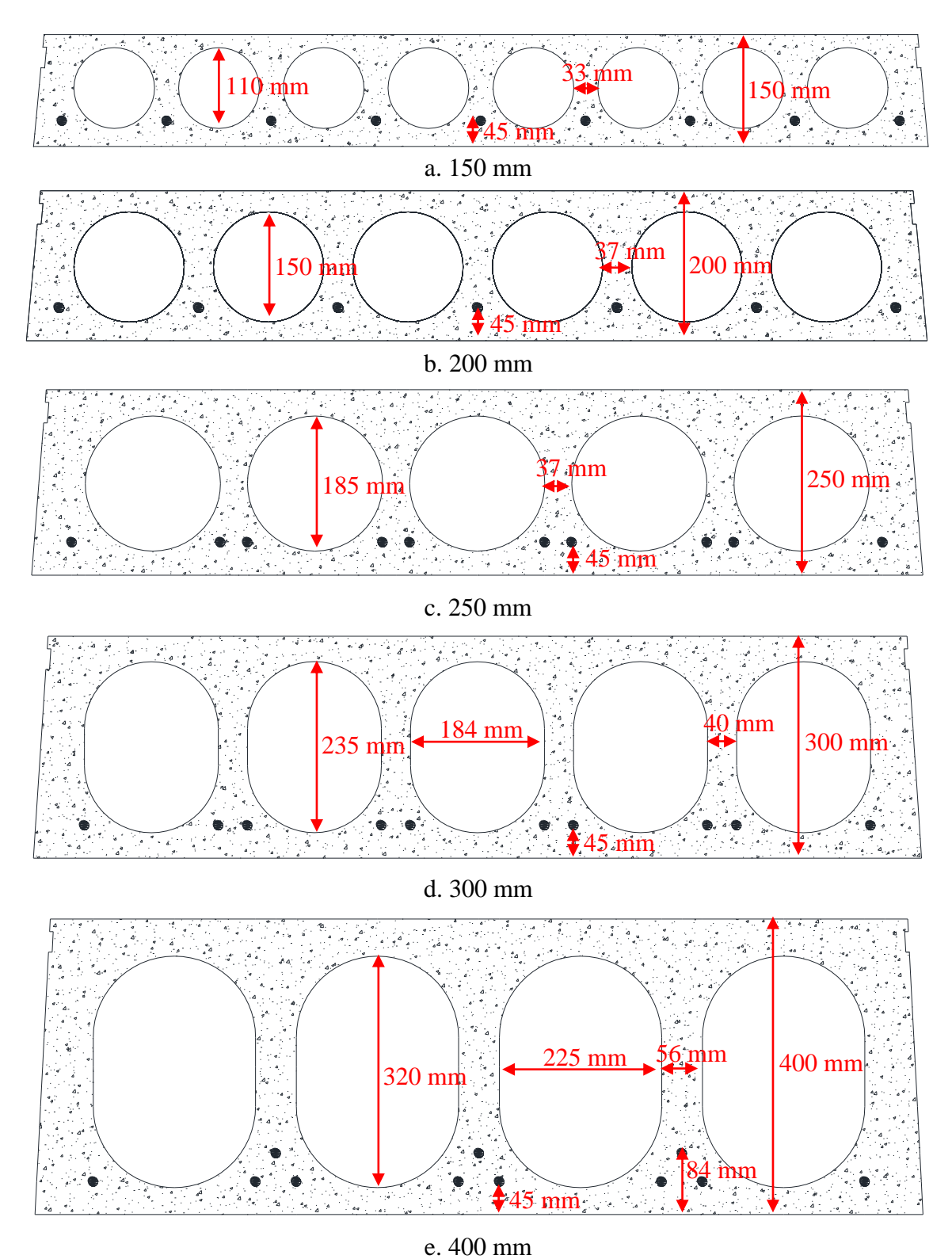
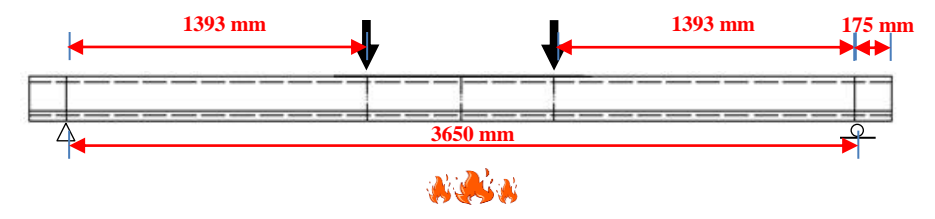


Figure 6.2. Cross-sectional configurations of various standard PC hollowcore slabs



a. Under four point loads inducing high bending load (BL)

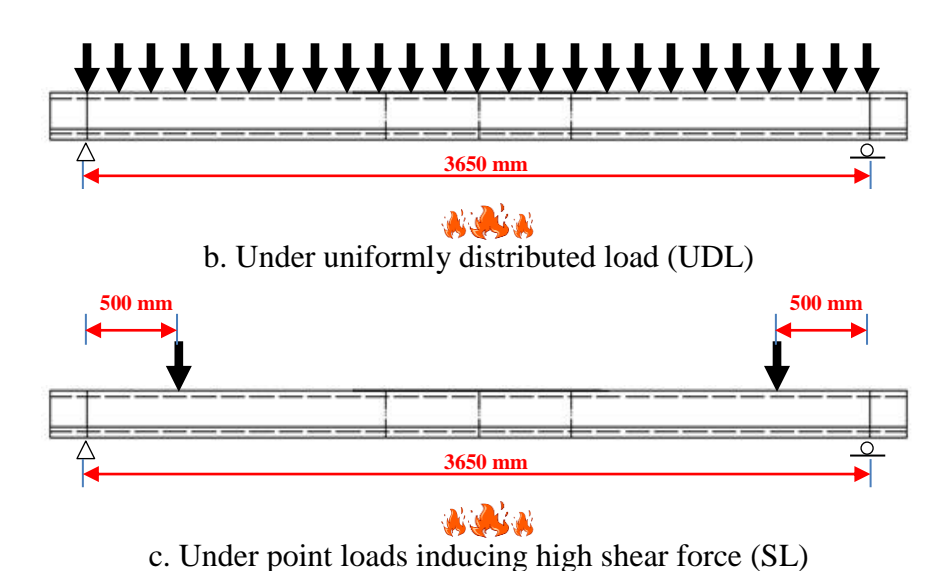


Figure 6.3. PC hollowcore slab subjected various loading scenarios

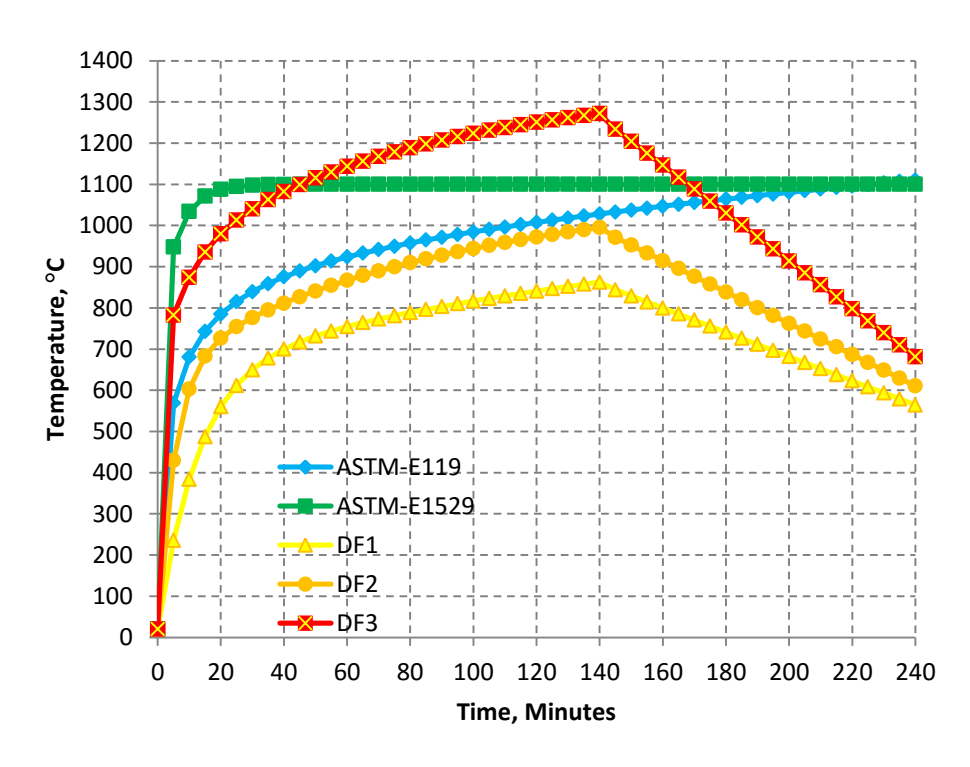


Figure 6.4. Various fire scenarios encountered in buildings and parking structures

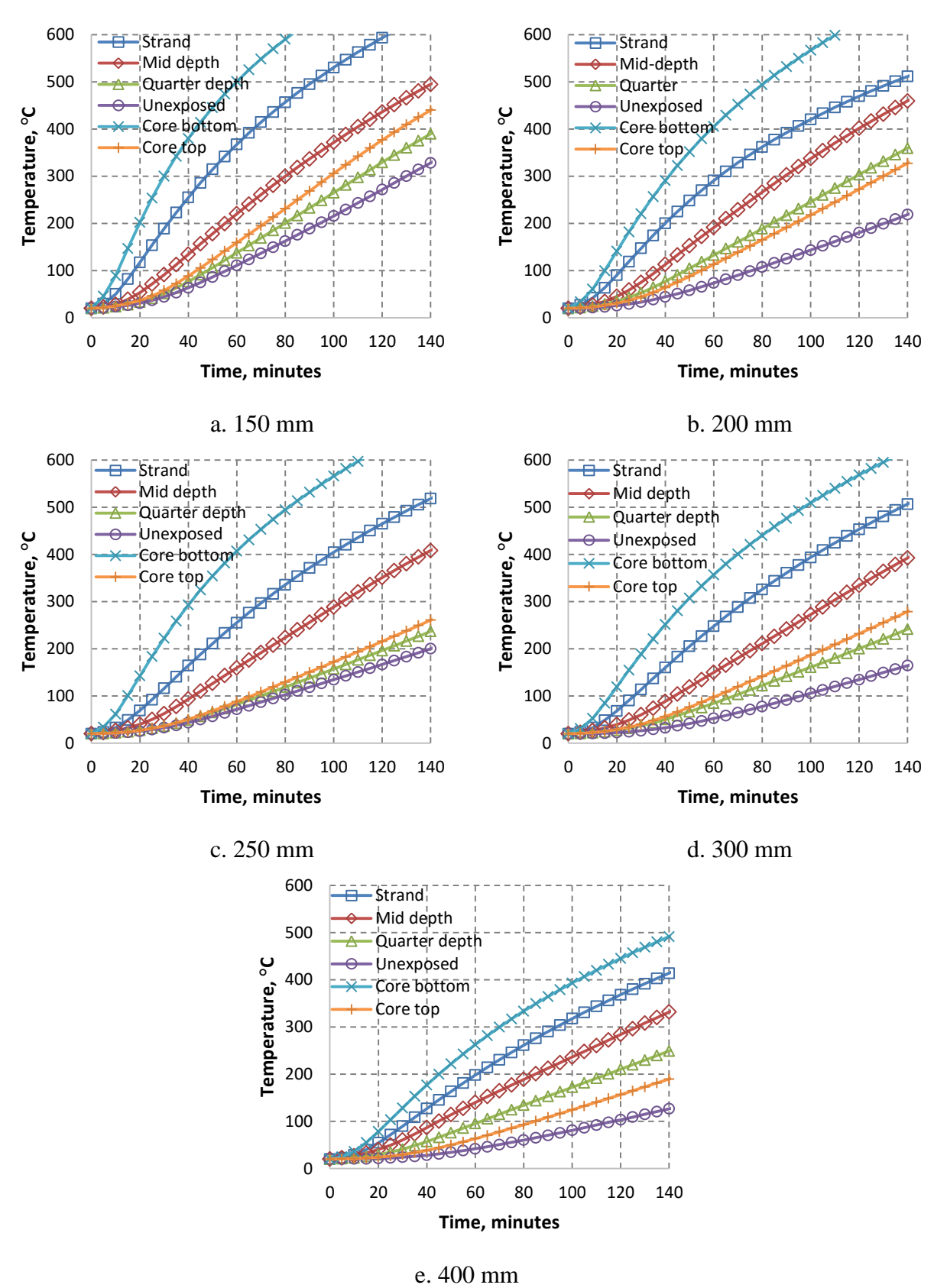
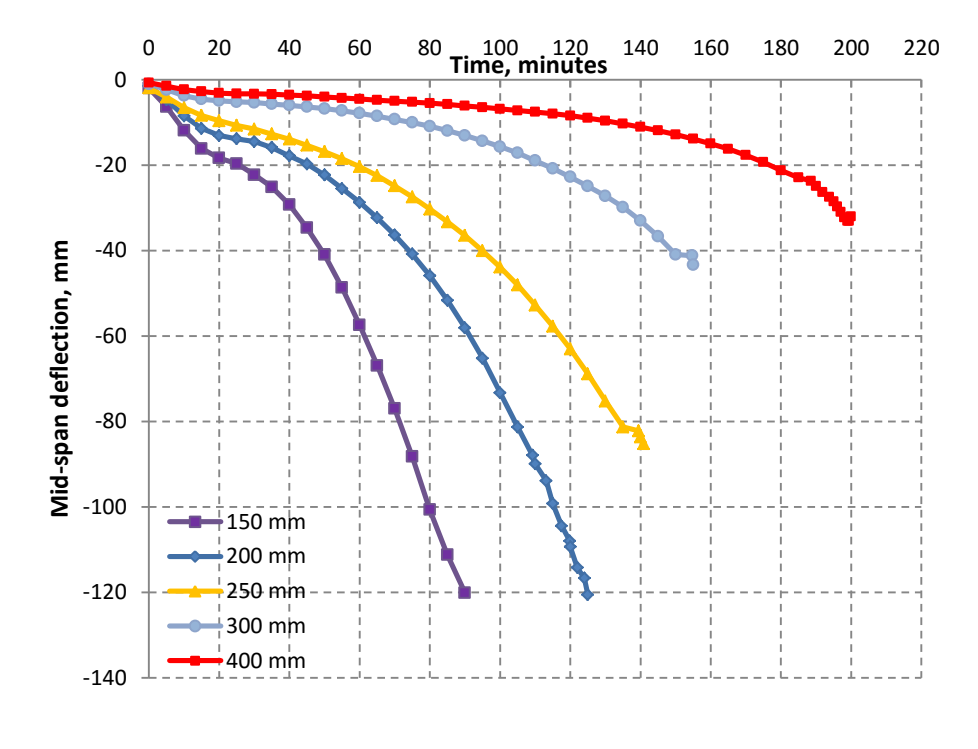
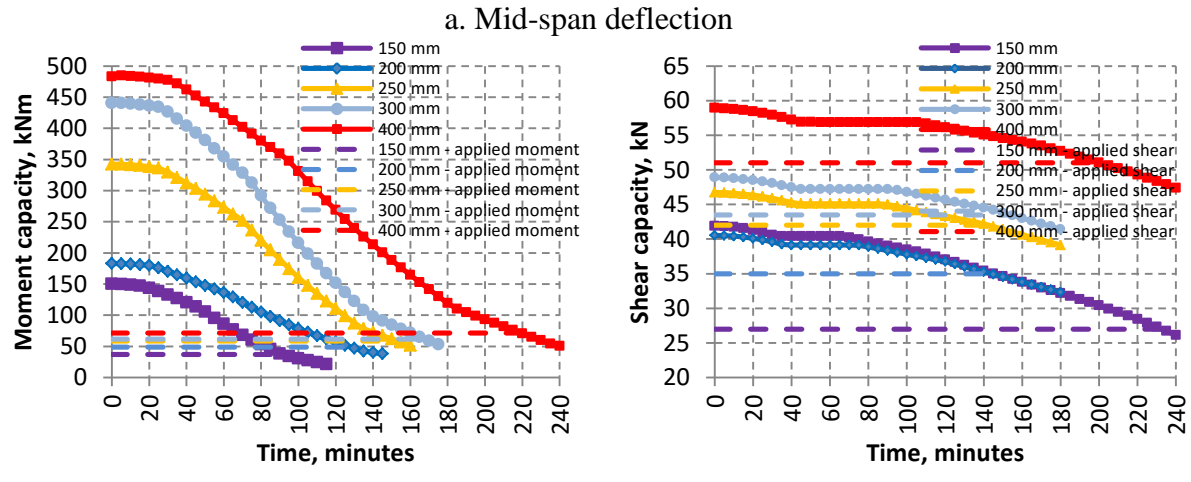


Figure 6.5. Variation of cross-sectional temperature in various hollowcore slabs under fire





a. Moment capacity c. Shear capacity
Figure 6.6. Effect of slab depth on mid-span deflection, moment and shear capacity of hollowcore slabs exposed to fire

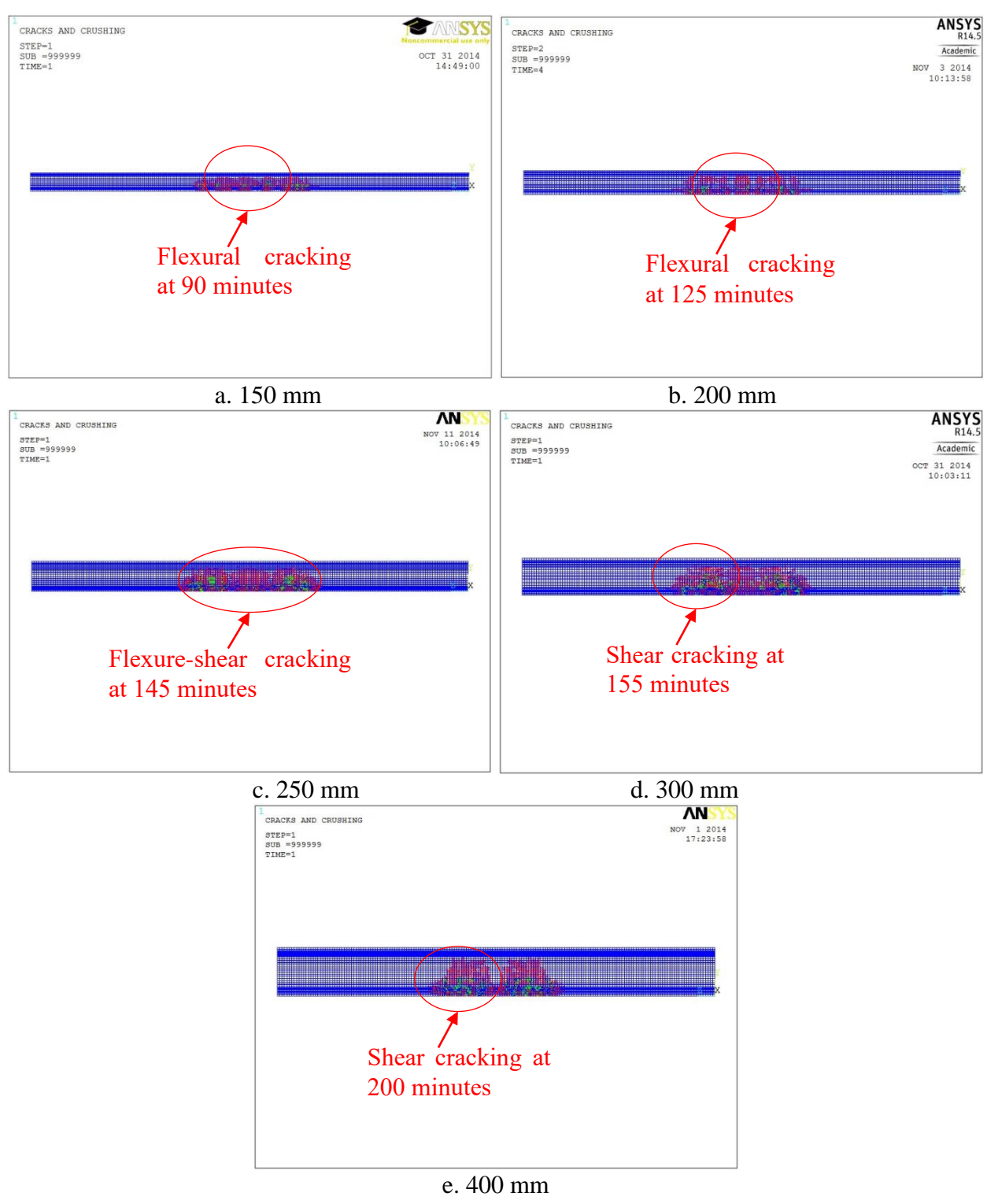
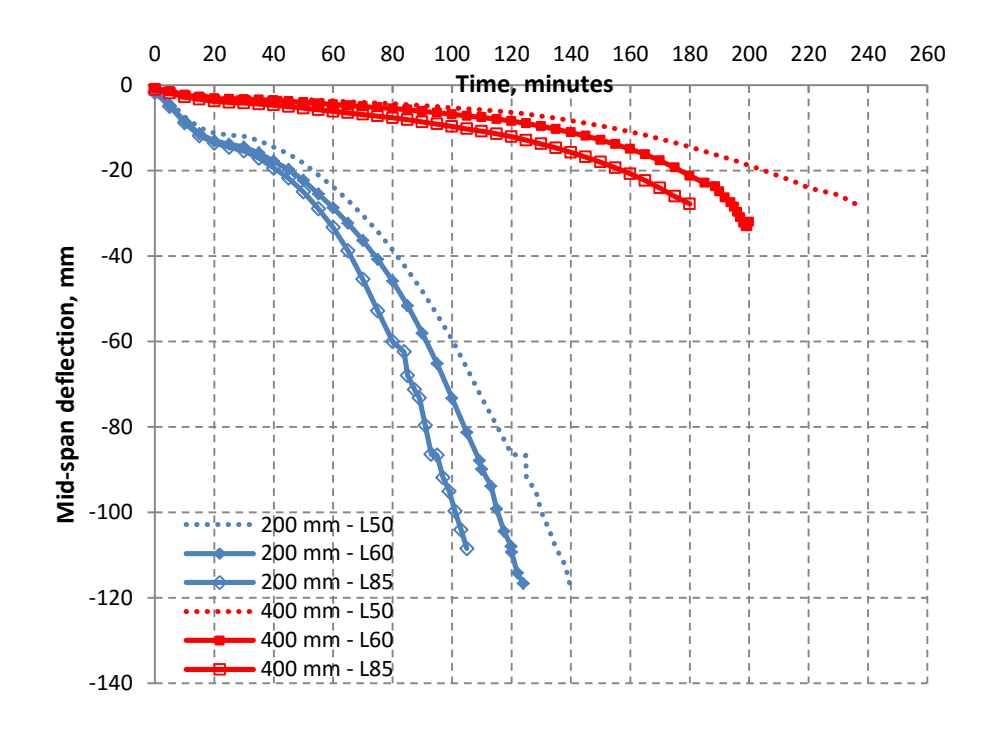
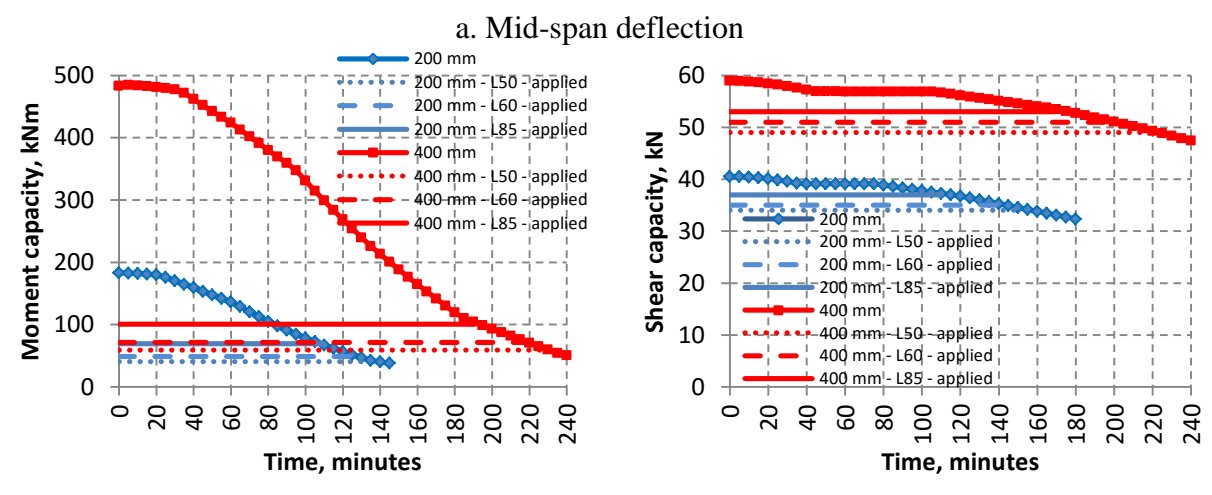
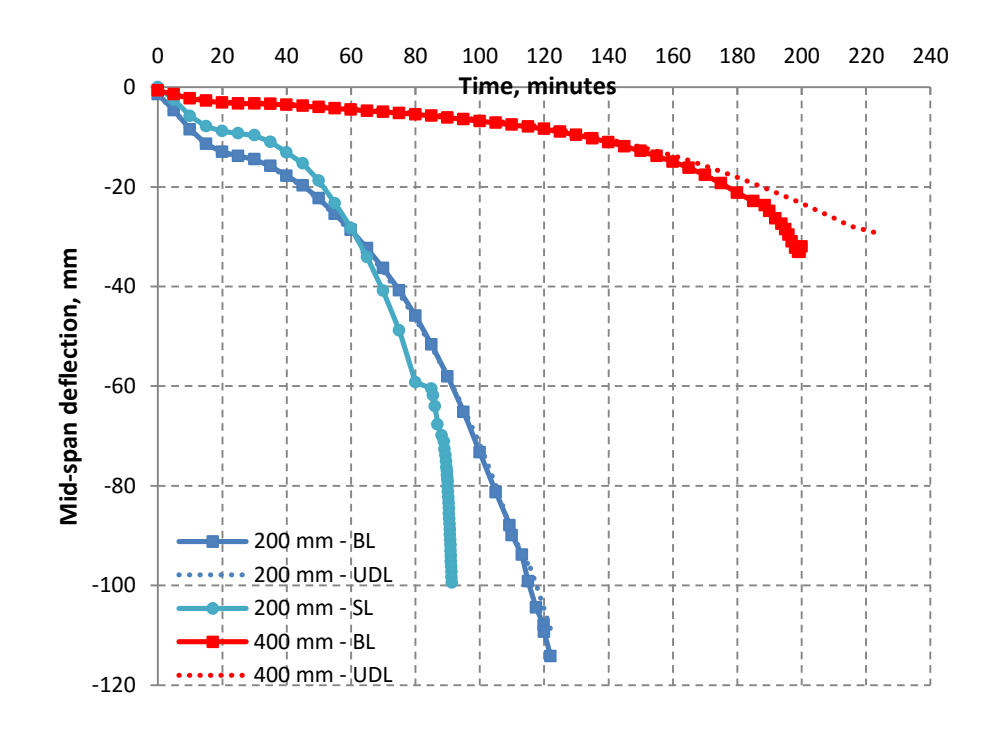


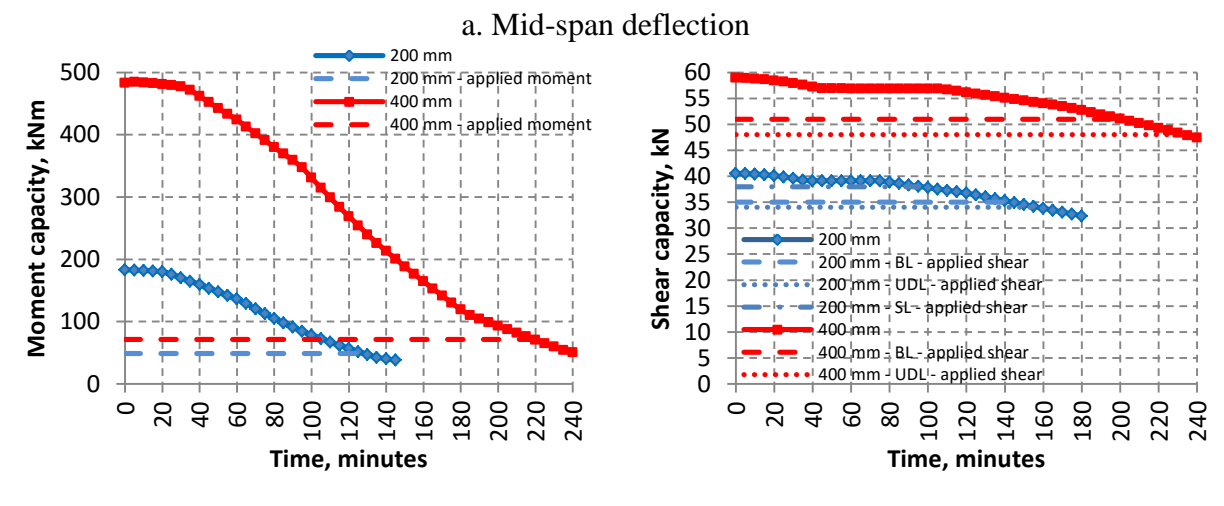
Figure 6.7. Effect of slab depth on crack pattern in hollowcore slabs under fire condition at failure





b. Moment capacity c. Shear capacity
Figure 6.8. Effect of load level on mid-span deflection, moment and shear capacity in hollowcore slabs exposed to fire





b. Moment capacity c. Shear capacity
Figure 6.9. Effect of loading scenario on mid-span deflection, moment and shear capacity in hollowcore slabs exposed to fire

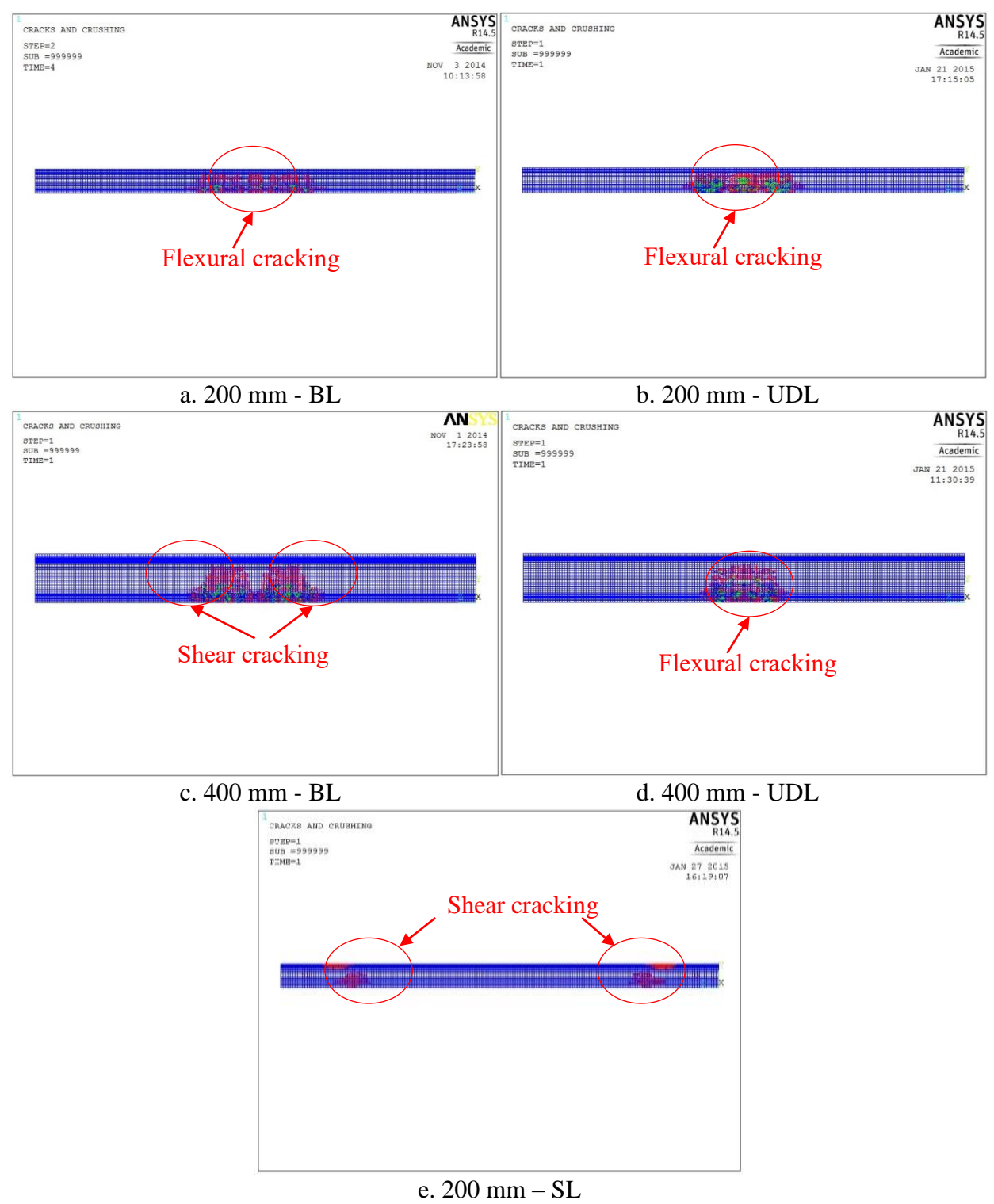
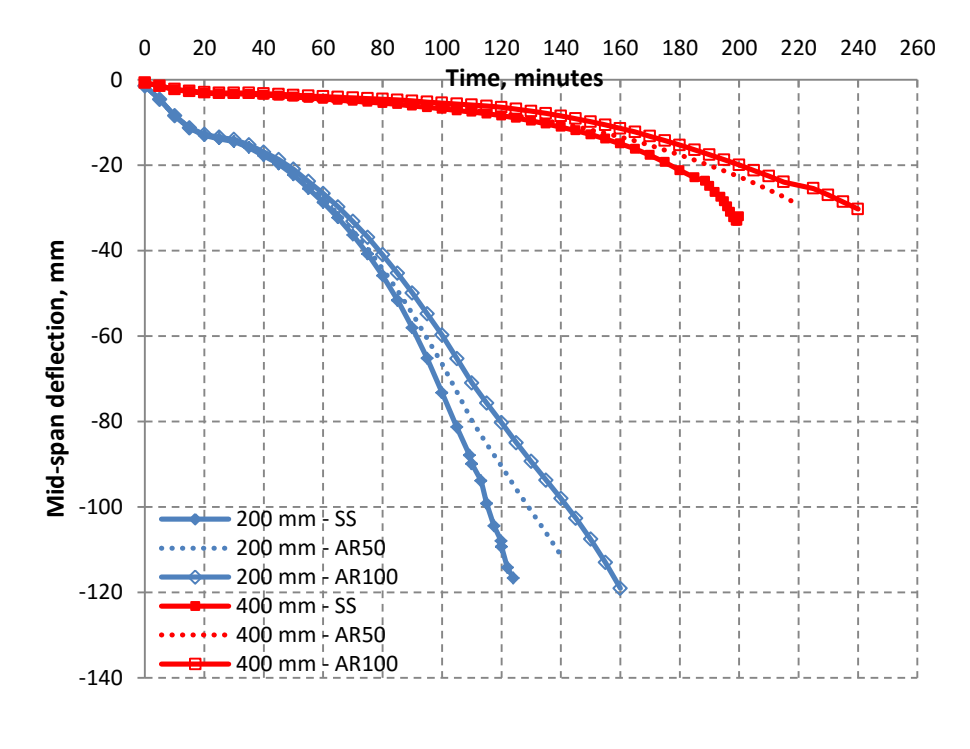
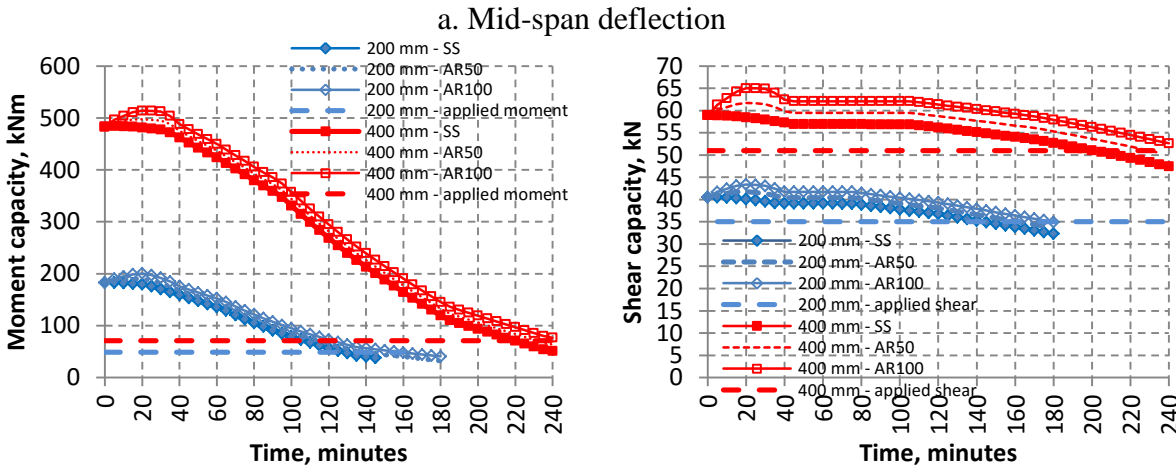


Figure 6.10. Effect of loading scenarios on crack pattern in hollowcore slabs exposed to fire





b. Moment capacity c. Shear capacity
Figure 6.11. Effect of axial restraint on mid-span deflection, moment and shear capacity in hollowcore slabs exposed to fire

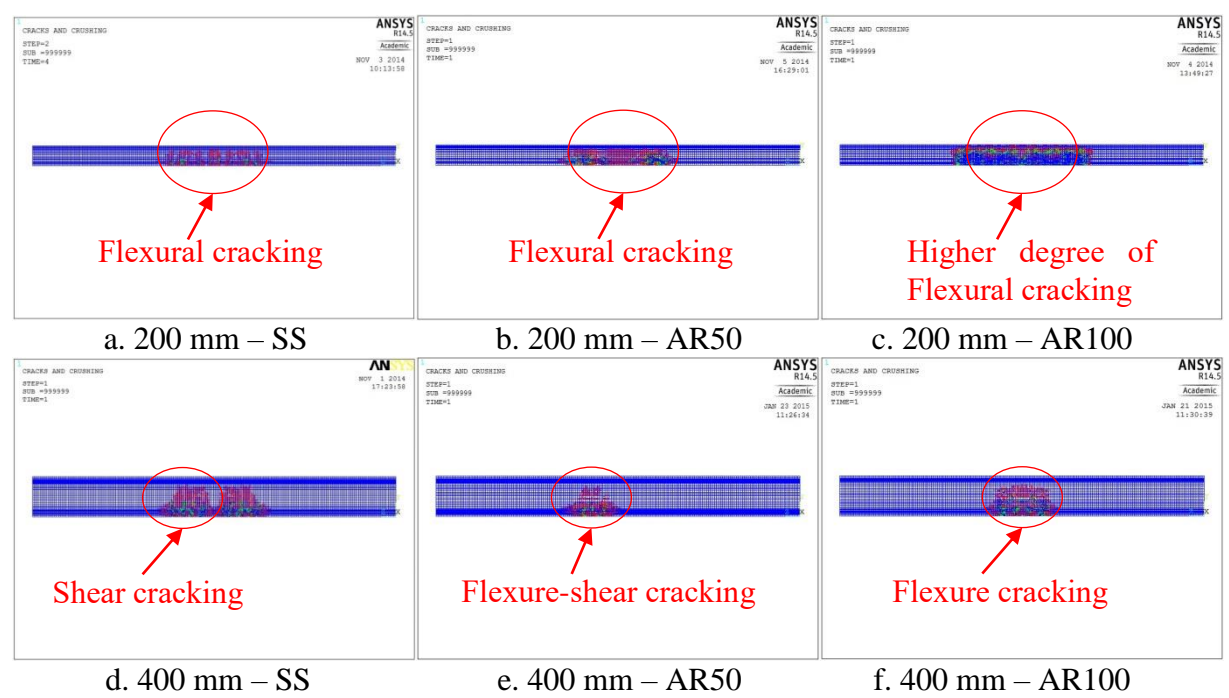
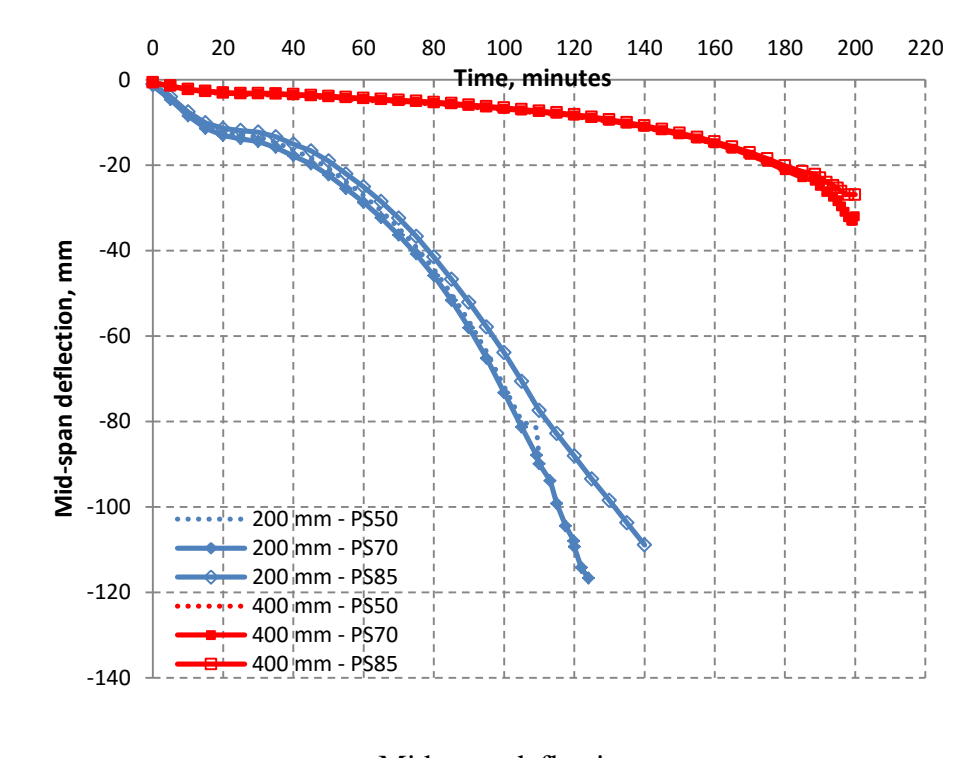
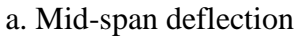
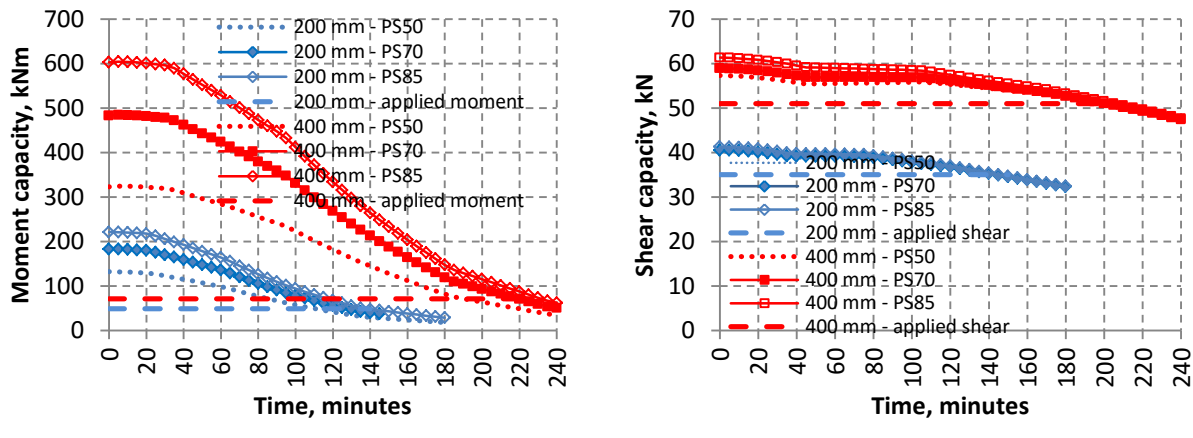


Figure 6.12. Effect of axial restraint on crack pattern in hollowcore slabs exposed to fire







b. Moment capacity

c. Shear capacity

re 6.13. Effect of level of prestressing on mid-span deflection, moment and she

Figure 6.13. Effect of level of prestressing on mid-span deflection, moment and shear capacity in hollowcore slabs exposed to fire

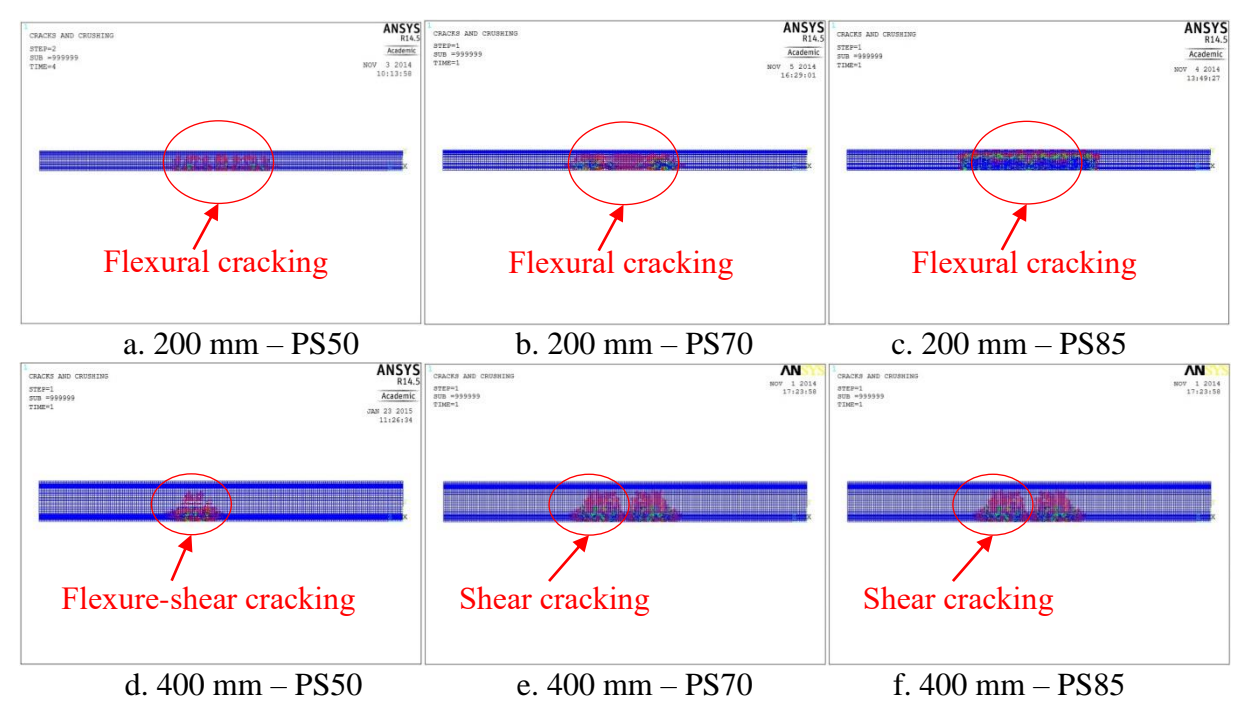


Figure 6.14. Effect of level of prestressing on crack pattern in hollowcore slabs exposed to fire

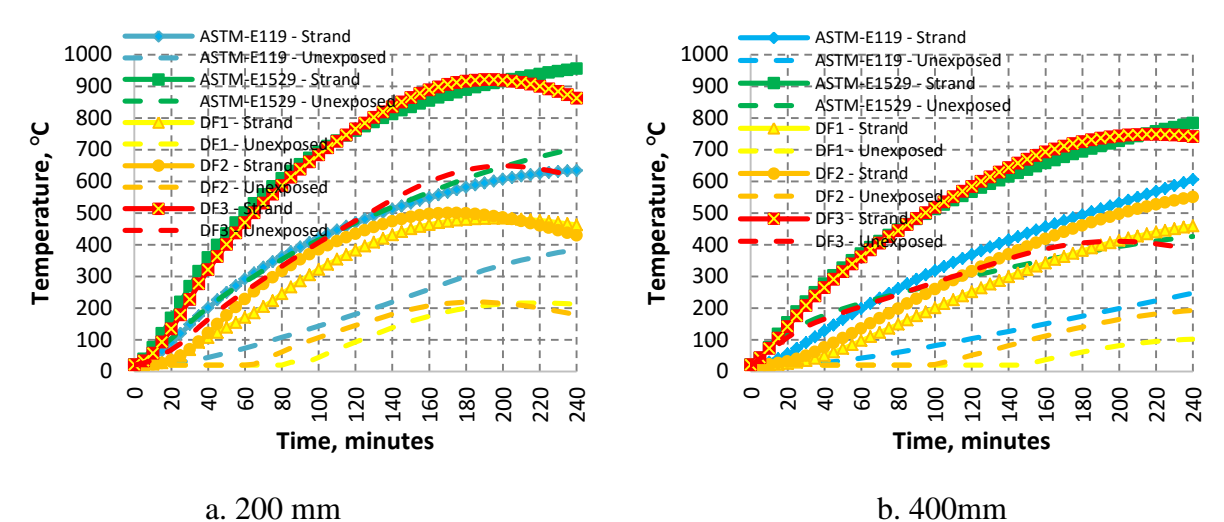
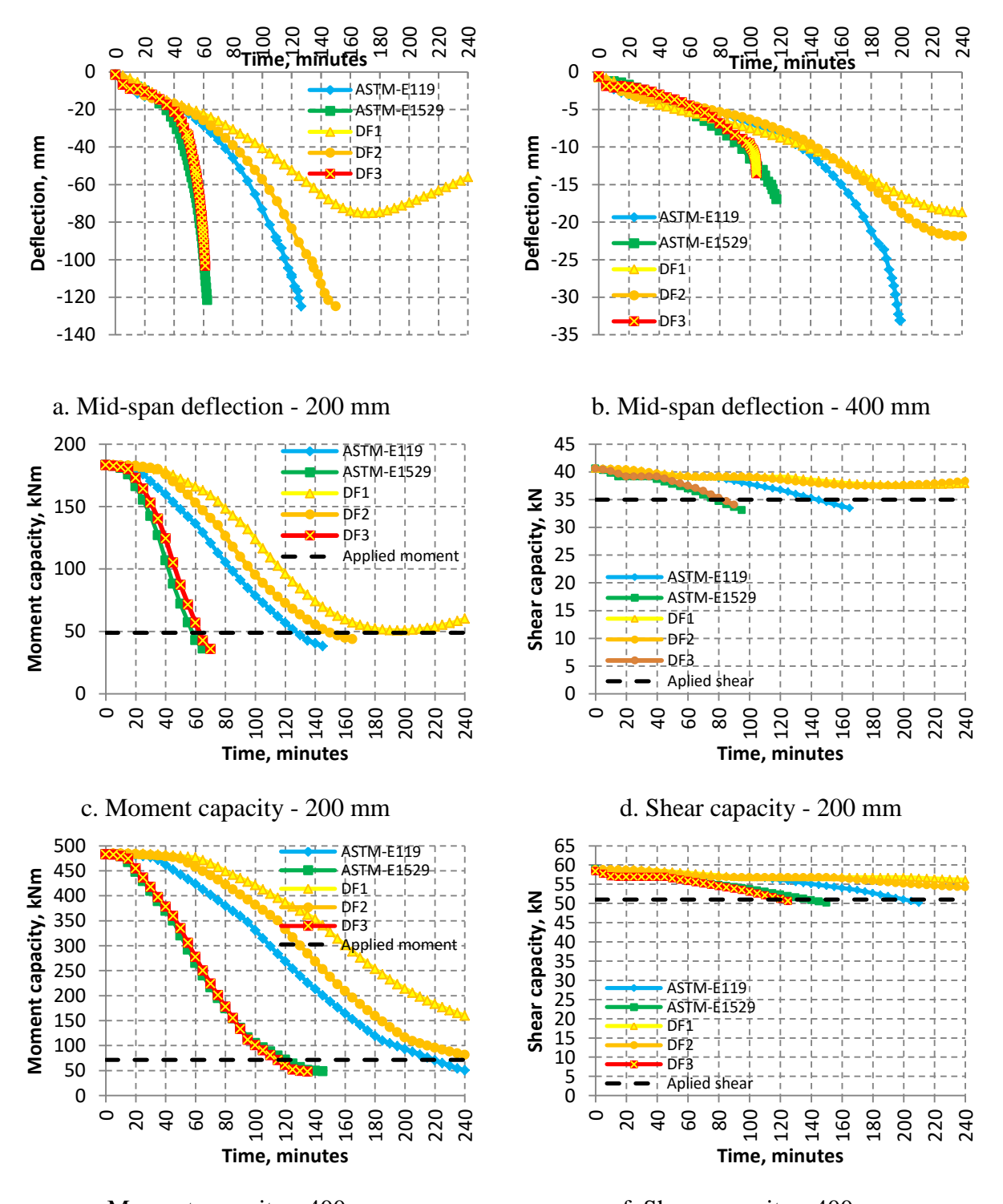


Figure 6.15. Effect of fire severity on sectional temperatures in hollowcore slabs



e. Moment capacity - 400 mm
f. Shear capacity - 400 mm
Figure 6.16. Effect of fire severity on mid-span deflection, moment and shear capacity in hollowcore slabs

6.5 Summary

Based on the results and observations presented in this chapter, following observations can be drawn on the fire behavior of PC hollowcore slabs:

- Slab depth has significant effect on mode of failure in hollowcore slabs under fire conditions, wherein failure is through flexural mode in thinner slabs (150 and 200 mm), flexure-shear mode in medium thickness slab (250 mm) and shear failure in thicker slabs (300 and 400 mm).
- Load intensity and loading pattern has significant effect on the shear response of PC
 hollowcore slabs under fire conditions. PC hollowcore slabs can undergo shear failure prior
 to attaining flexural failure under concentrated loads inducing high shear forces.
- Axial restraint has significant effect on shear response of PC hollowcore slabs under fire
 conditions, wherein presence of higher axial restraint at support can prevent shear failure in
 fire exposed hollowcore slabs.
- Fire severity has significant effect on fire behavior of PC hollowcore slabs, wherein a higher intensity fire results in lower fire resistance and can shift failure mode from shear to flexure in thicker hollowcore slabs.
- Simplified approach derived from Eurocode 2 for evaluating moment and shear capacity of PC hollowcore slabs under fire conditions reasonably predicts fire resistance of PC hollowcore. However, it is crucial to account for both flexural and shear limit states while evaluating fire resistance.

This chapter is mainly based on the following journal papers:

- V. K. R. Kodur, A. M. Shakya. Application of rational methodology for evaluating fire resistance of concrete structures, Building Materials, Szkoła Główna Służby Pożarniczej, Pages 82-87, Warsaw, Poland, October 2014.
- V. K. R. Kodur, A. M. Shakya, Performance based approach for evaluating fire resistance of prestressed concrete hollowcore slabs, Concrete in Australia – Concrete Performance in Fire, Concrete Institute of Australia, 40-3, Pages 54-61, September 2014.
- Shakya AM, Kodur VKR. Behavior of prestressed concrete hollowcore slabs under standard and design fire exposure. 8th Int. Conf. Struct. Fire, vol. 1, Shanghai China: 2014, p. 199–208.
- Shakya AM, Kodur VKR. Performance of prestressed concrete hollowcore slabs under standard and design fire exposure. PCI Conv. Natl. Bridge Conf., National Harbor, MD: Prestressed Concrete Institute; 2014.

7.1 General

The prevalent method of evaluating fire resistance of hollowcore slabs is through prescriptive methods as specified in ACI 216.1 (ACI 216.1-14 2014), PCI (PCI 2011) and Eurocode2 (Eurocode 2 2004a). The prescriptive methods mainly comprise of tabulated fire resistance ratings linked to concrete cover thickness and effective slab depth of hollowcore slabs and are derived based on standard fire tests. These prescriptive methods do not account for actual design

(fire scenario, load level and restraint level) conditions and realistic failure modes, and thus might not yield realistic fire resistance in PC hollowcore slabs.

Some codes such as PCI (PCI 2010) and Eurocode 2 (Eurocode 2 2004a) provide simplified design approaches for evaluating fire resistance of concrete structures. These approaches are typically based on sectional analysis and utilize temperature induced strength reduction factors to evaluate reduction in flexural capacity of a structural member at a given fire exposure time. When the degraded sectional capacity drops below applied loading effect (moment) during a fire event, failure is said to occur. Such a design approach for evaluating fire resistance of PC hollowcore slabs is not well established, as these approach are validated for flexural failure only without any considerations to other critical failure modes, especially shear failure (Jansze et al. 2012; Min et al. 2012). Thus, there is a critical need for a rational design approach to evaluate realistic fire resistance of PC hollowcore slabs that can account for all critical failure modes in PC hollowcore slabs under fire conditions.

7.2 Rational design approach

To overcome the drawbacks in current prescriptive based fire design approaches for PC hollowcore slabs, a rational approach is developed for evaluating the fire resistance of PC hollowcore slabs. As structural behavior of PC hollowcore slabs is mainly governed by flexural and shear response, fire resistance of PC hollowcore slab is evaluated by accounting for failure through both flexural and shear limit states. The proposed approach comprises of two main stages. First stage involves evaluating cross-sectional temperatures, which is followed by evaluating moment and shear capacities at any given time into fire exposure. Prestressing strand and web concrete temperatures are utilized to evaluate flexural and shear capacities at a given

fire exposure time. Since, the moment capacity at a critical section of hollowcore slab is mostly dependent on the strand, and the shear capacity is mostly dependent on the web concrete, temperatures at strand and web locations need to be evaluated during fire exposure. A flowchart illustrating the various steps in evaluating fire resistance of hollowcore slab is shown in Figure 7.1.

7.3 Simplified approach for predicting temperatures in PC hollowcore slabs

The behavior of fire exposed PC hollowcore slabs is mainly governed by flexural and shear response. Flexural and shear capacities at a section in PC hollowcore slabs are mainly influenced by temperature induced strength degradation in prestressing strand and concrete. Thus, first step in accurately predicting fire response of hollowcore slab is accurately predicting sectional temperature, as also illustrated in the flowchart (see Figure 7.1). Therefore, knowing the temperatures in strand and web concrete is critical for evaluating sectional moment and shear capacities, respectively, at any particular time during fire exposure.

7.3.1 General procedures

There are very few approaches in the literature for predicting sectional temperatures in concrete members under fire exposure. Kodur et al. (Kodur et al. 2013) recently proposed a simplified approach for evaluating sectional temperatures in concrete members. However, this simplified approach is not directly applicable due to presence of void cores in hollowcore slabs. Thus, the simplified approach developed by Kodur et al. (Kodur et al. 2013) is extended for evaluating sectional temperatures in hollowcore slabs.

To account for hollow cores in slabs, regression analysis is carried out for obtaining the coefficients in the simplified approach proposed by Kodur et al. (Kodur et al. 2013). The

regression analysis is carried out based on the temperature data generated in Chapter 6 for wide range of PC hollowcore slabs of various thicknesses. The sectional temperatures are dependent on the slab depth and core size, and thus, the coefficients needs to be individually calibrated for temperatures at different concrete layer. Thus, two sets of coefficients are calculated for predicting temperatures in hollowcore slabs at two critical locations; strand and mid depth, required for evaluating moment and shear capacity.

Further, there is large variability in cross-sectional core configurations in hollowcore slabs from one manufacturer to another and one country to another. Thus, it is extremely difficult to develop regression-based simplified approach for predicting sectional temperatures for all possible cross-sectional configurations. Thus, proposed simplified approach for evaluating sectional temperatures is established for commonly used core configurations in the United States, with depths ranging from 150 mm to 400 mm.

7.3.2 Nonlinear regression analysis

A large amount of temperature data is generated through numerical analysis on wide range of PC hollowcore slabs, as presented in Chapter 6. A nonlinear regression analysis on these temperature data, with corresponding fire-exposed time and cross-sectional locations was carried out using "solver" function in Microsoft Excel (Microsoft Excel n.d.). The "solver" function is able to calculate the optimum coefficients to match the original data with a given format of formula and applied "constraint" criteria. The coefficients are calibrated by minimizing the sum of square of error between the predictions and original data, which is highly dependent on the format of formula and constraint criteria. Thus, a general format of the equations and constraint criteria was adopted from the equation proposed by Kodur et al. (Kodur et al. 2013) for solid concrete slabs, before undertaking regression analysis. Since the heat transfer through

hollowcore slabs is one directional, the temperature equations are proposed for 1-dimentional heat transfer only. The general format for the 1-dimensional heat transfer can be expressed as:

$$T_z = c_1 \cdot \eta_Z \cdot (a \cdot t^n) \tag{7.1}$$

$$\eta_z = a_1 \cdot \ln\left(\frac{t}{z^{1.5}}\right) + a_2 \cdot \sqrt{z} + a_3 \tag{7.2}$$

where, T_z is the temperature resulting from 1-D heat transfer in °C, η_Z is the heat transfer factor induced through one fire-exposed surface, c_1 is the coefficients to account for concrete type, t is the fire exposure time in hours, z is the distance from the point in concrete section to fire exposure surface in meters, a_1 , a_2 and a_3 are the coefficients to be traced in the regression analysis. (a.tⁿ) is the temperature under standard fire exposure (Kodur et al. 2013). For ASTM E119 fire, a = 910 and n = 0.148 and the default values of c_1 for high strength carbonate aggregate concrete is 1.01 (Kodur et al. 2013).

The regression parameters (a₁, a₂ and a₃) are chosen to fit the data points in the critical range with the smallest discrepancy, and that have reasonable match in other regions using "constraint" criteria. The compressive strength of concrete and yield strength of prestressing steel are typically not influenced up to 300°C, and that these strengths become negligible after reaching 800°C (ACI 216.1-14 2014; Eurocode 2 2004a). Therefore, the regression result has to be highly reliable or slightly conservative in temperature-sensitive zone of 300-800°C. Further, the regression results in 20-300°C could be set as a secondary target since the variation in this temperature range does not significantly influence the strength of concrete and steel reinforcement. To achieve this objective, the following constraint criteria were applied in the regression analysis:

- a. When temperature is in 300-800°C range, the average of errors between temperatures by finite element approach and predicted temperatures by regression equations should be controlled to lie within 10%.
- b. For temperature higher than 800°C, predicted temperature using regression equations should not be smaller than those from FEA.
- c. For temperature in 100-300°C, the average of errors between temperatures by FEA and predicted temperatures by regression equations should be controlled to lie within 15%.
- d. For temperature from FEA smaller than 100°C, predicted temperatures by regression equations should not be lower than those from FEA by more than 50°C.

With the above developed equations and constrains, a regression analysis was conducted for 1-D equation for temperatures at strand and mid-depth level. The final formulae used for calculating temperature at a given point in a hollowcore slab are obtained as follows.

$$T_z = c_1 \cdot \eta_Z \cdot (a \cdot t^n) \tag{7.3}$$

$$\eta_z = a_1 \cdot \ln\left(\frac{t}{z^{1.5}}\right) - a_2 \cdot \sqrt{z} - a_3 \tag{7.4}$$

where, values of a_1 , a_2 and a_3 are evaluated to be 0.222, 0.425 and 0.634 for strand temperature and 0.233, 0.579 and 0.356 for mid-depth temperature respectively.

7.3.3 Regression analysis results

The temperature predictions from proposed equations (Eqns. 7.3 and 7.4) are compared with the temperature data obtained from detailed finite element analysis, as illustrated in Figure 7.2(a) to (e). These comparisons are presented for hollowcore slabs with five different depths namely, 150, 200, 250, 300 and 400 mm. These slabs are taken from PCI handbook (PCI 2010) and represent prevalent cross-sectional configurations used in practice. In these figures, a point below "-10% margin" line indicate that the predicted temperature from equations is higher than

that obtained using finite element approach by more than 10%. If a point lies above "+10% margin" line, the predicted temperature from equations is smaller than that obtained in finite element approach by more than 10%. It can be seen that for all five slabs, most data points lie within ±10% margin zone, especially for temperatures higher than 300°C. Therefore, the proposed equations are capable of reasonably predicting cross-sectional temperatures of PC hollowcore slabs exposed to standard fire. It is to be noted that there are a few points in the zone above "+10% margin" line, indicating un-conservative temperature predictions (see Figure 7.2(a)). These points correspond to 150 mm slab and this inaccuracy could be attributed to the fact that 150 mm slab has lower thermal inertia, which results in higher sectional temperatures in finite element analysis, but is not fully captured by the equations. Conversely, there are a few points in the zone below "-10% margin" line, indicating over-conservative temperature predictions (see Figure 7.2(e)). These points correspond to 400 mm slab and this inaccuracy could be attributed to the fact that 400 mm slab has higher thermal inertia, which results in lower sectional temperatures in finite element analysis, but is again not fully captured by the equations. Since the temperature predictions are slightly over-conservative for 400 mm slab, the proposed equations can be utilized for these slabs.

7.3.4 Verification of temperature equation

The validity of the proposed equations (Eqns. 7.3 and 7.4) is established by comparing the temperatures predicted utilizing the proposed equations with that measured in fire tests and that obtained from finite element approach. For this purpose fire tests conducted on hollowcore slabs (Slab 6 and Slab 4) as discussed in Chapter 3 and few other slabs reported in the literature were selected. The tests previously reported in the literature include hollowcore slabs tested by Janzse et al. (on Slab G6) (Jansze et al. 2012) and that by Breccolotti et al. (on Slab B) (Breccolotti et al.

2006). Slab 6 was exposed to ASTM-E119 standard fire (ASTM 2011) and Slab 4 was exposed to design fire (DF), whereas Slab G6 and Slab B were exposed to ISO834 standard fire (International Standard (E) 1999). ISO834 fire has slight higher intensity than ASTM-E119 fire and DF fire has slightly lower intensity than ASTM-E119 fire, as shown in Figure 7.3. The full details of slab configurations and fire tests are illustrated in Table 7.1.

The predicted temperatures in strand and mid-depth concrete for Slab 6, Slab 4, Slab G6 and Slab B are compared with that measured in the tests and that obtained from finite element approach in Figure 7.4, Figure 7.5, Figure 7.6 and Figure 7.7 respectively. It can be seen that the predicted temperatures are mostly in good agreement with the measured data in the tests. Further, verification of the proposed equations is illustrated by comparing strand temperature obtained from proposed approach and finite element approach at 1 hr, 2 hr and 3 hr into fire exposure in Table 7.2.

In Slab 6, as shown in Figure 7.4, there is a very good agreement between the temperatures (strand and mid-depth) from proposed equations and that from measured in test and from finite element approach. However, there is large difference in the temperature beyond 140 minutes when compared to test data, as Slab 6 failed at 140 minutes during the test. However, numerical analysis is continued beyond 140 minutes, and thus there is no drop in temperature from both finite element approach and proposed equations. Similarly in Slab 4, there is good correlation between the predicted temperatures obtained from proposed equation and that from test and finite element approach up to 120 minutes. Beyond 120 minutes, there is large discrepancy between temperatures, as the decay phase was initiated at 120 minutes in the test but not in numerical analysis (proposed equations and FEA).

In Slab G6 and Slab B, as shown in Figure 7.6 and Figure 7.7, it can be seen that there is higher discrepancies in the mid depth temperatures, as compared to that in Slab 6, as shown in Figure 7.4. This is due to the fact that the equations are calibrated for slab core configurations and depths typically used in the United States. In Figure 7.6, the slab depth is 266 mm and has slightly lower core area to gross area ratio than in those found in the US. Due to higher area of cross-sectional concrete, the temperatures in the inner layers increase at a slightly slower rate than that predicted by the equations. However, the effect of core configuration is less significant on the strand temperature, as strand is closer to the fire exposed surface.

In Slab B shown in Figure 7.7, the discrepancy in the mid-depth temperature is somewhat lower than that seen in Slab G6 and this can be attributed to the core configuration of Slab B, which has a depth of 200 mm and is very similar to that of 200 mm slab used in practice. However, the existing discrepancy can be attributed to the difference in concrete strength (lower strength) used for fabricating Slab B, which results in slightly lower concrete temperatures in the tests than that predicted by the equations. However, the predicted temperatures are higher than the measured temperature in the test, and thus can be deemed to be conservative.

A further examination indicates that there is relatively larger discrepancy between predicted and measured temperatures in 20-100°C range, in all above four slabs. This is because 20-100°C temperatures range is not primary objective in the regression analysis. As mentioned in Section 7.3.2, the regression analysis was performed to fit the data points in the critical temperature range (300-800°C). Since temperature variation in 20-100°C range does not significantly influence the strength in strand and concrete, the accuracy of temperature predictions in this range is set as a secondary target in the regression analysis. However, this does not significantly

affect further structural analysis of PC hollowcore slabs, since there is no strength loss in concrete and prestressing strands till 100°C.

Overall predicted temperatures using proposed equations show a good agreement with measured data throughout fire exposure duration, and this demonstrates the validity of the proposed simplified approach in predicting temperatures in commonly used hollowcore slabs.

7.4 Evaluating flexural and shear capacity under fire conditions

Knowing the sectional temperatures in PC hollowcore slabs, flexural and shear capacity can be evaluated at any given time into fire exposure by utilizing flexural and shear capacity equations specified in Eurocode 2 (Eurocode 2 2004a).

7.4.1 General procedures

Once sectional temperatures at various steps into fire exposure is known, temperature dependent strength properties of strand and concrete can be evaluated at any given time into fire exposure. These temperature dependent strength properties of prestressing strand and concrete can be evaluated using strength degradation ratio illustrated in Table 7.3 and Table 7.4. Then, the equations specified in Eurocode 2 (Eurocode 2 2004a) for ambient condition can be utilized to evaluate the flexural and shear capacities under fire exposure by accounting for temperature dependent strength properties. The equations for evaluating moment and shear capacity specified in ACI318 (ACI 318 2011) and PCI (PCI 2010) can also be used and are similar to that in Eurocode 2 (Eurocode 2 2004a).

7.4.2 Flexural and shear capacity at ambient conditions

The flexural capacity equations for PC hollowcore slabs specified in Eurocode 2 (Eurocode 2 2004a) for ambient condition are illustrated as follows.

$$M_n = A_{ps} f_{ps} \left(d - \frac{a}{2} \right)$$

$$M_n \ge 1.2 M_{cr}$$
(7.5)

where,

$$M_{cr} = \left(\frac{I}{y_t}\right) \left(6\lambda \sqrt{f_{cT}'} + f_{pe} - f_d\right)$$
$$f_{ps} = f_{pu} \left[1 - \frac{\gamma_p}{\beta_1} \left(\frac{\rho_p f_{pu}}{f_c'}\right)\right]$$

$$\beta_1 = 0.85 - \left(\frac{f_c'(in psi) - 4000}{1000}\right) \times 0.05$$

$$\rho_p = \frac{A_{ps}}{bd_p}$$

where,

 M_n = flexural capacity at ambient condition, kN-m

 A_{ps} = area of prestressed reinforcement, m²

 M_{cr} = flexural capacity at cracking, N-m

I = moment of inertia of section about centroidal axis, m⁴

 y_t = distance from centroidal axis of gross section, neglecting reinforcement, to tension face, m

 $f_{pe} = \frac{P_e}{S_b}$ = compressive stress in concrete due to effective prestress forces only (after allowance for all prestress losses) at extreme fiber of section where tensile stress is caused by externally applied loads, Pa (or N/m²)

 $f_d = \frac{P}{A}$ = stress due to unfactored dead load, at extreme fiber of section where tensile stress is caused by externally applied loads, Pa (or N/m²)

 S_b = section modulus for the bottom fiber, m³

 f_{ps} = stress in prestressed reinforcement at ambient condition, Pa (or N/m²)

 f_{pu} = tensile strength of prestressing steel at ambient condition, Pa (or N/m²)

 f'_c = compressive strength of concrete at ambient condition, Pa (or N/m²), utilize average sectional temperature to evaluate f'_{cT}

 γ_p = factor for type of prestressing strand (0.28 for low relaxation strand)

 β_1 = factor relating depth of equivalent rectangular compressive stress block to neutral axis depth

 ρ_p = ratio of prestressed reinforcement

d = distance from extreme compression fiber to centroid of prestressed reinforcement

 $a = \text{depth of equivalent compression stress block under fire conditions} = \frac{A_{ps}f_{ps}}{0.85f'_cb}$

Similarly, the shear capacity equations for hollowcore slabs specified in Eurocode 2 (Eurocode 2 2004a) for ambient conditions are illustrated as follows.

$$V_{Rd,c} = \left[C_{Rd,c} k \left(100 \rho_l f_{c,m} \right)^{\frac{1}{3}} + k_1 \sigma_{cp} \right] b_w d$$
 (7.6)

where,

 $V_{\rm Rd,c}$ = shear capacity in regions un-cracked in flexure in ambient condition in N

 $C_{\rm Rd,c} = 0.18/\gamma_{\rm c}$ ($\gamma_{\rm c}$ is partial safety factor for concrete)

$$k = 1 + \sqrt{(200/d)} \le 2.0$$

where,

d = effective depth at ambient temperature measured in mm

 $\rho_{I,=}$ force-equivalent ratio of longitudinal reinforcement $=\frac{A_{Sl}}{b_w d} \le 0.02$

where,

 A_{sl} = area of the tensile reinforcement (prestressing strands)

 b_w = smallest width of the cross-section in the tensile area measured in mm

 $f_{c,m}$ = average strength of concrete at ambient condition in MPa

$$k_1 = 0.15$$

$$\sigma_{cp} = N_{Ed}/A_c$$

where,

 N_{Ed} = axial force in the cross-section due to loading or prestressing in N

 A_c = area of concrete cross-sectional measured in mm²

7.4.3 Flexural and shear capacity under fire conditions

The above discussed ambient temperature flexural and shear capacity equations can be modified to evaluate the flexural and shear capacities under fire conditions by accounting for the temperature induced strength degradation in prestressing strands and concrete. Thus, the modified equations for evaluating flexural capacity under fire conditions are illustrated as follows.

$$M_{nT} = A_{ps} f_{psT} \left(d - \frac{a_T}{2} \right) \tag{7.7}$$

where,

$$f_{psT} = f_{puT} \left[1 - \frac{\gamma_p}{\beta_1} \left(\frac{\rho_p f_{puT}}{f'_{cT}} \right) \right]$$

$$\beta_1 = 0.85 - \left(\frac{f'_{cT}(in \, psi) - 4000}{1000}\right) \times 0.05$$

$$\rho_p = \frac{A_{ps}}{bd_p}$$

where,

 M_{nT} = flexural strength under fire conditions, kN-m

 A_{ps} = area of prestressed reinforcement, m²

 f_{psT} = stress in prestressed reinforcement under fire conditions, Pa (or N/m²)

 f_{puT} = tensile strength of prestressing steel under fire conditions, Pa (or N/m²)

 f'_{cT} = compressive strength of concrete under fire conditions, Pa (or N/m²), utilize average sectional temperature to evaluate f'_{cT}

 γ_p = factor for type of prestressing strand (0.28 for low relaxation strand)

 β_1 = factor relating depth of equivalent rectangular compressive stress block to neutral axis depth

 ρ_p = ratio of prestressed reinforcement

d = distance from extreme compression fiber to centroid of prestressed reinforcement

 a_T = depth of equivalent compression stress block under fire conditions = $\frac{A_{ps}f_{psT}}{0.85f_{cT}'b}$

Similarly, the modified equations for evaluating shear capacity of hollowcore slabs under fire conditions are illustrated as follows.

$$V_{Rd,c,fi} = \left[C_{Rd,c} k \left(100 \rho_{l,fi} f_{c,fi,m} \right)^{\frac{1}{3}} + k_1 \sigma_{cp,fi} \right] b_w d$$
 (7.8)

where,

 $V_{\mathrm{Rd,c,fi}} = \mathrm{design}$ shear strength in regions un-cracked in flexure under fire conditions in N

 $C_{\rm Rd,c} = 0.18/\gamma c$ (yc is partial safety factor for concrete)

$$k = 1 + \sqrt{(200/d)} \le 2.0$$

where,

d = effective depth at ambient temperature measured in mm

 $\rho_{I,fi} = \text{force-equivalent ratio of longitudinal reinforcement} = \frac{A_{sl}}{b_w d} \le 0.02$ where,

 A_{sl} = area of the tensile reinforcement (prestressing strands)

 b_w = smallest width of the cross-section in the tensile area measured in mm

 $f_{c,fi,m}$ = average strength of concrete under fire conditions in MPa ($f_{c,fi,m}$ can be taken equal to the strength of concrete for the temperature at mid height of the web)

 $k_1 = 0.15$

$$\sigma_{cp,fi} = N_{Ed}/A_c$$

where,

 N_{Ed} = axial force in the cross-section due to loading or prestressing in N A_c = area of concrete cross-sectional measured in mm²

Once moment and shear capacity is known at any given time in to fire exposure, failure can be evaluated by comparing with the applied moment and shear force. At room temperature, considering only dead loads and live loads for the strength limit state, most design codes ASCE 7 (McAllister et al. n.d.) and Eurocode 1 (Eurocode 1 2008) specify two load combinations as follows.

$$M_u = 1.4DL \tag{7.9}$$

$$M_u = 1.2DL + 1.6LL (7.10)$$

where, $M_{\rm u}$ is the ultimate load (moment) resulting from factored dead and live loads, DL is the dead load and LL is the live load.

However, in the event of fire, the applied loading is much lower than the maximum design loads specified for ambient conditions, since fire is a rare (accidental) event, ASCE 7 (McAllister et al. n.d.) recommends loading under fire conditions to be evaluated as

$$M_{fire} = 1.2DL + 0.5LL (7.11)$$

Similarly, Eurocode 1 (Eurocode 1 2008) recommends loading under fire conditions to be evaluated as

$$M_{fire} = DL + 0.5LL \tag{7.12}$$

where, M_{fire} is the applied moment under fire exposure. The applied shear force (V_{fire}) is evaluated based on the applied moment and loading scenario.

Thus, combining Eqns. 7.9-7.12, the following criteria should be applied to evaluate failure of PC hollowcore slabs:

At room temperature:
$$M_u \le \emptyset M_n$$
 (7.13)

$$V_{n} \leq \emptyset V_{n}$$

Under fire exposure:
$$M_{fire} \le M_{n,T}$$
 (7.14)

$$V_{fire} \leq V_{n,T}$$

where, ϕ is the strength reduction factor specified in ACI318 (ACI 318 2011). Under fire conditions, no reduction factor is applied.

Utilizing the above simplified equations 7.7 and 7.8, moment capacity and shear capacity of PC hollowcore slab can be calculated at any given fire exposure time. Failure in the slab occurs, when the moment or shear capacity drops below bending moment or shear force due to external loading, and the corresponding time is the fire resistance of PC hollowcore slab. A flowchart illustrating the approach for evaluating fire resistance of a PC hollowcore slab is illustrated in

Figure 7.1. To further illustrate detailed procedure of the proposed rational approach, a design example for evaluating fire resistance of a PC hollowcore slab is illustrated in Appendix A.

7.4.4 Case study

To illustrate the usefulness of this approach, the moment capacity is evaluated using the proposed approach (Equation 7.7) for test slabs discussed in Section 7.3.4, which include Slab 6 and Slab 4 discussed in Chapter 3, hollowcore slab tested by Janzse et al. (on Slab G6) (Jansze et al. 2012) and that by Breccolotti et al. (on Slab B) (Breccolotti et al. 2006). The degradation in moment capacity in these slabs evaluated using the proposed equation are compared that from finite element approach in Figure 7.8(a), Figure 7.9(a), Figure 7.10(a) and Figure 7.11(a) respectively. It is evident that predicted moment capacity degradation using proposed approach is in good agreement with that from finite element. This can be attributed to the fact that the moment capacity is mainly dependent on the strand strength and the proposed temperature equations reasonably predict strand temperature.

The shear capacity is also evaluated using the proposed approach (Equation 7.8) for test slabs discussed in Section 7.3.4, which include Slab 6 and Slab 4 discussed in Chapter 3, hollowcore slab tested by Janzse et al. (on Slab G6) (Jansze et al. 2012) and that by Breccolotti et al. (on Slab B) (Breccolotti et al. 2006). The shear capacity degradation evaluated using the proposed approach is compared with that evaluated based on finite element approach in Figure 7.8(b), Figure 7.9(b), Figure 7.10(b) and Figure 7.11(b) respectively. Overall, the discrepancy in the shear capacity results is slightly higher than that observed in moment capacity results, illustrated in Section 7.4. This can be attributed to the fact that the temperature equations does not fully account for the effect of hollow cores. However, the prediction of shear capacity degradation using proposed approach is very close to that using finite element approach for Slab 6 and Slab

4, as shown in Figure 7.8(b). This is mainly due to the fact that the temperature equations are derived based on temperature data obtained from typical cross-sectional configurations in the US. In the case of Slab G6, as shown in Figure 7.10(b), the equation predicts faster rate of degradation in shear capacity, as the equation predicts slightly higher mid-depth temperature. As also discussed in 7.3.4, this is due to lower core area to gross area ratio of the Slab G6, which results in lower temperatures in the test. In the case of Slab B, the discrepancy in the degradation in shear capacity (see Figure 7.11(b)) evaluated using the proposed approach and that evaluated based on finite element approach is due to discrepancy in the mid-depth temperature (see Figure 7.7). However, this result does not affect the fire resistance, as the fire resistance of Slab B is governed by flexural limit state.

7.4.5 Validation of flexural and shear capacity equations

The validity of the above proposed approach is established by comparing the predicted response of slabs with results from fire tests. For this purpose, hollowcore slabs discussed in Section 7.3.4 (Slab 6 and Slab 4), hollowcore slab tested by Janzse et al. (on Slab G6) (Jansze et al. 2012) and that by Breccolotti et al. (on Slab B) (Breccolotti et al. 2006) are selected. The details of slab configurations and fire tests are also illustrated in Table 7.1. Since the variation of moment and shear capacities with fire exposure time cannot be directly measured in fire tests, the measured fire resistance (failure times) of tested slabs is compared with those predicted from the proposed approach. It can be seen in that the proposed approach provides reasonable predictions on fire resistance of PC hollowcore slabs, as also illustrated in Table 7.5. It is to be noted that the proposed approach best works for slabs having cross sectional configuration similar to that commonly used in the US. In the case of Slab 6 and Slab 4, proposed equation predicts fire resistance of 130 minutes which is conservative than that measured in the test. The proposed approach also shows that Slab 6

and Slab 4 fail through flexural limit state, as measured in tests. In the fire tests, Slab 6 failed through flexural failure, but Slab 4 did not fail as decay phase was initiated at 120 minutes into fire exposure. Similarly, in the case of Slab G6, failure did not occur at 120 minutes of fire exposure during the test, when the fire exposure was stopped. The proposed approach predicts a fire resistance of 135 minutes of fire resistance in Slab G6, showing that the slab does not fail at 120 minutes. The proposed approach also shows that failure in Slab G6 occurs through shear limit state as seen in test, wherein Slab G6 failed through shear cracking, when loading was increased at 120 minutes. In the case of Slab B, the proposed approach predicts failure at 125 minutes through flexural limit state, as observed in the test. However, the predicted fire resistance is slightly under conservative than that measured in the test. This is due to occurrence of some degree of spalling in Slab B during the fire test which is not predicted the proposed approach.

7.5 Limitations of proposed approach

Due to large variability in the cross-sectional configurations of PC hollowcore slabs from one country to another, it is not possible to develop an unified approach or model that covers all possible core configurations through regression analysis. Thus, the current proposed approach is only applicable over certain range of parameters. The following limitations need to be taken into consideration, while using the proposed approach.

- 1) The proposed approach is applicable for evaluating temperatures or fire resistance in PC hollowcore slabs exposed to standard fire only. These equations are not applicable for design fires, which have a cooling phase following the growth phase.
- 2) The proposed approach is applicable for core configurations specified in PCI manual (prevalent in the US) and having depth ranging from 150 mm to 400 mm. However, the proposed approach is typically conservative for other configurations.

- 3) The proposed simplified approach for moment capacity is applicable to simply supported PC hollowcore slabs only, since the effect of axial restraint is not accounted for in the simplified approach.
- 4) The temperature predictions on strand and mid-depth concrete using proposed equations does not account for uncertainty factors such as fire-induced spalling and cracking of concrete.

Table 7.1. Summary of slab details and test parameters

Test slab	Aggregate type	Dimensions length (m) ×width (m) ×depth (mm)	Cross sectional configurations	Test day compressive strength (f'c), MPa	Applied loading (% of capacity)	Support condition	Fire scenario
Slab 6 (Shakya and Kodur 2015)	Carbonate	3.65×1.2×200	6-150 mm cores 7-12.5 mm strands	75	60	SS	ASTM-E119
Slab 4 (Shakya and Kodur 2015)	Siliceous	3.65×1.2×200	6-150 mm cores 7-12.5 mm strands	91	60	SS	DF
Slab G6 (Jansze et al. 2012)	Carbonate	3.9×1.2×265	5-167 mm × 200 mm cores 7-9.5 mm strands	56	70	SS	ISO 834
Slab B (Breccolotti et al. 2006)	Carbonate	4×1.2×200	6-150 mm cores 7-9.5 mm strands	48	60	SS	ISO 834

Note: SS = simply supported

Table 7.2. Comparison of temperature in prestressing strand at 1, 2 and 3 hour of fire exposure

	Strand temperature									
Test slab		FEA		Proposed approach						
	1 hr	2 hr	3 hr	1 hr	2 hr	3 hr				
Slab 6 (Shakya and Kodur 2015)	290	469	580	284	469	596				
Slab 4 (Shakya and Kodur 2015)	288	450	490	284	469	596				
Slab G6 (Jansze et al. 2012)	227	427	n.a.	245	429	n.a.				
Slab B (Breccolotti et al. 2006)	217	401	n.a.	267	453	n.a.				

Note: 'n.a.' = not available

Table 7.3. Values for the main parameters of the stress-strain relationships of NSC and HSC at elevated temperatures (Eurocode 2)

Temp.	Temp.	NSC							HSC			
		Siliceous Agg.			Calc	areous A	gg.	$f_{c,T}^{'}/f_{c}^{'}(20^{\circ}C)$				
		$\frac{f_{c,T}^{'}}{f_c^{'}(20^{\circ}C)}$	$arepsilon_{cl,T}$	$\mathcal{E}_{cu1,T}$	$\frac{f_{c,T}^{'}}{f_c^{'}(20^{\circ}C)}$	$\mathcal{E}_{cl,T}$	$\varepsilon_{cul,T}$	Class1	Class2	Class3		
68	20	1	0.0025	0.02	1	0.0025	0.02	1	1	1		
212	100	1	0.004	0.0225	1	0.004	0.023	0.9	0.75	0.75		
392	200	0.95	0.0055	0.025	0.97	0.0055	0.025	0.9	0.75	0.70		
572	300	0.85	0.007	0.0275	0.91	0.007	0.028	0.85	0.75	0.65		
752	400	0.75	0.01	0.03	0.85	0.01	0.03	0.75	0.75	0.45		
932	500	0.6	0.015	0.0325	0.74	0.015	0.033	0.60	0.60	0.30		
1112	600	0.45	0.025	0.035	0.6	0.025	0.035	0.45	0.45	0.25		
1292	700	0.3	0.025	0.0375	0.43	0.025	0.038	0.30	0.30	0.20		
1472	800	0.15	0.025	0.04	0.27	0.025	0.04	0.15	0.15	0.15		
1652	900	0.08	0.025	0.0425	0.15	0.025	0.043	0.08	0.113	0.08		
1832	1000	0.04	0.025	0.045	0.06	0.025	0.045	0.04	0.075	0.04		
2012	1100	0.01	0.025	0.0475	0.02	0.025	0.048	0.01	0.038	0.01		
2192	1200	0	-	-	0	-	_	0	0	0		

Table 7.4. Values for the main parameters of the stress-strain relationships of prestressing steel at elevated temperatures (Eurocode 2)

cievated temperatures (Eurocode 2)									
Steel temp.	$\frac{F_{py,T}}{\beta f_{yp}}$				$g_{pp,T} \over g_{yp}$	$rac{E_{p,T}}{E_p}$		$\varepsilon_{pt,T}[-]$	$arepsilon_{pu,T}[-]$
Т°С			1.				1.	cw,	cw,
	Class A	Class B	q and t	cw	q and t	cw	q and t	q and t	q and t
1	2a	2b	3	4	5	6	7	8	9
20	1	1	1	1	1	1	1	0.05	0.1
100	1	0.99	0.98	0.68	0.77	0.98	0.76	0.05	0.1
200	0.87	0.87	0.92	0.51	0.62	0.95	0.61	0.05	0.1
300	0.7	0.72	0.86	0.32	0.58	0.88	0.52	0.055	0.105
400	0.5	0.46	0.69	0.13	0.52	0.81	0.41	0.06	0.11
500	0.3	0.22	0.26	0.07	0.14	0.54	0.2	0.065	0.115
600	0.14	0.1	0.21	0.05	0.11	0.41	0.15	0.07	0.12
700	0.06	0.08	0.15	0.03	0.09	0.1	0.1	0.075	0.125
800	0.04	0.05	0.09	0.02	0.06	0.07	0.06	0.08	0.13
900	0.02	0.03	0.04	0.01	0.03	0.03	0.03	0.085	0.135
1000	0	0	0	0	0	0	0	0.09	0.14
1100	0	0	0	0	0	0	0	0.095	0.145
1200	0	0	0	0	0	0	0	0.1	0.15

Note: For intermediate values of temperature, linear interpolation may be used.

Where,

cw = cold worked, q and t = quenched and tempered

$$\beta = \begin{cases} \left(\frac{\varepsilon_{ud} - f_{po,1T} / E_p}{\varepsilon_{uT} - \varepsilon_{po,1T} / E_p}\right) \times \left(\frac{f_{pT} - f_{po,1T}}{f_{pT}}\right) + \frac{f_{po,1T}}{f_{pT}} & ClassA \\ 0.9 & ClassB \end{cases}$$

$$\varepsilon_{ud}, \varepsilon_{uT}, f_{po,1T}, f_{pT} \ and \ E_p \ are \ material \ properties \ at \ room \ temperature \ as \ per \ EN1992-1-1$$

Table 7.5. Comparison of predicted and test fire resistance

-	Dimensions	Fire resistance, minutes						
Test slab	length (m)	Te	st	Proposed approach				
Test sido	×width (m) ×depth (mm)	Flexure	Shear	Flexure	Shear			
Slab 6								
(Shakya and Kodur 2015)	3.65×1.2×200	140	n.f.	130	150			
Slab 4 (Shakya and Kodur 2015)	3.65×1.2×200	n.f.	n.f.	130	150			
Slab G6 (Jansze et al. 2012)	3.9×1.2×265	>120	>120	180	135			
Slab B (Breccolotti et al. 2006)	4×1.2×200	105	n.f	125	n.f.			

Note: 'n.f.' = not failed

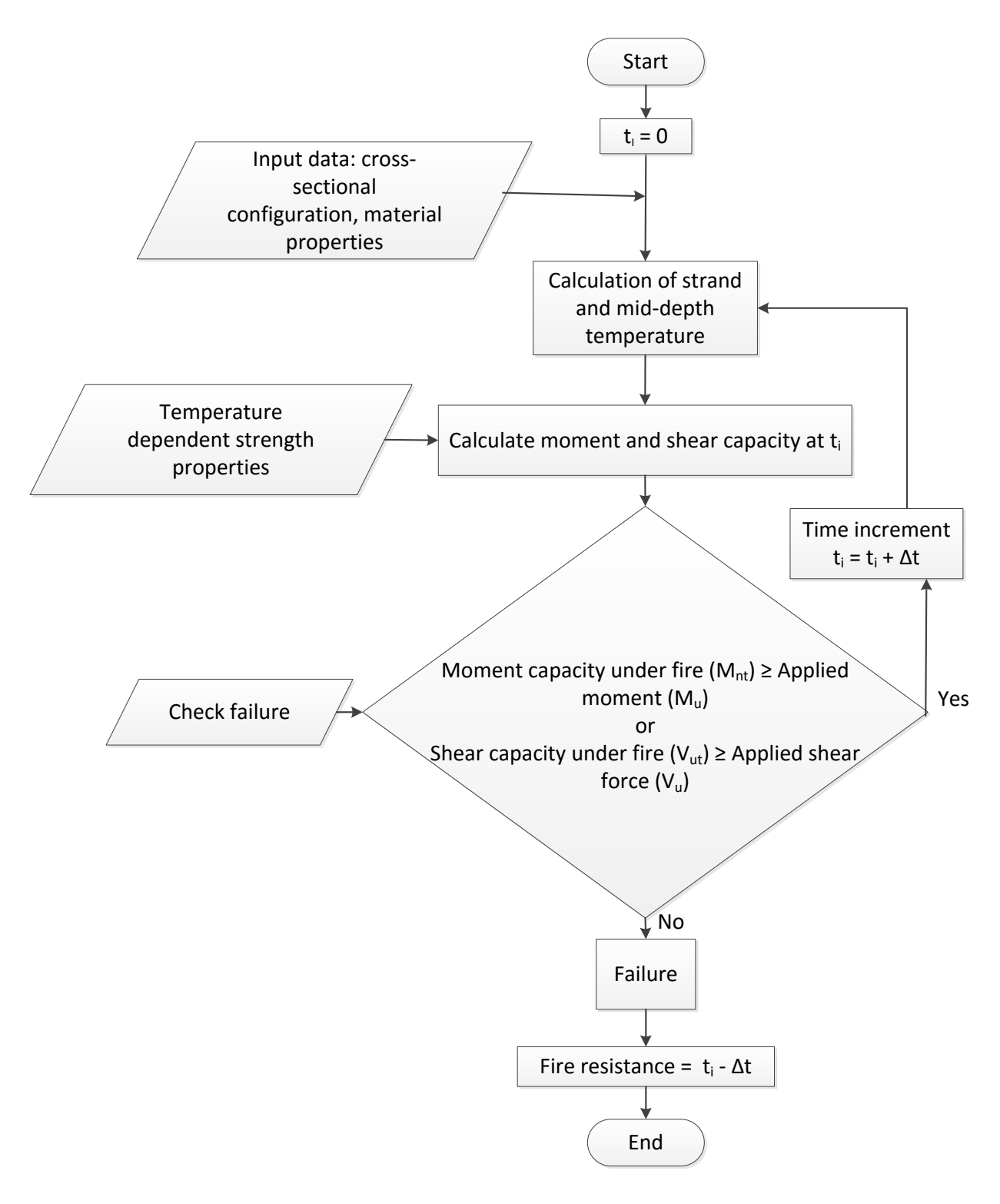


Figure 7.1. Flowchart illustrating rational design approach for evaluating fire resistance of PC hollowcore slabs

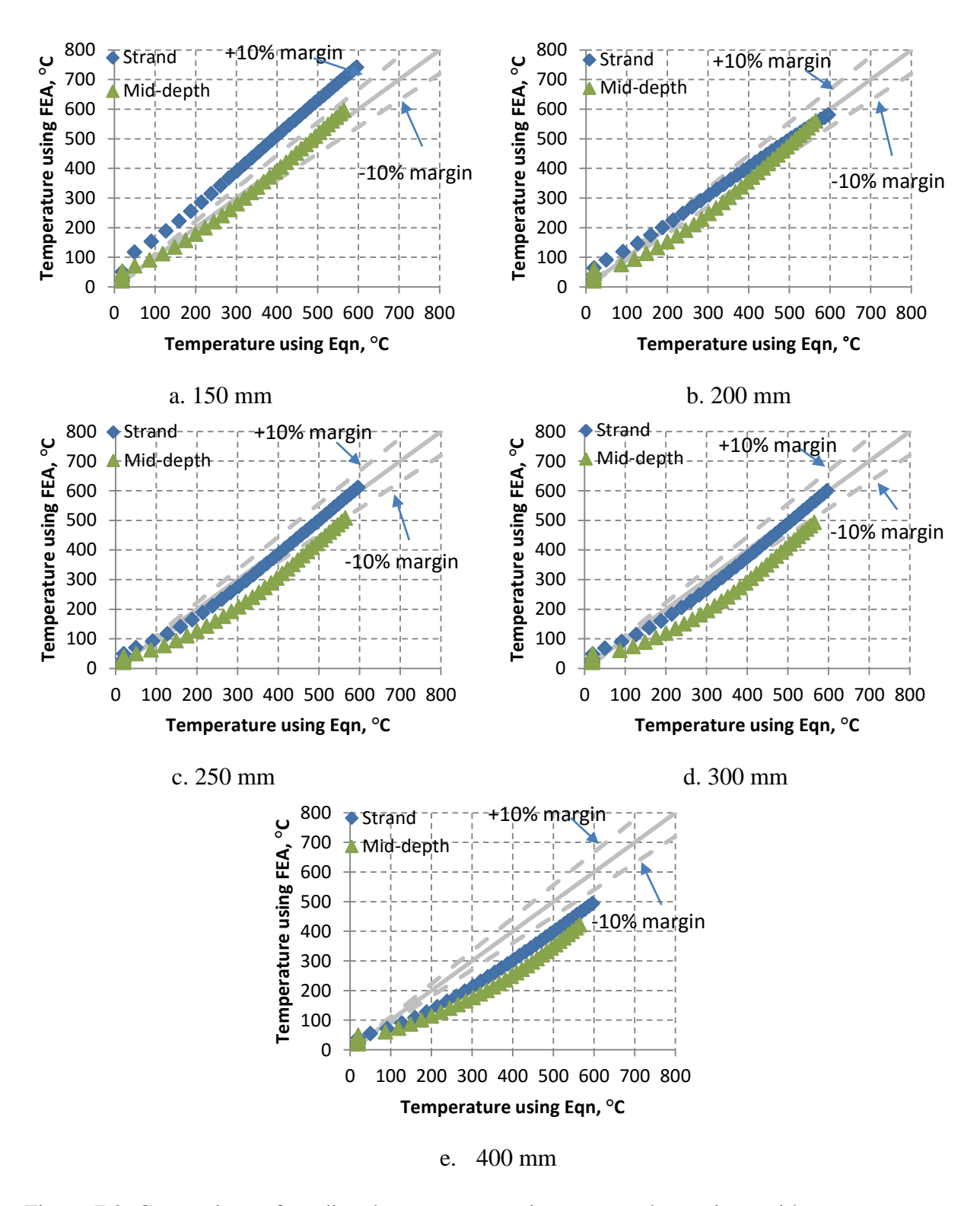


Figure 7.2. Comparison of predicted temperature using proposed equations with temperatures obtained using finite element analysis for various depth hollowcore slabs

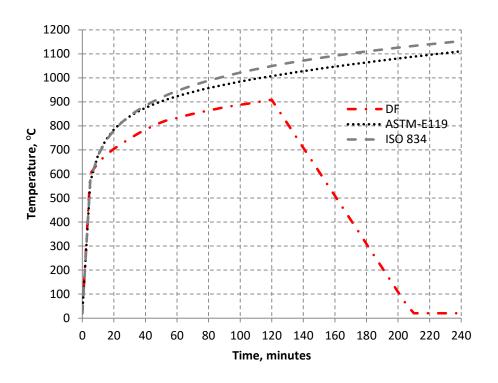


Figure 7.3. Time-temperature curves, simulated during fire tests

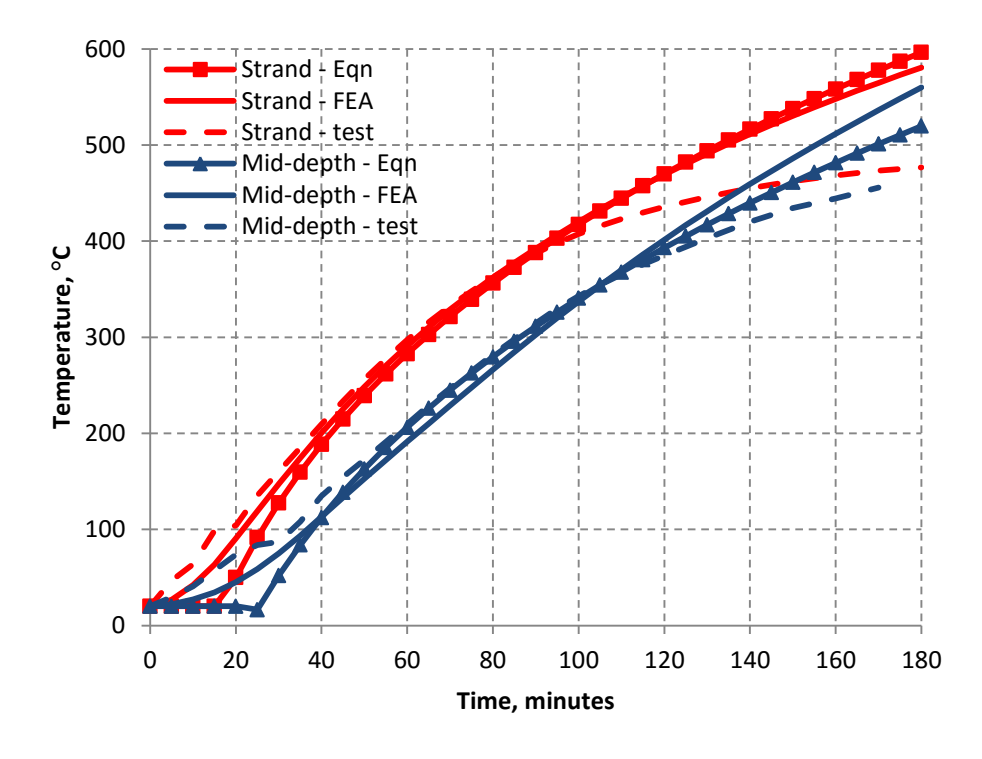


Figure 7.4. Comparison of predicted temperature in Slab 6 with that obtained from test conducted by Shakya and Kodur

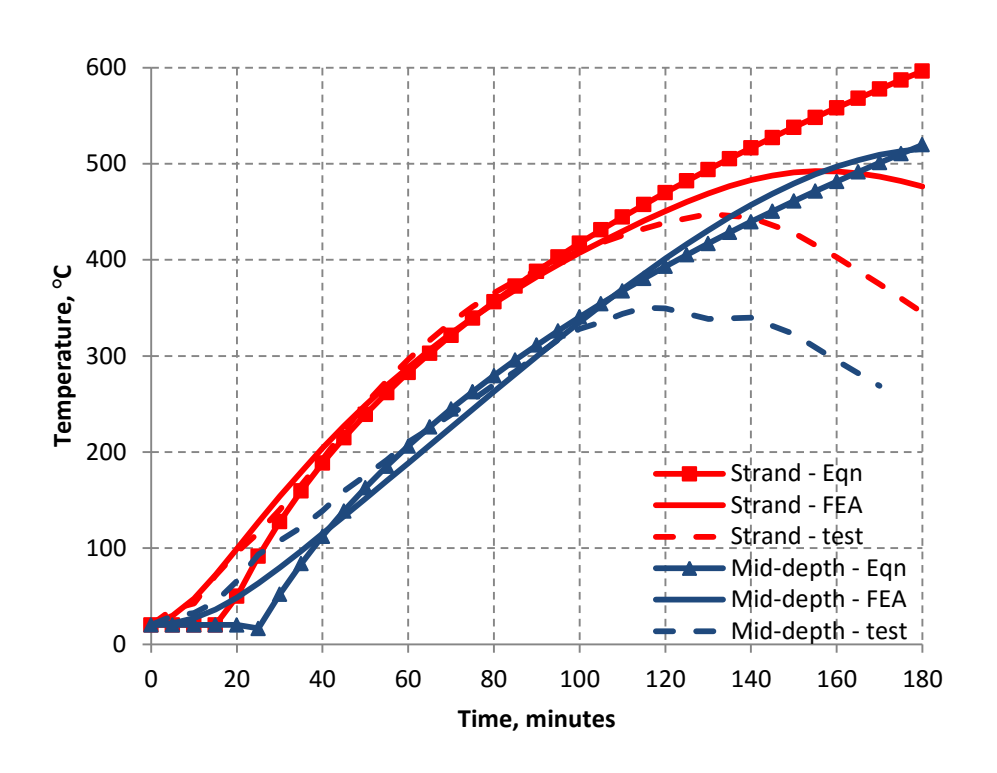


Figure 7.5. Comparison of predicted temperature in Slab 4 with that obtained from test conducted by Shakya and Kodur

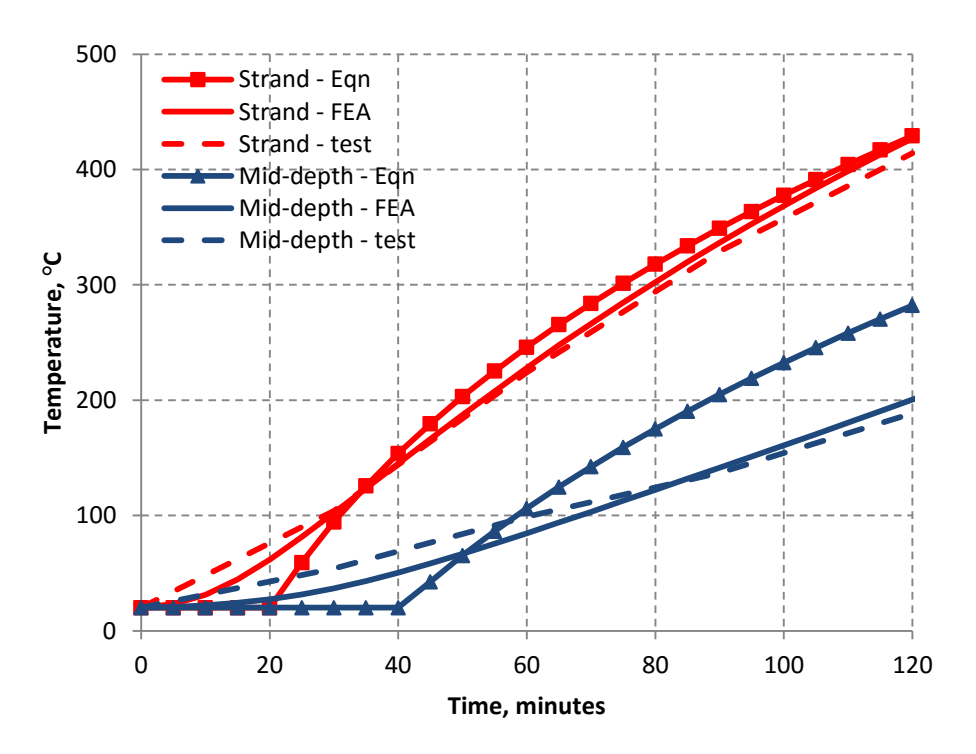


Figure 7.6. Comparison of predicted temperature in Slab G6 with that obtained from test conducted by Jansze et al.

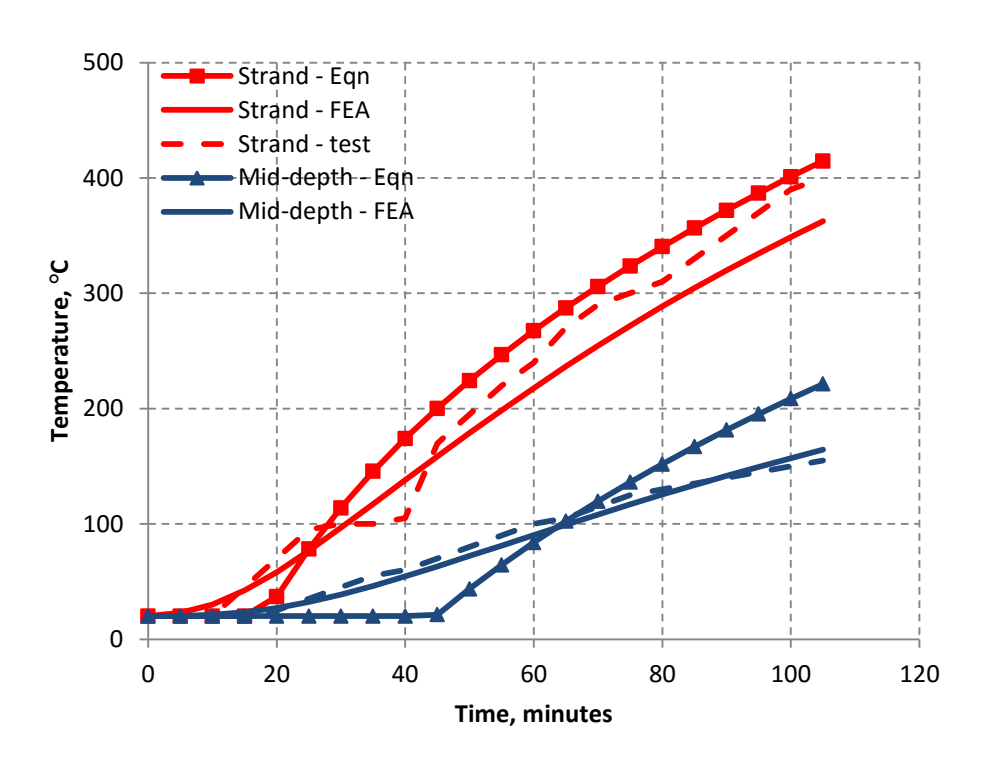
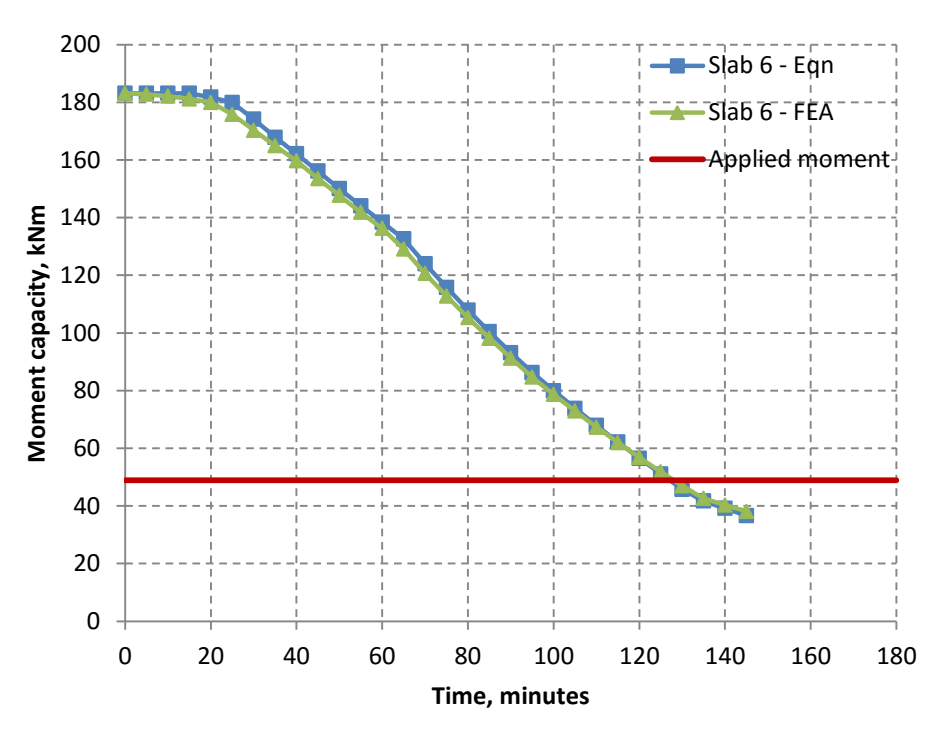


Figure 7.7. Comparison of predicted temperature in hollowcore slab with that obtained from test conducted by Breccolotti et al.



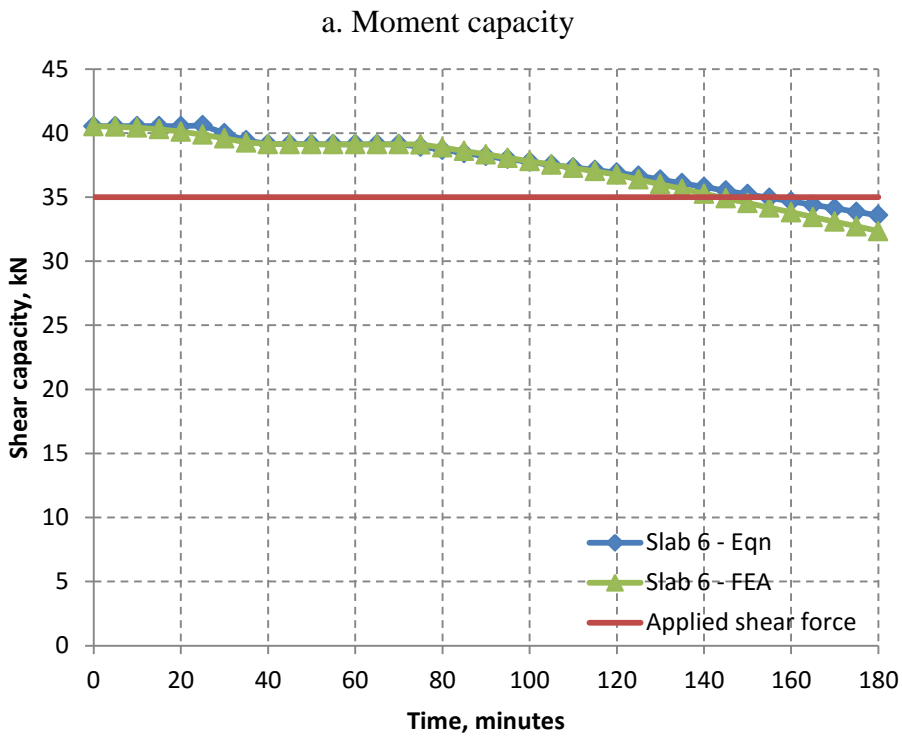
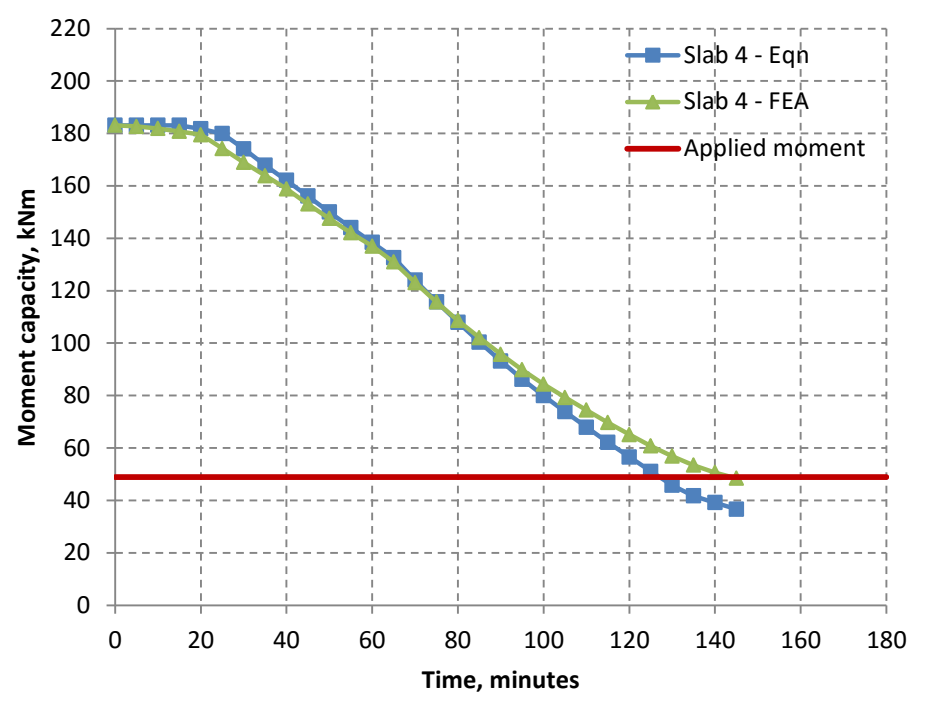
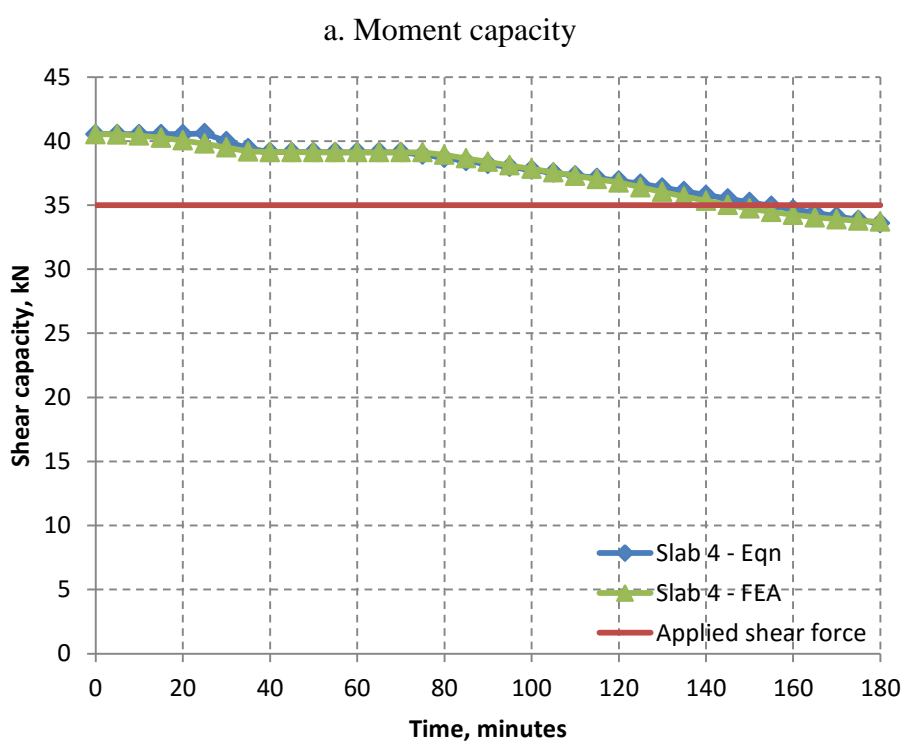


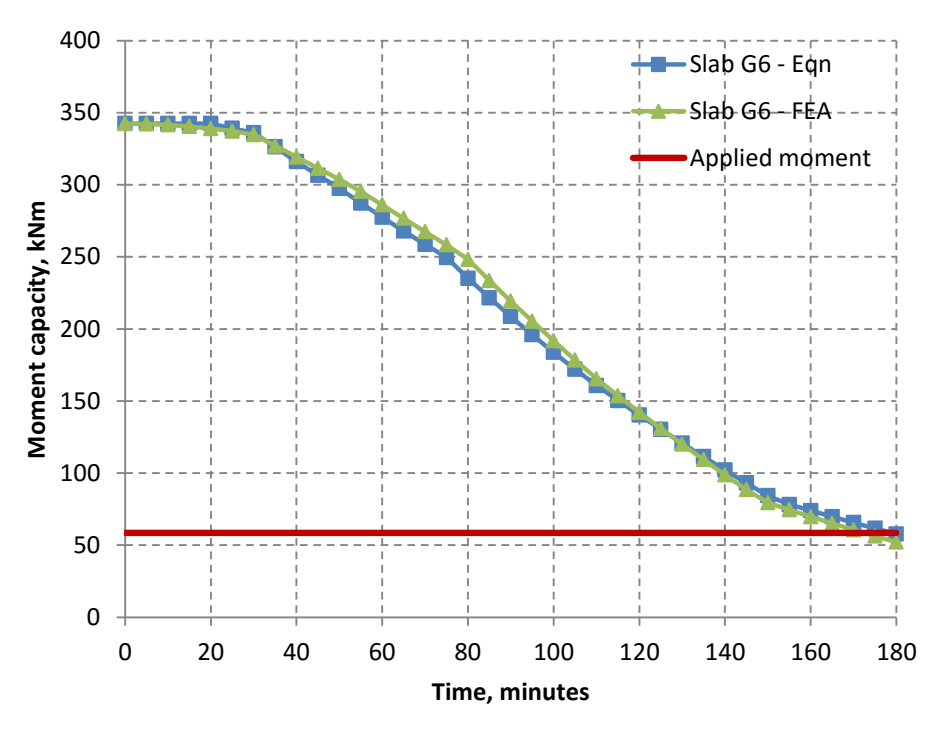
Figure 7.8. Comparison of moment and shear capacity degradation using proposed equations and FEA in tested Slab 6

b. Shear capacity





b. Shear capacity
Figure 7.9. Comparison of moment and shear capacity degradation using proposed equations and
FEA in tested Slab 4



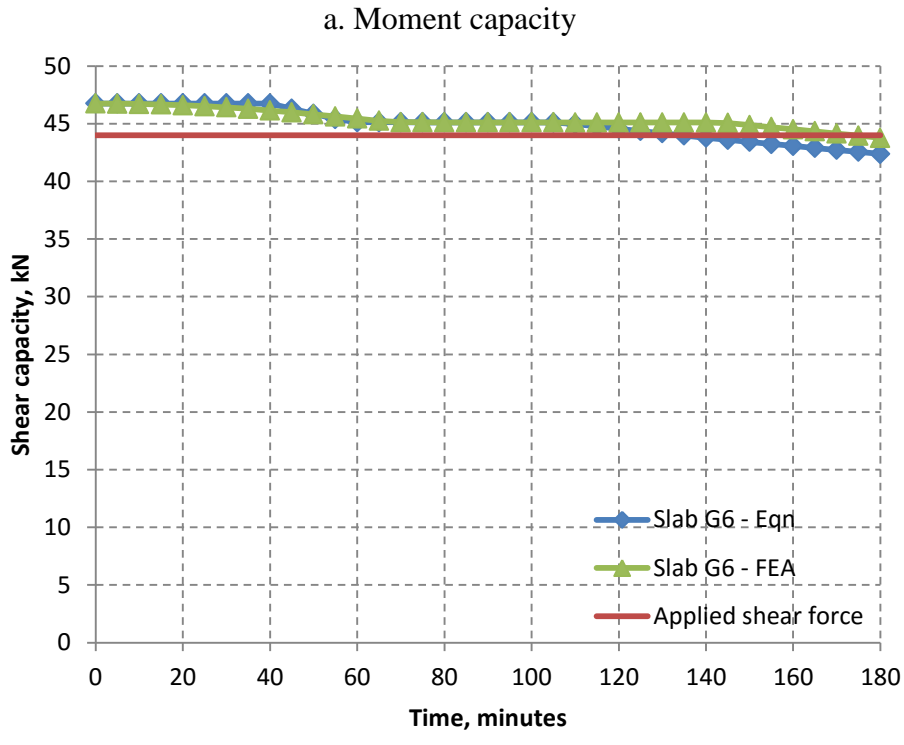
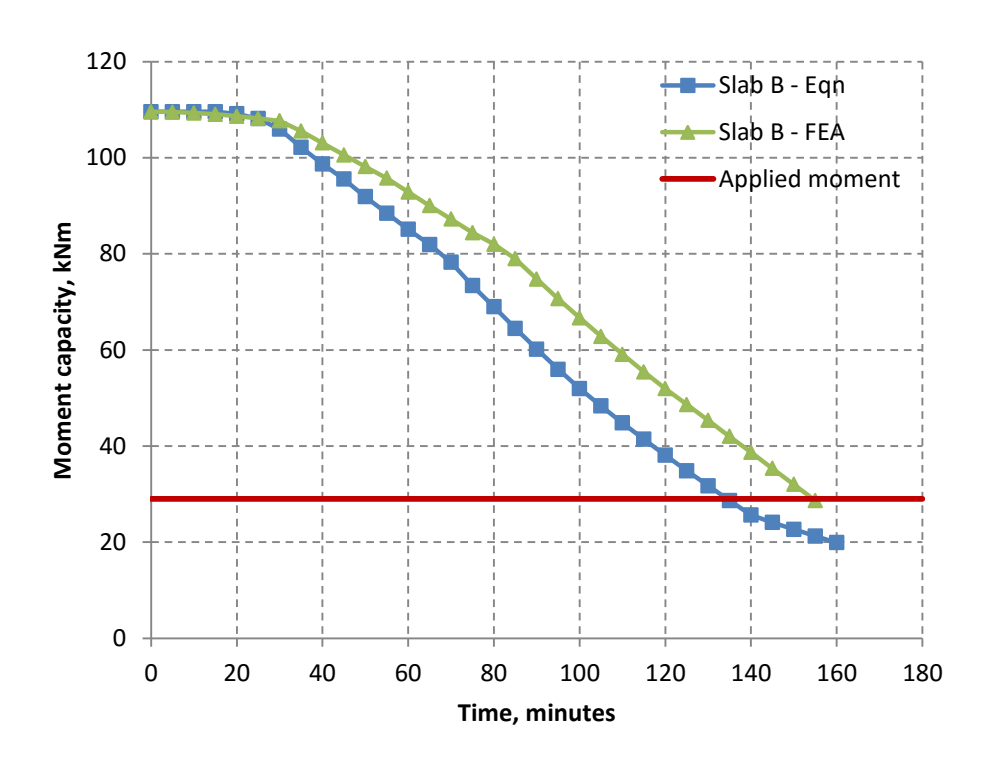


Figure 7.10. Comparison of moment and shear capacity degradation using proposed equations and FEA in tested Slab G6

b. Shear capacity



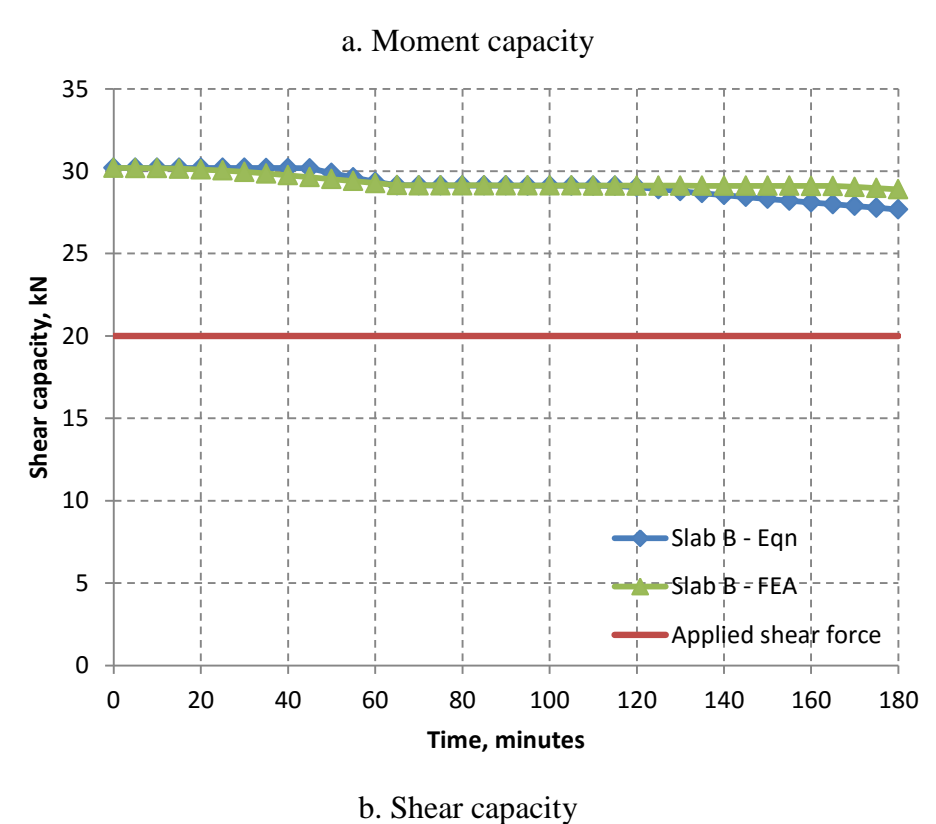


Figure 7.11. Comparison of moment and shear capacity degradation using proposed equations and FEA in tested Slab B

7.6 Summary

This chapter presents a simplified approach for assessing fire resistance of PC hollowcore slabs exposed to standard fire. This approach is developed by applying an analogy as that of room temperature design as specified in Eurocode 2, by accounting for the temperature induced strength degradation in strand and concrete. Temperature equations are also proposed for predicting temperatures at strand and mid-depth concrete throughout the fire exposure duration.

- Through this approach, moment and shear capacity can be evaluated at any given fire exposure time.
- The validity of the proposed approach is established by comparing temperature, moment and shear capacity and failure time predictions with those obtained from fire tests and finite element analysis. The applicability of the proposed approach in design situation is also illustrated through detailed examples.
- Overall the proposed approach provides a simple and rational method for evaluating fire response of PC hollowcore slabs exposed to standard fires.

8 CONCLUSIONS AND RECOMMENDATIONS

8.1 General

This dissertation presented a comprehensive study on the behavior of prestressed concrete (PC) hollowcore slabs under fire conditions. Both experimental and numerical studies were carried out to evaluate fire response of PC hollowcore slabs and to quantify the influence of critical factors influencing the fire response. As part of experimental studies, a series of tensile strength tests were carried out at various temperatures to develop data on variation of mechanical properties of prestressing strand with temperature. Data from these tests was utilized to develop empirical relations for mechanical properties of low relaxation prestressing strand over 20-800°C temperature range. Further, full-scale fire resistance tests were carried out on six PC hollowcore slabs. Data from these fire tests was utilized to gauge the effect of load level, fire scenario, aggregate type and axial restraint on fire resistance of PC hollowcore slabs.

As a part of numerical studies, a three-dimensional finite element based numerical model was developed to model the response and failure modes of PC hollowcore slabs under realistic fire, loading and restraint conditions. This numerical model, developed in ANSYS software (ANSYS 2014), accounts for temperature induced degradation of properties of concrete and prestressing strands, cracking in concrete, material and geometrical nonlinearities, realistic fire, loading and restraint conditions, as well as different failure limit states these slabs undergo under fire conditions. The validity of the model is established by comparing predicted response parameters from the numerical model against data and observations obtained through fire resistance tests undertaken as part of this thesis and also with that obtained from the literature.

The validated numerical model was applied to conduct a series of parametric studies to quantify the influence of critical factors on fire response and critical failure modes of PC hollowcore slabs. Results generated from parametric studies were utilized to develop a rational design methodology for evaluating fire resistance of PC hollowcore slabs. This methodology comprises of two main steps, namely cross-sectional temperature evaluation, and moment and shear capacity evaluation in a fire exposed slab at any given time. For calculating temperature profiles in a PC hollowcore slab, a set of empirical equations is proposed by utilizing temperature data generated through parametric study. For evaluating moment and shear capacity of PC hollowcore slabs at any given fire exposure time, room temperature capacity equations specified in Eurocode 2 (Eurocode 2 2004a) are modified to account for temperature-induced strength degradation in concrete and prestressing steel. The proposed approach provides a useful tool for estimating failure times in PC hollowcore slabs.

8.2 Key findings

Based on the information presented in this dissertation, the following key conclusions are drawn:

- There have been numerous fire resistance tests on PC hollowcore slabs. However, there is very limited information on the specific variations in behavior and failure mechanisms of these slabs under fire conditions. Thus, there is lack of understanding on the causes for variations in failure mode of the slabs under fire conditions, especially through shear.
- 2. Prestressing strand exhibits higher strength degradation, as compared to that of reinforcing bar, throughout 20 to 800°C temperature range. Prestressing strand does not experience any loss of yield strength and only slight loss of ultimate strength in 20 to 200°C range. Beyond 200°C, prestressing strand undergoes a rapid reduction in

- yield and ultimate strength. At 800°C, prestressing strand loses about 80% of yield strength and 95% of its ultimate strength.
- 3. PC hollowcore slabs with depths exceeding 200 mm can provide a minimum of two hours of fire resistance under 60% loading during typical building (design) fires. Hollowcore slabs exhibit better performance under design fire scenarios than under standard fire scenarios. In addition, provision of fire axial restraint enhances fire resistance of PC hollowcore slabs.
- 4. The proposed numerical model accounts for various failure limit states, including shear, and is capable of tracing the behavior of PC hollowcore slabs under realistic fire, loading and support conditions. The model also accounts for temperature induced property degradation in concrete and prestressing strands, and cracking in concrete.
- 5. Results from experimental and numerical studies indicate that slab depth, load intensity, loading scenario, axial restraint and fire severity have significant influence on the fire response and failure mode of PC hollowcore slabs.
 - a. Thinner slabs (150 and 200 mm), subjected to 60% of load, undergo failure through flexural mode, while thicker slabs undergo failure (300 and 400 mm) through shear. Slabs with medium depth (250 mm) undergo failure through flexure-shear failure mode.
 - b. Load intensity and loading pattern has significant effect on the shear response of PC hollowcore slabs under fire conditions. PC hollowcore slabs can undergo shear failure prior to attaining flexural failure at high shear regions inducing high shear forces.

- c. Axial restraint has significant effect on shear response of PC hollowcore slabs under fire conditions, wherein presence of higher axial restraint at supports can minimize shear failure in fire exposed hollowcore slabs.
- d. Higher levels of prestressing can lead to improved structural (moment and shear) performance in PC hollowcore slabs at ambient conditions. However, the effectiveness of prestressing on slab performance gets diminished at elevated temperatures, due to loss in strand strength, which leads to marginal improvement in the overall fire resistance.
- e. Severity of fire exposure has significant effect on the behavior of PC hollowcore slabs, wherein a higher intensity fire results in lower fire resistance and can shift failure mode from shear to flexural mode in thicker (more than 250 mm) hollowcore slabs.
- 6. The proposed approach for evaluating temperature and moment and shear capacity can be applied to assess fire response of PC hollowcore slabs under standard fire exposure. This simplified approach is capable of predicting cross sectional temperatures at critical locations (strand and web concrete) of fire exposed hollowcore slab and evaluate moment and shear capacities at any given fire exposure time. The simplicity of the proposed rational approach makes it attractive for incorporation in design standards.

8.3 Recommendations for future research

Although this study has advanced the state-of-the-art with respect to fire response of prestressed concrete hollowcore slabs, additional research is required to gain further insight into some of the complexities on the behavior of hollowcore slabs exposed to fire. The following are some of the key recommendations for future research in this area:

Due to large variability in the cross-sectional configurations of PC hollowcore slabs from one manufacturer to another and from one country to another, it is extremely difficult to develop an unified approach or model that covers all possible core configurations through regression analysis. The proposed simplified approach presented in this thesis is applicable to hollowcore slabs typically used in buildings, with depths ranging from 200 mm to 400 mm. Further, the simplified approach for temperature equations can be applied for recalibrating the coefficients in temperature equations to account for country- or manufacture-specific cross-sectional configurations.

- Further fire resistance experiments are needed to develop data on fire response of PC
 hollowcore slabs with different configurations including cross-sectional configuration,
 various levels of axial restraints and loading scenarios.
- Further fire resistance experiments are needed to develop data on the hollowcore slabs provided with topping concrete.
- Further work is required to incorporate more advanced features into numerical model namely, accounting for fire-induced spalling of concrete and accounting for temperatureinduced air movement in the cores for accurately predicting convection inside the cores.
- More work is needed to extend the proposed rational design methodology to account for the response of PC hollowcore slabs exposed to design fire scenario (with cooling phase).

8.4 Research impact

In recent years prestressed concrete (PC) hollowcore slabs are increasingly used in building applications due to numerous advantages these slabs offer over other floor systems. Structural fire safety is one of the primary considerations in buildings and hence, building codes specify fire resistance requirements for slabs. At present, fire resistance ratings of slabs is assessed through standard fire tests and prescriptive rules wherein, fire resistance is determined based on slab thickness and concrete cover thickness to reinforcement. These prescriptive rules, developed based on data from standard fire tests, ignore critical failure limit states and consider only limited parameters, and thus often do not yield realistic fire performance.

The studies presented in this dissertation provide a comprehensive understanding of the behavior of PC hollowcore slabs under fire conditions. The effects of critical influencing factors, such as slab depth, load intensity, loading scenario, axial restraint and fire severity are quantified through experimental and numerical studies. It is apparent from these studies that the realistic fire resistance can only be evaluated through a rational approach by accounting for all critical failure limit states, including flexure and shear.

Further, the numerical model presented in this study provides an effective alternative to fire resistance tests for evaluating fire response of PC hollowcore slabs. This model accounts for all critical factors that affect the behavior of hollowcore slab under fire conditions, namely temperature induced property degradation of concrete and prestressing strands, cracking in concrete, and different failure limit states. Thus, the developed model can be used to perform detailed fire resistance analysis on PC hollowcore slabs.

In addition, the proposed rational design approach is capable of predicting various response parameters such as cross sectional temperature, and moment and shear capacity of hollowcore slab at any given fire exposure time. Thus, a quick and reliable evaluation on fire resistance of PC hollowcore slabs can be performed, as an alternative to detailed finite element analysis. This approach can be applied over a wide range of PC hollowcore slabs used in the United States, so is attractive for incorporation in codes and standards. Overall, the research presented in this dissertation developed a comprehensive understanding on the behavior of PC hollowcore slabs under realistic fire, loading and restraint scenarios.

APPENDIX

APPENDIX

Design and Load Calculations

This Appendix summarizes the design and load calculations on PC hollowcore slabs using PCI hand book and Eurocode 2. The cross-section, shear force diagram, and bending moment diagram for the tested slabs are shown in Figure A.1. Step-by-step example for evaluating fire resistance of a PC hollowcore slab utilizing proposed rational fire design method is also illustrated.

A.1 Design of PC hollowcore slab

A.1.1 Configurations:

The configuration of a tested hollowcore slabs is illustrated in Figure A.1.

$$A_c = 126129 \; mm^2 = 0.126 \; m^2$$

$$b = 1200 \ mm = 1.2 \ m$$

$$b_w = 259 \ mm = 0.259 \ m$$

$$I_g = 6.601 \times 10^8 \ mm^4 = 0.00066 \ m^4$$

$$Y_b \cong Y_t = 100 \ mm = 0.1 \ m$$

$$S_b \cong S_t = \frac{I_g}{Y_b or Y_t} = 6.6 \times 10^6 \ mm^3 = 0.0066 \ m^3$$

$$w_t = 2490 \, Pa$$

$$Span(L) = 3660 mm = 3.66 m$$

 $d = 200 - 44 = 156 \, mm = 0.156 \, m$ (Distance of center of strand to the exposed surface is 44 mm)

$$e = 57 \ mm = 0.057 \ m$$

7 – 12.5 mm diameter prestressing strands

$$d_b = 12.5 \ mm = 0.0125 \ m$$

A.1.2 Material properties:

Concrete: Class 1 high strength concrete (HSC);

$$f_c^\prime~=~70~MPa=70\times 10^6 Pa$$
 , $\varepsilon_c=0.003, E_c=27500~MPa=~2.75\times 10^{10} Pa$

Prestressing strand: Cold-worked (cw) Class B low relaxation (LR) prestressing strands;

$$f_{pu} = 1860 \, MPa \, = 1860 \times 10^6 Pa, E_{ps} = 2 \times 10^{11} Pa$$

A.1.3 Transfer stresses and allowable concrete strength at release of prestressing

Stresses will be checked at transfer point and at mid-span

$$A_{ps} = 7 \times 97.52 \, m^2 = 682.64 \, mm^2 = 0.000683 \, m^2$$

Assume 5% initial prestress loss

Initial prestressing = 70% of f_{pu}

At release prestress force $(P_o) = 0.7 \times 0.95 \times 682.64 \times 1860 = 844357 \, N$

A.1.3.1 Due to prestress effect

Prestress effect =
$$\frac{P_o}{A_c} \pm \frac{P_o e}{s_b or s_t} = \frac{844357}{0.126} \pm \frac{844357 \times 0.057}{0.0066}$$

= $1.4 \times 10^7 \ Pa \ (bottom) \ and - 5.9 \times 10^5 \ Pa \ (top)$

A.1.3.2 Due to self-weight only at transfer points

$$Transfer\ length\ (l_t) = 50d_b = 50 \times 0.0125 = 0.625\ m$$

At transfer points, 0.625 m from the slab ends

$$Moment~0.625~m~from~slab~ends~(M_d) = \left(\frac{L \times l_t}{2} - \frac{l_t^2}{2}\right) \times w_t \times b$$

$$= \left(\frac{3.66 \times 0.625}{2} - \frac{0.625^2}{2}\right) \times 2490 \times 1.2 = 2833.9 N - m$$

$$\frac{M_d}{s} = \frac{2833.9}{0.0066} = -429384 \, Pa \, (bottom) \, and \, 429384 \, Pa \, (top)$$

Net concrete stress at transfer point

$$1.4 \times 10^7 - 429384 = 1.36 \times 10^7 Pa (bottom)$$

$$-5.9 \times 10^5 + 429384 = -1.6 \times 10^5 (top)$$

A.1.3.3 Due to self-weight only at mid-span

$$Moment~0.625~m~from~slab~ends~(M_d) = \frac{(w_t \times b \times L^2)}{8} = \frac{2490 \times 1.2 \times 3.66^2}{8}$$

$$= 5003.3 N - m$$

$$\frac{M_d}{s} = \frac{5003.3}{0.0066} = 758069 \, Pa \, (bottom) \, and - 758069 \, Pa \, (top)$$

Net concrete stress at mid-span

$$1.4 \times 10^7 + 758069 = 1.476 \times 10^7 Pa (bottom)$$

$$-5.9 \times 10^5 - 758069 = -1.35 \times 10^6 (top)$$

Thus, the permissible stress at transfer is governed by the stresses at transfer points

$$=-1.6\times10^5 Pa~(top-tension)~and~1.36\times10^7 Pa~(bottom-compression)$$

Extreme fiber stress in tension at tranfer points = $6\sqrt{f_c' \times 0.000145(psi)}$

$$=> f_c' = \left(1.6 \times 10^5 \times \frac{0.000145}{6}\right)^2 = 14.95 \ psi = 103111 \ Pa = 0.1 \ MPa$$

Extreme fiber stress in compression at transfer points = $0.6f_c'$

$$=> f_c' = 1.36 \times \frac{10^7}{0.6} = 2.27 \times 10^7 Pa = 22.7 MPa$$

Thus, allowable concrete strength at release is 22.7 MPa.

A.1.4 Loss of prestress

Dead load (DL) =
$$w_t \times b = 2490 \ Pa \times 1.2 = 2988 \frac{N}{m}$$

Live load (LL) = $(manufacturer\ safe\ super-imposed\ load\times b)=23509\ Pa\times 1.2$

$$=28211\frac{N}{m}$$

A.1.4.1 Elastic shortening (ES)

$$P_i = 0.7(A_{ps} \times f_{pu}) = 0.7 \times 682.64 \times 1860 = 844357 N$$

$$M_g = \left(\frac{DL \times L^2}{8}\right) = \frac{2988 \times 3.66^2}{8} = 5003.3 N - m$$

$$f_{cir} = k_{cir} \left(\frac{p_i}{A_c} + P_i \times \frac{e^2}{I_g} \right) - M_g \times \frac{e}{I_g}$$

$$= 0.9 \left(\frac{844357}{0.126} + 844357 \times \frac{0.057^2}{0.00066} \right) - 5003.3 \times \frac{0.057}{0.00066} = 9.34 \times 10^6 N$$

$$ES = \frac{K_{es} \times E_s}{E_{ci}} f_{cir} = 1.0 \times \frac{2 \times 10^{11}}{2.75 \times 10^{10}} \times 9.34 \times 10^6 = 6.79 \times 10^7 Pa = 9.85 \text{ ksi}$$

A.1.4.2 Concrete creep (CR)

$$f_{cds} = M_{sd} \times \frac{e}{I_g} = \left(2988 \times \frac{3.66^2}{8}\right) \times \frac{0.057}{0.00066} = 432099 Pa$$

$$CR = \frac{K_{cr} \times E_s}{E_{ci}} (f_{cir} - f_{cds}) = 2.0 \times \frac{2 \times 10^{11}}{2.75 \times 10^{10}} \times (9.34 \times 10^6 - 432099) = 1.29 \times 10^8 Pa = 0.00 \times 10^{11} = 0.00 \times 1$$

18.7 ksi

A.1.4.3 Shrinkage of concrete (SH)

$$\frac{Area}{perimeter} = \frac{V}{S} = 48.8 mm = 1.92 in$$

Using relative humidity (RH) = 70%

$$SH = 8.2 \times 10^{-6} K_{sh} \times E_s(ksi) \left(1 - 0.06 \times \frac{V}{S}(in) \right) \times (100 - RH)$$

$$= 8.2 \times 10^{-6} \times 1.0 \times 29000(ksi) \left(1 - 0.06 \times 1.92(in) \right) \times (100 - 70)$$

$$= 6.3 \, ksi = 4.3 \times 10^7 \, Pa$$

A.1.4.4 Steel relaxation (RE)

From Table 2.2.3.1 (PCI)

$$K_{re} = 5000, J = 0.04$$

From Table 2.2.3.2 (PCI)

$$C = 0.75 \, for \frac{f_{si}}{f_{pu}} = 0.7$$

$$RE = [K_{re} - J(SH + CR + ES)]C = \left[\frac{5000}{1000} - 0.04(9.85 + 18.7 + 6.3)\right] \times 0.75 = 2.7 \text{ ksi}$$
$$= 1.86 \times 10^7 Pa$$

A.1.4.5 Total loss at mid-span (TS)

$$TS = ES + CR + SH + RE = 37.55 \text{ ksi} = 2.58 \times 10^8 \text{ Pa}$$

Thus, percentage loss =
$$\frac{2.58 \times 10^8}{0.7 \times 1860 \times 10^6} \times 100 = 19.8\% \approx 20\%$$

A.1.5 Service load stresses (PCI)

Dead load (DL) =
$$w_t \times b = 2490 \ Pa \times 1.2 = 2988 \frac{N}{m}$$

Live load (LL) = $(manufacturer\ safe\ super-imposed\ load\times b)=23509\ Pa\times 1.2$

$$=28211\frac{N}{m}$$

$$M_{service} = (DL + LL) \times \frac{L^2}{8} = (2988 + 28211) \times \frac{3.66^2}{8} = 52241.2 N - m$$

with prestress losses of 20%, $A_{ps} \times f_{se} = 0.7 \times 682.64 \times 1860 \times (1-0.2) = 711038$ N

Top fiber compression under service loads

$$f_{top} = \frac{A_{ps} \times f_{se}}{A_c} - \frac{A_{ps} \times f_{se} \times e}{s_t} + \frac{M_{service} \times b}{s_t}$$

$$= \frac{711038}{0.126} - 711038 \times \frac{0.057}{0.0066} + 52241.2 \times \frac{1.2}{0.0066} = 9 \times 10^6 Pa < 0.6 \times f_c'$$

$$= 0.6 \times 70 \times 10^6 = 4.2 \times 10^7 Pa \ (OK)$$

Bottom fiber tension under service loads

$$f_{bottom} = \frac{A_{ps} \times f_{se}}{A_c} + \frac{A_{ps} \times f_{se} \times e}{s_b} - \frac{M_{service} \times b}{s_b}$$

$$= \frac{711038}{0.126} + 711038 \times \frac{0.057}{0.0066} - 52241.2 \times \frac{1.2}{0.0066} = 2.28 \times 10^6 Pa$$

$$< 7.5 \sqrt{f_c' \times 0.000145(psi)} = 7.5 \sqrt{70 \times 145(psi)} = 755 psi$$

$$= 5.2 \times 10^6 Pa (OK)$$

A.1.6 Flexural capacity (Eurocode 2)

$$M_n = A_{ps} \times f_{ps} \left(d - \frac{a}{2} \right) = 0.000683 \times 1.78 \times 10^9 \left(0.156 - \frac{0.017}{2} \right) = 179322 N - m$$

 $\approx 180 \ kN - m$

where,

$$f_{ps} = f_{pu} \left[1 - \frac{\gamma_p}{\beta_1} \left(\rho_p \times \frac{f_{pu}}{f_c'} \right) \right] = 1860 \times 10^6 \left[1 - \frac{0.28}{0.65} \left(0.00365 \times \frac{1860 \times 10^6}{70 \times 10^6} \right) \right]$$
$$= 1.78 \times 10^9 Pa$$

 $\gamma_p = 0.28$ for LR strands

$$\beta_1 = 0.65 \ for \ f_c' = 70 \ MPa$$

$$\rho_p = \frac{A_{ps}}{b \times d_p} = \frac{0.000683}{1.2 \times 0.156} = 0.00365$$

$$w_p = \frac{\rho_p \times f_{ps}}{f_c'} = \frac{0.00365 \times 1.78 \times 10^9}{70 \times 10^6} = 0.093 < 0.36 \times \beta_1 = 0.234 (OK)$$

$$a = \frac{A_{ps} \times f_{ps}}{0.85 \times f_c' \times b} = \frac{0.000683 \times 1.78 \times 10^9}{0.85 \times 70 \times 10^6 \times 1.2} = 0.017 m$$

A.1.7 Shear capacity (Eurocode 2)

$$V_{Rd,c,fi} = \left[C_{Rd,c} k (100\rho_1 f_c')^{\frac{1}{3}} + k_1 \sigma_{cp} \right] b_w d$$

$$= \left[0.1 \times 2 \times (100 \times 0.0169 \times 70)^{\frac{1}{3}} + 0.15 \times 0 \right] \times 259 \times 156 = 39668.8 \, N$$

$$\approx 40 \, kN$$

where,

$$C_{Rd,c} = \frac{0.18}{\gamma_c} = \frac{0.18}{1.5} \approx 0.1 \ (\gamma_c \ from \ 2.4.2.4 \ EC2)$$

$$f_c' = 70 MPa$$

$$k = 1 + \sqrt{\frac{200}{d}} \le 2.0 \text{ with d in } mm = 1 + \sqrt{\frac{200}{156}} = 2.133 => k = 2.00$$

$$k_1 = 0.15$$

$$\rho_1 = \frac{A_{ps}}{b_w d} = \frac{682.64}{259 \times 156} = 0.0169 < 0.02 (OK)$$

$$\sigma_{cp} = \frac{f_{ps} \times A_{ps}}{A_c} = 1780 \times \frac{682.64}{126129} = 9.64 \, MPa < 0.2 f_c' = 0.2 \times 70 = 14 \, MPa(OK)$$

However, the compressive stress due to prestressing is ignored under fire conditions, thus σ_{cp} = 0 MPa

A.1.8 Load calculation under fire conditions based on ASTM-E119

Dead load (DL) =
$$w_t \times b = 2490 \ Pa \times 1.2 = 2988 \frac{N}{m}$$

Live load (LL) or applied load = $(manufacturer\ safe\ super-imposed\ load\times b)$

$$= 23509 \, Pa \times 1.2 = 28211 \frac{N}{m}$$

$$w_u = 1.2 \times DL + 1.6 \times LL = 1.2 \times 2988 + 1.6 \times 28211 = 48723.2 \frac{N}{m}$$

$$M_u = \frac{w_u \times L^2}{8} = \frac{48723.2 \times 3.66^2}{8} = 81584.6 N - m$$

$$w_{fire} = 1.2 \times DL + 0.5 \times LL = 1.2 \times 2988 + 0.5 \times 28211 = 17691.1$$

$$M_{fire} = \frac{w_{fire} \times L^2}{8} = \frac{17691.1 \times 3.66^2}{8} = 29622.9 N - m$$

$$w_{test} = DL + LL = 2988 + 28211 = 3.1 \times 10^4 \frac{N}{m} (ASTM - E119)$$

$$\begin{split} M_{test} &= w_{test} \times \frac{L^2}{8} = 3.1 \times 10^3 \times \frac{3.66^2}{8} \cong 5 \times 10^5 N - m \\ &\cong 50 \ kN - m \ (applied \ moment - ASTM - E119) \\ V_{test} &= \frac{M_{test}}{L} = \frac{50}{1.4} \cong 35 \ kN - m \ (applied \ shear - ASTM - E119) \end{split}$$

Applied load ratio =
$$\frac{5 \times 10^5}{8.1 \times 10^5} \approx 0.6 \approx 60\%$$

A.2 Calculation of fire resistance using proposed rational design approach

Based on the proposed rational approach, strand and mid-depth temperatures is evaluated first and then moment capacity and shear capacity at 1 hr, 1½ hr and 2 hr and at failure times is evaluated.

A.2.1 Strand and mid-depth temperatures

A.2.1.1 At 1 hr into fire exposure

$$T_z = c_1 \cdot \eta_Z \cdot (a \cdot t^n)$$

$$\eta_z = a_1 \cdot \ln\left(\frac{t}{a^{1.5}}\right) + a_2 \cdot \sqrt{z} + a_3$$

where,

$$c_1 = 1.01, a = 910, n = 0.148, t = 1 hr$$

$$a_1 = 0.222, a_2 = 0.425, a_3 = 0.634, z = 0.045 m for strand$$

$$a_1 = 0.233, a_2 = 0.579, a_3 = 0.356, z = 0.105 \ m \ for \ mid-depth$$

Strand temperature $T_z = 1.01 \times 0.309 \times (910 \times 1^{0.148}) = 284^{\circ}C$

where,
$$\eta_z = 0.222 \cdot \ln \left(\frac{1}{0.045^{1.5}} \right) - 0.425 \cdot \sqrt{0.045} - 0.356 = 0.309$$

$$Mid-depth\ temperature\ T_z=1.01\times0.23\times(910\times1^{0.148})=211^{\circ}C$$

where,
$$\eta_z = 0.233 \cdot \ln \left(\frac{1}{0.105^{1.5}} \right) - 0.579 \cdot \sqrt{0.105} - 0.356 = 0.23$$

A.2.1.2 At $1\frac{1}{2}$ hr into fire exposure

Strand temperature
$$T_z = 1.01 \times 0.39 \times (910 \times 1.5^{0.148}) = 388^{\circ}C$$

where,
$$\eta_z = 0.222 \cdot \ln \left(\frac{1.5}{0.045^{1.5}} \right) - 0.425 \cdot \sqrt{0.045} - 0.356 = 0.39$$

$$\mathit{Mid-depth\ temperature\ T_z=1.01\times0.32\times(910\times1.5^{0.148})=312^{\circ}C}$$

where,
$$\eta_z = 0.233 \cdot \ln \left(\frac{1.5}{0.105^{1.5}} \right) - 0.579 \cdot \sqrt{0.105} - 0.356 = 0.32$$

A.2.1.3 At 2 hr into fire exposure

Strand temperature
$$T_z = 1.01 \times 0.46 \times (910 \times 2^{0.148}) = 469^{\circ}C$$

where,
$$\eta_z = 0.222 \cdot \ln\left(\frac{2}{0.045^{1.5}}\right) - 0.425 \cdot \sqrt{0.045} - 0.356 = 0.46$$

$$\mathit{Mid-depth\ temperature\ T_z=1.01\times0.39\times(910\times2^{0.148})=397^{\circ}C}$$

where,
$$\eta_z = 0.233 \cdot \ln\left(\frac{2}{0.105^{1.5}}\right) - 0.579 \cdot \sqrt{0.105} - 0.356 = 0.39$$

A.2.1.4 At 130 minutes (2.1 hr) into fire exposure

Strand temperature
$$T_z=1.01\times0.47\times(910\times2.1^{0.148})=482^{\circ}C$$

where,
$$\eta_z = 0.222 \cdot \ln \left(\frac{2.1}{0.045^{1.5}} \right) - 0.425 \cdot \sqrt{0.045} - 0.356 = 0.47$$

$$Mid-depth\ temperature\ T_z=1.01\times0.4\times(910\times2.1^{0.148})=410^{\circ}C$$

where,
$$\eta_z = 0.233 \cdot \ln \left(\frac{2.1}{0.105^{1.5}} \right) - 0.579 \cdot \sqrt{0.105} - 0.356 = 0.4$$

A.2.2 Moment capacity

A.2.2.1 At 1 hr into fire exposure

$$M_{nT} = A_{ps} \times f_{psT} \left(d - \frac{a}{2} \right) = 0.000683 \times 1.34 \times 10^{9} \left(0.156 - \frac{0.015}{2} \right)$$
$$= 135910 \ N - m \cong 136 \ kN - m$$

where,

$$\frac{f_{puT}}{f_{pu}} = \left(0.87 - \frac{284 - 200}{300 - 200}(0.87 - 0.72)\right) = 0.744 \text{ for Class B, cw, LR strands}$$

$$\frac{f'_{cT}}{f'_{c}} = \left(0.9 - \frac{284 - 200}{300 - 200}(0.9 - 0.85)\right) = 0.86 \text{ for Class 1 HSC}$$

$$\begin{split} f_{psT} &= f_{puT} \left[1 - \frac{\gamma_p}{\beta_1} \left(\rho_p \times \frac{f_{puT}}{f_c'} \right) \right] \\ &= 1860 \times 10^6 \times 0.744 \left[1 - \frac{0.28}{0.65} \left(0.00365 \times \frac{0.744 \times 1860 \times 10^6}{0.86 \times 70 \times 10^6} \right) \right] \\ &= 1.34 \times 10^9 Pa \\ a &= \frac{A_{ps} \times f_{psT}}{0.85 \times f_{cT}' \times b} = \frac{0.000683 \times 1.34 \times 10^9}{0.85 \times 0.86 \times 70 \times 10^6 \times 1.2} = 0.015 \, m \end{split}$$

A.2.2.2 At 1½ hr into fire exposure

$$M_{nT} = A_{ps} \times f_{psT} \left(d - \frac{a}{2} \right) = 0.000683 \times 8.87 \times 10^8 \left(0.156 - \frac{0.011}{2} \right)$$
$$= 91176 N - m \approx 91 kN - m$$

where,

$$\begin{split} \frac{f_{puT}}{f_{pu}} &= \left(0.72 - \frac{388 - 300}{400 - 300}(0.72 - 0.46)\right) = 0.49 \text{ for Class B, cw, LR strands} \\ \frac{f'_{cT}}{f'_{c}} &= \left(0.85 - \frac{388 - 300}{400 - 300}(0.85 - 0.75)\right) = 0.76 \text{ for Class 1 HSC} \\ f_{psT} &= f_{puT} \left[1 - \frac{\gamma_{p}}{\beta_{1}} \left(\rho_{p} \times \frac{f_{puT}}{f'_{c}}\right)\right] \\ &= 1860 \times 10^{6} \times 0.49 \left[1 - \frac{0.28}{0.65} \left(0.00365 \times \frac{0.49 \times 1860 \times 10^{6}}{0.76 \times 70 \times 10^{6}}\right)\right] \\ &= 8.87 \times 10^{8} Pa \\ a &= \frac{A_{ps} \times f_{psT}}{0.85 \times f'_{cT} \times b} = \frac{0.000683 \times 8.87 \times 10^{8}}{0.85 \times 0.76 \times 70 \times 10^{6} \times 1.2} = 0.011 \, m \end{split}$$

A.2.2.3 At 2 hr into fire exposure

$$M_{nT} = A_{ps} \times f_{psT} \left(d - \frac{a}{2} \right) = 0.000683 \times 5.35 \times 10^8 \left(0.156 - \frac{0.008}{2} \right)$$
$$= 55541.6 N - m \approx 56 kN - m$$

A.2.2.4 At 130 minutes (2.1 hr) into fire exposure

$$M_{nT} = A_{ps} \times f_{psT} \left(d - \frac{a}{2} \right) = 0.000683 \times 4.8 \times 10^8 \left(0.156 - \frac{0.007}{2} \right)$$
$$= 49995.6 N - m \approx 50 kN - m$$

A.2.3 Shear capacity

A.2.3.1 At 1 hr into fire exposure

$$V_{Rd,c,fi} = \left[C_{Rd,c} k (100\rho_1 f_c')^{\frac{1}{3}} + k_1 \sigma_{cp} \right] b_w d$$

$$= \left[0.1 \times 2 \times (100 \times 0.0169 \times 0.9 \times 70)^{\frac{1}{3}} + 0.15 \times 0 \right] \times 259 \times 156$$

$$= 39036.4 \, N \cong 39 \, kN$$

where,

$$\frac{f'_{cT}}{f'_{c}} = \left(0.9 - \frac{211 - 200}{300 - 200}(0.9 - 0.85)\right) = 0.9 \text{ for Class 1 HSC}$$

$$C_{Rd,c} = \frac{0.18}{\gamma_c} = \frac{0.18}{1.5} \approx 0.1 \ (\gamma_c \ from \ 2.4.2.4 \ EC2)$$

$$k = 1 + \sqrt{\frac{200}{d}} \le 2.0 \text{ with } d \text{ in } mm = 1 + \sqrt{\frac{200}{156}} = 2.133 => k = 2.00$$

$$k_1 = 0.15$$

$$\rho_1 = \frac{A_{ps}}{b_w d} = \frac{682.64}{259 \times 156} = 0.0169 < 0.02 (OK)$$

$$\sigma_{cp} = \frac{f_{ps} \times A_{ps}}{A_c} = 1780 \times \frac{682.64}{126129} = 9.64 \, MPa < 0.2 f_c' = 0.2 \times 70 = 14 \, MPa(OK)$$

However, the compressive stress due to prestressing is ignored under fire conditions,

thus
$$\sigma_{cp} = 0 MPa$$

A.2.3.2 At 1½ hr into fire exposure

$$V_{Rd,c,fi} = \left[C_{Rd,c} k (100 \rho_1 f_c')^{\frac{1}{3}} + k_1 \sigma_{cp} \right] b_w d$$

$$= \left[0.1 \times 2 \times (100 \times 0.0169 \times 0.84 \times 70)^{\frac{1}{3}} + 0.15 \times 0 \right] \times 259 \times 156$$

$$= 38148.9 \, N \cong 38 \, kN$$

where,

$$\frac{f'_{cT}}{f'_{c}} = \left(0.85 - \frac{312 - 300}{400 - 300}(0.85 - 0.75)\right) = 0.84 \text{ for Class 1 HSC}$$

A.2.3.3 At 2 hr into fire exposure

$$V_{Rd,c,fi} = \left[C_{Rd,c} k (100\rho_1 f_c')^{\frac{1}{3}} + k_1 \sigma_{cp} \right] b_w d$$

$$= \left[0.1 \times 2 \times (100 \times 0.0169 \times 0.76 \times 70)^{\frac{1}{3}} + 0.15 \times 0 \right] \times 259 \times 156$$

$$= 36897.2 \ N \cong 37 \ kN$$

A.2.3.4 At 155 minutes (2.6 hr) into fire exposure

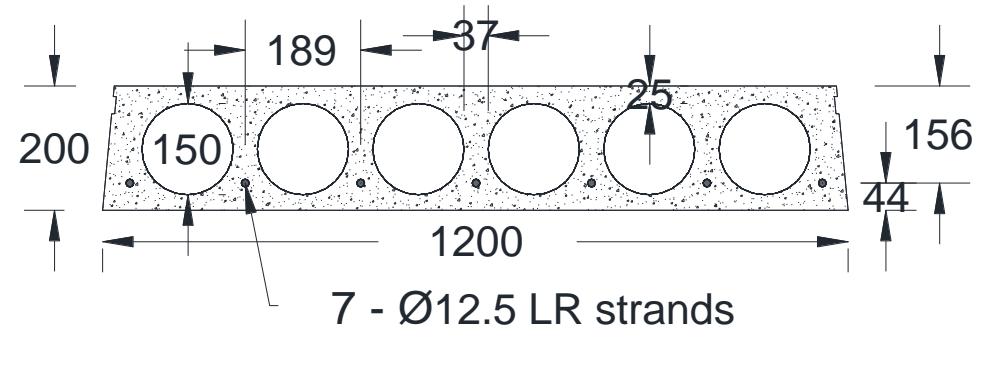
$$V_{Rd,c,fi} = \left[C_{Rd,c} k (100 \rho_1 f_c')^{\frac{1}{3}} + k_1 \sigma_{cp} \right] b_w d$$

$$= \left[0.1 \times 2 \times (100 \times 0.0169 \times 0.64 \times 70)^{\frac{1}{3}} + 0.15 \times 0 \right] \times 259 \times 156$$

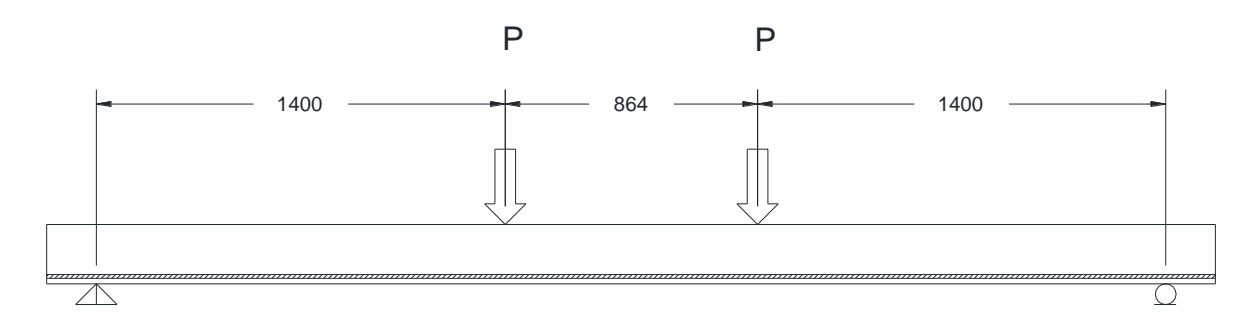
$$= 34843 \ N \cong 35 \ kN$$

A.2.4 Fire resistance

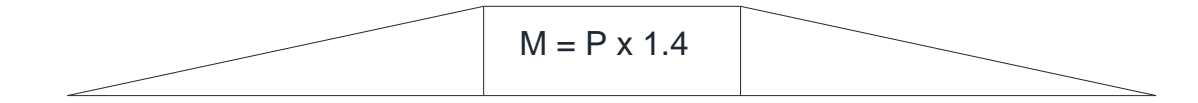
Finally, fire resistance can be evaluated by comparing the moment capacity and shear capacity under fire exposure with the applied bending moment and shear force respectively. Applied bending moment = 50 kN-m and applied shear force = 35 kN-m. The moment capacity is 50 kN-m at 125 minutes and shear capacity is 35 kN-m at 155 minutes. Thus, the fire resistance of the PC hollowcore slab is 130 minutes.



a. Cross-section



b. Elevation



c. Bending moment diagram



d. Shear force diagram

Figure A.1. Cross section, elevation and internal force diagram of PC hollowcore slab

REFERENCES

REFERENCES

- Abiko, K. (1995). "Hot Ductility and High Temperature Microstructure of High Purity Iron Alloys." *Le Journal de Physique IV*, 05(C7), C7–77–C7–84.
- Abrams, M. S. (1976). "Fire tests of hollow-core specimens with and without roof insulation." *PCI Journal*.
- ACI 216.1-14. (2014). Code requirements for determining fire resistance of concrete and masonry construction assemblies. American Concrete Institute, Farmington, MI.
- ACI 318. (2011). Building code requirements for structural concrete. American Concrete Institute, Farmington, MI.
- Acker, V. A. (2003). "Shear resistance of prestressed hollowcore floors exposed to fire." *Structural Concrete, Journal of the FIB and Thoman Telford and fib*, 4(2), 65–74, 1464–4177.
- Aguado, J. V., Espinos, A., Hospitaler, A., Javier, O., and Romero, M. L. (2012). "Fire resistance of hollowcore slabs. Influence of reinforcement arrangement." Zurich, Switzerland.
- Andersen, N. E., and Lauridsen, D. H. (1999). *Danish Institute of Fire Technology Technical Report X* 52650 Part 2 Hollowcore concrete slabs. DIFT, Denmark.
- ANSYS. (2014). Finite element computer code. ANSYS, Inc.
- AS 3600. (2001). Concrete Structures. Australian Standard AS 3600-2001, Sydney, Australia.
- ASCE. (1992). Structural Fire Protection. American Society of Civil Engineers, New York.
- AS/NZS. (2002). AS/NZS 1170:2002. Structural design actions. Standards New Zealand, Wellington, New Zealand.
- ASTM. (2003). Standard Test Methods for Elevated Temperature Tension Tests of Metallic Materials E21. ASTM International, West Conshohocken, PA.
- ASTM. (2011). Standard test methods for fire tests of building construction and materials. Test Method E119. American Society for Testing and Materials, West Conshohocken, PA.
- ASTM. (2012a). Standard specification for steel strand, uncoated seven-wire for prestressed concrete A416. American Society for Testing and Materials, West Conshohocken, PA.

- ASTM. (2012b). Standard specification for deformed and plain carbon-steel bars for concrete reinforcement A615. American Society for Testing and Materials, West Conshohocken, PA.
- ASTM. (2014). Test Methods for Determining Effects of Large Hydrocarbon Pool Fires on Structural Members and Assemblies E1529. ASTM International, West Conshohocken, PA.
- Bailey, C. G., and Lennon, T. (2008). "Full-scale fire tests on hollowcore floors." *The Structural Engineer*, 86(6), 33–39.
- Borgogno, W. (1997). "Structural behavior of slim floor covering with concrete hollow slabs at room temperature and elevated temperature." Dissertation, Swiss Federal Institute of Technology, Zurich, Germany.
- Breccolotti, M., Materazzi, A. L., and Venanzi, I. (2006). "Fire performance of HPLWC hollow core slabs." *4th international workshop Structures in Fire SiF'06*, Universidade De Aveiro Campus Universitário De Santiago, Aveiro, Portugal.
- BS 476–20. (1987). Fire tests on building materials and structure—part 20: method for determination of the fire resistance of elements of construction. CEN: European Committee for Standardization, Brussels, Belgium.
- Chang, J. J., Buchanan, A. H., Dhakal, R. P., and Moss, P. J. (2008). "Hollowcore concrete slab exposed to fire." *Fire and Materials*, 32(6), 321–331.
- Chawla, K. K. (2008). *Mechanical Behavior of Materials*. Cambridge University Press, Cambridge; New York.
- DIANA. (2000). Finite element package. Delft, TNO, Netherlands.
- Dolzhenkov, I. E. (1971). "The nature of blue brittleness of steel." *Metal Science and Heat Treatment*, 13(3), 220–224.
- Dotreppe, J., and Franssen, J. (2004). "Precast hollow core slabs in fire: Numerical simulation and experimental tests." National Research Council Canada and University of Liege, Belgium, Ottawa, Canada.
- Engström, B., Lundgren, K., and Broo, H. (2007). "Shear and torsion in prestressed hollow core units: finite element analyses of full-scale tests." *Structural Concrete*, 8(2), 87–100.
- Eurocode 1. (2008). Actions on structures, Part 1–1: General actions Densities, self-weight, imposed loads for buildings. CEN: European Committee for Standardization, UK.
- Eurocode 2. (2004a). Design of concrete structures, Part 1-2: General rules-structural fire design. ENV 1992-1-2. CEN: European Committee for Standardization, UK.

- Eurocode 2. (2004b). Design of concrete structures, Part 1–1: General rules and rules for buildings. CEN: European Committee for Standardization, UK.
- Eurocode 3. (2005). Design of steel structures, Part 1-2: General rules-structural fire design. ENV 1992-1-2. CEN: European Committee for Standardization, UK.
- Felicetti, R., Gambarova, P. G., and Meda, A. (2009). "Residual behavior of steel rebars and R/C sections after a fire." *Construction and Building Materials*, 23(12), 3546–3555.
- Fellinger, J. H. H., Stark, J., and Walraven, J. (2005). "Shear and anchorage behavior of fire exposed hollow core slabs." *HERON*, 50(4).
- FIP. (1999). *Practical design of structural concrete*. Recommendation, The International Federation for Structural Concrete, Lausanne, Switzerland, 114.
- Franssen, J. M., Kodur, V. K. R., and Mason, J. (2004). SAFIR: A computer program for analysis of structures subjected to fire. University of Liege, Liege, Belgium.
- Gales, J. A., Bisby, L. A., and Stratford, T. (2012). "New Parameters to Describe High-Temperature Deformation of Prestressing Steel Determined Using Digital Image Correlation." *Structural Engineering International*, 22(4), 476–486.
- Gales, J., Bisby, L. A., and Gillie, M. (2011). "Unbonded Post Tensioned Concrete Slabs in Fire Part I Experimental Response of Unbonded Tendons under Transient Localized Heating." *Journal of Structural Fire Engineering*, 2(3), 139–154.
- Gálvez, F., Atienza, J. M., and Elices, M. (2011). "Behaviour of steel prestressing wires under extreme conditions of strain rate and temperature." *Structural Concrete*, 12(4), 255–261.
- Hou, X., Zheng, W., Kodur, V., and Sun, H. (2014). "Effect of temperature on mechanical properties of prestressing bars." *Construction and Building Materials*, 61, 24–32.
- ICC. (2012). *International Building Code*. International Code Council Inc., Country Club Hills, IL.
- Ichikawa, Y., and England, G. L. (2004). "Prediction of moisture migration and pore pressure build-up in concrete at high temperatures." *Nuclear Engineering and Design*, 228(1–3), 245–259.
- Iding, R., Bresler, B., and Nizamuddin, Z. (1977). Fires T3 A computer program for the fire response of structures. University of California at Berkeley.
- International Standard (E). (1999). Fire resistance tests: Elements of building construction. Part 1: General Requirements. ISO834-1-1999. International Organization for Standardization, Geneva, Switzerland.

- Jansze, W., Acker, A. van, Lindstrom, G., and Klein-Holte, R. (2014). *Structural behaviour of prestressed concrete hollow core floors exposed to fire*. Uitgeverij BOXpress B.V., 's-Hertogenbosch.
- Jansze, W., Acker, A. V., Bella, B. D., Klein-Holte, R., Lindstrom, G., Nitsch, A., Py, J. P., Robert, F., and Scalliet, M. (2012). "Fire resistance of hollowcore floors regarding shear and anchorage capacity." *Structures in Fire Sif '12*, Zurich, Switzerland.
- Jensen, J. F. (2005). *Hollowcore slabs and fire Documentation on shear capacity*. Danish Prefab Concrete Association, Danish Institute of Fire Technology, Denmark.
- Kodur, V. (2014). "Properties of Concrete at Elevated Temperatures." *International Scholarly Research Notices*, 2014, e468510.
- Kodur, V. K. R. (2000). "Spalling in High Strength Concrete Exposed to Fire: Concerns, Causes, Critical Parameters and Cures." *Advanced Technology in Structural Engineering*, 1–9.
- Kodur, V. K. R., and Dwaikat, M. (2007). "Performance-based Fire Safety Design of Reinforced Concrete Beams." *Journal of Fire Protection Engineering*, 17(4), 293–320.
- Kodur, V. K. R., and Harmathy, T. Z. (2012). "Properties of building materials. Section 1, Chapter 10." *SFPE handbook of fire protection engineering*, Society of Fire Protection Engineers, Bethesda, MD.
- Kodur, V. K. R., and McGrath, R. (2001). "Performance of High Strength Concrete Columns Under Severe Fire Conditions." *Proceedings Third International Conference on Concrete Under Severe Conditions*, Vancouver, BC, Canada, pp. 254–268.
- Kodur, V. K. R., and Shakya, A. M. (2013). "Effect of temperature on thermal properties of spray applied fire resistive materials." *Fire Safety Journal*, 61(0), 314 323.
- Kodur, V. K. R., and Shakya, A. M. (2014). "Application of rational methodology for evaluating fire resistance of concrete structures." *Building Materials, Szkoła Główna Służby Pożarniczej, Warsaw, Poland*, 2014(10), 82–87.
- Kodur, V. K. R., Yu, B., and Dwaikat, M. M. S. (2013). "A simplified approach for predicting temperature in reinforced concrete members exposed to standard fire." *Fire Safety Journal*, 56, 39–51.
- Lennon, T. (2003). "Precast concrete hollowcore slabs in fire." *The Structural Engineer*, 81(8), 30–47.
- McAllister, T., LaMalva, K., and Garlock, M. (n.d.). "ASCE/SEI 7 Appendix E Proposal: Performance-Based Design Procedures for Fire Effects on Structures." *Structures Congress* 2015, American Society of Civil Engineers, 807–818.

- Microsoft Excel. (n.d.). Microsoft Excel. Microsoft Corporation.
- Min, J., Dhakal, R., Abu, A., Moss, P., and Buchanan, A. (2012). "Prediction of shear failure of hollowcore slabs exposed to fire." *From Materials to Structures: Advancement through Innovation*, CRC Press, 555–560.
- Min, J. K., Moss, P. J., Dhakal, R. P., and Buchanan, A. H. (2010). "Modeling the fire resistance of prestressed concrete floors using multi-spring connection elements." *Structures in Fire Structure in Fire '10*, DEStech Publications, Michigan State University, Lansing.
- NRC/CNRC. (2010). *National Building Code of Canada*. National Research Council Canada, Vancouver, Canada.
- PCI. (2010). PCI Design Handbook. Precast Prestressed Concrete Institute, Chicago, IL.
- PCI. (2011). Design for Fire Resistance of Precast/Prestressed Concrete.
- Peltonen, S., and Plum, C. M. (November). *Fire resistance of hollowcore slabs supported on non-fire protected Deltabeams*. Peikko News, Peikko Group Oy, Finland, 4–8.
- Rahman, M. K., Baluch, M. H., Said, M. K., and Shazali, M. A. (2012). "Flexural and Shear Strength of Prestressed Precast Hollow-Core Slabs." *Arabian Journal for Science and Engineering*, 37(2), 443–455.
- Schepper, L., and Anderson, N. E. (2000). *Danish Institute of Fire Technology and COWI Technical Report PG 10724 Fire test of deck elements*. COWI and DEFT, Denmark.
- Shakya, A. M., and Kodur, V. K. R. (2015). "Response of precast prestressed concrete hollowcore slabs under fire conditions." *Engineering Structures*, 87, 126–138.
- Tao, Z., Wang, X., and Uy, B. (2013). "Stress-Strain Curves of Structural and Reinforcing Steels after Exposure to Elevated Temperatures." *Journal of Materials in Civil Engineering*, 25(9), 1306–1316.
- Twilt, L. (1988). "Strength and deformation properties of steel at elevated temperatures: Some practical implications." *Fire Safety Journal*, 13(1), 9–15.
- Wang, W., Liu, B., and Kodur, V. (2013). "Effect of Temperature on Strength and Elastic Modulus of High-Strength Steel." *Journal of Materials in Civil Engineering*, 25(2), 174–182.
- Wang, Y. C., Wong, P. M. H., and Kodur, V. (2007). "An experimental study of the mechanical properties of fibre reinforced polymer (FRP) and steel reinforcing bars at elevated temperatures." *Composite Structures*, 80(1), 131–140.

- Willam, K., and Warnke, E. (1975). "Constitutive model for the triaxial behavior of concrete." *International Association for Bridge and Structural Engineering*, Bergamo, Italy, 1–30.
- Williams B. K. (2004). "Fire Performace of FRP-Strengthened Reinforced Concrete Flexural Members." PhD Thesis, Queen's University, Kongston, Ontario, Canada.
- Zheng, W., Hu, Q., and Zhang, H. (2007). "Experimental research on the mechanical property of prestressing steel wire during and after heating." Frontiers of Architecture and Civil Engineering in China, 1(2), 247–254.
- Zheng, W. Z., Hou, X. M., Shi, D. S., and Xu, M. X. (2010). "Experimental study on concrete spalling in prestressed slabs subjected to fire." *Fire Safety Journal*, 45, 283–297.